INTERNATIONAL ATOMIC ENERGY AGENCY

INDC(NDS)-452
Distr. SD/EL

I N D C INTERNATIONAL NUCLEAR DATA COMMITTEE

WORKSHOP

ON NUCLEAR STRUCTURE AND DECAY DATA:

THEORY AND EVALUATION

MANUAL – PART 1

Editors: A.L.Nichols and P.K.McLaughlin
IAEA Nuclear Data Section
Vienna, Austria

November 2004

IAEA NUCLEAR DATA SECTION, WAGRAMER STRASSE 5, A-1400 VIENNA

INDC documents may be downloaded in electronic form from http://www-nds.iaea.or.at/indc_sel.html or sent as an e-mail attachment. Requests for hardcopy or e-mail transmittal should be directed to services@iaeand.iaea.org or to:

Nuclear Data Section
International Atomic Energy Agency
PO Box 100
Wagramer Strasse 5
A-1400 Vienna
Austria

Produced by the IAEA in Austria
December 2004

INDC(NDS)-452
Distr. SD/EL

WORKSHOP
ON NUCLEAR STRUCTURE AND DECAY DATA: THEORY AND EVALUATION

MANUAL – PART 1

ICTP Trieste, Italy

17 – 28 November 2003

Edited by

A.L. Nichols and P.K. McLaughlin

IAEA Nuclear Data Section

Vienna, Austria

Abstract

A two-week Workshop on Nuclear Structure and Decay Data was organized and administrated by the IAEA Nuclear Data Section, and hosted at the Abdus Salam International Centre for Theoretical Physics (ICTP) in Trieste, Italy from 17 to 28 November 2003. The aims and contents of this workshop are summarized, along with the agenda, list of participants, comments and recommendations. Workshop materials are also included that are freely available on CD-ROM (all relevant PowerPoint presentations and manuals along with appropriate computer codes):

e-mail: services@iaeand.iaea.org
fax: (+43-1)26007
post to: International Atomic Energy Agency
Nuclear Data Section
P.O. Box 100
Wagramer Strasse 5
A-1400 Vienna
Austria

January 2004

TABLE OF CONTENTS

1. SUMMARY 1
   - 1.1 Objectives 3
   - 1.2 Programme 3
     - 1.2.1 Agenda 3
     - 1.2.2 List of participants 7
   - 1.3 Presentations available in electronic form on cd-rom 10
   - 1.4 Other workshop materials on cd-rom 12
   - 1.5 Recommendations and conclusions 12
   - 1.6 Reference 13
2. WORKSHOP INTRODUCTION 14
3. EVALUATIONS: A Very Informal History 17
4. NUCLEAR THEORY 31
   - 4.1 The Nuclear Shell Model 31
   - 4.2 The Interacting Boson Model 51
   - 4.3 Self-consistent Mean-field Models: Structure of Heavy Nuclei 67
   - 4.4 Self-consistent Relativistic Mean-field Models: Structure of Heavy Nuclei 99
   - 4.5 Geometrical Symmetries in Nuclei 135
5. EXPERIMENTAL NUCLEAR SPECTROSCOPY 181
   - 5.1 Introduction 183
   - 5.2 Nuclear Shapes 189
   - 5.3 Measurements of Lifetimes 219
6. STATISTICAL ANALYSES 251
   - 6.1 Evaluation of Discrepant Data I 252
   - 6.2 Evaluation of Discrepant Data II 265
7. EVALUATED NUCLEAR STRUCTURE DATA BASE 281
8. BIBLIOGRAPHIC DATABASES in support of NSDD Evaluations 293
9. ENSDF – EVALUATIONS: Methodology and Worked Examples 307
   - 9.1 Decay Data Evaluations 308
   - 9.2 Decay Data Evaluations : Model Exercises 334
   - 9.3 ENSDF – Reaction Data 346
   - 9.4 ENSDF – Adopted Levels and Gammas: Model Exercises 361
10. EVALUATION OF DECAY DATA: Relevant IAEA Co-ordinated Research Projects 371
11. NUCLEAR STRUCTURE AND DECAY DATA: Introduction to relevant web pages 419

WORKSHOP ON NUCLEAR STRUCTURE AND DECAY DATA: THEORY AND EVALUATION

Summary

ICTP Trieste, Italy

17 – 28 November 2003

Prepared by

A.L. Nichols

IAEA Nuclear Data Section

Vienna, Austria

Abstract

Basic aspects of a two-week Workshop on Nuclear Structure and Decay Data: Theory and Evaluation are outlined in this short note for the record. The aims and contents of this workshop are summarized, along with the agenda, list of participants, comments and recommendations. Much was achieved and one aim will be to hold this specific workshop at various time intervals for training purposes (with agreed changes and regular modifications) on the advice of the International Nuclear Data Committee (INDC) and Network of Nuclear Structure and Decay Data Evaluators.

January 2004

1. OBJECTIVES

The International Atomic Energy Agency organised a two-week Workshop on "Nuclear Structure and Decay Data: Theory and Evaluation" at the Abdus Salam International Centre for Theoretical Physics (ICTP) in Trieste from 17 to 28 November 2003. This workshop was conceived and directed by A.L. Nichols (IAEA Nuclear Data Section), J. Tuli (NNDC, Brookhaven National Laboratory, USA) and A. Ventura (ENEA, Bologna, Italy).

The primary objective of the ICTP-hosted workshop was to familiarize nuclear physicists and engineers from both developed and developing countries with

- (i) modern nuclear models;
- (ii) relevant experimental techniques;
- (iii) statistical analyses procedures to derive recommended data sets;
- (iv) evaluation methodologies for nuclear structure and decay data;
- (v) international efforts to produce the Evaluated Nuclear Structure Data File (ENSDF).

Reliable nuclear structure and decay data are important in a wide range of nuclear applications and basic research. Participants were introduced to both the theory and measurement of nuclear structure data, and the use of computer codes to evaluate decay data.

Detailed presentations were given by invited lecturers, along with computer exercises and workshop tasks. Participants were also invited to contribute their own thoughts and papers of direct relevance to the workshop.

2. PROGRAMME

The workshop programme is listed in Section 2.1 of this brief summary, based on a one-week pilot workshop in November 2002 (1) and subsequent debate between the workshop directors.

2.1 Agenda

MONDAY, 17 November 2003

09:00 – 10:30	Registration & Coffee
10:30 – 12:30	Opening Session
	Welcome (Alan Nichols (IAEA) and Jag Tuli (BNL))
	Aims (Jag Tuli)
	NSDD – general features (Jag Tuli)
	IAEA-NDS – NSDD network and recent relevant CRPs (Alan Nichols)
12:30 – 14:00	Lunch
14:00 – 15:30	Introduction
	ICTP computer facilities (ICTP staff/Kevin McLaughlin)
15:30 – 15:45	Coffee break
15:45 – 17:30	Introduction (cont.)
	Web capabilities (Tom Burrows and Alan Nichols)
	Bibliographic databases (Tom Burrows)

TUESDAY, 18 November 2003

09:00 – 10:30	Nuclear theory (Piet Van Isacker)
10:30 – 10:45	Coffee break
10:45 – 12:30	ENSDF format (Jag Tuli)
12:30 – 14:00	Lunch
14:00 – 15:30	ENSDF programs (Tom Burrows)
15:30 – 15:45	Coffee break
15:45 – 17:30	Students' presentations

WEDNESDAY, 19 November 2003

09:00 – 10:30	Nuclear theory (Piet Van Isacker and Ashok Jain)
10:30 – 10:45	Coffee break
10:45 – 12:30	ENSDF - decay (Eddie Browne)
12:30 – 14:00	Lunch
14:00 – 15:30	Model exercise – format (lead by Jag Tuli)
15:30 – 15:45	Coffee break
15:45 – 17:30	Students' presentations

THURSDAY, 20 November 2003

09:00 – 10:30	Nuclear theory (Dario Vretenar)
10:30 – 10:45	Coffee break
10:45 – 12:30	ENSDF - reaction (Coral Baglin)
12:30 – 14:00	Lunch
14:00 – 15:30	Model exercise – decay (lead by Eddie Browne)
15:30 – 15:45	Coffee break
15:45 – 17:30	Students' presentations

FRIDAY, 21 November 2003

09:00 – 10:30	Nuclear theory (Dario Vretenar)
10:30 – 10:45	Coffee break
10:45 – 12:30	Model exercise- reaction (lead by Coral Baglin)
12:30 – 14:00	Lunch
14:00 – 15:30	Theory (Ashok Jain)
15:30 – 15:45	Coffee break
15:45 – 17:30	ENSDF programs (Tom Burrows)

Saturday, 22 November 2003
Sunday, 23 November 2003

MONDAY, 24 November 2003

09:00 – 10:30	ENSDF – evaluation policies (Jag Tuli)
10:30 – 10:45	Coffee break
10:45 – 12:30	ENSDF - adopted levels and gammas (Coral Baglin)
12:30 – 14:00	Lunch

14:00 – 15:30	Model exercise – programs (lead by Tom Burrows)
15:30 – 15:45	Coffee break
15:45 – 17:30	Workshop activities (JT, TB, CB, EB, KMc)

TUESDAY, 25 November 2003

09:00 – 10:30	Model exercise - adopted levels and gammas (Coral Baglin)
10:30 – 10:45	Coffee break
10:45 – 12:30	Workshop activities (JT, TB, CB, EB, KMc)
12:30 – 14:00	Lunch
14:00 – 15:30	Workshop activities (JT, TB, CB, EB, KMc)
15:30 – 15:45	Coffee break (JT, TB, CB, EB, KMc)
15:45 – 17:30	Workshop activities (JT, TB, CB, EB, KMc)

WEDNESDAY, 26 November 2003

09:00 – 10:30	Experimental techniques (Peter von Brentano)
10:30 – 10:45	Coffee break
10:45 – 12:30	Experimental techniques (Peter von Brentano)
12:30 – 14:00	Lunch
14:00 – 15:30	Workshop activities (TB, CB, EB, KMc)
15:30 – 15:45	Coffee break
15:45 – 17:30	Workshop activities (TB, CB, EB, KMc)

THURSDAY, 27 November 2003

09:00 – 10:30	Statistical analyses (Desmond MacMahon)
10:30 – 10:45	Coffee break
10:45 – 12:30	Statistical analyses (Desmond MacMahon)
12:30 – 14:00	Lunch
14:00 – 15:30	Workshop activities (TB, EB, KMc)
15:30 – 15:45	Coffee break
15:45 – 17:30	Workshop activities (TB, EB, KMc)

FRIDAY, 28 November 2003

09:00 – 10:30	Workshop activities (TB, EB, KMc)
10:30 – 10:45	Coffee break
10:45 – 12:30	Review of workshop (Eddie Browne, Tom Burrows and Alan Nichols)
12:30 – 14:00	Lunch

2.2 Participants

Twenty-four participants (predominantly from developing countries) with full or partial support from the IAEA were selected to attend the workshop in November 2003. Selection was undertaken by Nuclear Data Section staff in association with the workshop directors.

<u>First row, sitting from left to right</u>:
Thomas W. BURROWS (USA), Edgardo BROWNE-MORENO (USA), Dario VRETENAR (Croatia), Jagdish K. TULI (USA), Alan NICHOLS (IAEA), Ashok Kumar JAIN (India), Coral M. BAGLIN (USA), Andrea SCHERBAUM (IAEA).

Second row, standing from left to right:
Elsayed M.K. Ahmed ELMAGHRABY (Egypt), Reza NAZARI (Iran), Gopal MUKHERJEE (India), Nagappa M. BADIGER (India), Houshyar NOSHAD (Iran), Suresh Kumar PATRA (India), Kevin MCLAUGHLIN (IAEA), Youssef ABDEL-FATTAH (Egypt), A.K.M. HARUN-AR-RASHID (Bangladesh), Alejandro ALGORA (Hungary), Maitreyee NANDY (India), Mohini GUPTA (India), Sham S. MALIK (India), Guilherme Soares ZAHN (Brazil), Hai NGUYEN (Vietnam), Guillermo V. MARTI (Argentina), Zhimin WANG (China), Young Ae KIM (Korea), Jing QIAN (China), Elena LITVINOVA (Russia), Vitaly PRONSKIKH (Russia).

<u>Unavailable</u>:
Kripamay MAHATA (India), Luc PERROT (France), Prakash Kumar SAHU (India), Renju George THOMAS (India).

LIST OF PARTICIPANTS

Mr. Youssef **ABDEL-FATTAH**
Atomic Energy Authority of Egypt
Egyptian Second Research Reactor-ETRR2
Enshas, Cairo
EGPYT
Tel: +20-2-4691753
Fax: +20-2-4691757
E-mail: afattah@etrr2-aea.org.eg

Mr. Alejandro **ALGORA**
Institute of Nuclear Research
Hungarian Academy of Sciences
Bem ter 18/C
H-4026 Debrecen
HUNGARY
Tel: +36-52-417-266
Fax: +36-52-416-181
E-mail: algora@atomki.hu

Mr. Nagappa Mahadevappa **BADIGER**
Department of Physics
Karnatak University
Dharwad - 580 003
INDIA
Tel: +91-836-747121
Fax: +91-836-747884
E-mail: nagappa123@yahoo.co.in

Mr. Elsayed M.K. Ahmed **ELMAGHRABY**
Nuclear Physics Department
Nuclear Research Center
Atomic Energy Authority
Anshas Location
Cairo 13759
EGYPT
Tel: +20-2-2875924
Fax +20-2-2876031
E-mail: maghraby@techemail.com

Ms. Mohini **GUPTA**
Manipal Academy of Higher Education (MAHE)
University Building
Karnataka, Manipal - 576 119
INDIA
Tel: +91-22-2202-5254
Fax: +91-22-2283-3977
E-mail: nuclear@rolta.net

Mr. A.K.M. **HARUN-AR-RASHID**
Department of Physics
University of Chittagong
Chittagong 4331
BANGLADESH
Tel: +88-31-726311
Fax: +88-31-726310
E-mail: harashid@yahoo.com

Ms. Young Ae **KIM**
Nuclear Data Evaluation Laboratory
Korea Atomic Energy Research Institute
P.O. Box 105
Yuseong-gu, Daejon 305-353
KOREA
Tel: +82-42-868-8795
Fax: +82-42-868-2636
E-mail: ex-psi@kaeri.re.kr

Ms. Elena **LITVINOVA**
State Scientific Center of RF
Institute of Physics and Power Engineering (IPPE)
Bondarenko Sq. 1
249020 Obninsk
RUSSIA
Tel: +7-08439-98207
Fax: +7-08439-68225
E-mail: litva@aport.ru

Mr. Kripamay **MAHATA**
Nuclear Physics Division
Bhabha Atomic Research Centre
Trombay, Mumbai - 400 085
INDIA
Tel: +91-22-25593457
Fax: +91-22-25505151
E-mail: kmahata@magnum.barc.ernet.in

Mr. Sham S. **MALIK**
Physics Department
G.N.D. University
Amritsar - 143 005
INDIA
Tel: +91-183-2258809, Ext. 3475
Fax: +91-183-2258819
E-mail: shammalik@yahoo.com

Mr. Guillermo V. **MARTI**
Dpto. de Física – Lab. TANDAR - CAC
Comisión Nacional de Energía Atómica (CNEA)
Avda. Gral Paz 1499 (1650)
Pdo. de Gral. San Martín
Prov. de Buenos Aires
ARGENTINA
Tel: +54-11-6772-7073
Fax: +54-11-6772-7121
E-mail: marti@tandar.cnea.gov.ar

Mr. Gopal **MUKHERJEE**
Nuclear and Atomic Physics Division
Room No. 368
Saha Institute of Nuclear Physics
1/AF Bidhannagar
Kolkata - 700 064
INDIA
Tel: +91-33-2337-5345, Ext. 368
Fax: +91-33-2337-4637
E-mail: gopal@lotus.saha.ernet.in

Ms. Maitreyee **NANDY**
Saha Institute of Nuclear Physics
1/AF, Bidhannagar
Kolkata - 700 064
INDIA
Tel: +91-33-23375345, Ext. 213
Fax: +91-33-23374637
E-mail: mnandy98@yahoo.com

Mr. Reza **NAZARI**
National Nuclear Safety Department (NNSD)
Atomic Energy Organization of Iran
End of North Karegar Ave.
P.O.Box 14155-1339
Tehran
IRAN
Tel: +98-21-61383653
Fax: +98-21-8009379
E-mail: rnazari@aeoi.org.ir

Mr. Hai **NGUYEN**
Department of Nuclear Physics and Technology
Nuclear Research Institute
1, Nguyen Tu Luc Street
Dalat City
VIETNAM
Tel: +84-63-829436
Fax: +84-63-821107
E-mail: nchai@hcm.vnn.vn.

Mr. Houshyar **NOSHAD**
Center for Theoretical Physics and Mathematics
Atomic Energy Organization of Iran (AEOI)
P.O. Box 14155-1339
Tehran
IRAN
Tel: +9821-61384266
Fax: +9821-8021412
E-mail: hnoshad@aeoi.org.ir

Mr. Suresh Kumar **PATRA**
Institute of Physics
Sachivalaya Marg
Bhubaneswar - 751 005
INDIA
Tel: +91-674-2301058
+91-674-2301083
Fax: +91-674-2300142
E-mail: patra@iopb.res.in

Mr. Luc **PERROT**
SPhN/DAPNIA CEA Saclay
Orme des Merisiers
F-91191 Gif sur Yvette Cedex
FRANCE
Tel: +33-1-69087387 Fax: +33-1-69087584
E-mail: lperrot@cea.fr
*(as of 10 March 2004: 9 rue de Florence,
F-75008 Paris, France; Tel: +33-1-53040330,
E-mail: luc_perrot@yahoo.fr)*

Mr. Vitaly **PRONSKIKH**
Laboratory of High Energies
Joint Institute for Nuclear Research
Jolio-Curie str. 6
141980 Dubna, Moscow Region
RUSSIA
Tel: +7-09621-63941
Fax: +7-09621-65891
E-mail: vitali.pronskikh@jinr.ru

Ms. Jing **QIAN**
China Nuclear Data Center
China Institute of Atomic Energy
P.O. Box 275 (41)
Beijing 102413,
CHINA
Tel: +86-10-69357275
Fax: +86-10-69357008
E-mail: qjcrue@iris.ciae.ac.cn

Mr. Prakash Kumar **SAHU**
Nuclear Physics Division
Bhabha Atomic Research Centre
Trombay, Mumbai – 400 085
INDIA
Tel: +91-22-25592087
Fax: +91-22-25505151
E-mail: pksahu@magnum.barc.ernet.in

Mr. Renju George **THOMAS**
Nuclear Physics Division
Bhabha Atomic Research Centre
Trombay, Mumbai – 400 085
INDIA
Tel: +91-22-25592609
Fax: +91-22-25505151
E-mail: rgthomas@magnum.barc.ernet.in

Mr. Zhimin **WANG**
Department of Nuclear Physics
China Institute of Atomic Energy
P.O. Box 275 (10)
Beijing 102413
CHINA
Tel: +86-10-69357663
Fax: +86-10-69357787
E-mail: wangzm@iris.ciae.ac.cn
*(as of 1 November 2003 for one year: Instituto
Nazionale de Fisica Nucleare Sezione di Padova
(INFN), Padova, Italy)*

Mr. Guilherme Soares **ZAHN**
Research Nuclear Reactor Center (CRPq)
Instituto de Pesquisas Energeticas e Nucleares (IPEN)
P.O. Box 11049 – CEP 05422-970 – Pinheiros
São Paulo SP
BRAZIL
Tel: +55-11-38169181
Fax: +55-11-38169188
E-mail: gzahn@curiango.ipen.br

LIST OF LECTURERS

Ms. Coral M. **BAGLIN**
Nuclear Science Division
Lawrence Berkeley National Laboratory
University of California
1 Cyclotron Road
MS 88R0192
Berkeley, CA 94720
USA
Tel: +1-510-486-6152
Fax: +1-510-486-5757
E-mail: cmbaglin@lbl.gov

Mr. Edgardo **BROWNE-MORENO**
Nuclear Science Division
Lawrence Berkeley National Laboratory
University of California
1 Cyclotron Road
MS 88R0192
Berkeley, CA 94720-8101
USA
Tel: +1-510-486-7647
Fax: +1-510-486-5757
E-mail: ebrowne@lbl.gov

Mr. Thomas W. **BURROWS**
National Nuclear Data Center
Building 197D
Brookhaven National Laboratory
P.O. Box 5000
Upton, NY 11973-5000
USA
Tel: +1 631 344 5084
Fax: +1 631 344 2806
E-mail: burrows@bnl.gov

Mr. Ashok Kumar **JAIN**
Department of Physics
Indian Institute of Technology
Uttaranchal, Roorkee – 247 667
INDIA
Tel: +91-1332-285753
Fax: +91-1332-273560
E-mail: ajainfph@iitr.ernet.in

Mr. Desmond **MACMAHON**
Centre for Acoustics and Ionising Radiation
National Physical Laboratory
Queens Road
Teddington, Middlesex TW11 0LW
UNITED KINGDOM
Tel: +44-20-8943-8573
Fax: +44-20-8943-6161
E-mail: desmond.macmahon@npl.co.uk

Mr. Jagdish K. **TULI** (Director)
National Nuclear Data Center
Building 197D
Brookhaven National Laboratory
P.O. Box 5000
Upton, NY 11973-5000
USA
Tel: +1-631-344-5080
Fax: +1-631-344-2806
E-mail: tuli@bnl.gov

Mr. Piet **VAN ISACKER**
Groupe Physique
Grand Accelerateur National d'Ions Lourds (GANIL)
BP 55027
F-14076 Caen Cedex 5
FRANCE
Tel: +33-2-31 45 45 65
Fax: +33-2-31 45 44 21
E-mail: isacker@ganil.fr

Mr. Peter **VON BRENTANO**
Institut für Kernphysik der Universität Köln
Zülpicher Strasse 77
D-50937 Köln
GERMANY
Tel: +49-221-470-6960
Fax: +49-221-470-5168
E-mail: brentano@ikp.uni-koeln.de

Mr. Dario **VRETENAR**
Department of Physics
Faculty of Science
University of Zagreb
Bijenicka c.32
P.O. Box 162
1000 Zagreb
CROATIA
Tel: +385-1-4680-321
Fax: +385-1-4680-336
E-mail: vretenar@phy.hr

IAEA STAFF

Mr. Alan L. **NICHOLS** (Director)
Nuclear Data Section
International Atomic Energy Agency
Wagramerstrasse 5
A-1400 Vienna
Austria
Tel: +43-1-2600-21709
Fax: +43-1-26007
E-mail: a.nichols@iaea.org

Mr. Kevin **MCLAUGHLIN** (Tutor)
Nuclear Data Section
International Atomic Energy Agency
Wagramerstrasse 5
A-1400 Vienna
Austria
Tel: +43-1-2600-21713
Fax: +43-1-26007
E-mail: p.mclaughlin@iaea.org

Mr. Andrea **SCHERBAUM** (Workshop Secretary)
Nuclear Data Section
International Atomic Energy Agency
Wagramerstrasse 5
A-1400 Vienna
Austria
Tel: +43-1-2600-21710
Fax: +43-1-26007
E-mail: a.scherbaum@iaea.org

3. PRESENTATIONS AVAILABLE IN ELECTRONIC FORM ON CD-ROM

Presentations by Lecturers

Aims of the Workshop - General features of NSDD, J. Tuli

Nuclear Theory:
Nuclear Shell Model, P. Van Isacker
Interacting Boson Model, P. Van Isacker
Geometrical Symmetries in Nuclei – An Introduction, A. Jain
Geometrical Symmetries in Nuclei, A. Jain
Lectures on Geometrical Symmetries in Nuclei, A. Jain
Hartree-Foch-Bogoliubov Method, D. Vretenar
Self-consistent Mean-field Models – Structure of Heavy Nuclei, D. Vretenar

Experimental Nuclear Spectroscopy:
Introduction, P. Von Brentano
Lecture I – Nuclear Shapes, P. Von Brentano
Lecture II – Measurement of Lifetimes, P. Von Brentano

Statistical Analyses:
Evaluation of Discrepant Data I, D. MacMahon
Evaluation of Discrepant Data II, D. MacMahon
Convergence of Techniques for the Evaluation of Discrepant Data: D. MacMahon, A. Pearce, P. Harris
Techniques for Evaluating Discrepant Data, M.U. Rajput, D. MacMahon
Possible Advantages of a Robust Evaluation of Comparisons, J.W. Muller (presented by D. MacMahon)

ENSDF:
Evaluated Nuclear Structure Data Base, J.K. Tuli
Evaluations – A Very Informal History, J.K. Tuli
Evaluated Nuclear Structure Data File – A Manual for Preparation of Data Sets, J.K. Tuli
Guidelines for Evaluators, M.J. Martin, J.K. Tuli
Bibliographic Databases, T.W. Burrows
ENSDF Analysis and Utility Codes, T.W. Burrows:
- Their Descriptions and Uses, T.W. Burrows
- FMTCHK (Format and Syntax Checking), T.W. Burrows
- PowerPoint presentations, T.W. Burrows
- LOGFT (Calculates log *ft* for beta decay), T.W. Burrows
- GTOL (Gamma to Level), T.W. Burrows
- HSICC (Hager-Seltzer Internal Conversion Coefficients), T.W. Burrows

ENSDF – Decay Data, E. Browne
Model Exercises – Decay, E. Browne
ENSDF – Reaction Data, C. Baglin
ENSDF – Adopted Levels and Gammas, C. Baglin
ENSDF – Examples 1, 2, 3, 4 and 5, C. Baglin

Additional Material:
IAEA: NSDD Network, Recent Relevant CRPs and Other Activities (PowerPoint presentation), A.L. Nichols
IAEA: NSDD Network, Recent Relevant CRPs and Other Activities (draft paper), A.L. Nichols
Nuclear Structure and Decay Data: Introduction to Relevant Web Pages (draft paper), T.W. Burrows, P.K. McLaughlin, A.L. Nichols

Presentations by Participants

Study of Isomers in Heavy Nuclei, G. Mukherjee
Optimisation of the Performance of the ETRR-2 Facilities, A. Fattah-Youssef
Target/Projective Structure Dependence in Transfer Reactions, P.K. Sahu
Comparison of Thomas-Fermi and Rotating Finite Range Model Fission Barriers, K. Mahata
Use of Nuclear Reaction Modeling Codes at Low and Intermediate Energies, M. Nandy
Fission of ^{209}Bi and ^{197}Au Nuclei Induced by 30 MeV Protons, H. Noshad
γ-γ Studies of β^- decay ^{193}Os → ^{193}Ir, G. Zahn
Neutron Cross Sections of Er Isotopes, A.K.M. Harun-ar-Rashid
Nuclear Reaction Analysis Using Pre-developed Programs – EMPIRE and Abarax, E. Elmaghraby
ETFFS Calculations of the Low-lying Dipole Strength in Ca Isotopes, E. Litvinova
Bremsstrahlung in the Optical Region, N. Badiger
^{152}Gd Excited States – Preliminary Discussion, V. Pronskikh
Beta-decay Studies Using Total Absorption Spectroscopy, A. Algora
A = 193 Mass Chain Evaluation, G. Marti

4. OTHER WORKSHOP MATERIALS ON CD-ROM

Atomic Masses
Access to ENSDF Codes and Tools
Isotope Explorer
PCNuDat
Access to NSDD Resources

NNDC Online Data Service Manual and Data Citation Guidelines

1.Introduction to International Nuclear Structure and Decay Data Network
Contact names and addresses

Access to ENSDF Format Summary and Examples

Nuclear Structure Manuals

5. RECOMMENDATIONS AND CONCLUSIONS

A number of important points can be made concerning the workshop:

1. Twenty-four participants were selected and attended a two-week workshop that covered nuclear theory and modeling, relevant experimental techniques, statistical analyses, and the philosophy and methodology for comprehensive mass chain evaluations. Support materials and information were also provided on the network of international nuclear structure and decay data evaluators and the most relevant CRPs undertaken through the IAEA Nuclear Data Section.

2. Workshop participants were introduced to mass chain evaluations through group and individual PC/computing activities (50% of agenda of second week) CD-ROM and hardcopy materials were provided by IAEA staff for all students/lecturers.

3. Administrative functions leading up to and during the course of the workshop worked smoothly, including visa arrangements, travel and subsistence payments to students and lecturers, additional banking transactions, and hotel/guest-house accommodation – as an ICTP-hosted workshop many of the administrative details for these functions were organized by IAEA staff.

4. Specific participants were identified for future involvement in NSDD and mass chain evaluations.

5. Lessons were learnt by the IAEA staff involved in this ICTP-hosted event, and much experience was gained in ensuring future success in the organization of such "at-distance" workshops. This particular workshop ran extremely smoothly, and all participants were able to attend (i.e., 100% success with visas). Students were given the opportunity to review the workshop through a written questionnaire and direct discussions (on 28 November). Their major recommendations are as follows:

(a) provide exercises as homework beyond normal workshop hours;
(b) provide sample questions and answers (answers also to be worked out during the course of individual lectures);
(c) increase PC activities within the main body of the workshop, and their introduction much earlier during the first week.
(d) establish stronger links between ENSDF and nuclear theory lectures (i.e., between ENSDF nuclear parameters (and those data used to derive such parameters) and topics to be discussed within nuclear theory).

Combination of Thursday questionnaire and Friday face-to-face review session produced constructive feedback. The overall opinion of all of the students was that they had thoroughly enjoyed the 2-week workshop, made useful new contacts with lecturers, IAEA-NDS staff and other students, and learnt much about nuclear structure and decay data; all of the primary objectives of the workshop were successfully achieved.

REFERENCE

1. PRONYAEV, V.G., NICHOLS, A.L., Summary Report on Workshop on Nuclear Structure and Decay Data Evaluation, 18-22 November 2002, INDC(NDS)-439, January 2003.

Workshop on
Nuclear Structure and Decay Data: Theory and Evaluation

17-28 November 2003

ICTP, Miramare - Trieste, Italy

Introduction

The International Atomic Energy Agency (IAEA, Vienna, Austria) in co-operation with the Abdus Salam International Centre for Theoretical Physics (ICTP, Trieste, Italy) and the Ente per le Nuove Tecnologie, l'Energia e l'Ambiente (ENEA, Bologna, Italy) organized a *"Workshop on Nuclear Structure and Decay Data: Theory and Evaluation"* at the ICTP in Trieste from 17 to 28 November 2003. This workshop was co-directed by Drs. A. Ventura (ENEA, Bologna), A.L. Nichols (IAEA, Vienna) and J.K. Tuli (Brookhaven National Laboratory, USA).

The workshop constituted a unique opportunity for scientists to gain extensive and up-to-date training on the evaluation of nuclear structure and decay data, as developed for the Evaluated Nuclear Structure Data File (ENSDF) and *Nuclear Data Sheets* for the nuclear physics community. Reliable evaluated nuclear structure and decay data are of vital importance in a large number of nuclear applications such as power generation, material analysis, dosimetry and medical diagnostics, as well as basic nuclear physics and astrophysics. Important features of these needs are satisfied by the work undertaken by the international Nuclear Structure and Decay Data Evaluators' Network (NSDD). The main products of this worldwide network are the recommended data files and evaluated decay data.

ENSDF is an enormous source of nuclear data and information for basic research and applications. Both the maintenance and further developments of these files are vitally important, and require continuing scientific effort. While the input to ENSDF from developing countries has been limited in the past, the time has come for scientists from these countries to make a significant contribution to these on-going efforts. The workshop represented the initiation of a suitable mechanism to achieve this aim by focusing on advances in nuclear structure physics and evaluation methodologies through practical training.

Aims

The primary objective of the workshop was to familiarize nuclear physicists from both developing and developed countries with:

(i) new data that characterize the decay properties of nuclei and their nuclear structure;
(ii) nuclear models;
(iii) evaluation methodologies for nuclear structure and decay data.

Participants were introduced to the rigorous criteria adopted to evaluate nuclear structure data, and how these data are entered into ENSDF. Important aspects of the workshop included the use of computer codes to evaluate the nuclear structure and decay data, and the construction of data files for ENSDF. Presentations were given by invited lecturers, along with well-defined exercises involving the use of the relevant computer codes. Participants were also be invited to contribute their own thoughts of direct technical relevance to the workshop.

The workshop programme included coverage of the following topics:
review of modern nuclear models and new data obtained at experimental installations;
ENSDF and related bibliographic databases;
computer codes used for NSDD evaluations;
computer exercises with real NSDD evaluations and preparation of the data sets for inclusion in ENSDF;
network of NSDD evaluators, their products and communication links;
participants' presentations of their own work in NSDD.
Scientists attended from countries that are members of the United Nations, UNESCO or IAEA. Although the main purpose of the ICTP is to help scientists from developing nations through a programme of training activities within a framework of international cooperation, applicants from developed countries were also encouraged to attend.

Workshop manual

Significant quantities of written material were prepared for the workshop. Their accumulation in various forms acted as aid to the participants in their understanding of nuclear theory, measurement techniques, data analysis and ENSDF mass-chain evaluations, representing an important combination of technical information for future reference and other NSDD workshops. Therefore, a relatively large fraction of these presentations, background papers and manuals have been assembled in the form of this document for further use.

Our intention is to use and develop this material in the years to come, particularly for other workshops of this type. Another aim is to ensure that such presentations are not lost, and can be readily at hand for new mass-chain and decay-data evaluators to assist them in their preparation of recommended data for the ENSDF files.

Acknowledgements

I wish to thank my fellow co-directors of the NSDD Workshop for their support leading up to November 2003, and particularly the lecturers (all experts in their fields) for their enthusiasm during the workshop and provision of the various technical input to this document. Administrative aspects of the workshop were considerable leading up to and during the course of November 2003 – as an ICTP-hosted activity, all such features and problems were handled by Ms Andrea Scherbaum (IAEA Nuclear Data Section), and her efforts were much appreciated. Finally, none of the lectures and associated materials would have been delivered without the enthusiastic involvement of all participants at this workshop and an equivalent one-week pilot course in November 2002 (INDC(NDS)-439. January 2003).

A. L. Nichols
Head, Nuclear Data Section
Department of Nuclear Sciences and Applications
International Atomic Energy Agency
Wagramer Strasse 5
A-1400 Vienna
Austria

30 April 2004

Evaluations:
A Very Informal History

J. Tuli

NNDC, BNL

E-mail: tuli@bnl.gov

Nuclear Structure and Decay Data Evaluations - an informal history

Jagdish K. Tuli

National Nuclear Data Center,

Brookhaven National Laboratory, USA

E-mail: tuli@bnl.gov

BROOKHAVEN NATIONAL LABORATORY

Informal Evaluation History

Webster's Dictionary defines "to compile" as

"to put together, in a new form, out of materials already existing"

In scientific fields: to compact and serve as a convenient source of detailed information - a good "compilation" always involves "evaluation"

BROOKHAVEN NATIONAL LABORATORY

Informal Evaluation History – cont.

First compilation of known nuclides was published by Giorgio Fea in 1935:

Tabelle Riassunitive E Bibliografia delle Transmutazioni Artificiali,

Nuovo Cimento 6, 1 (1935)

BROOKHAVEN NATIONAL LABORATORY

Informal Evaluation History – cont.

First evaluation as "Table of Isotopes" published by J.J. Livingwood and G. T. Seaborg,

Rev Mod Phys 12, 30 (1940)

Evaluation limited to artificially produced nuclear species – immediate use in identification and radiotracers

BROOKHAVEN NATIONAL LABORATORY

Informal Evaluation History – cont.

Subsequent editions of "Table of Isotopes" included all nuclear species:

- G.T. Seaborg, Rev Mod Physics 16, 1 (1944)
- G.T. Seaborg, I. Perlman, *ibid*., 20, 585 (1948)
- J. M. Hollander, I. Perlman and G. T. Seaborg, *ibid*., 25, 469 (1953)
- D. Strominger, J.M. Hollander and G.T. Seaborg, *ibid.,* 30, 585 (1958)

BROOKHAVEN
NATIONAL LABORATORY

Informal Evaluation History – cont.

Subsequent editions of "Table of Isotopes" published by John Wiley:

6th Edition: C. M. Lederer, J. M. Hollander and I. Perlman

7th Edition: C. M. Lederer, V. S. Shirley, Editors; E. Browne, J.M. Dairiki, R.E. Doebler, Principal Authors; A.A. Shihab-Eldin, L.J. Jardine, J.K. Tuli, A.B. Buyrn, Authors

BROOKHAVEN
NATIONAL LABORATORY

Informal Evaluation History – cont.

8^{th} (and last) edition of “Table of Isotopes” was also published by John Wiley in two volumes, ~ 3000 pages + CD ROM:

R.B. Firestone, V.S. Shirley, Editor
C.M. Baglin, S.Y. Chu, J. Zipkin, Assistant Editors

Unlike previous editions, 8^{th} edition is derived, and not an independent evaluation

BROOKHAVEN NATIONAL LABORATORY

Informal Evaluation History – cont.

An Editor of “Table of Isotopes” observed in 1941

“The rate at which radioactivities are discovered may be reduced very considerably and the table would itself become stable.”

That clearly did not happen!

BROOKHAVEN NATIONAL LABORATORY

Informal Evaluation History – cont.

There were other parallel evaluation efforts
Some of these were:

T. Lauritsen (and later F. Ajzenberg-Selove) (1948-on)

B.S. Dzhelepov (and later with L. Peker and others) in USSR (1950-on)

P. M. Endt (and later with C. van der Leun)
(1954 – on)

Informal Evaluation History – cont.

Wall Chart

Emilio Segre (as part of Enrico Fermi's group) introduced first chart, with Z along the x-axis and N along the Y axis.

Segre's chart was published in 5/1945 as Los Alamos report with classified data omitted!

1948: G. Friedlander and M. Perlman (GE Research Lab) created the first GE chart with Z and N reversed. Sixteen editions have since been published by Knolls Atomic Power Lab

Informal Evaluation History – cont.

Nuclear Data Sheets

Katherine Way as part of Manhattan Project working at Clinton Lab (later renamed ORNL) began collecting nuclear data.

1948: Way headed the Nuclear Data Project at US National Bureau of Standards (later renamed US National Institute of Standards and Technology)

Informal Evaluation History – cont.

"Nuclear Data" report was published in 1950.

Data included measured values with references of isotopic abundances, methods of production, n cross sections, half-lives, decay modes, energies and intensities of radiations, conversion coefficients, and some reaction data and decay schemes. No recommended values or uncertainties were given.

Informal Evaluation History – cont.

1953: Nuclear Data Project moved under the control of the US National Academy of Sciences-National Research Council in Washington, DC

Published data (AEC reports) now also included coincidence, mass assignments, n,p separation energies, total disintegration energies, spins, magnetic and electric moments. Uncertainties were given with a single decay scheme for all isobars and given A.

Data were in form of loose leaf pages called "NUCLEAR DATA SHEETS"

BROOKHAVEN NATIONAL LABORATORY

Informal Evaluation History – cont.

1964: Nuclear Data Project under the leadership of Katherine Way moved back to Oak Ridge National Lab, where her effort had originally started in 1948.

Nuclear Data Sheets were once again to be published in book form by Academic Press, rather than as single sheets of data.

BROOKHAVEN NATIONAL LABORATORY

Informal Evaluation History – cont.

Nuclear Data Sheets

February 1966: Nuclear Data Sheets started as section B of the journal Nuclear Data, and later as simply Nuclear Data Sheets published by Academic Press

December 1965: Section A of Nuclear Data was started as Atomic Data Tables.

August 1973: Two journals (Atomic Data and Atomic Data A) merged as Atomic and Nuclear Data Tables, with K. Way as Editor

Informal Evaluation History – cont.

Evaluations limited to NDP-ORNL effort

Time lag in evaluations (1970-71)

Employment situation was not good for Ph.D.students

NSF/NAS joined forces to ensure that evaluations became more current:

- created three-year NIRA program
- recruited two sets of 12 young Ph.Ds for two-year terms
- some stayed in the evaluation business at the end of the program (1971-74)

Informal Evaluation History – cont.

- Hand-written data sheets. Draftsman were drawing the decay schemes
- Bruce Ewbank at ORNL was instrumental in computerization of recent references (NSR)
- Computerization of various drawings
- Common input format for tables and drawing
- Evaluated Nuclear Structure Data File

BROOKHAVEN NATIONAL LABORATORY

Informal Evaluation History – cont.

- Subsequent to the completion of NIRA program, proposed in 1975 that the evaluation activity be decentralized with international involvement under the auspice of IAEA, Nuclear Data Section.
- Evaluation responsibility was divided amongst various data centers within and outside the US.
- NNDC at BNL coordinated the national and international effort for US/DOE.
- Lead role in editing and processing evaluations continued at NDP/ORNL.

BROOKHAVEN NATIONAL LABORATORY

Informal Evaluation History - cont

1980: change of production responsibility to NNDC, when ORNL management support for the activity declined.

1981: NNDC became responsible for production of Nuclear Data Sheets and computerized the process. Photo-ready copy of the journal has since been supplied to the publisher.

BROOKHAVEN NATIONAL LABORATORY

Informal Evaluation History – cont.

ORNL and NNDC edited the journal jointly until June 1998 when Murray Martin retired (started evaluation work with Katherine Way and served as the Editor-in-Chief of the journal while working at the Nuclear Data Project, ORNL).

With Murray's retirement the editing responsibility shifted completely to the National Nuclear Data Center, BNL.

BROOKHAVEN NATIONAL LABORATORY

Nuclear Structure and Decay Data Network

J. K. Tuli
National Nuclear Data Center
Brookhaven National Laboratory
Upton, NY 11973
USA

BROOKHAVEN NATIONAL LABORATORY

Nuclear Structure and Decay Data Network

US Network (~ 6 FTE)

BNL
INEEL
LBNL
McMaster, Canada
ORNL
TUNL

BROOKHAVEN NATIONAL LABORATORY

Nuclear Structure and Decay Data Network

Non-US Contributors

Belgium
Canada
China
France
Japan
Kuwait
Russia
Sweden

Nuclear Structure and Decay Data Network

WHAT DO WE DO?

Primary mission:

Evaluate (or compile) structure and decay data, A = 1-293, for inclusion in ENSDF (or XUNDL) database.

Other responsibilities:

- Maintenance of checking and evaluation software
- Peer review of evaluations
- Dissemination of data

Nuclear Structure and Decay Data Network

OUR PRINCIPAL DATABASES

Web accessible from NNDC or mirror sites; http://www.nndc.bnl.gov links you to them

- **NSR** - Nuclear Science References
- **ENSDF** - Evaluated Nuclear Structure Data File
- **XUNDL** - Unevaluated data compiled from recently published literature

BROOKHAVEN NATIONAL LABORATORY

Nuclear Theory:
The Nuclear Shell Model

P. Van Isacker

GANIL, France

E.mail: isaker@ganil.fr

Nuclear Shell Model

Context and assumptions of the model

Symmetries of the shell model:

Racah's SU(2) pairing model

Wigner's SU(4) symmetry

Elliott's SU(3) model of rotation

Overview of nuclear models

- *Ab initio* methods: description of nuclei starting from the bare nn and nnn interactions
- Nuclear shell model: nuclear average potential + (residual) interaction between nucleons
- Mean-field methods: nuclear average potential with global parametrization (+ correlations)
- Phenomenological models: specific nuclei or properties with local parametrization

Ab initio methods

- Faddeev-Yakubovsky: A ≤ 4
- Coupled-rearrangement-channel Gaussian-basis variational: A ≤ 4 (higher with clusters)
- Stochastic variational: A ≤ 7
- Hyperspherical harmonic variational: A ≤ 4
- Green's function Monte Carlo: A ≤ 7
- No-core shell model: A ≤ 12
- Effective interaction hyperspherical: A ≤ 6

Benchmark calculation for *A* = *4*

- Test calculation with realistic interaction: all methods agree

$$\langle \Psi | \sum_{k<l}^{4} \delta(r - r_{kl}) | \Psi \rangle$$

Method	$\langle T \rangle$	$\langle V \rangle$	E_b	$\sqrt{\langle r^2 \rangle}$
FY	102.39(5)	−128.33(10)	−25.94(5)	1.485(3)
CRCGV	102.30	−128.20	−25.90	1.482
SVM	102.35	−128.27	−25.92	1.486
HH	102.44	−128.34	−25.90(1)	1.483
GFMC	102.3(1.0)	−128.25(1.0)	−25.93(2)	1.490(5)
NCSM	103.35	−129.45	−25.80(20)	1.485
EIHH	100.8(9)	−126.7(9)	−25.944(10)	1.486

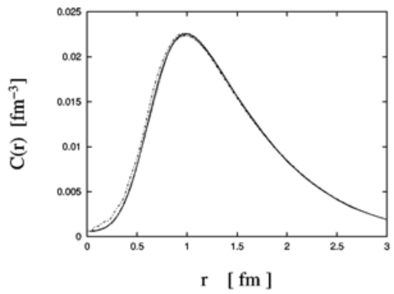

But E_{expt} = -28.296 MeV ⇒ need for three-nucleon interaction

• Basic symmetries

- Non-relativistic Schrödinger equation:

$$H=\sum_{k=1}^{A}\frac{p_k^2}{2m_k}+\sum_{k<l}^{A}W_2(\xi_k,\xi_l)+\sum_{k<l<m}^{A}W_3(\xi_k,\xi_l,\xi_m)+\cdots$$
$$\left[\xi_k\equiv\{\vec{r}_k,\vec{\sigma}_k,\vec{\tau}_k\},\vec{p}_k=-i\hbar\vec{\nabla}_k\right]$$

- Symmetry or invariance under:

— translations ⇒ linear momentum ***P***

— rotations ⇒ angular momentum ***J***=***L***+***S***

— space reflection ⇒ parity π

— time reversal

Nuclear shell model

- Separation in mean field + residual interaction:

$$H=\sum_{k=1}^{A}\frac{p_k^2}{2m_k}+\sum_{k<l}^{A}W(\xi_k,\xi_l)$$
$$=\underbrace{\sum_{k=1}^{A}\left[\frac{p_k^2}{2m_k}+V(\xi_k)\right]}_{\text{mean field}}+\underbrace{\left[\sum_{k<l}^{A}W(\xi_k,\xi_l)-\sum_{k=1}^{A}V(\xi_k)\right]}_{\text{residualinteraction}}$$

- Independent-particle assumption - choose V and neglect residual interaction:

$$H\approx H_{\mathrm{IP}}=\sum_{k=1}^{A}\left[\frac{p_k^2}{2m_k}+V(\xi_k)\right]$$

Independent-particle shell model

- Solution for one particle:

$$\left[\frac{p_k^2}{2m_k}+V(\xi_k)\right]\phi_i(k)=E_i\phi_i(k) \qquad [\phi_i(k)\equiv\phi_i(\vec{r}_k,\vec{\sigma}_k,\vec{\tau}_k)]$$

- Solution for many particles:

$$\Phi_{i_1 i_2\ldots i_A}(1,2,\ldots,A)=\prod_{k=1}^{A}\phi_{i_k}(k)$$

$$H_{\mathrm{IP}}\Phi_{i_1 i_2\ldots i_A}(1,2,\ldots,A)=\left(\sum_{k=1}^{A}E_{i_k}\right)\Phi_{i_1 i_2\ldots i_A}(1,2,\ldots,A)$$

Independent-particle shell model

- Antisymmetric solution for many particles (Slater determinant):

$$\Psi_{i_1 i_2\ldots i_A}(1,2,\ldots,A)=\frac{1}{\sqrt{A!}}\begin{vmatrix}\phi_{i_1}(1) & \phi_{i_1}(2) & \ldots & \phi_{i_1}(A)\\ \phi_{i_2}(1) & \phi_{i_2}(2) & \ldots & \phi_{i_2}(A)\\ \vdots & \vdots & \ddots & \vdots\\ \phi_{i_A}(1) & \phi_{i_A}(2) & \ldots & \phi_{i_A}(A)\end{vmatrix}$$

- Example for $A=2$ particles:

$$\Psi_{i_1 i_2}(1,2)=\frac{1}{\sqrt{2}}\left[\phi_{i_1}(1)\phi_{i_2}(2)-\phi_{i_1}(2)\phi_{i_2}(1)\right]$$

Hartree-Fock approximation

- Vary ϕ_i (*i.e., V*) to minize the expectation value of H in a Slater determinant:

$$\delta \frac{\int \Psi^*_{i_1 i_2 \ldots i_A}(1,2,\ldots,A) H \Psi_{i_1 i_2 \ldots i_A}(1,2,\ldots,A) d\xi_1 d\xi_2 \ldots d\xi_A}{\int \Psi^*_{i_1 i_2 \ldots i_A}(1,2,\ldots,A) \Psi_{i_1 i_2 \ldots i_A}(1,2,\ldots,A) d\xi_1 d\xi_2 \ldots d\xi_A} = 0$$

- Application requires choice of H - many global parametrizations (Skyrme, Gogny…) have been developed

Poor man's Hartree-Fock

- Choose a simple, analytically solvable V that approximates the microscopic HF potential:

$$H_{\mathrm{IP}} = \sum_{k=1}^{A} \left[\frac{p_k^2}{2m} + \frac{1}{2} m\omega^2 r_k^2 - \zeta_{\mathrm{ls}} \vec{l}_k \cdot \vec{s}_k - \zeta_{\mathrm{ll}} l_k^2 \right]$$

- Contains
  - — Harmonic oscillator potential with constant ω
  - — Spin-orbit term with strength $\zeta_{\mathbf{ls}}$
  - — Orbit-orbit term with strength $\zeta_{\mathbf{ll}}$
  - — Adjust ω, $\zeta_{\mathbf{ls}}$ and $\zeta_{\mathbf{ll}}$ to best reproduce HF

Energy levels of harmonic oscillator

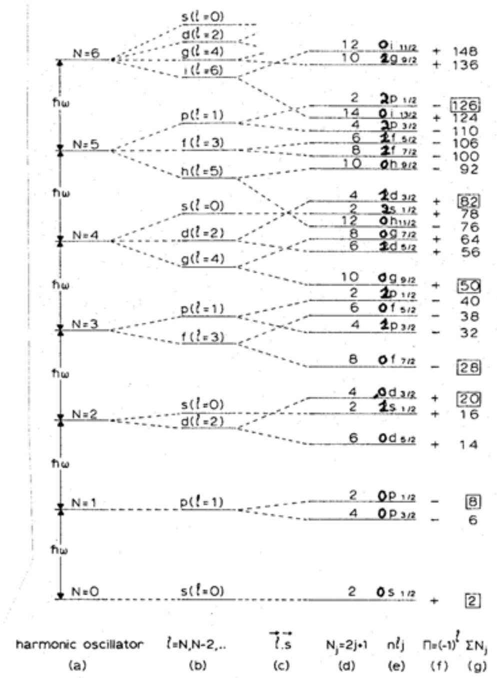

Typical parameter values:

$\hbar\omega \approx 41A^{-1/3}\text{MeV}$

$\zeta_{ls}\hbar^2 \approx 20A^{-2/3}\text{MeV}$

$\zeta_{ll}\hbar^2 \approx 0.1\text{MeV}$

$\therefore b \approx 1.0A^{1/6}\text{fm}$

'Magic' numbers at 2, 8, 20, 28, 50, 82, 126, 184,…

Evidence for shell structure

- Evidence for nuclear shell structure from
  - Excitation energies in even-even nuclei
  - Nucleon-separation energies
  - Nuclear masses
  - Nuclear level densities
  - Reaction cross sections
- Is nuclear shell structure modified away from the line of stability?

Shell structure from $E_x(2_1)$

High $E_x(2_1)$ indicates stable shell structure:

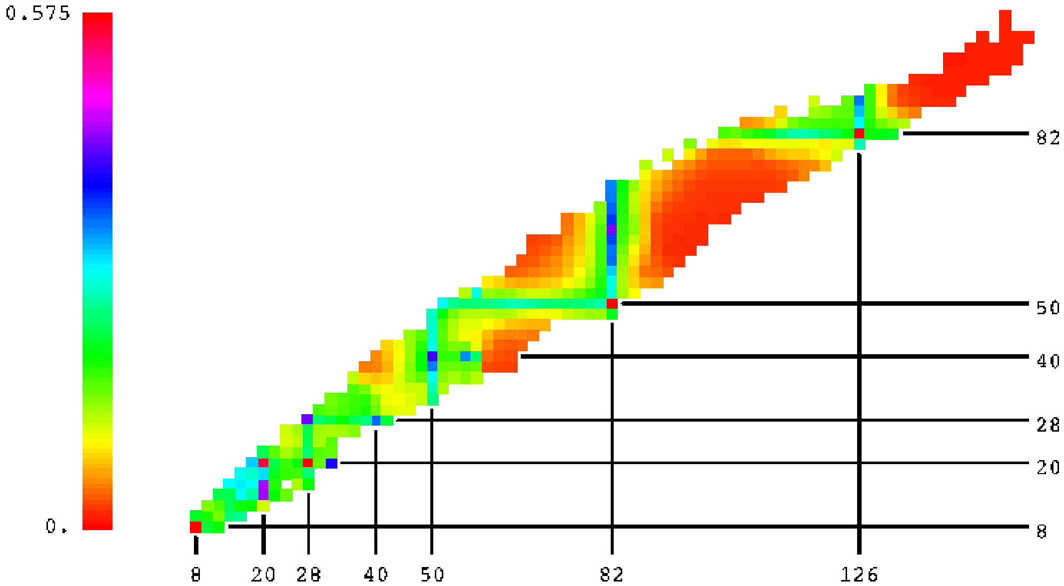

Shell structure from S_n or S_p

- Change in slope of S_n (S_p) indicates neutron (proton) shell closure (constant N-Z plots):

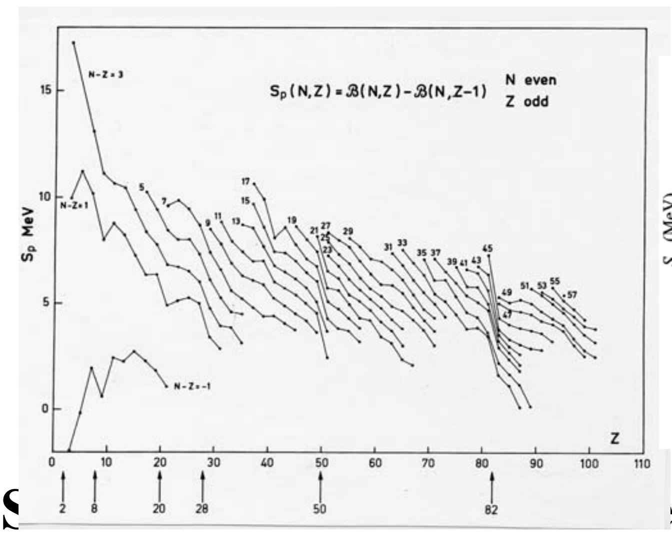

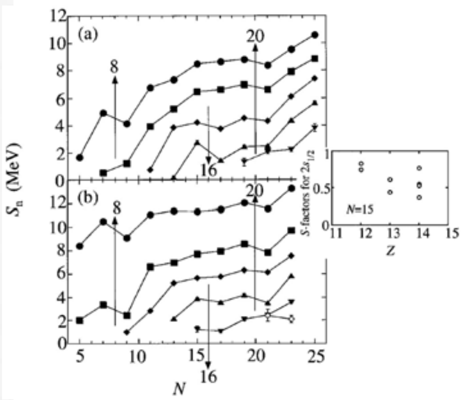

Shell structure from masses

- Deviations from Weizsäcker mass formula:

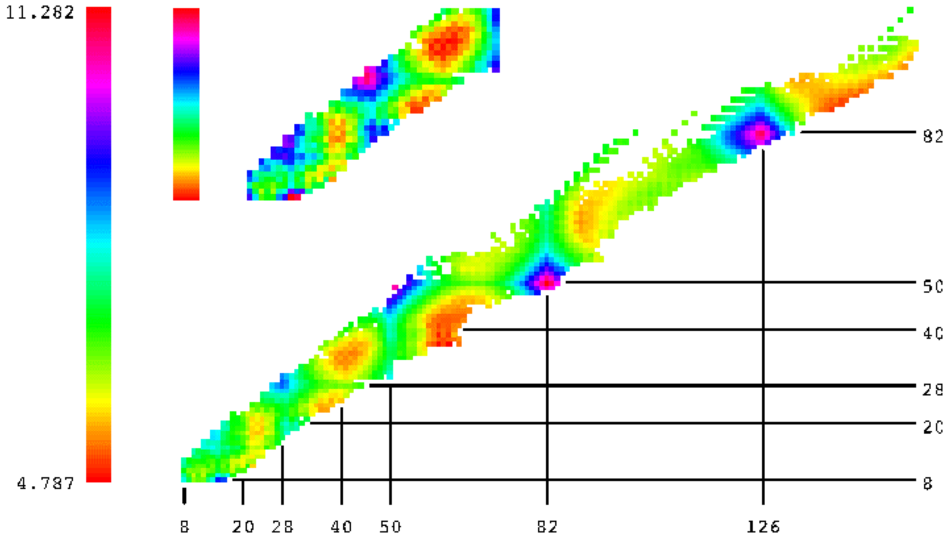

Shell structure from masses

- Deviations from improved Weizsäcker mass formula that includes $n_\nu n_\pi$ and $n_\nu + n_\pi$ terms:

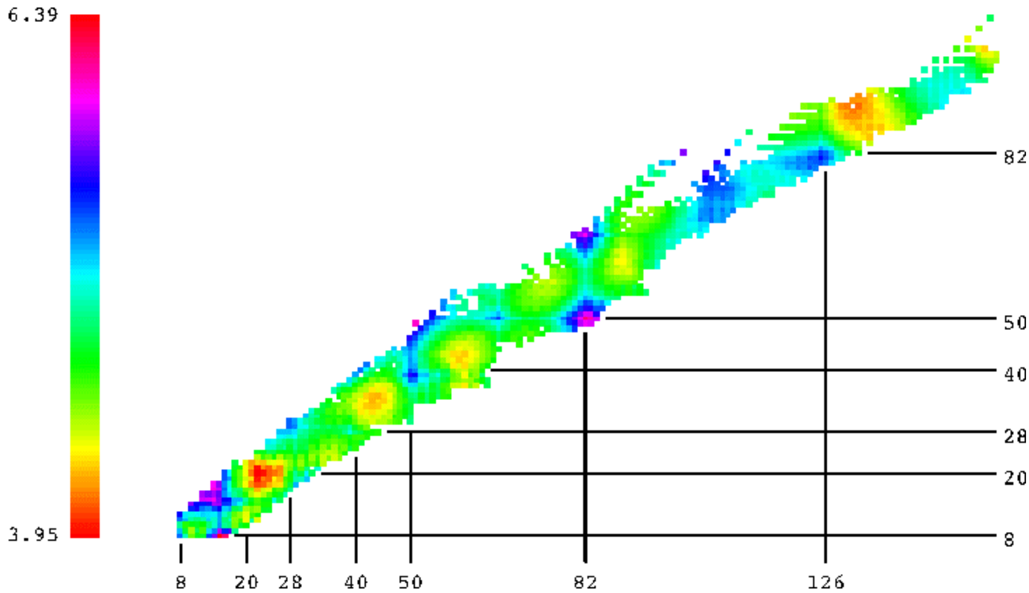

Validity of SM wave functions

- Example: Elastic electron scattering on ^{206}Pb and ^{205}Tl, differing by a 3s proton

- Measured ratio agrees with shell-model prediction for 3s orbit with modified occupation

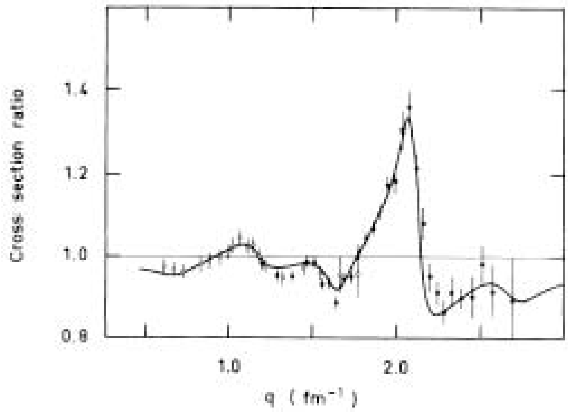

Nuclear shell model

- The full shell-model Hamiltonian:

$$H = \sum_{k=1}^{A} \left[\frac{p_k^2}{2m} + V(\xi_k) \right] + \sum_{k<l}^{A} V_{\mathrm{RI}}(\xi_k, \xi_l)$$

- Valence nucleons: neutrons or protons that are in excess of the last, completely filled shell

- Usual approximation: consider the residual interaction V_{RI} among valence nucleons only

- Sometimes include selected core excitations ('intruder' states)

The shell-model problem

- Solve the eigenvalue problem associated with the matrix (n active nucleons):

$$\left\langle i_1' \ldots i_n' \left| \sum_{k<l}^{n} V_{\mathrm{RI}}(\xi_k,\xi_l) \right| i_1 \ldots i_n \right\rangle \qquad \left[\left\langle 1 \ldots n \middle| i_1 \ldots i_n \right\rangle \equiv \Psi_{i_1 \ldots i_n}(1 \ldots n)\right]$$

- Methods of solution:

— Diagonalization (Strasbourg-Madrid): 10^9

— Monte-Carlo (Pasadena-Oak Ridge):

— Quantum Monte-Carlo (Tokyo):

— Group renormalization (Madrid-Newark): 10^{120}

Residual shell-model interaction

- Four approaches:

— Effective: derive from free nn interaction taking account of the nuclear medium

— Empirical: adjust matrix elements of residual interaction to data; examples: p, sd and pf shells

— Effective-empirical: effective interaction with some adjusted (monopole) matrix elements

— Schematic: assume a simple spatial form and calculate its matrix elements in a harmonic-oscillator basis; example: δ interaction

Schematic short-range interaction

- Delta interaction in harmonic-oscillator basis.
- Example of ^{42}Sc$_{21}$ (1 active neutron + 1 active proton):

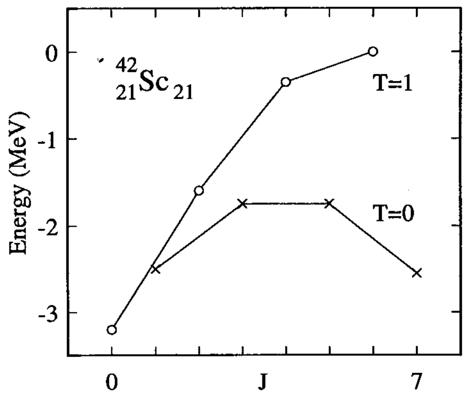

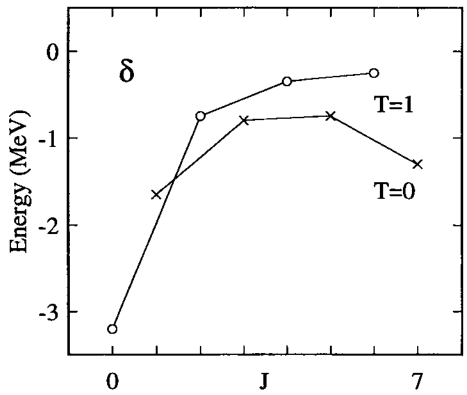

Symmetries of the shell model

- Three bench-mark solutions:

— no residual interaction ⇒ IP shell model

— pairing (in *jj* coupling) ⇒ **Racah**'s SU(2)

— quadrupole (in *LS* coupling) ⇒ **Elliott**'s SU(3)

- Symmetry triangle:

$$H_{\mathrm{IP}} = \sum_{k=1}^{A}\left[\frac{p_k^2}{2m} + \frac{1}{2}m\omega^2 r_k^2 - \zeta_{\mathrm{ls}}\vec{l}_k\cdot\vec{s}_k - \zeta_{\mathrm{ll}}l_k^2\right]$$
$$+\sum_{k<l}^{A}V_{\mathrm{RI}}(\xi_k,\xi_l)$$

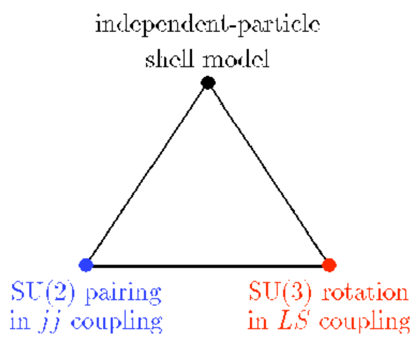

Racah's SU(2) pairing model

- Assume large spin-orbit splitting ζ_{ls} which implies a jj coupling scheme

- Assume pairing interaction in a single-j shell:

$$\left\langle j^2 JM_J \middle| V_{\mathrm{pairing}} \middle| j^2 JM_J \right\rangle = \begin{cases} -\frac{1}{2}(2j+1)g, & J=0 \\ 0, & J\neq 0 \end{cases}$$

- Spectrum of ^{210}Pb:

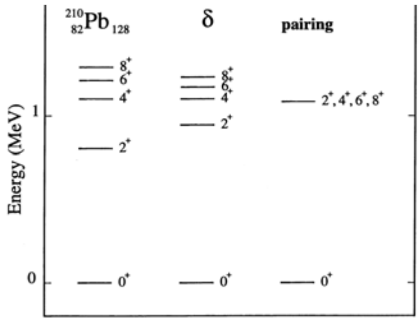

Solution of pairing Hamiltonian

- Analytic solution of pairing hamiltonian for identical nucleons in a single-j shell:

$$\left\langle j^n \upsilon J \middle| \sum_{k<l}^{n} V_{\mathrm{pairing}}(\xi_k, \xi_l) \middle| j^n \upsilon J \right\rangle = -\frac{1}{4} G(n-\upsilon)(2j-n-\upsilon+3)$$

- Seniority υ (number of nucleons not in pairs coupled to $J=0$) is a good quantum number

- Correlated ground-state solution (*cf.* super-fluidity in solid-state physics)

Pairing and superfluidity

- Ground states of a pairing Hamiltonian have *superfluid* character:

  — even-even nucleus (υ=*0*): $\left(S_+\right)^{n_j/2}|o\rangle$

  — odd-mass nucleus (υ=*1*): $a_j^+\left(S_+\right)^{n_j/2}|o\rangle$

- Nuclear superfluidity leads to

  — constant energy of first 2^+ in even-even nuclei

  — odd-even staggering in masses

  — two-particle (2n or 2p) transfer enhancement

Superfluidity in semi-magic nuclei

- Even-even nuclei:

  — ground state has υ=*0*.

  — first-excited state has υ=*2*.

  — pairing produces constant energy gap:

$$E_x\left(2_1^+\right)=\tfrac{1}{2}\left(2j+1\right)g$$

- Example of Sn nuclei:

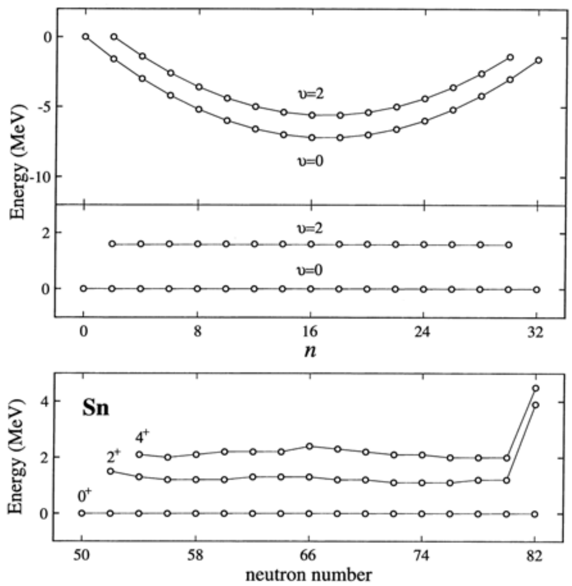

Two-nucleon separation energies

- Two-nucleon separation energies S_{2n}:

  (a) shell splitting dominates over interaction

  (b) interaction dominates over shell splitting

  (c) S_{2n} in tin isotopes

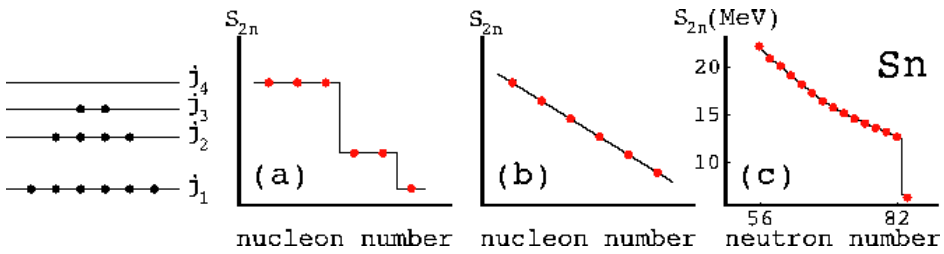

Generalized pairing models

- Trivial generalization from a single-j shell to several degenerate j shells:

$$S_+ \propto \frac{1}{2}\sum_j \sqrt{2j+1}\left(a_j^+ \times a_j^+\right)_0^{(0)}$$

- Pairing with neutrons and protons:

  — $T=1$ pairing: SO(5).

  — $T=0$ and $T=1$ pairing: SO(8)

- Non-degenerate shells:

  — Talmi's generalized seniority

  — Richardson's integrable pairing model

Pairing with neutrons and protons

- For neutrons and protons *two* pairs, and hence *two* pairing interactions are possible:

— Isoscalar ($S=1,T=0$):

$$-S_+^{10}\cdot S_-^{10},\quad S_+^{10}=\sqrt{l+\tfrac{1}{2}}\left(a^+_{l\frac{1}{2}\frac{1}{2}}\times a^+_{l\frac{1}{2}\frac{1}{2}}\right)^{(010)},\quad S_-^{10}=\left(S_+^{10}\right)^+$$

— Isovector ($S=0,T=1$):

$$-S_+^{01}\cdot S_-^{01},\quad S_+^{01}=\sqrt{l+\tfrac{1}{2}}\left(a^+_{l\frac{1}{2}\frac{1}{2}}\times a^+_{l\frac{1}{2}\frac{1}{2}}\right)^{(001)},\quad S_-^{01}=\left(S_+^{01}\right)^+$$

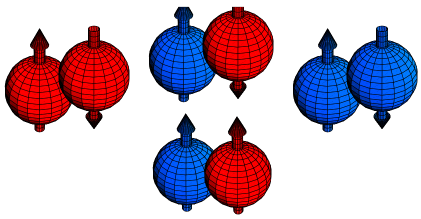

Superfluidity of *N*=*Z* nuclei

- Ground state of a $T=1$ pairing Hamiltonian for identical nucleons is superfluid, $(S_+)^{n/2}|\mathrm{o}\rangle$
- Ground state of a $T=0$ and $T=1$ pairing Hamiltonian with equal number of neutrons and protons has *different* superfluid character:

$$\left(\cos\theta\, S_+^{10}\cdot S_+^{10}-\sin\theta\, S_+^{01}\cdot S_+^{01}\right)^{n/4}|\mathrm{o}\rangle$$

- $\Rightarrow$ Condensate of α s (θ depends on g_0/g_1)
- Observations:

— isoscalar component in condensate survives only in $N\sim Z$ nuclei, if anywhere at all

— spin-orbit term *reduces* isoscalar component

Wigner's SU(4) symmetry

- Assume the nuclear Hamiltonian is invariant under spin *and* isospin rotations:

$$\left[H_{\text{nucl}}, S_\mu\right] = \left[H_{\text{nucl}}, T_\nu\right] = \left[H_{\text{nucl}}, Y_{\mu\nu}\right] = 0$$

$$S_\mu = \sum_{k=1}^{A} s_\mu(k), \quad T_\nu = \sum_{k=1}^{A} t_\nu(k), \quad Y_{\mu\nu} = \sum_{k=1}^{A} s_\mu(k) t_\nu(k)$$

- Since $\{S_\mu, T_\nu, Y_{\mu\nu}\}$ form an SU(4) algebra:

— H_{nucl} has SU(4) symmetry

— total spin ***S***, total orbital angular momentum ***L***, total isospin ***T*** and SU(4) labels ($\lambda\mu\nu$) are conserved quantum numbers

Physical origin of SU(4) symmetry

- SU(4) labels specify the separate spatial and spin-isospin symmetry of the wavefunction:

particle number	spatial symmetry	L	spin–isospin symmetry	$(\lambda\mu\nu)$	(S,T)
2	$\square\square$ (S)	$0^2, 2^2, 4$	$\begin{smallmatrix}\square\\\square\end{smallmatrix}$ (A)	(010)	(0,1) (1,0)
	$\begin{smallmatrix}\square\\\square\end{smallmatrix}$ (A)	$1, 2, 3$	$\square\square$ (S)	(200)	(0,0) (1,1)

- Nuclear interaction is short-range attractive and hence *favours maximal spatial symmetry*

Breaking of SU(4) symmetry

- Breaking of SU(4) symmetry as a consequence of
  - — spin-orbit term in nuclear mean field
  - — coulomb interaction
  - — spin-dependence of residual interaction
- Evidence for SU(4) symmetry breaking from
  - — masses: rough estimate of nuclear BE from

$$B(N,Z) \propto a + bg(\lambda\mu\nu) = a + b\langle \lambda\mu\nu | C_2[\mathrm{SU}(4)] \lambda\mu\nu \rangle$$

  - — β decay: Gamow-Teller operator $Y_{\mu,\pm 1}$ is a generator of SU(4) $\Rightarrow$ selection rule in $(\lambda\mu\nu)$

SU(4) breaking from masses

- Double binding energy difference δV_{np}

$$\delta V_{\mathrm{np}}(N,Z) = \tfrac{1}{4}\left[B(N,Z) - B(N-2,Z) - B(N,Z-2) + B(N-2,Z-2)\right]$$

- δV_{np} in *sd*-shell nuclei:

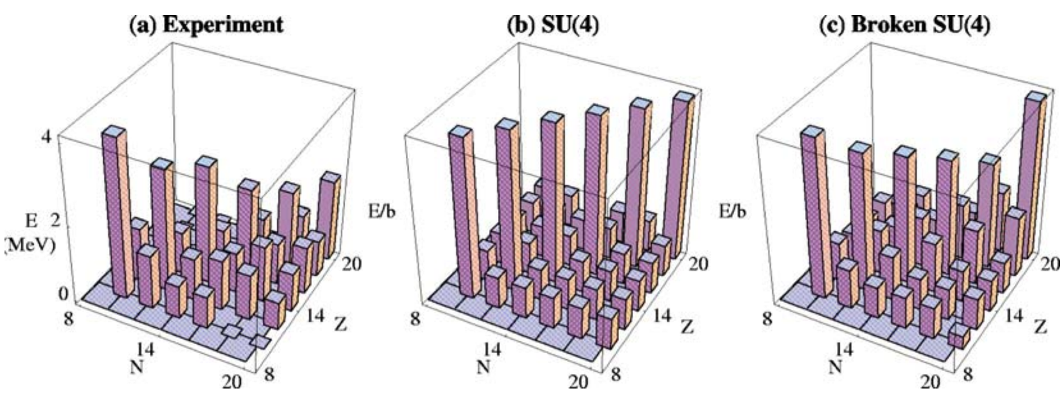

SU(4) breaking from β decay

- Gamow-Teller decay into odd-odd or even-even N=Z nuclei:

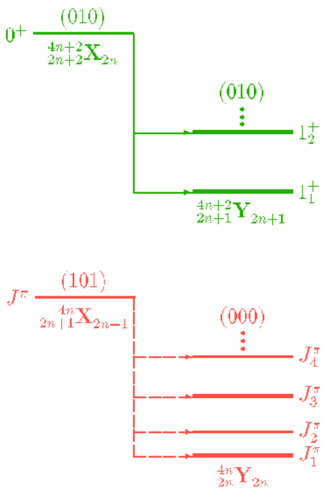

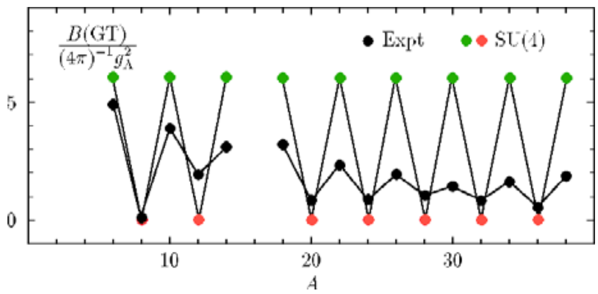

Elliott’s SU(3) model of rotation

- Harmonic oscillator mean field (*no* spin-orbit) with residual interaction of quadrupole type:

$$H = \sum_{k=1}^{A}\left[\frac{p_k^2}{2m} + \frac{1}{2}m\omega^2 r_k^2\right] - \kappa Q\cdot Q,$$

$$Q_\mu = \sqrt{\frac{4\pi}{5}}\left(\sum_{k=1}^{A} r_k^2 Y_{2\mu}(\hat{r}_k) + \sum_{k=1}^{A} p_k^2 Y_{2\mu}(\hat{p}_k)\right)$$

Importance and limitations of SU(3)

- Historical importance:

  — bridge between the spherical shell model and the liquid droplet model through mixing of orbits

  — spectrum generating algebra of Wigner's SU(4) supermultiplet

- Limitations:

  — *LS* (Russell-Saunders) coupling, *not jj* coupling (zero spin-orbit splitting) $\Rightarrow$ beginning of *sd* shell

  — Q is the *algebraic* quadrupole operator $\Rightarrow$ no major-shell mixing

Generalized SU(3) models

- How to obtain rotational features in a *jj*-coupling limit of the nuclear shell model?

- Several efforts since Elliott:

  — pseudo-spin symmetry

  — quasi-SU(3) symmetry (Zuker)

  — effective symmetries (Rowe)

  — FDSM: fermion dynamical symmetry model

  — etc.

Nuclear Theory:
The Interacting Boson Model

P. Van Isacker

GANIL, France

E-mail: isaker@ganil.fr

The interacting boson model (IBM)

Dynamical symmetries of the IBM

Neutrons, protons and F-spin (IBM-2)

$T=0$ and $T=1$ bosons: IBM-3 and IBM-4

Overview of collective models

- Pure collective models:
  - (rigid) rotor model
  - (harmonic quadrupole) vibrator model
  - liquid-drop model of vibrations and rotations
  - interacting boson model
- With inclusion of particle degrees of freedom:
  - Nilsson model
  - particle-core coupling model
  - interacting boson-fermion model

Rigid rotor model

- Hamiltonian of quantum mechanical rotor in terms of 'rotational' angular momentum ***R***:

$$\hat{H}_{\text{rot}} = \frac{\hbar^2}{2}\left[\frac{R_1^2}{\Im_1} + \frac{R_2^2}{\Im_2} + \frac{R_3^2}{\Im_3}\right] = \frac{\hbar^2}{2}\sum_{i=1}^{3}\frac{R_i^2}{\Im_i}$$

- nuclei have an additional intrinsic part H_{intr} with 'intrinsic' angular momentum ***J***

- total angular momentum is ***I***=***R***+***J***

Modes of nuclear vibration

- nucleus is considered as a droplet of nuclear matter with an equilibrium shape - vibrations are modes of excitation around that shape

- character of vibrations depends on symmetry of equilibrium shape. Two important cases in nuclei:

  – spherical equilibrium shape

  – spheroidal equilibrium shape

Vibrations about a spherical shape

- Vibrations are characterized by a multipole quantum number λ in surface parametrization:

$$R(\theta,\varphi) = R_0\left(1 + \sum_{\lambda}\sum_{\mu=-\lambda}^{+\lambda}\alpha_{\lambda\mu}Y^*_{\lambda\mu}(\theta,\varphi)\right)$$

  - $\lambda = 0$: compression (high energy)
  - $\lambda = 1$: translation (not an intrinsic excitation)
  - $\lambda = 2$: quadrupole vibration

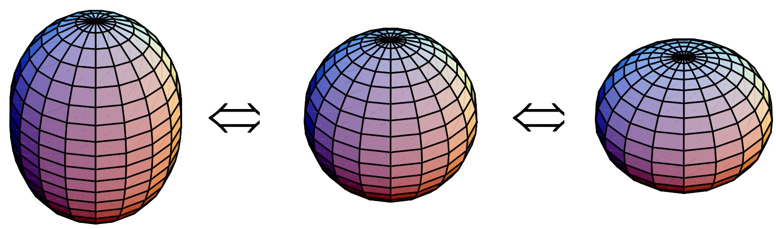

Vibrations about a spheroidal shape

- Vibration of a shape with axial symmetry is characterized by $a_{\lambda\nu}$
- Quadrupolar oscillations:
  - $\nu = 0$: along the axis of symmetry (β)
  - $\nu = \pm 1$: spurious rotation
  - $\nu = \pm 2$: perpendicular to axis of symmetry (γ)

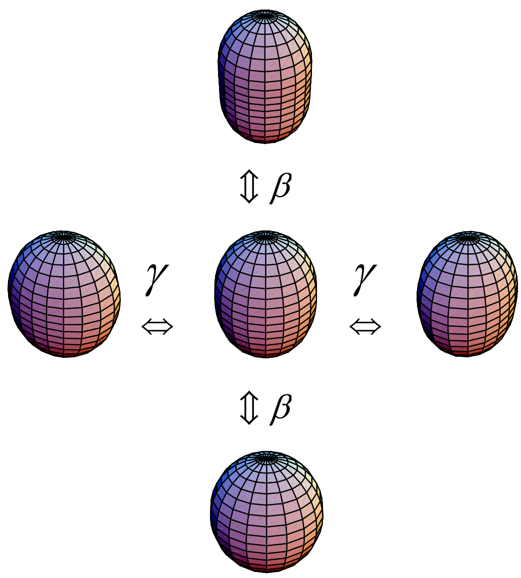

Interacting boson model (IBM)

- Nuclear collective excitations are described in terms of N s and d bosons

- Spectrum generating algebra for the nucleus is U(6) - all physical observables (Hamiltonian, transition operators…) are expressed in terms of the generators of U(6)

- Formally, nuclear structure is reduced to solving the problem of N interacting s and d bosons

Justifications for IBM

- Bosons are associated with *fermion pairs* which approximately satisfy Bose statistics:

$$S^+ = \sum_j \alpha_j \left(a_j^+ \times a_j^+\right)_0^{(0)} \to s^+ ,\; D_m^+ = \sum_{jj'} \alpha_{jj'} \left(a_j^+ \times a_{j'}^+\right)_m^{(2)} \to d_m^+$$

- Microscopic justification: IBM is a truncation and subsequent bosonization of the *shell model* in terms of S and D pairs

- Macroscopic justification: in the classical limit ($N \to \infty$) the expectation value of the IBM Hamiltonian between coherent states reduces to a *liquid-drop* Hamiltonian

IBM Hamiltonian

- Rotational invariant Hamiltonian with up to N-body interactions (usually up to 2):

$$H_{\mathrm{IBM}} = \varepsilon_s n_s + \varepsilon_d n_d + \sum_{ijklJ} \upsilon_{ijkl}^{L} \left(b_i^+ \times b_j^+\right)^{(L)} \cdot \left(\tilde{b}_k \times \tilde{b}_l\right)^{(L)} + \cdots$$

- For what choice of single-boson energies ε_s and ε_d and boson-boson interactions υ^{L}_{ijkl} is the IBM Hamiltonian solvable?

- This problem is equivalent to the enumeration of all algebras G that satisfy

$$\mathrm{U}(6) \supset G \supset \mathrm{SO}(3) \equiv \left\{L_\mu = \sqrt{10}\left(d^+ \times \tilde{d}\right)^{(1)}_\mu\right\}$$

U(5) vibrational limit

- Spectrum of an anharmonic oscillator in 5 dimensions associated with the quadrupole oscillations of a droplet's surface

- Conserved quantum numbers: n_d, υ, L

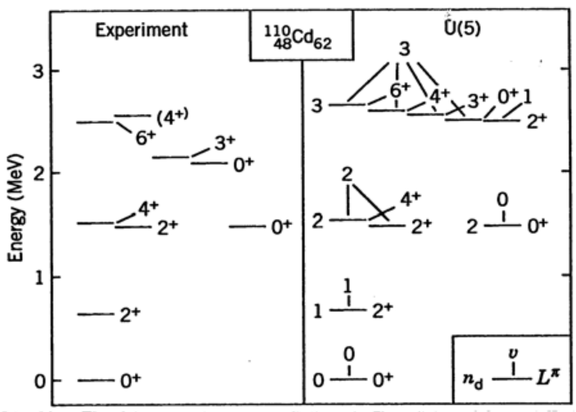

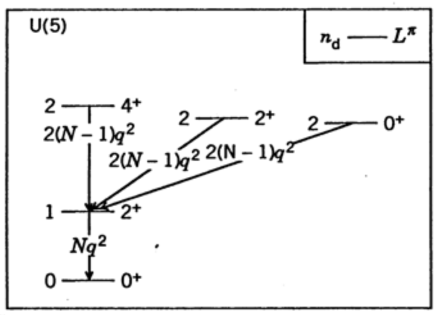

A. Arima & F. Iachello, Ann. Phys. (NY) **99** (1976) 253
D. Brink *et al.*, Phys. Lett. **19** (1965) 413

SU(3) rotational limit

- Rotation-vibration spectrum with β- and γ-vibrational bands
- Conserved quantum numbers: (λ,μ), L

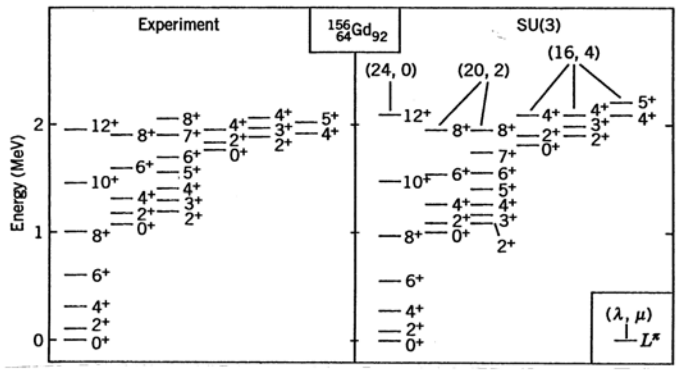

A. Arima & F. Iachello, Ann. Phys. (NY) **111** (1978) 201
A. Bohr & B.R. Mottelson, Dan. Vid. Selsk. Mat.-Fys. Medd. **27** (1953) No 16

SO(6) γ-unstable limit

- Rotation-vibration spectrum of a γ-unstable body
- Conserved quantum numbers: σ, υ, L

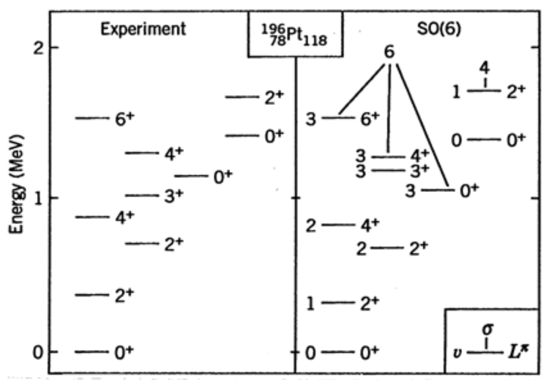

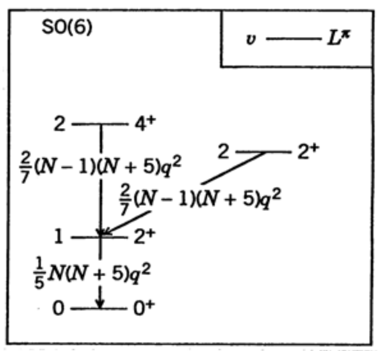

A. Arima & F. Iachello, Ann. Phys. (NY) **123** (1979) 468
L. Wilets & M. Jean, Phys. Rev. **102** (1956) 788

Synopsis of IBM symmetries

- Symmetry triangle of IBM:
  - three standard solutions: U(5), SU(3), SO(6)
  - SU(1,1) analytic solution for U(5) →SO(6)
  - hidden symmetries (parameter transformations)
  - deformed-spherical coexistent phase
  - partial dynamical symmetries
  - critical-point symmetries?

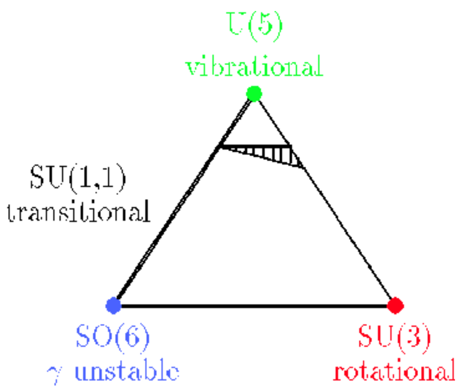

Extensions of IBM

- Neutron and proton degrees freedom (IBM-2):
  - *F*-spin multiplets ($N_\nu + N_\pi$ = constant)
  - scissors excitations
- Fermion degrees of freedom (IBFM):
  - odd-mass nuclei
  - supersymmetry (doublets and quartets)
- Other boson degrees of freedom:
  - isospin $T=0$ and $T=1$ pairs (IBM-3 and IBM-4)
  - higher multipole (g…) pairs

Scissors excitations

- Collective displacement modes between neutrons and protons:

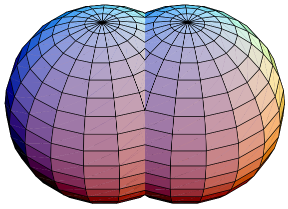

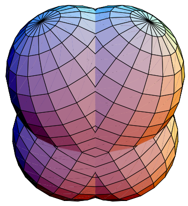

  - *linear* displacement (giant dipole resonance): $\boldsymbol{R}_\nu$-$\boldsymbol{R}_\pi \Rightarrow E1$ excitation
  - *angular* displacement (scissors resonance): $\boldsymbol{L}_\nu$-$\boldsymbol{L}_\pi \Rightarrow M1$ excitation

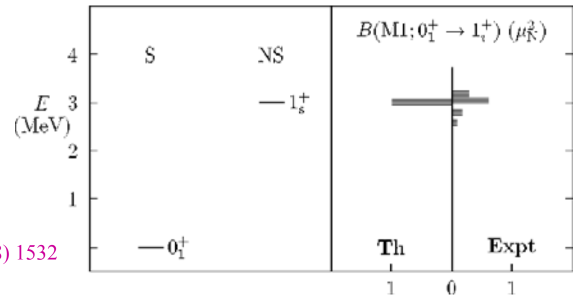

N. Lo Iudice & F. Palumbo, Phys. Rev. Lett. **41** (1978) 1532
F. Iachello, Phys. Rev. Lett. **53** (1984) 1427
D. Bohle *et al.*, Phys. Lett. B **137** (1984) 27

Supersymmetry

- Simultaneous description of even- and odd-mass nuclei (*doublets*) or of even-even, even-odd, odd-even and odd-odd nuclei (*quartets*)
- Example of ^{194}Pt, ^{195}Pt, ^{195}Au and ^{196}Au:

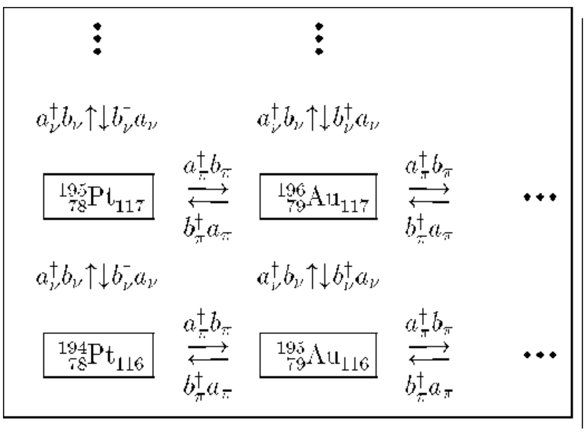

F. Iachello, Phys. Rev. Lett. **44** (1980) 772
P. Van Isacker *et al.*, Phys. Rev. Lett. **54** (1985) 653
A. Metz *et al.*, Phys. Rev. Lett. **83** (1999) 1542

Example of ^{195}Pt

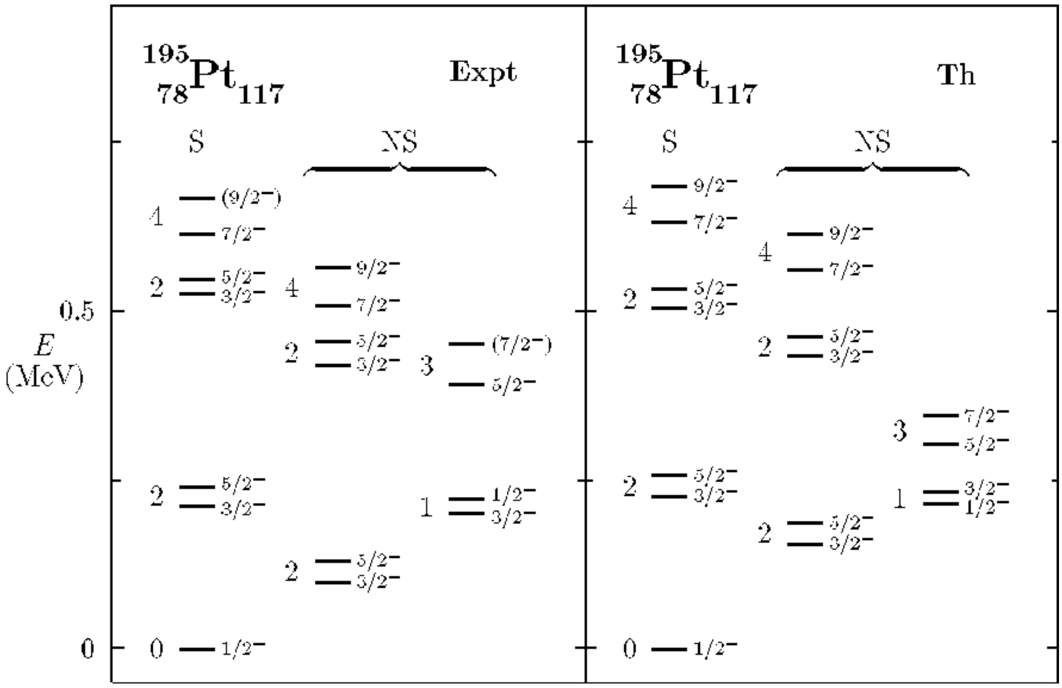

Example of ^{196}Au

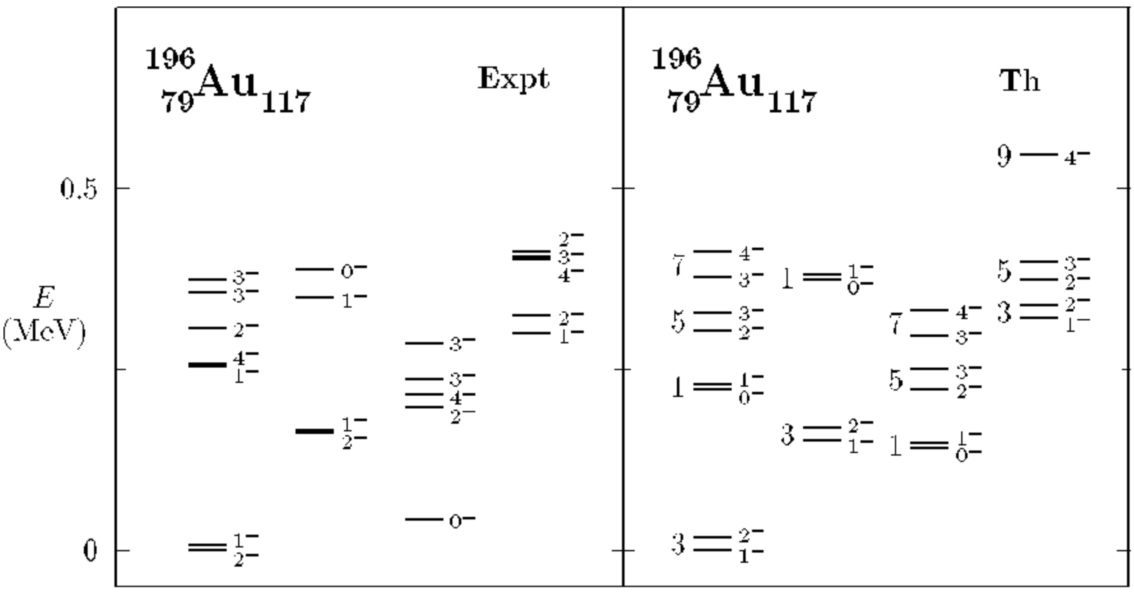

Isospin invariant boson models

- Several versions of IBM depending on the fermion pairs that correspond to the bosons:
  - IBM-1: single type of pair
  - IBM-2: $T=1$ nn ($M_T=-1$) and pp ($M_T=+1$) pairs
  - IBM-3: full isospin $T=1$ triplet of nn ($M_T=-1$), np ($M_T=0$) and pp ($M_T=+1$) pairs
  - IBM-4: full isospin $T=1$ triplet and $T=0$ np pair (with $S=1$)
- Schematic IBM-k has only S ($L=0$) pairs, full IBM-k has S ($L=0$) and D ($L=2$) pairs

IBM-4

•Shell-model justification in LS coupling:

particle number	spatial symmetry	L	spin–isospin symmetry	$(\lambda\mu\nu)$	(S,T)
2	$\square\square$ (S)	$0^2,2^2,4$	$\begin{smallmatrix}\square\\\square\end{smallmatrix}$ (A)	(010)	(0,1) (1,0)
	$\begin{smallmatrix}\square\\\square\end{smallmatrix}$ (A)	$1,2,3$	$\square\square$ (S)	(200)	(0,0) (1,1)

- Advantages of IBM-4:
  - boson states carry L, S, T, J and $(\lambda\mu\nu)$
  - mapping from the shell model to IBM-4 $\Rightarrow$ shell-model test of the boson approximation
  - includes np pairs $\Rightarrow$ important for N~Z nuclei

IBM-4 with *L=0* bosons

- Schematic IBM-4 with bosons
  - $L=0, S=1, T=0 \Rightarrow J=1$ (p boson, $\pi=+1$)
  - $L=0, S=0, T=1 \Rightarrow J=0$ (s boson, $\pi=+1$)
- Two applications:
  - microscopic (but schematic) study of the influence of spin-orbit coupling on the structure of the superfluid condensate in $N = Z$ nuclei
  - phenomenological mass formula for $N \sim Z$ nuclei

Boson mapping of SO(8)

- Pairing Hamiltonian in non-degenerate shells,

$$H = \sum_j \varepsilon_j n_j - g_0 S_+^{10} \cdot S_-^{10} - g_1 S_+^{01} \cdot S_-^{01}$$

  is non-solvable in general but can be treated (numerically) via a boson mapping

- Correspondence $S_+^{10} \to p^+$ and $S_+^{01} \to s^+$ leads to a schematic IBM-4 with $L=0$ bosons

- Mapping of shell-model pairing Hamiltonian completely determines boson energies and boson-boson interactions (*no* free parameters)

P. Van Isacker *et al.*, J. Phys. G **24** (1998) 1261

Pair structure and spin-orbit force

- Fraction of p bosons in the lowest $J=1$, $T=0$ state for $N = Z = 5$ in the pf shell:

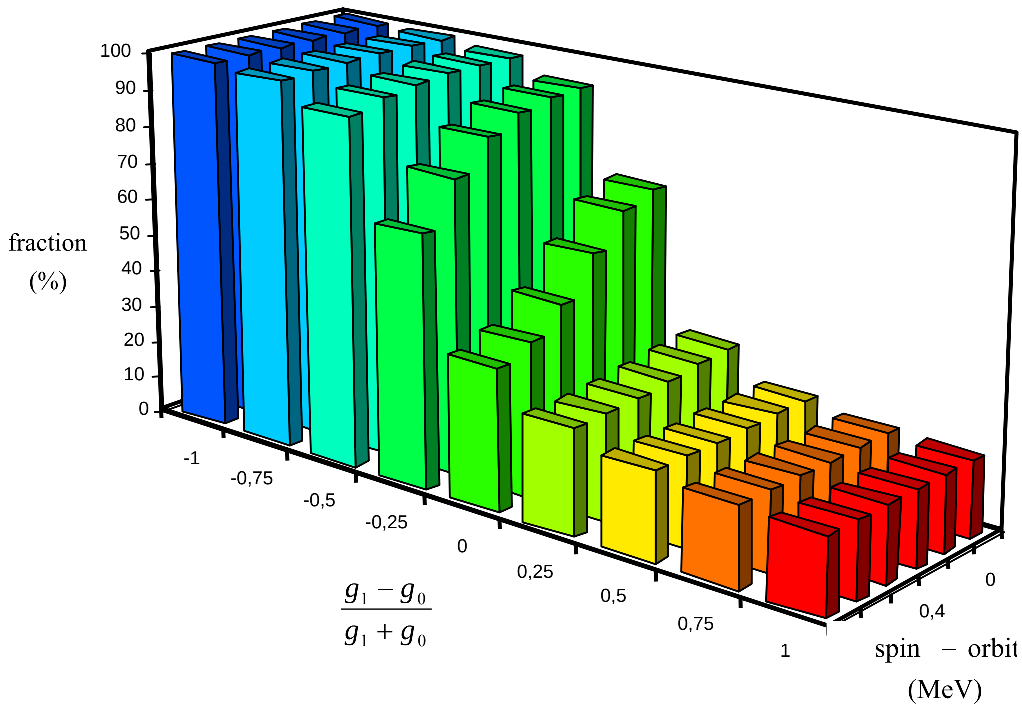

O. Juillet & S. Josse, Eur. Phys. A **2** (2000) 291

Mass formula for $N \sim Z$ nuclei

- Schematic IBM-4 with $L = 0$ bosons has U(6) algebraic structure

- Symmetry lattice of the model:

$$\mathrm{U}(6) \supset \left\{ \begin{matrix} \mathrm{U}_S(3) \otimes \mathrm{U}_T(3) \\ \mathrm{SU}(4) \end{matrix} \right\} \supset \mathrm{SO}_S(3) \otimes \mathrm{SO}_T(3)$$

- Simple IBM-4 Hamiltonian suggested by microscopy with *adjustable* parameters:

$$H = aC_1[\mathrm{U}(6)] + bC_2[\mathrm{U}(6)] + cC_2[\mathrm{SO}_T(3)] + dC_2[\mathrm{SU}(4)] + eC_2[\mathrm{U}_S(3)]$$

E. Baldini-Neto *et al.*, Phys. Rev. C **65** (2002) 064303

Binding energies of *sd* $N = Z$ nuclei

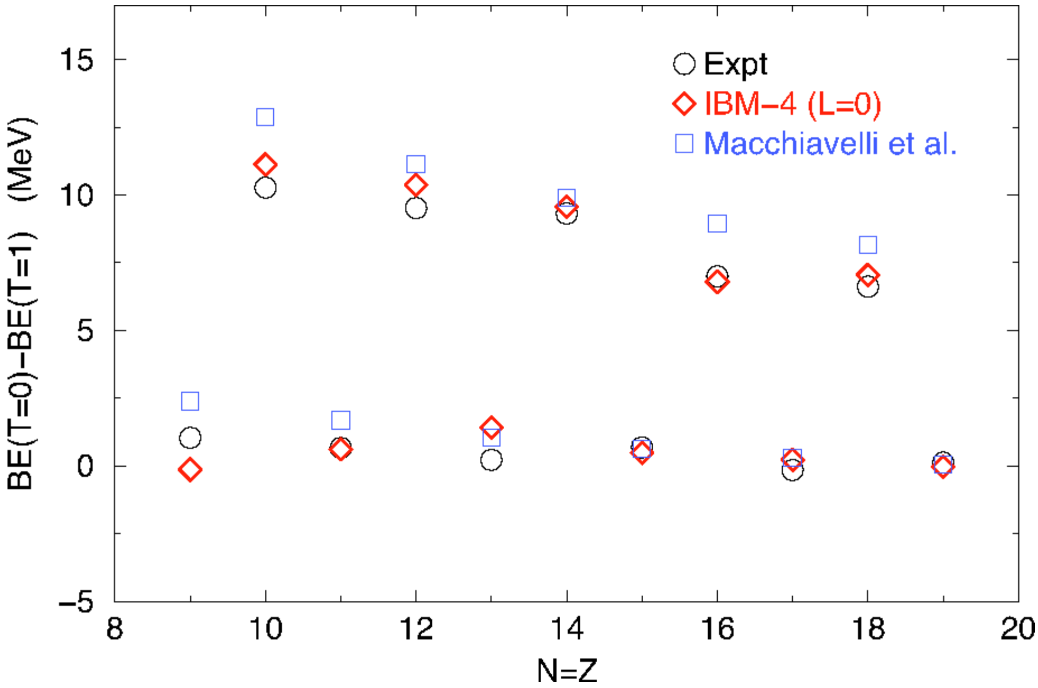

Binding energies of *pf*-shell nuclei

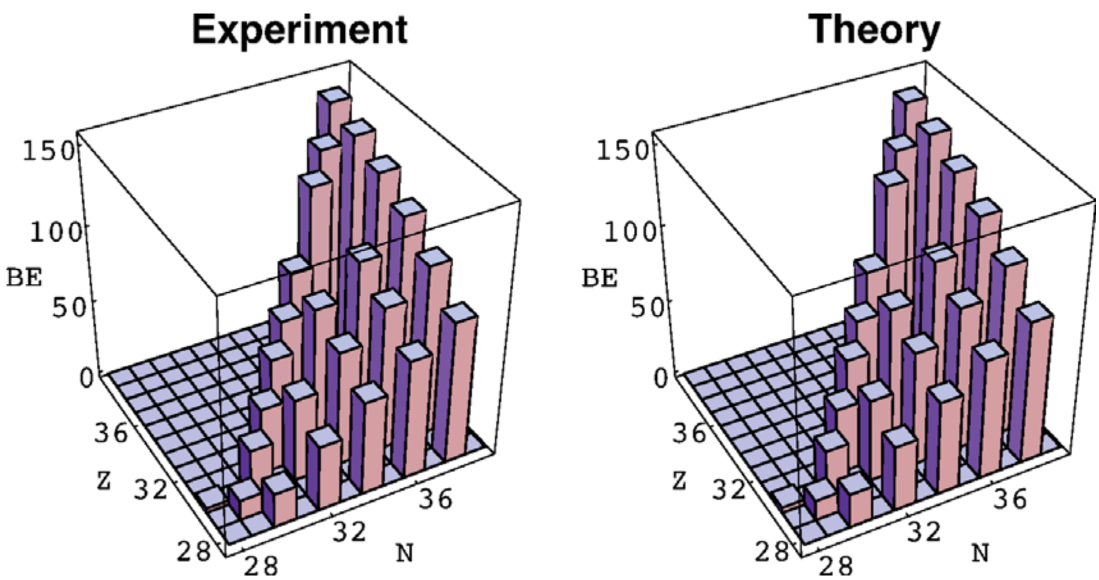

Algebraic many-body models

- Integrability of any quantum many-body (bosons and/or fermions) system can be analyzed with algebraic methods
- Two nuclear examples:
  - pairing *vs*. quadrupole interaction in the nuclear shell model
  - spherical, deformed and γ-unstable nuclei with *s*,*d*-boson IBM

$$\mathrm{U}(6) \supset \left\{ \begin{array}{c} \mathrm{U}(5) \supset \mathrm{SO}(5) \\ \mathrm{SU}(3) \\ \mathrm{SO}(6) \supset \mathrm{SO}(5) \end{array} \right\} \supset \mathrm{SO}(3)$$

Other fields of physics

- Molecular physics:
  - U(4) vibron model with *s*,*p*-bosons

$$\mathrm{U}(4) \supset \left\{ \begin{array}{c} \mathrm{U}(3) \\ \mathrm{SO}(4) \end{array} \right\} \supset \mathrm{SO}(3)$$

  - coupling of many SU(2) algebras for polyatomic molecules
- Similar applications in hadronic, atomic, solid-state, polymer physics, quantum dots…
- Use of *non-compact* groups and algebras for scattering problems

Nuclear Theory:

Self-consistent Mean-field Models
Structure of Heavy Nuclei

D. Vretenar

University of Zagreb

E.mail: vretenar@phy.hr

The Hartree-Fock-Bogoliubov Method

1. Basics of a mean-field description

The basic building block of any mean-field model is a set of single-nucleon wave functions:

$$\{\psi_i(\mathbf{x}), i = 1, \ldots, N_{\mathsf{wf}}\}, \quad \mathbf{x} = (\mathbf{r}, \sigma, \tau)$$

- the number of single-particle wave functions (N_{wf}) is larger than number of nucleons A = Z + N.

$$\hat{a}_i^+ = \int d^3r \sum_{\sigma t} \psi_i(\mathbf{x})\, \hat{a}_x^+$$

Creation operator for a nucleon in a single-particle state i

Creation operator for eigenstates of position

Independent single-particle model: state of a nucleus is described by a Slater determinant:

$$|\Phi\rangle \equiv \det\{\psi_i(\mathbf{x}), i=1, \ldots, A\}$$

$\hat{a}_i^+|\Phi\rangle = 0$ for occupied states $1 \leq I \leq A$

$\hat{a}_i|\Phi\rangle = 0$ for unoccupied states $(i > A)$

Pairing correlations $\Longrightarrow$ concept of independent quasi-particles defined by the Bogoliubov transformation

$$\hat{b}_n^+ = \sum_i (U_{in}\,\hat{a}_i^+ + V_{in}\,\hat{a}_i)$$

- Ground state of the system is given by the condition defined as the quasi-particle vacuum:

$$\hat{b}_n|\Phi\rangle = 0$$

- quasi-particle wave functions in coordinate space:

$$\phi_n = \begin{pmatrix} \phi_n^{(U)}(\mathbf{x}) \\ \phi_n^{(V)}(\mathbf{x}) \end{pmatrix} = \begin{pmatrix} \sum_i U_{in}\psi_i(\mathbf{x}) \\ \sum_i V_{in}\psi_i(\mathbf{x}) \end{pmatrix}$$

one-body density

$$\rho_{ij} = \langle\Phi|\hat{a}_j^+\hat{a}_i|\Phi\rangle = (V^*V^T)_{ij} = \rho_{ji}^*$$

pair tensor

$$\kappa_{ij} = \langle\Phi|\hat{a}_j\hat{a}_i|\Phi\rangle = (V^*U^T)_{ij} = -\kappa_{ji}$$

$$\mathcal{R} = \begin{pmatrix} \rho & \kappa \\ -\kappa^* & 1\!\!1 - \rho^* \end{pmatrix}$$

Generalized density matrix: eigenvalues either 0 or 1

Coordinate space representation

$$\rho(\mathbf{x},\mathbf{x}') = \langle\Phi|\hat{a}_{x'}^+\hat{a}_x|\Phi\rangle \equiv \sum_n \phi_n^{(V)}(\mathbf{x})\phi_n^{(V)^*}(\mathbf{x}')$$

$$\kappa(\mathbf{x},\mathbf{x}') = \langle\Phi|\hat{a}_{x'}\hat{a}_x|\Phi\rangle \equiv \sum_n \phi_n^{(U)}(\mathbf{x})\phi_n^{(V)^*}(\mathbf{x}')$$

2. Hartree-Fock-Bogoliubov equation

Ground state |Φ› of HFB is obtained by minimization of the total energy:

$$E = \langle\Psi|\hat{H}|\Psi\rangle = E[\rho, \kappa, \kappa^*]$$

with constraints on the proton and neutron numbers $\langle\Psi|\hat{N}_q|\Psi\rangle = N_q$

- Minimization of the total Routhian: $E^\lambda = E - \lambda_q \langle\Psi|\hat{N}_q|\Psi\rangle$ ⇨

HFB equation

$$\boxed{\mathcal{H}\begin{pmatrix} U_n \\ V_n \end{pmatrix} = e_n \begin{pmatrix} U_n \\ V_n \end{pmatrix} \quad \text{with} \quad \mathcal{H} = \begin{pmatrix} h-\lambda & \Delta \\ -\Delta^* & -h^*+\lambda \end{pmatrix}}$$

- Mean-field Hamiltonian and the pairing field:

$$h_{ij} = \frac{\delta E}{\delta\rho_{ji}} = h^*_{ji} \qquad \Delta_{ij} = \frac{\delta E}{\delta\kappa^*_{ij}} = -\Delta_{ji}$$

$$h_{ij} = T_{ij} + \sum_{kl} V_{ikjl}\,\rho_{lk} \qquad \Delta_{ij} = \frac{1}{2}\sum_{kl} V_{ijkl}\,\kappa_{kl}$$

1. Quasiparticle basis Φ_n → diagonalizes the generalized one-body matrix *R*
2. Canonical basis ψ_i → diagonalizes the one-body density p
3. Hartee-Fock basis → diagonalizes the mean-field Hamiltonian *h*

3. Symmetries and Constraints

i) symmetries related to the shape of the nucleus – spherical, axial quadrupole, triaxial quadrupole, octupole
ii) time reversal symmetry – for even-even non-rotating nuclei - creation of a quasiparticle or rotation of the nucleus breaks time-reversal symmetry

- Landscape of the energy as a function of a shape degree of freedom is explored with the help of constraints

  Equations of motion are obtained by minimization of a Routhian:

  $$E = \langle \hat{H} \rangle - \sum_{q=p,n} \lambda_q \langle \hat{N}_q \rangle - \sum_\alpha \lambda_\alpha \langle \hat{Q}_\alpha \rangle$$

  constraint on the expectation value: $\langle \hat{Q}_\alpha \rangle \equiv \langle \Psi | \hat{Q}_\alpha | \Psi \rangle = Q_\alpha$

- Quadratic constraint:

$$E = \langle \hat{H} \rangle - \sum_{q=p,n} \lambda_q \langle \hat{N}_q \rangle + \frac{1}{2} \sum_\alpha C_\alpha \left(\langle \hat{Q}_\alpha \rangle - \mu_\alpha \right)^2$$

Constant

Desired value of the Operator expectation

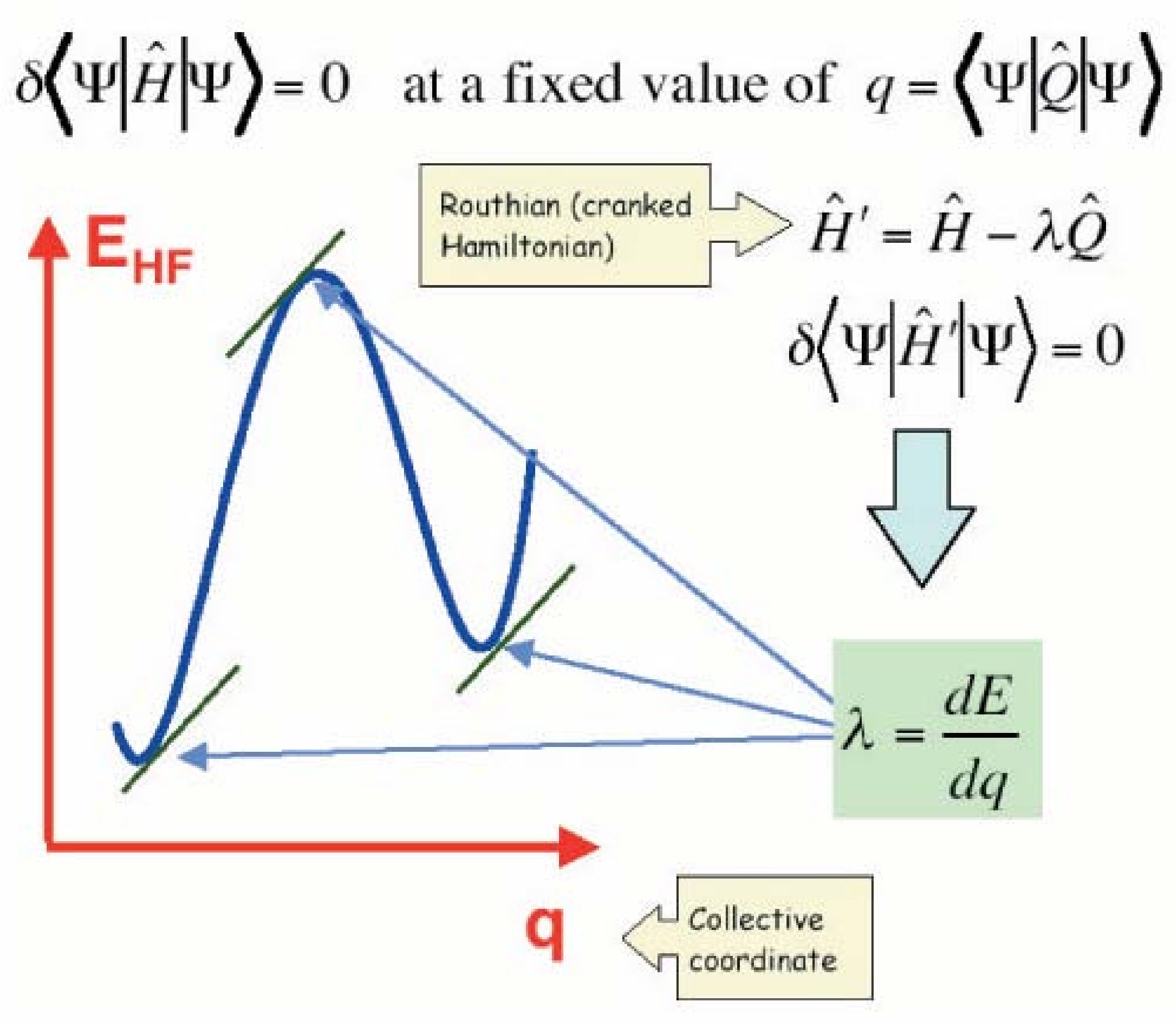

$\delta\langle\Psi|\hat{H}|\Psi\rangle = 0$ at a fixed value of $q = \langle\Psi|\hat{Q}|\Psi\rangle$
Routhian (cranked Hamiltonian)
$\hat{H}' = \hat{H} - \lambda\hat{Q}$
$\delta\langle\Psi|\hat{H}'|\Psi\rangle = 0$
E_{HF}
$\lambda = \frac{dE}{dq}$
q
Collective coordinate

4. BCS approximation

- well defined only in the case of time-reversal invariance $\longrightarrow$ Kramer's degeneracy of single-particle states:

$$\epsilon_n = \epsilon_{\bar{n}} \quad \text{for time} - \text{conjugate partners} \quad \varphi_n, \varphi_{\bar{n}}$$

$$h = \begin{pmatrix} h & 0 \\ 0 & \bar{h}^* \end{pmatrix} \qquad \Delta = \begin{pmatrix} 0 & d \\ -d^T & 0 \end{pmatrix}$$

- BCS approximation: forces the pairing potential to be diagonal on the basis of the eigenstates of the mean-field potential

$$d_{n\bar{m}} = \delta_{nm} d_{n\bar{m}} \qquad \hat{h}\varphi_n = \varepsilon_n \varphi_n$$

Pairing problem reduces to the determination of occupation amplitudes by solving the gap equation:

$$\boxed{(\varepsilon_n - \lambda)(u_n^2 - v_n^2) + 2 d_{n\bar{n}} u_n v_n = 0}$$

Density matrices become

One-body density: $\rho(\mathbf{x}, \mathbf{x}') = 2 \sum_{n>0} v_n^2 \, \varphi_n(\mathbf{x}) \varphi_n^*(\mathbf{x}')$

Pair density: $\tilde{\rho}(\mathbf{x}, \mathbf{x}') = -2 \sum_{n>0} u_n v_n \, \varphi_n(\mathbf{x}) \varphi_n^*(\mathbf{x}')$

5. Local densities and Currents

Full density matrix can be decomposed into four separate spin-isospin terms:

$$\rho(\mathbf{r}\sigma\tau, \mathbf{r}'\sigma'\tau') = \frac{1}{4}\Big\{\Big[\rho_{00}(\mathbf{r},\mathbf{r}')\,\delta_{\sigma\sigma'} + \mathbf{s}_{00}(\mathbf{r},\mathbf{r}')\cdot\boldsymbol{\sigma}_{\sigma'\sigma}\Big]\delta_{\tau\tau'} + \sum_{\alpha=-1}^{+1}\Big[\rho_{1\alpha}(\mathbf{r},\mathbf{r}')\,\delta_{\sigma\sigma'} + \mathbf{s}_{1\alpha}(\mathbf{r},\mathbf{r}')\cdot\boldsymbol{\sigma}_{\sigma'\sigma}\Big](\boldsymbol{\tau}_{\tau'\tau})_\alpha\Big\}$$

where $\boldsymbol{\sigma}_{\sigma'\sigma} = (\sigma'|\hat{\boldsymbol{\sigma}}|\sigma)$ $\quad\boldsymbol{\tau}_{\tau'\tau} = (\tau'|\hat{\boldsymbol{\tau}}|\tau)$

- For pure proton and neutron states, only $\alpha = 0$ components of the isovector densities contribute

- There are six local densities and currents that can be derived from the full density matrix.

Omit the second index in the densities and, with T = 0 or 1, local densities and currents:

T = 0 density: $$\rho_0(\mathbf{r}) \;=\; \rho_0(\mathbf{r},\mathbf{r}) = \sum_{\sigma\tau} \rho(\mathbf{r}\sigma\tau;\mathbf{r}\sigma\tau)$$

T = 1 density: $$\rho_1(\mathbf{r}) \;=\; \rho_1(\mathbf{r},\mathbf{r}) = \sum_{\sigma\tau} \rho(\mathbf{r}\sigma\tau;\mathbf{r}\sigma\tau)\,\tau$$

T = 0 spin density: $$\mathbf{s}_0(\mathbf{r}) \;=\; \mathbf{s}_0(\mathbf{r},\mathbf{r}) = \sum_{\sigma\sigma'\tau} \rho(\mathbf{r}\sigma\tau;\mathbf{r}\sigma'\tau)\,\boldsymbol{\sigma}_{\sigma'\sigma}$$

T = 1 spin density: $$\mathbf{s}_1(\mathbf{r}) \;=\; \mathbf{s}_1(\mathbf{r},\mathbf{r}) = \sum_{\sigma\sigma'\tau} \rho(\mathbf{r}\sigma\tau;\mathbf{r}\sigma'\tau)\,\boldsymbol{\sigma}_{\sigma'\sigma}\,\tau$$

Current: $$\mathbf{j}_T(\mathbf{r}) \;=\; \tfrac{i}{2}(\nabla' - \nabla)\,\rho_T(\mathbf{r},\mathbf{r}')\Big|_{\mathbf{r}=\mathbf{r}'}$$

Spin-current tensor: $$\mathcal{J}_T(\mathbf{r}) \;=\; \tfrac{i}{2}(\nabla' - \nabla)\otimes\mathbf{s}_T(\mathbf{r},\mathbf{r}')\Big|_{\mathbf{r}=\mathbf{r}'}$$

Kinetic density: $$\tau_T(\mathbf{r}) \;=\; \nabla\cdot\nabla'\,\rho_T(\mathbf{r},\mathbf{r}')\Big|_{\mathbf{r}=\mathbf{r}'}$$

Kinetic spin-density: $$\mathbf{T}_T(\mathbf{r}) \;=\; \nabla\cdot\nabla'\,\mathbf{s}_T(\mathbf{r},\mathbf{r}')\Big|_{\mathbf{r}=\mathbf{r}'}$$

CHOICES FOR THE EFFECTIVE INTERACTION

A. MEAN-FIELD EFFECTIVE INTERACTIONS

1. Gogny interaction: sum of two Gaussians with space, spin and isospin exchange mixtures - also a density-dependent interaction plus a spin-orbit term:

parameters

$$\hat{v}_{\mathrm{Gogny}}(\mathbf{r}_{12}) = \sum_{j=1}^{2} e^{-(\mathbf{r}_{12}/\mu_j)^2}\left(W_j + B_j \hat{P}_\sigma - H_j \hat{P}_\tau - M_j \hat{P}_\sigma \hat{P}_\tau\right)$$

parameters

$$+ t_3 (1 + x_0 \hat{P}_\sigma)\,\delta(\mathbf{r}_{12})\,\rho^\alpha\left(\frac{\mathbf{r}_1+\mathbf{r}_2}{2}\right)$$

$$+ \mathrm{i} W_{ls}(\hat{\boldsymbol{\sigma}}_1 + \hat{\boldsymbol{\sigma}}_2)\cdot \hat{\mathbf{k}}^\dagger \times \delta(\mathbf{r}_{12})\,\hat{\mathbf{k}}$$

Exchange operators: $\hat{P}_\sigma = \frac{1}{2}(1 + \hat{\boldsymbol{\sigma}}_1 \cdot \hat{\boldsymbol{\sigma}}_2)$ $\quad \hat{P}_\tau = \frac{1}{2}(1 + \hat{\tau}_1 \cdot \hat{\tau}_2)$

$$\mathbf{r}_{12} = \mathbf{r}_1 - \mathbf{r}_2 \qquad \mathbf{k} = -\frac{\mathrm{i}}{2}(\nabla_1 - \nabla_2)$$

- Finite-range Gogny interaction is used simultaneously in both the mean-field and pairing channels

2. Skyrme interactions

Skyrme Hartree-Fock approach: total binding energy is given by the sum of kinetic energy, Skyrme energy functional that models the effective interaction between nucleons, Coulomb energy, pair energy and corrections for spurious motions:

$$\boxed{E = E_{\mathrm{kin}} + \int d^3r\, \mathcal{E}_{\mathrm{Sk}} + E_{\mathrm{Coul}} + E_{\mathrm{pair}} - E_{\mathrm{corr}}}$$

The Skyrme energy functional $\mathcal{E}_{\mathrm{Sk}} = \sum_{T=0,1} \left(\mathcal{E}_T^{\mathrm{even}} + \mathcal{E}_T^{\mathrm{odd}} \right)$

Density-dependent coefficients

Contains only time-even dens.

Dependences on time-odd currents

$$\mathcal{E}_T^{\mathrm{even}} = C_T^{\rho} \rho_T^2 + C_T^{\Delta\rho}\, \rho_T \Delta \rho_T + C_T^{\tau}\, \rho_T \tau_T + C_T^{J} \mathcal{J}_T^2 + C_T^{\nabla J}\, \rho_T\, \nabla \mathbf{J}_T$$

$$\mathcal{E}_T^{\mathrm{odd}} = C_T^{s}\, \mathbf{s}_T^2 + C_T^{\Delta s}\, \mathbf{s}_T \cdot \Delta \mathbf{s}_T + C_T^{sT}\, \mathbf{s}_T \cdot \mathbf{T}_T + C_T^{\nabla s} (\nabla \cdot \mathbf{s}_T)^2 + C_T^{j}\, \mathbf{j}_T^2 + C_T^{\nabla j}\, \mathbf{s}_T \cdot \nabla \times \mathbf{j}_T$$

Does not contribute in stationary calculations of even-even nuclei

Single-particle Hamiltonians

Contribution from Skyrme interaction to the single-particle Hamiltonian:

$$\boxed{\hat{h}_q = U_q - \nabla \cdot B_q \nabla - \tfrac{\mathrm{i}}{2}\{\mathcal{W}_q, \nabla\sigma\} + \mathbf{S}_q \cdot \hat{\boldsymbol{\sigma}} - \nabla \cdot (\hat{\boldsymbol{\sigma}} \cdot \mathbf{C}_q) \nabla - \tfrac{\mathrm{i}}{2}\{\mathbf{A}_q, \nabla\}}$$

where $\{\mathcal{W}_q, \nabla\sigma\} = \sum_{ij}\{W_{ij}, \nabla_i \hat{\sigma}_j\}$ (q = p, n)

- Local potentials are calculated from:

$$\text{time-even}: \quad U_q = \frac{\delta E}{\delta \rho_q}, \quad B_q = \frac{\delta E}{\delta \tau_q}, \quad \mathcal{W}_q = \frac{\delta E}{\delta \mathcal{J}_q},$$

$$\text{time-odd}: \quad \mathbf{A}_q = \frac{\delta E}{\delta \mathbf{j}_q}, \quad \mathbf{S}_q = \frac{\delta E}{\delta \mathbf{s}_q}, \quad \mathbf{C}_q = \frac{\delta E}{\delta \mathbf{T}_q}$$

Time-odd fields:

Time-odd fields **A**, **C**, and **S** contribute to the single-particle Hamiltonian only when the intrinsic time-reversal symmetry is broken and the Kramer's degeneracy of single-particle levels is removed

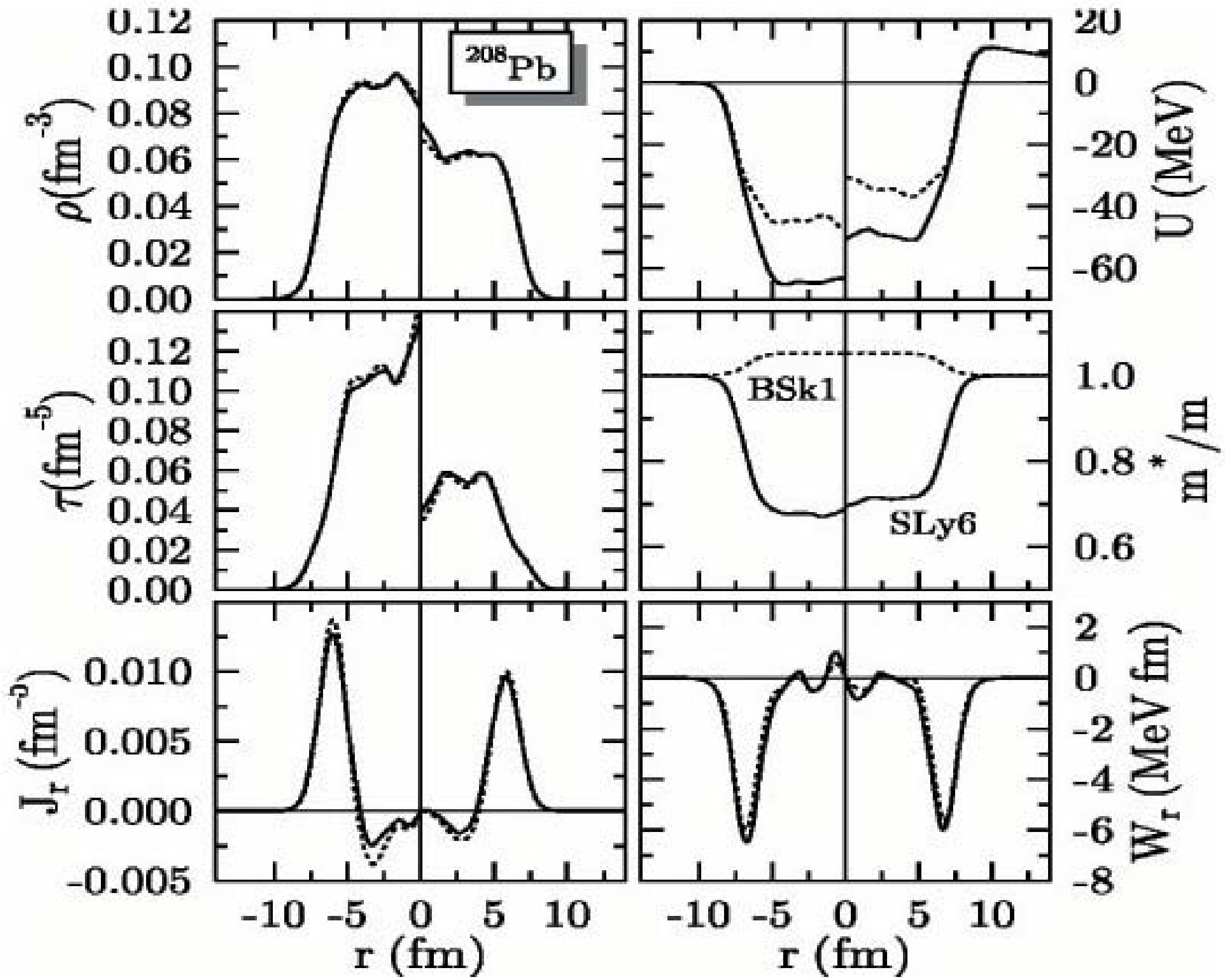

Time-even densities and potentials in ^{208}Pb, for neutrons (left) and protons (right), calculated with Skyrme interactions SLy6 (solid lines) and BSk1 (dotted lines)

Choices for coupling constants

1. Energy functional is derived from the Hartree-Fock expectation value

$$\mathcal{E}_{\mathsf{Sk}}^{\mathsf{HF}} = \langle \mathsf{HF} | \hat{v}_{\mathsf{Sk}} | \mathsf{HF} \rangle$$

of the zero-range momentum dependent two-body force introduced by Skyrme:

$$\begin{aligned}
\hat{v}_{\mathsf{Sk}}(\mathbf{r}_{12}) \; = \; & t_0 \,(1 + x_0 \hat{P}_\sigma)\, \delta(\mathbf{r}_{12}) \\
& + \tfrac{1}{2} t_1 \,(1 + x_1 \hat{P}_\sigma) \left(\hat{\mathbf{k}}^{\dagger 2}\, \delta(\mathbf{r}_{12}) + \delta(\mathbf{r}_{12})\, \hat{\mathbf{k}}^2 \right) \\
& + t_2 \,(1 + x_2 \hat{P}_\sigma)\, \hat{\mathbf{k}}^{\dagger} \cdot \delta(\mathbf{r}_{12})\, \hat{\mathbf{k}} \\
& + \tfrac{1}{6} t_3 \,(1 + x_3 \hat{P}_\sigma)\, \delta(\mathbf{r}_{12})\, \rho^{\alpha} \left(\tfrac{\mathbf{r}_1 + \mathbf{r}_2}{2} \right) \\
& + \mathrm{i} W_0 \,(\hat{\boldsymbol{\sigma}}_1 + \hat{\boldsymbol{\sigma}}_2) \cdot \hat{\mathbf{k}}^{\dagger} \times \delta(\mathbf{r}_{12})\, \hat{\mathbf{k}}
\end{aligned}$$

2. Energy functional is parameterized directly without reference to an effective two-body force - contains systematically all possible bilinear terms in the local densities and currents up to second order in the derivatives which are invariant with respect to parity, time-reversal, rotational, translational and isospin transformations

B. PAIRING CORRELATIONS

- Pairing-energy functional:

$$E_{\text{pair}} = \sum_{q=p,n} \frac{V_q}{4} \int d^3r \left[1 - \left(\frac{\rho(\mathbf{r})}{\rho_c}\right)^{\beta}\right] \tilde{\rho}_q^2(\mathbf{r})$$

corresponds to the density-dependent two-body zero-range local pairing force:

$$\boxed{v_{\text{pair}} = \frac{V_0}{2}(1 - \hat{P}_\sigma)\left[1 - \left(\frac{\rho(\mathbf{r}_1)}{\rho_c}\right)^{\beta}\right] \delta(\mathbf{r}_1 - \mathbf{r}_2)}$$

Volume pairing
$\rho_c \to \infty$

Surface pairing
$\rho_c \approx \rho_{nm}$

- Pairing strengths $V_{p,n}$ are adjusted phenomenologically to reproduce the odd-even staggering of energies in selected chains of nuclei

- Pairing-active space of single-particle states ⟸ Cutoff recipe ?

CORRELATIONS BEYOND THE STATIC MEAN-FIELD APPROACH: CONFIGURATION MIXING

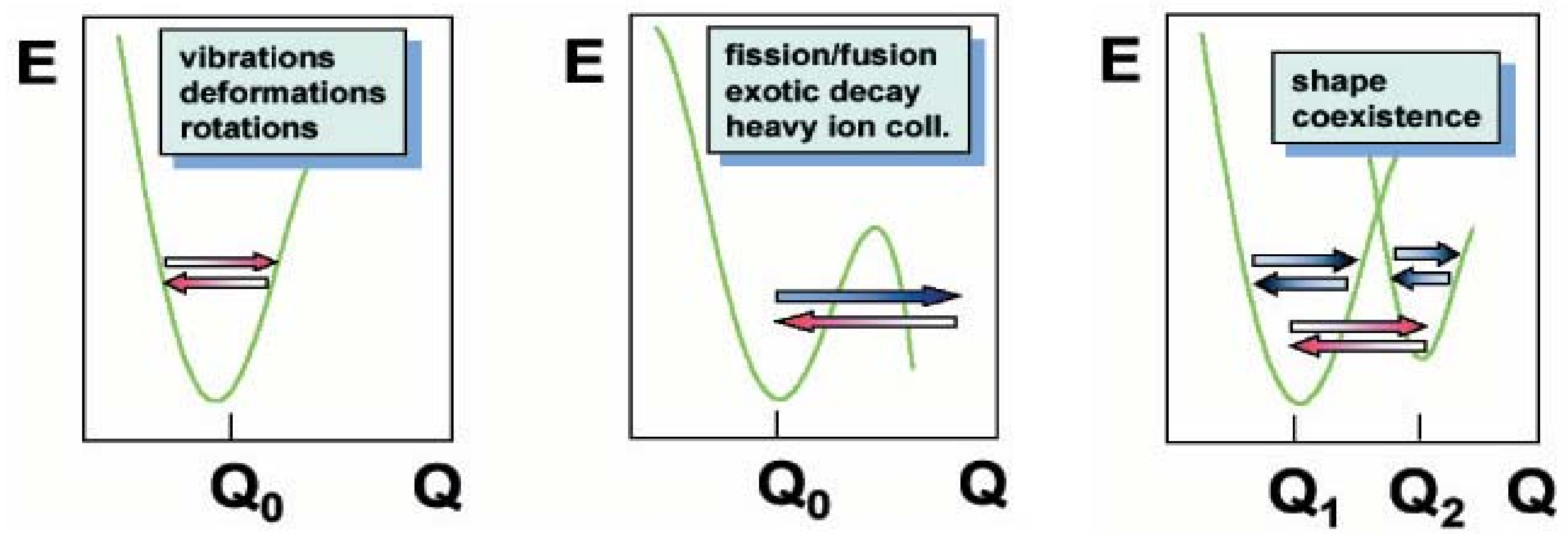

Most important correlation effects in nuclear structure stem from large amplitude collective motion. Low-lying excited states are mixed into the calculated mean-field ground state that can be removed by configuration mixing: superposition of several mean-field states

Includes nuclear surface vibrations related to low-lying excitation spectra and zero-energy modes (translation, rotation ...) associated with restoration of symmetries broken by the mean-field ground state

Generator Coordinate Method

- Determines approximate eigenstates of Hamiltonian H:

Weight functions

$$|\Psi_k\rangle = \int dq\, |\Phi(q)\rangle\, f_k(q)$$

Generator coordinate (collective variable)

Intrinsic (e.g. HFB) wave functions

- Requires expectation value $E_k = \frac{\langle \Psi_k|\hat{H}|\Psi_k\rangle}{\langle \Psi_k|\Psi_k\rangle}$ to be stationary with respect to an arbitrary variation δf_k $\Rightarrow$ Hill-Wheeler equation

$$\int dq' \left[\mathcal{H}(q,q') - E_k \mathcal{I}(q,q')\right] f_k(q') = 0$$

Hamiltonian kernel
$\mathcal{H}(q,q') = \langle \Phi(q)|\hat{H}|\Phi(q')\rangle$

Overlap kernel
$\mathcal{I}(q,q') = \langle \Phi(q)|\Phi(q')\rangle$

- Collective wave functions for the variable ***q*** $g_k(q) = \int dq' \, \mathcal{I}^{1/2}(q,q') \, f_k(q')$

- Matrix element of any operator O between two GCM states can be expressed in terms of the gk values as:

$$\langle \Psi_k | \hat{O} | \Psi_l \rangle = \iint dq \, dq' \, g_k^*(q) \, \tilde{\mathcal{O}}(q,q') \, g_l(q')$$

$$\tilde{\mathcal{O}}(q,q') = \iint dq'' \, dq''' \, \mathcal{I}^{1/2}(q,q'') \, \mathcal{O}(q'',q''') \, \mathcal{I}^{1/2}(q''',q')$$

- GCM energies $\mathbf{E_k}$ and functions $\mathbf{g_k}$ are the eigenvalues and eigenvectors of the hermitian integral operator

$$\int dq' \, \tilde{\mathcal{H}}(q,q') \, g_k(q') = E_k g_k(q)$$

Gaussian Overlap Approximation: overlap kernel is replaced by a Gaussian function of the form:

$$\mathcal{I}(q,q') \simeq \mathcal{I}_G(q,q') = \exp\left\{ -\frac{1}{2} \left[\frac{(q-q')}{a(\bar{q})} \right]^2 \right\}$$

based on the rapid decrease of the matrix elements between wave functions corresponding to different values of the collective variable

Choice of the collective coordinate

1. RESTORATION OF BROKEN SYMMETRIES: family of wave functions $|\Phi(q)\rangle$ is generated by the symmetry operations: rotation in coordinate space for angular momentum, rotation in gauge space for particle number - generating function $\mathbf{f_k(q)}$ is a priori determined by the properties of the symmetry operator.

2. SHAPE DEGREES OF FREEDOM: collective space is generated by constrained mean-field calculations - the generating function is unknown and has to be determined by diagonalization of the Hill-Wheeler equation.

Example: Projected GCM+HF+BCS

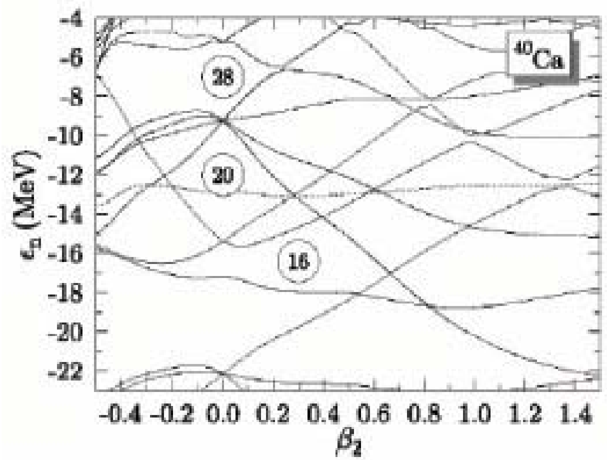

M.Bender, H.Flocard, P.-H. Heenan
Nucl-th/0305021

Usual starting point: deformed mean fields

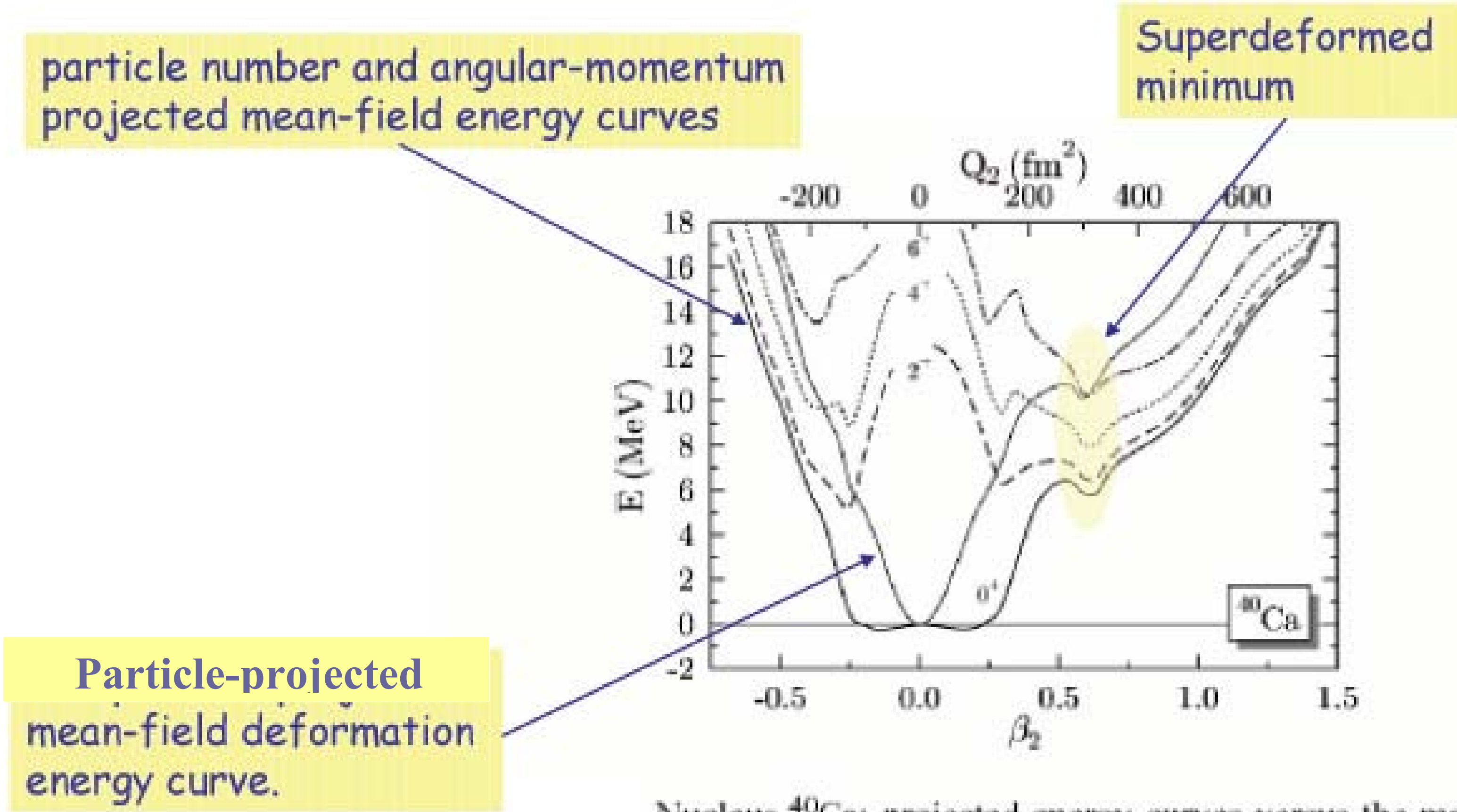

Nucleus ^{40}Ca; projected energy curves versus the mass deformation (β_2 and Q_2). The thin solid curve gives $\langle\beta_2|\hat{H}|\beta_2\rangle$ (MF), while the thick solid, dashed, dotted, and dash-dotted curves correspond to $\langle J,\beta_2|\hat{H}|J,\beta_2\rangle$ (PMF) for the values J=0, 2, 4, and 6, respectively. The energy origin is taken at $\langle\beta_2=0|\hat{H}|\beta_2=0\rangle$.

The Hamiltonian is diagonalized within each of the collective subspaces of the nonorthogonal bases $|J, \boldsymbol{\beta_2} >$ by using GCM.

PES and GCM eigenstates

Collective wave functions

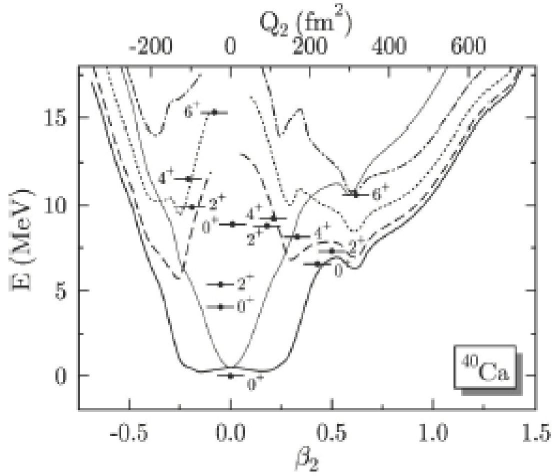

Nucleus ^{40}Ca; MF $\langle \beta_2|\hat{H}|\beta_2\rangle$ (thin solid) and PMF $\langle J,\beta_2|\hat{H}|J,\beta_2\rangle$ (thick solid) deformation energy curves. The ordinates of short horizontal segments give the energy $E_{J,k}$ of the GCM states [Eq. (5)]. The abscissa of the black points indicates the mean deformation $(\bar{\beta}_2)$ of the corresponding collective wave function $g_{J,k}$ [Eq. (6)]. The energy origin is taken at $E_{0,1}$.

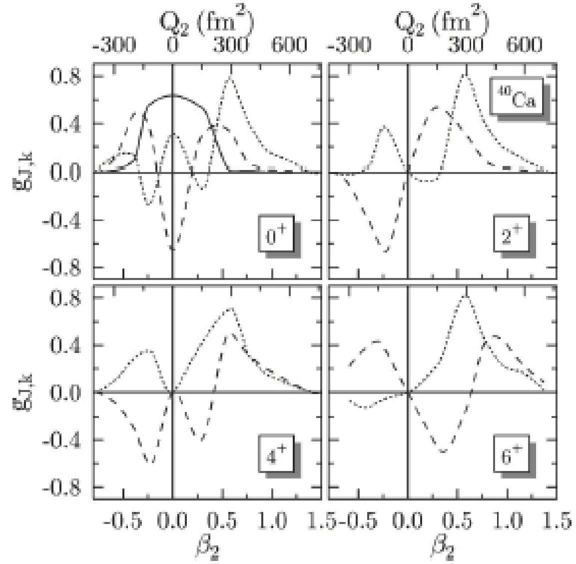

Collective GCM wave functions $g_{J,k}$ for low-spin states of ^{40}Ca. The ground-state 0^+ wave function is drawn with a thick solid line. The wave functions of the ND and SD bands are drawn with dashed and dotted lines, respectively.

CORRELATIONS BEYOND THE STATIC MEAN-FIELD APPROACH: SYMMETRY RESTORATION

Necessarily, a self-consistent mean-field (SCMF) wave function breaks several symmetries of the nuclear Hamiltonian. Any SCMF solution is degenerate with respect to the SCMF wave functions created by the symmetry operation which is broken. One must superpose all these equivalent wave functions to restore symmetry.

1. Particle-number projection BCS (or HFB) states are not eigenstates of the particle-number operator

an eigenstate |Φ(N,Z)]}> of the particle-number operators with N neutrons and Z protons acts on any wave SCMF function |Ψ> with projection operators:

$|\Phi(N,Z)\rangle = \hat{P}_N \hat{P}_Z |\Psi\rangle$ where $\hat{P}_N = \frac{1}{2\pi}\int_0^{2\pi} d\phi_N \, e^{i\phi_N(\hat{N}-N)}$

Variation before or after projection

PAV: $$E_k = \frac{\langle\Phi(N,Z)|\hat{H}|\Phi(N,Z)\rangle}{\langle\Phi(N,Z)|\Phi(N,Z)\rangle}$$

2. Angular-number projection

Deformed mean-field states are not eigenstates of the total angular momentum.
An eigenstate with eigenvalue J is obtained by projecting the mean-field wave function |Ψ›

$$|\Phi, JM\rangle = \frac{\sum_K g_K \hat{P}^J_{MK}|\Psi\rangle}{\sqrt{\sum_K |g_K|^2 \langle\Psi|\hat{P}^J_{KK}|\Psi\rangle}}$$

Euler angles

rotation operator

where the projector is given by $\hat{P}^J_{MK} = \frac{2J+1}{8\pi^2} \int d\Omega\, D^{J*}_{MK}(\Omega)\, \hat{R}(\Omega)$

- Rotational Correction as approximate projection: $\boxed{E_{\text{rot}} = -\frac{\langle \hat{\mathbf{J}}^2\rangle}{2\mathcal{J}}}$

3. Center-of-mass projection

Mean field is localized in space, violating translational invariance which has to be restored by projection onto good centre-of-mass momentum zero

$$|\Phi(\mathbf{P}_{\text{cm}} = 0)\rangle = \int d^3R \exp\left(-i\mathbf{R}\cdot\hat{\mathbf{P}}_{\text{cm}}\right)|\Psi\rangle$$

- Exact projection is numerically expensive – a simple expression for a center-of-mass correction to the energy and second order in $\mathbf{P}_{\text{cm}}$

$$\boxed{E_{\text{cm}} = -\frac{\langle \hat{\mathbf{P}}^2_{\text{cm}}\rangle}{2mA}}$$

Example: GOA + HF(B) Gogny calculations

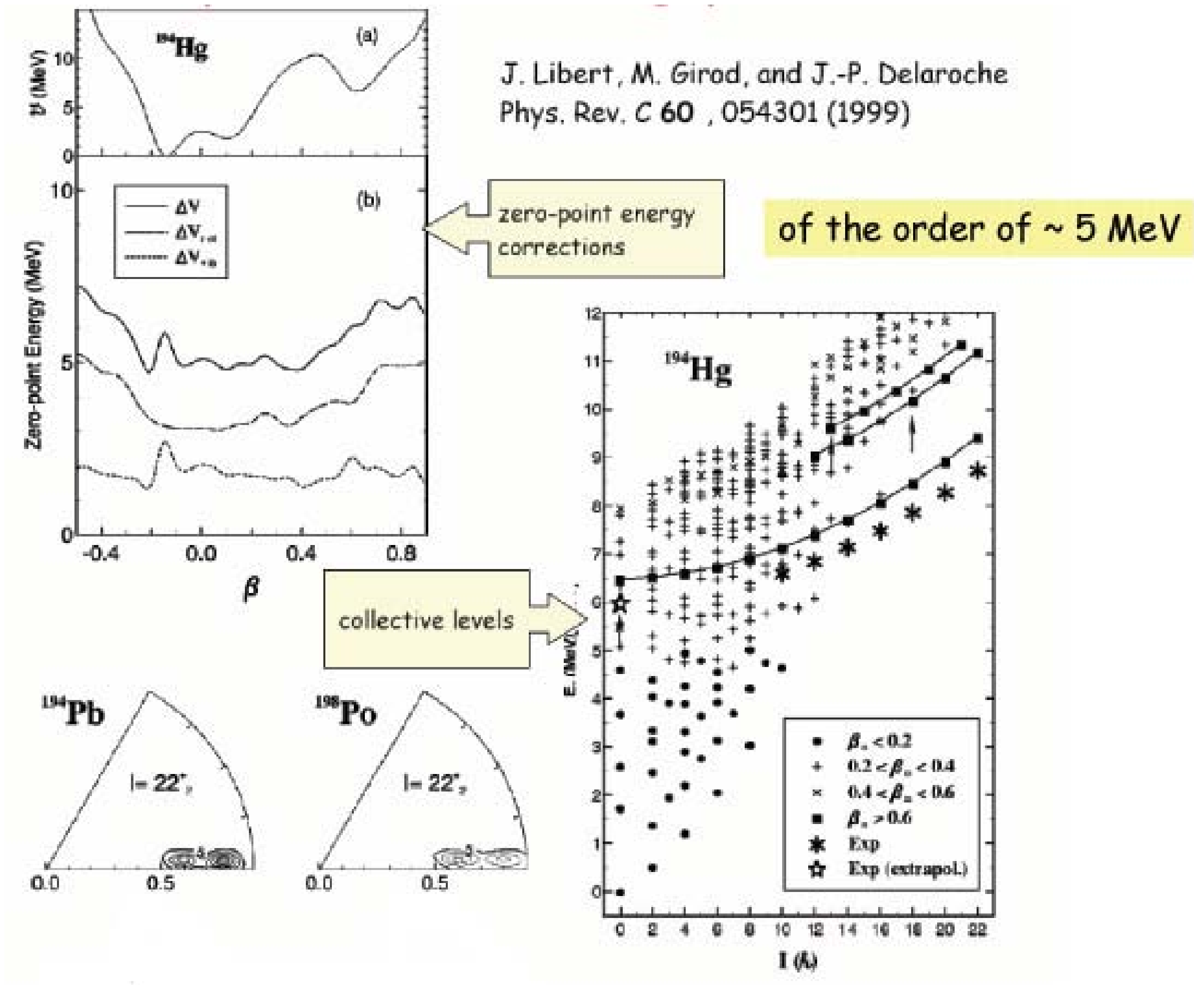

Applications

1. Binding Energies

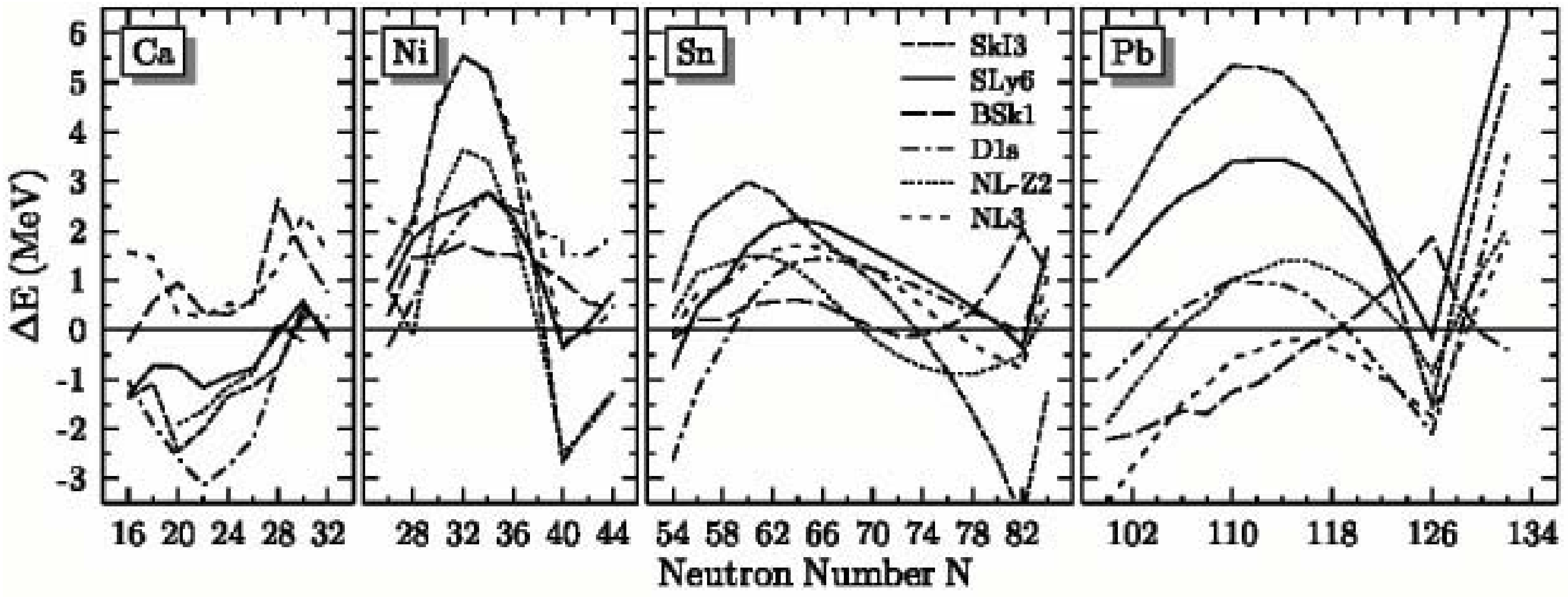

Error on the total binding energy for the isotopic chains and forces as indicated - positive (negative) **ΔE** denote underbound (overbound) nuclei with respect to experiment (results obtained by spherical mean-field calculations)

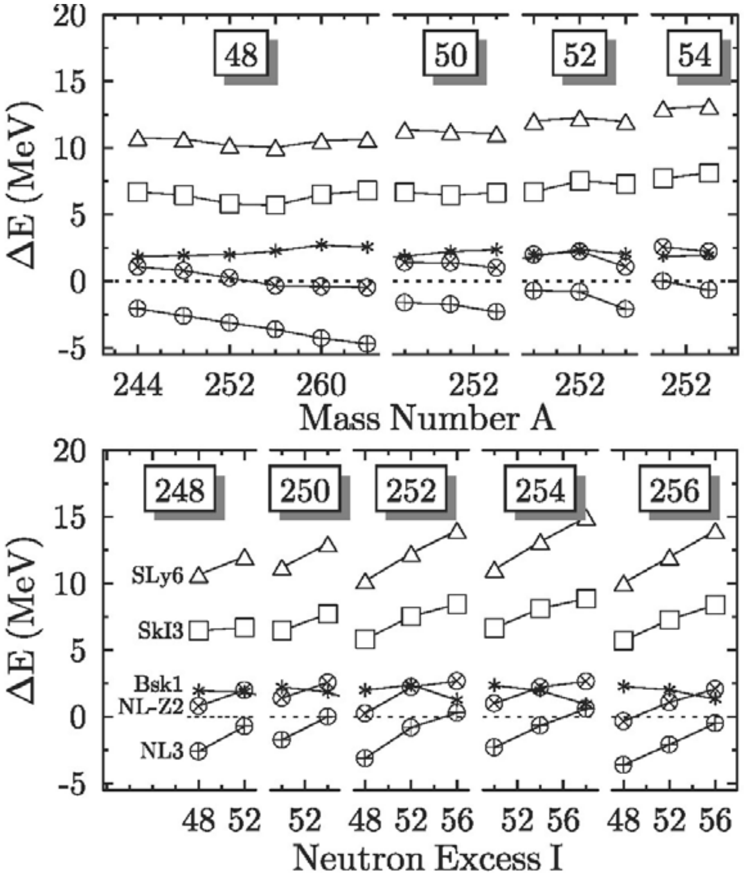

Error on the binding energy for the heaviest nuclei whose experimental mass is known: calculations include quadrupole axial deformations

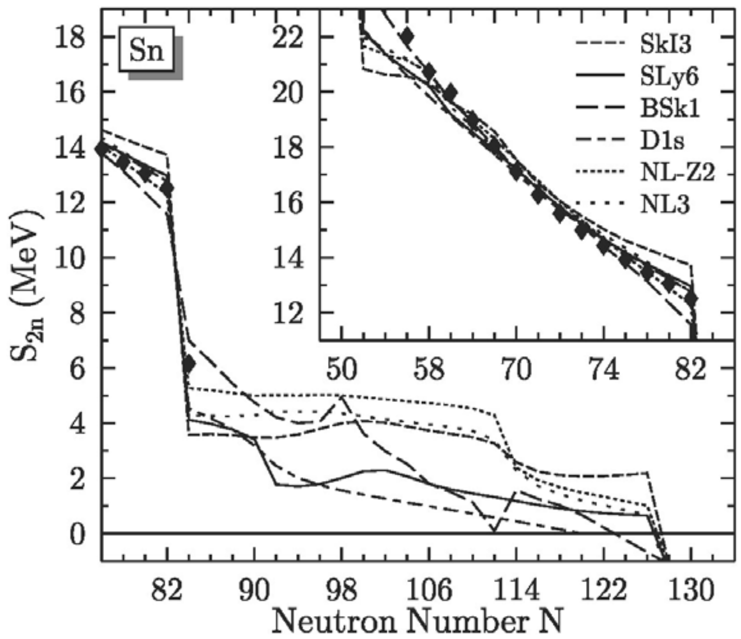

Two-neutron separation energy for the chain of Sn isotopes

2. Shell structure

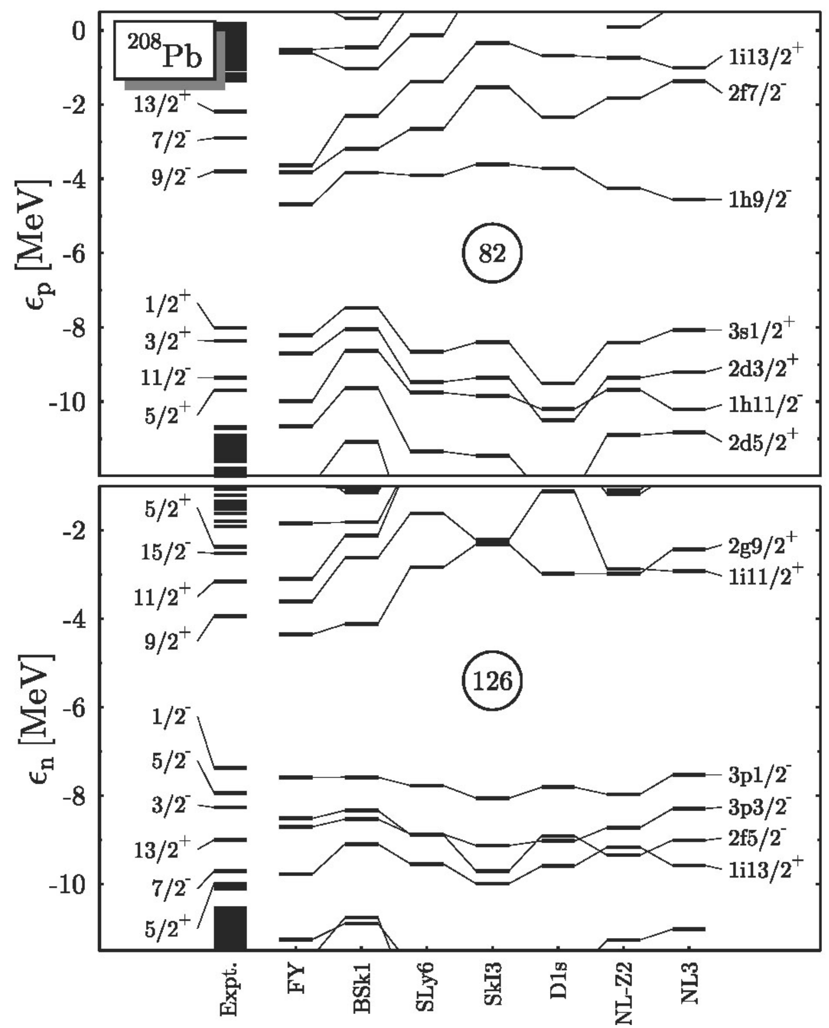

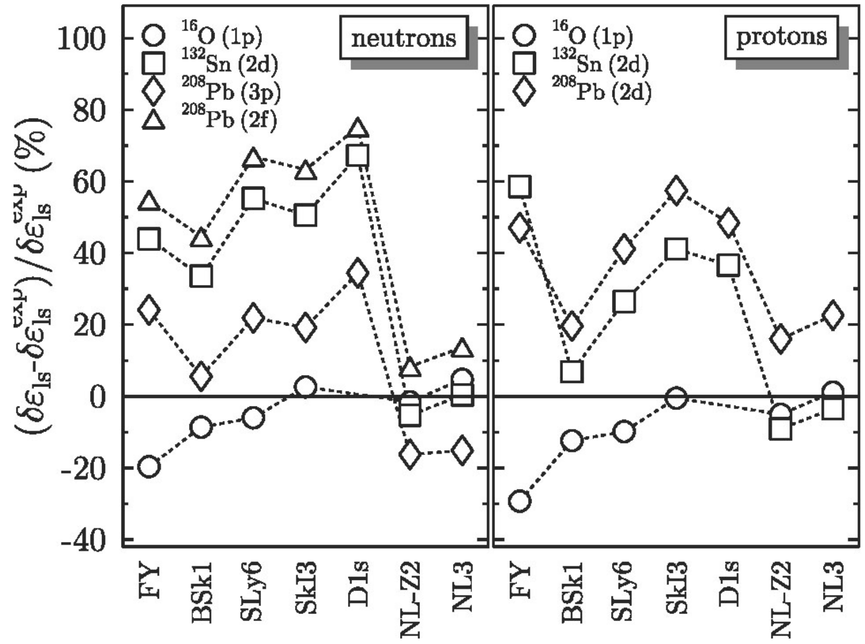

Relative error on spin-orbit
Splitting in doubly-magic nuclei

Eigenvalues ε_k of the single-particle Hamiltonian for neutrons in ^{208}Pb and ^{132}Sn calculated with Skyrme forces BSk1, SLy6 and SkI3, Gogny force D1S, and RMF forces NL3 and NL-Z2; results obtained with Folded-Yukawa model (FY) used in mic-mac models are shown for comparison

3. Observables of the Density Distribution

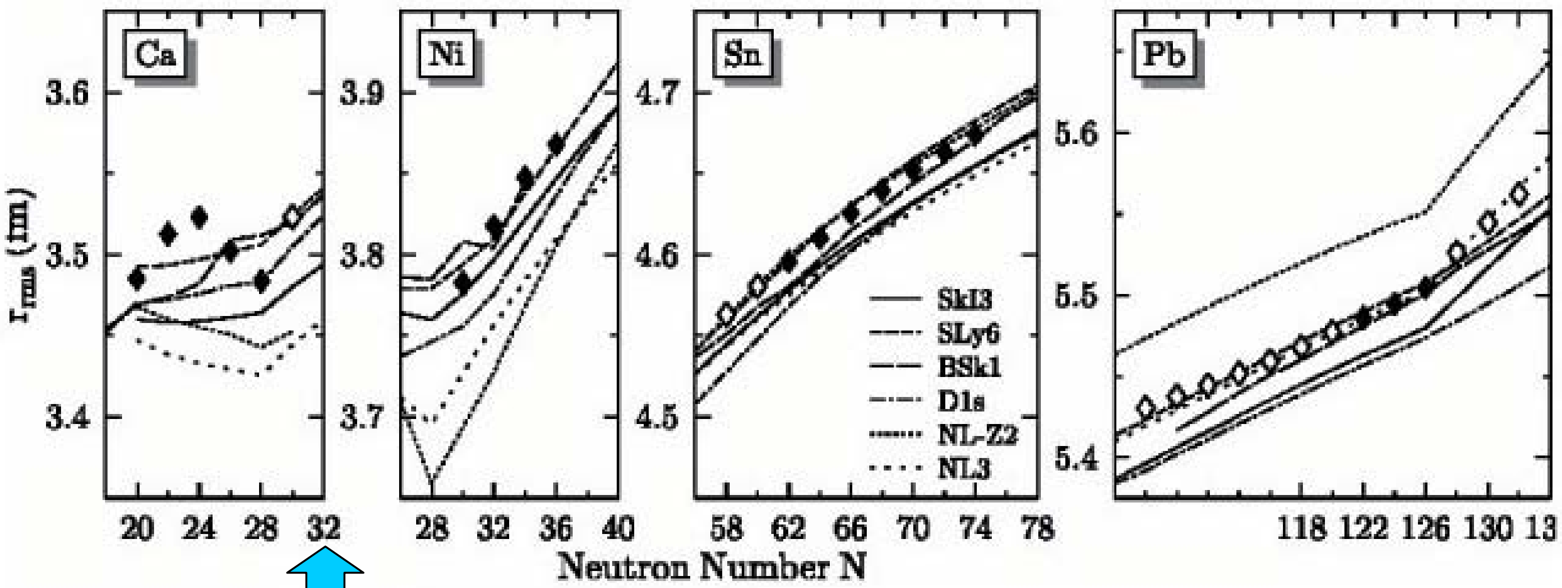

Comparison of rms radii of charge distributions from spherical mean-field calculations

- ◆ direct radius measurements;
- ◊ measurements of isotopic shifts

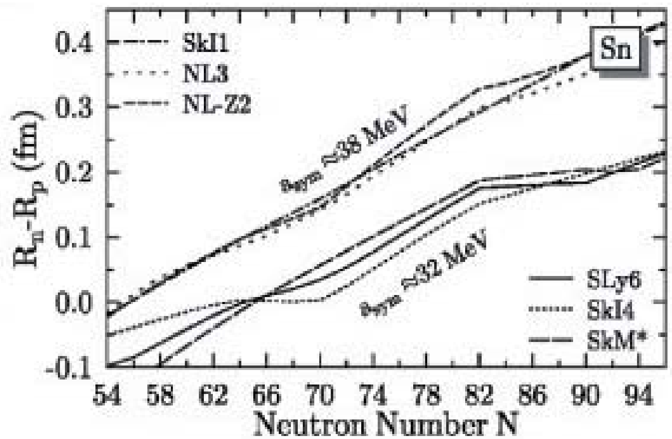

Neutron skin **Rn-Rp** along the chain of Sn isotopes: results are shown for two groups of forces, one with low and one with high asymmetry energy

4. Deformations

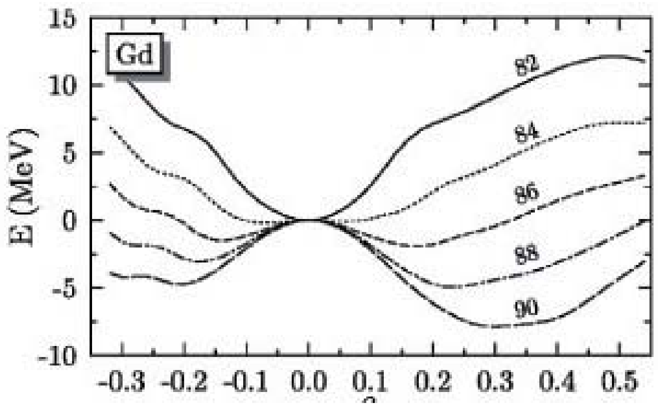

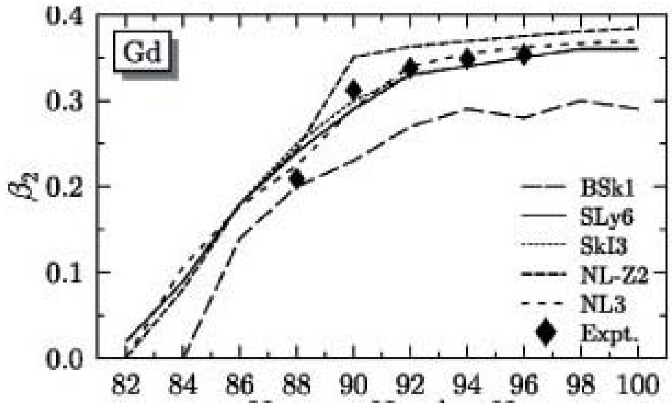

Transition from spherical to deformed shapes in the chain of Gd isotopes
Left panel: HF+BCS PES for Gd isotopes with 82 < N < 90 (SLy6 interaction)
Right panel: Ground state deformation of Gd isotopes with several forces

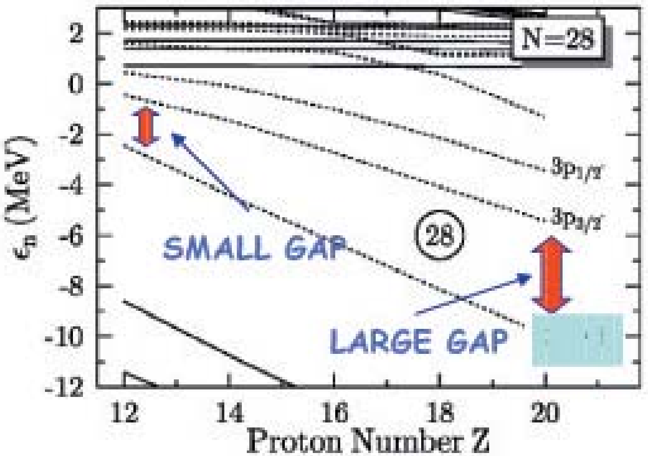

Disappearance of spherical N = 28 shell
in neutron-rich nuclei; neutron single-particle energies at spherical shape for N = 28 isotones

Fission Barriers

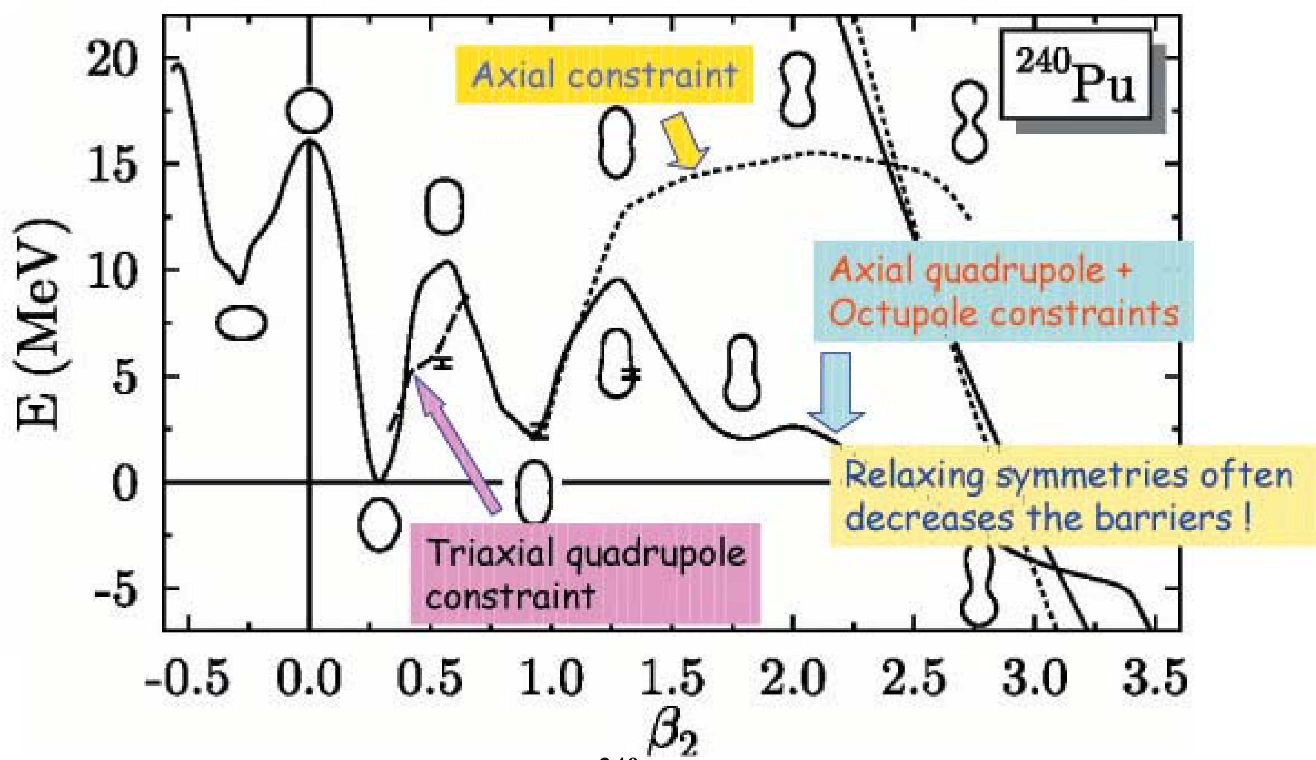

Paths in the deformation energy landscape of ^{240}Pu calculated with the SkI4 force

- solid line corresponds to axial quadrupole and octupole (reflexion asymmetric) constraints
- dashed line corresponds to triaxial quadrupole constraints
- dotted line corresponds to axial quadrupole constraint only
- two steep lines correspond to the symmetric (dotted line) and asymmetric(full line) fusion paths

5. Excitations

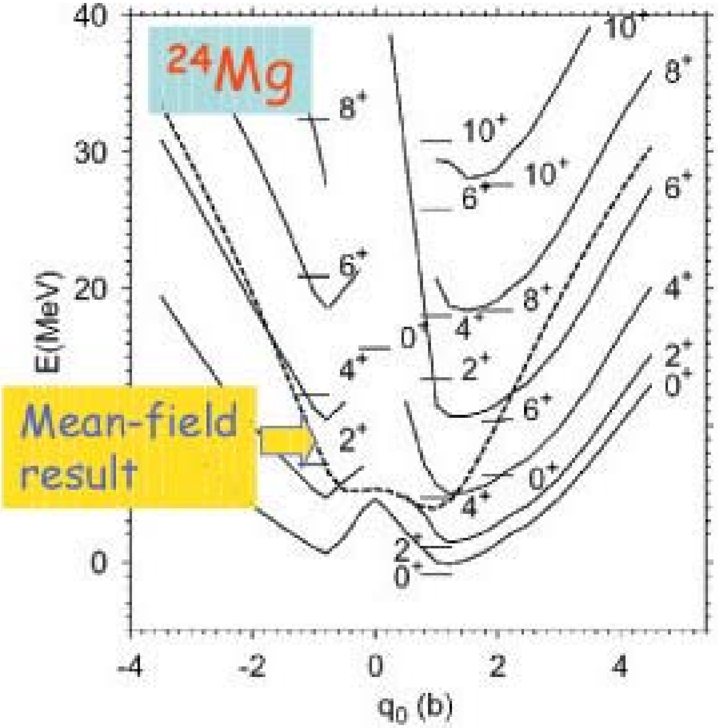

Ground-state correlations and mass sytematics

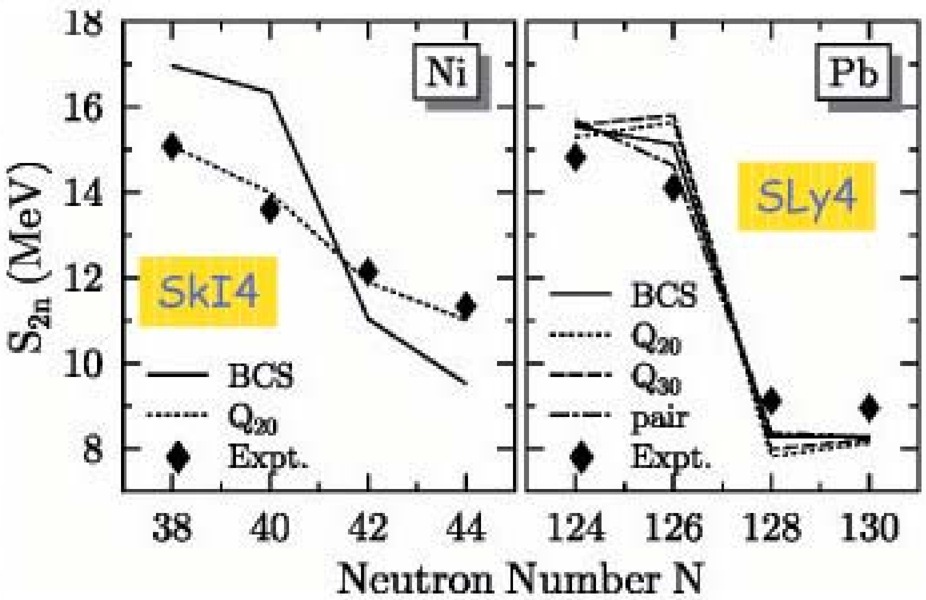

Projected ^{24}Mg PES for angular momentum J = 0 to 10, as a function of the axial quadrupole moment q_0 of the state projected.
First three energies obtained for each J in a GCM calculation: horizontal bars at the value of q_0 where the respective collective wave functions are maximum.

Influence of ground-state correlations on S_{2n} mean-field Skyrme-HF+BCS+LN calculations . Correlations beyond mean-field are included in both cases.
Ni: GOA approximation of the GCM
Pb: particle-number projected GCM calculations

Giant Resonances

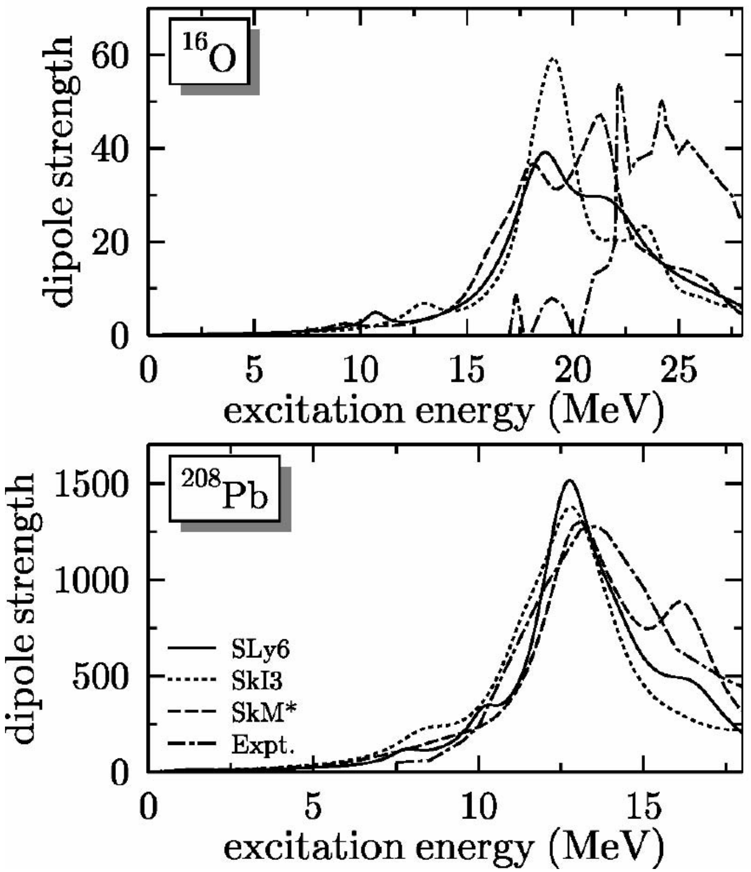

RPA results for the dipole strength distribution in ^{16}O and ^{208}Pb for various interactions. Discrete RPA spectra are folded with a Lorenzian of width 1 MeV to account roughly for escape width and collision broadening.

The peak positions of giant resonances in ^{208}P computed with RPA for various forces and compare with experimental values (all energies are given i MeV).

	$L=1, T=1$	$L=2, T=0$	$L=0, T=0$
Expt.	13.6	11.2	14.2
SIII	14.1	12.0	17.5
SkM*	13.0	11.6	14.0
SkP	12.5	10.3	13.2
SLy6	12.8	12.5	14.5
SkI3	12.7	13.7	15.3
SkI4	12.7	13.0	15.1
MSk5	11.4	10.3	14.1
SkT6	14.5	12.4	9.9
NL3	12.9	11.3	13.8

Nuclear Theory:

Self-consistent Relativistic Mean-Field Models
Structure of Heavy Nuclei

D. Vretenar

University of Zagreb

E.mail: vretenar@phy.hr

Self-consistent Relativistic Mean-Field Models

Quantum Hadrodynamics → low-energy, large-distance, effective field theory (EFT) representation of **QCD**

- models based on QHD provide a microscopic description of the nuclear many-body problem that is consistent with:

quantum mechanics

special relativity

unitarity and causality

symmetries of QCD →

Lorentz invariance
parity consevation
isospin symmetry
spontaneously broken chiral symmetry

1. MODELS WITH NON-LINEAR SELF-INTERACTIONS

system of Dirac nucleons coupled to the exchange mesons and the photon field through an effective Lagrangian

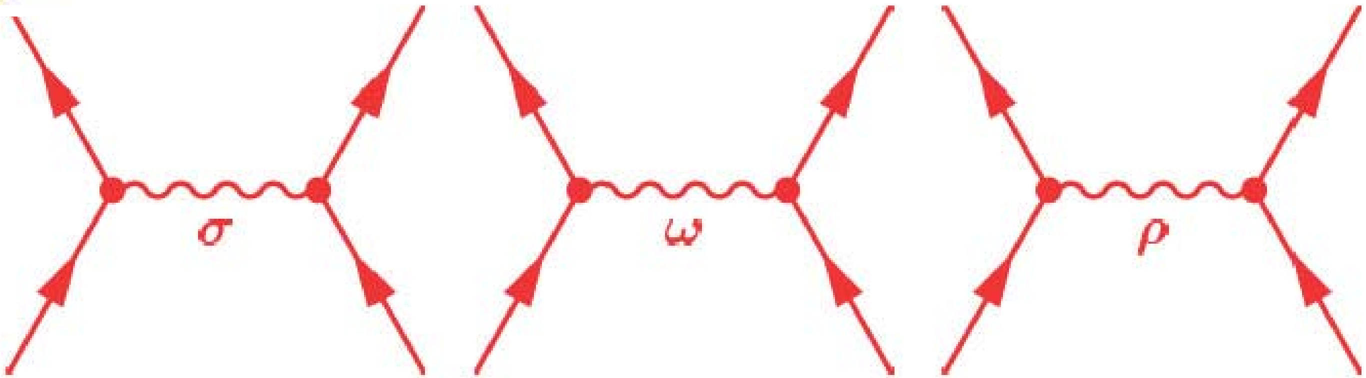

$(J^{\pi},T)=(0^{+},0)$

Sigma-meson: attractive Scalar field

$(J^{\pi},T)=(1^{-},0)$

Omega-meson: short-range repulsive field

$(J^{\pi},T)=(1^{-},1)$

Rho-meson: isovector field

Model defined by the Lagrangian density:

$$\mathcal{L} = \mathcal{L}_N + \mathcal{L}_m + \mathcal{L}_{int}$$

- Lagrangian of the free nucleon $\mathcal{L}_N = \bar{\psi}\,(i\gamma^\mu \partial_u - m)\,\psi$
- Lagrangian of the free meson fields and the electromagnetic field:

$$\begin{aligned}\mathcal{L}_m &= \frac{1}{2}\partial_\mu\sigma\partial^\mu\sigma - \frac{1}{2}m_\sigma^2\sigma^2 - \frac{1}{4}\Omega_{\mu\nu}\Omega^{\mu\nu} + \frac{1}{2}m_\omega^2\omega_\mu\omega^\mu \\ &\quad -\frac{1}{4}\vec{R}_{\mu\nu}\vec{R}^{\mu\nu} + \frac{1}{2}m_\rho^2\vec{\rho}_\mu\vec{\rho}^\mu - \frac{1}{4}F_{\mu\nu}F^{\mu\nu}\end{aligned}$$

$$\begin{aligned}\Omega_{\mu\nu} &= \partial_\mu\omega_\nu - \partial_\nu\omega_\mu \\ \vec{R}_{\mu\nu} &= \partial_\mu\vec{\rho}_\nu - \partial_\nu\vec{\rho}_\mu \\ F_{\mu\nu} &= \partial_\mu A_\nu - \partial_\nu A_\mu.\end{aligned}$$

- minimal set of interaction terms:

$$\mathcal{L}_{int} = -\bar{\psi}\Gamma_\sigma\sigma\psi - \bar{\psi}\Gamma_\omega^\mu\omega_\mu\psi - \bar{\psi}\vec{\Gamma}_\rho^\mu\vec{\rho}_\mu\psi - \bar{\psi}\Gamma_e^\mu A_\mu\psi.$$

with vertices

$$\Gamma_\sigma = g_\sigma, \quad \Gamma_\omega^\mu = g_\omega\gamma^\mu, \quad \vec{\Gamma}_\rho^\mu = g_\rho\vec{\tau}\gamma^\mu, \quad \Gamma_e^m = e\tfrac{1-\tau_3}{2}\gamma^\mu$$

Simple linear model does not provide a quantitative description of complex nuclear systems.
Effective density dependence is introduced through a non-linear potential:

$$U(\sigma) = \frac{1}{2}m_\sigma^2\sigma^2 + \frac{g_2}{3}\sigma^3 + \frac{g_3}{4}\sigma^4$$

From the Lagrangian-density model, the classical variation principle leads to the equations of motion:

time-dependent Dirac equation for the nucleon:

$$[\gamma^\mu(i\partial_\mu + V_\mu) + m + S]\,\psi = 0$$

Neglecting retardation effects for the meson fields, a self-consistent solution is obtained when the time-dependent mean-field potentials:

$$S(\mathbf{r},t) = g_\sigma\sigma(\mathbf{r},t)$$
$$V_\mu(\mathbf{r},t) = g_\omega\omega_\mu(\mathbf{r},t) + g_\rho\vec{\tau}\vec{\rho}_\mu(\mathbf{r},t) + eA_\mu(\mathbf{r},t)\frac{(1-\tau_3)}{2}$$

are calculated at each step in time from the solution of the stationary Klein-Gordon equations

$$-\Delta\phi_m + U'(\phi_m) = \pm\left\langle\bar{\psi}\Gamma_m\psi\right\rangle$$

Mean-field approximation:
meson field operators are replaced by their expectation values

No-sea approximation:
no contributions from the Dirac sea of negative energy states

Pairing correlations and relativistic Hartree-Bogoliubov theory

- Description of ground-state properties of exotic nuclei far from stability

  $\Rightarrow$ unified description of mean-field and pairing correlations

- relativistic Hartree-Bogoliubov (RHB) equations:

Pairing field

Quasiparticle energy

$$\begin{pmatrix} \hat{h}_D - m - \lambda & \hat{\Delta} \\ -\hat{\Delta}^* & -\hat{h}_D + m + \lambda \end{pmatrix} \begin{pmatrix} U_k(\mathbf{r}) \\ V_k(\mathbf{r}) \end{pmatrix} = E_k \begin{pmatrix} U_k(\mathbf{r}) \\ V_k(\mathbf{r}) \end{pmatrix}$$

Dirac Hamiltonian

chemical potential

nucleon mass

RHB equations are solved self-consistently, with potentials determined in the mean-field approximation from solutions of static Klein-Gordon equations:

$$\begin{aligned} \left[-\Delta + m_\sigma^2\right] \sigma(\mathbf{r}) &= -g_\sigma \rho_s(\mathbf{r}) - g_2 \sigma^2(\mathbf{r}) - g_3 \sigma^3(\mathbf{r}) \\ \left[-\Delta + m_\omega^2\right] \omega^0(\mathbf{r}) &= g_\omega \rho_v(\mathbf{r}) \\ \left[-\Delta + m_\rho^2\right] \rho^0(\mathbf{r}) &= g_\rho \rho_3(\mathbf{r}) \\ -\Delta A^0(\mathbf{r}) &= e \rho_p(\mathbf{r}) \end{aligned}$$

Source terms are sums of bi-linear products of nucleon amplitudes:

$$\rho_s(\mathbf{r}) = \sum_{k>0} V_k^\dagger(\mathbf{r})\gamma^0 V_k(\mathbf{r}) \qquad \rho_3(\mathbf{r}) = \sum_{k>0} V_k^\dagger(\mathbf{r})\tau_3 V_k(\mathbf{r})$$

$$\rho_v(\mathbf{r}) = \sum_{k>0} V_k^\dagger(\mathbf{r}) V_k(\mathbf{r}) \qquad \rho_{em}(\mathbf{r}) = \sum_{k>0} V_k^\dagger(\mathbf{r})\frac{1-\tau_3}{2} V_k(\mathbf{r})$$

no-sea approximation

- Gogny pairing interaction:

$$V^{pp}(1,2) = \sum_{i=1,2} e^{-((\mathbf{r}_1-\mathbf{r}_2)/\mu_i)^2}\,(W_i + B_i P^\sigma - H_i P^\tau - M_i P^\sigma P^\tau)$$

EFFECTIVE INTERACTIONS

model parameters: meson masses m_σ, m_ω, m_ρ, meson-nucleon coupling constants g_σ, g_ω, g_ρ, nonlinear self-interactions coupling constants g_2, g_3 ...

- mean-field model does not contain explicit correlation effects – parameters are determined from the properties of nuclear matter (symmetric and asymmetric) and bulk properties of finite nuclei (binding energies, charge radii, neutron radii, surface thickeness ...)

Least-squares adjustment to empirical nuclear matter properties and experimental data on ground-state properties of spherical nuclei constrains only six or seven parameters in the general expansion of an effective Lagrangian

calculated values

exp. data

Minimization of

$$\chi^2 = \sum_i \frac{(O_i^{\mathrm{th}} - O_i^{\mathrm{expt}})^2}{(\Delta O_i)^2}$$

assumed errors

- Uncorrelated error of a parameter is the allowed variation of that isolated parameter (while all other parameters are kept fixed) which enhances χ^2 just by a value of 1

- Correlated error of a parameter is the allowed change of that parameter, i.e. within χ^2+1, if all the other parameters are readjusted

Correlated and uncorrelated error of a particular parameter would be the same if that parameter was completely independent from all other parameters

Ground-state properties of Ni and Sn isotopes

Combination of the NL3 effective interaction for the RMF Lagrangian, and the Gogny interaction with the parameter set D1S in the pairing channel

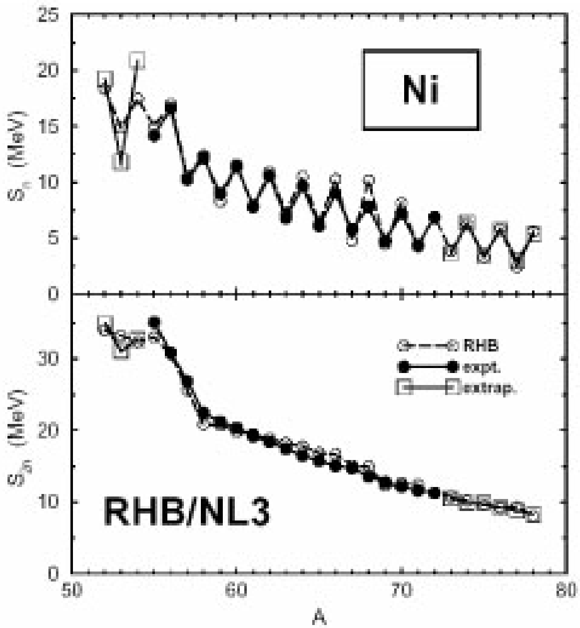

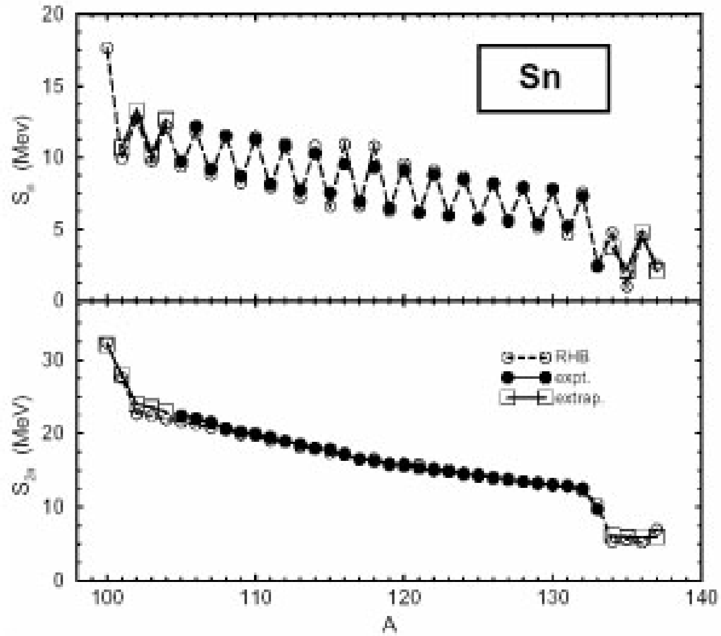

One- and two-neutron separation energies

$$S_n(Z,N) = B_n(Z,N) - B_n(Z,N-1)$$
$$S_{2n}(Z,N) = B_n(Z,N) - B_n(Z,N-2)$$

Differences between RHB model and experimental binding energies for Ni and Sn isotopes

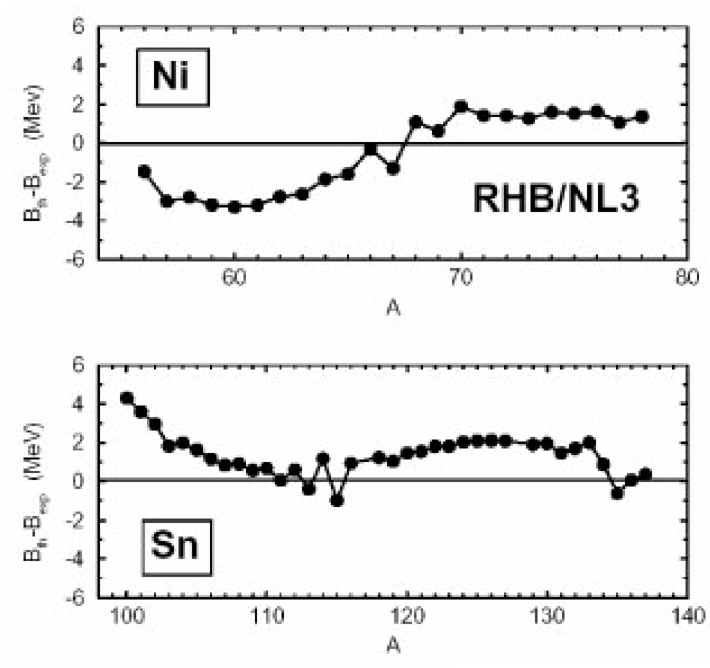

Self-consistent RHB single-neutron density distributions

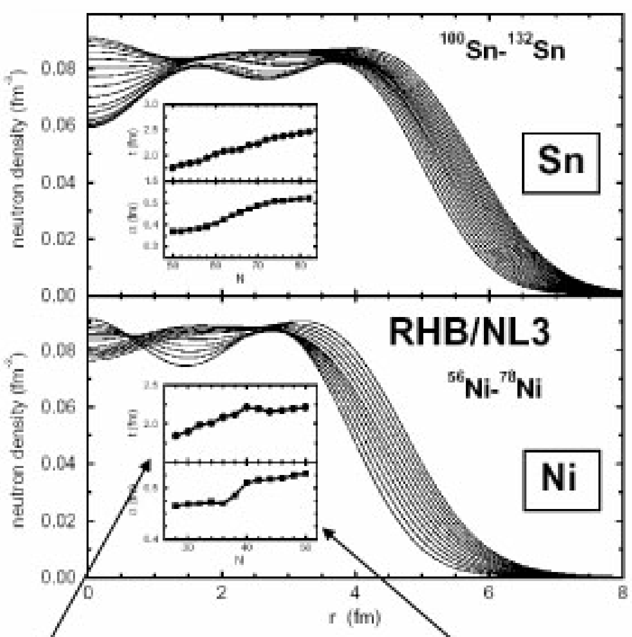

surface thickness

surface diffuseness α

$$\rho(r) = \rho_0 \left(1 + exp(\frac{r-R_0}{\alpha})\right)^{-1}$$

Reduction of the spin-orbit potential in neutron-rich nuclei

Spin-orbit potential originates from the addition of two large fields - field of the vector mesons (short range repulsion), and scalar field of the sigma meson (intermediate attraction)

First order approximation, and assuming spherical symmetry: spin-orbit term can be written as

$$V_{s.o.} \approx \frac{1}{r}\frac{\partial}{\partial r}V_{ls}(r)$$

$$V_{ls} = \frac{m}{m_{eff}}(V - S)$$

Weakening of the effective single-neutron spin-orbit potential in neutron-rich isotopes is reflected in the calculated energy spacings between spin-orbit

$$\boxed{\Delta E_{ls} = E_{n,l,j=l-1/2} - E_{n,l,j=l+1/2}}$$

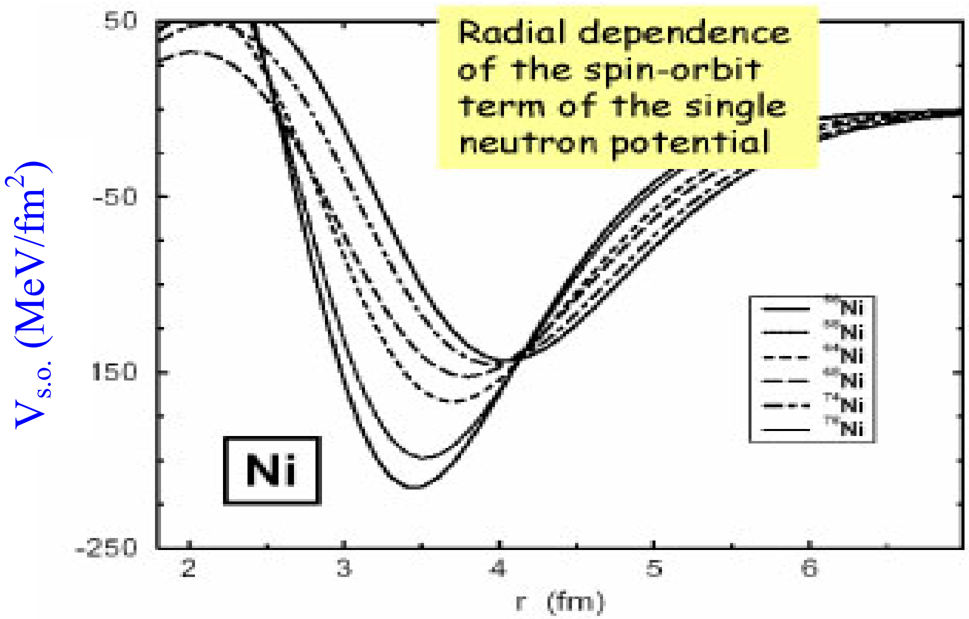

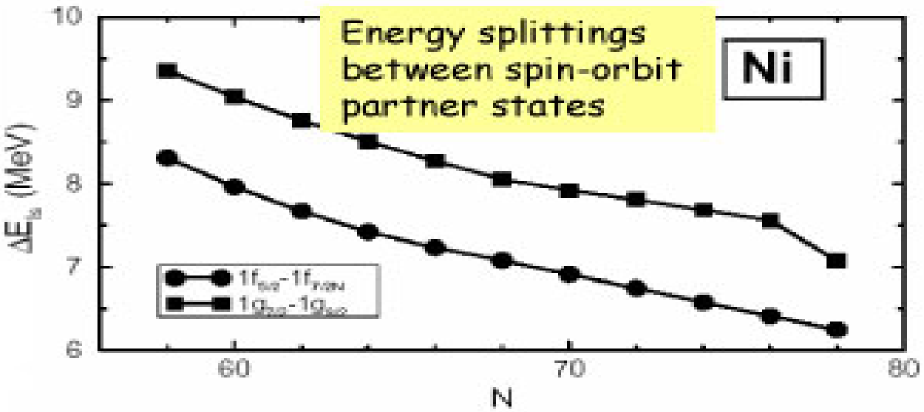

2. MODELS WITH DENSITY-DEPENDENT MESON-NUCLEON COUPLINGS

A. LAGRANGIAN

$$
\begin{aligned}
\mathcal{L} \;=\; & \bar{\psi}\,(i\gamma\cdot\partial - m)\,\psi \;+\; \frac{1}{2}(\partial\sigma)^2 - \frac{1}{2}m_\sigma\sigma^2 \\
& - \frac{1}{4}\Omega_{\mu\nu}\Omega^{\mu\nu} + \frac{1}{2}m_\omega^2\omega^2 \;-\; \frac{1}{4}\vec{R}_{\mu\nu}\vec{R}^{\mu\nu} + \frac{1}{2}m_\rho^2\vec{\rho}^{\,2} \;-\; \frac{1}{4}F_{\mu\nu}F^{\mu\nu} \\
& - g_\sigma\bar{\psi}\sigma\psi \;-\; g_\omega\bar{\psi}\gamma\cdot\omega\psi \;-\; g_\rho\bar{\psi}\gamma\cdot\vec{\rho}\vec{\tau}\psi \;-\; e\bar{\psi}\gamma\cdot A\frac{(1-\tau_3)}{2}\psi
\end{aligned}
$$

B. DENSITY DEPENDENCE OF THE COUPLINGS

Meson-nucleon couplings g_σ, g_ω, g_ρ $\longrightarrow$ functions of Lorentz-scalar bi-linear forms of the nucleon operators; simplest choice

a) functions of the vector density $\quad \rho_v = \sqrt{j_\mu j^\mu} \qquad j_\mu = \bar{\psi}\gamma_\mu\psi$

b) functions of the scalar density $\quad \rho_s = \bar{\psi}\psi$

a) is a more natural choice.
$\int \rho_v\, d^3r$ = baryon number (conserved quantity)
ρ_s is a dynamical quantity (determined by the selfconsistency condition $\partial\,\varepsilon/\partial M^* = 0$ in nuclear matter)

C. MESON FIELD EQUATIONS

$$
\begin{aligned}
(-\Delta + m_\sigma)\sigma(\mathbf{r}) &= -g_\sigma(\rho_v)\rho_s(\mathbf{r}) \\
(-\Delta + m_\omega)\omega(\mathbf{r}) &= g_\omega(\rho_v)\rho_v(\mathbf{r}) \\
(-\Delta + m_\rho)\rho_3(\mathbf{r}) &= g_\rho(\rho_v)(\rho_n(\mathbf{r}) - \rho_p(\mathbf{r}))
\end{aligned}
$$

D. SINGLE-NUCLEON DIRAC EQUATION

Variation of the Lagrangian: $\frac{\delta \mathcal{L}}{\delta \bar{\psi}} = \frac{\partial \mathcal{L}}{\partial \bar{\psi}} + \frac{\partial \mathcal{L}}{\partial \rho_v}\frac{\delta \rho_v}{\delta \bar{\psi}}$

Second term produces rearrangement contributions to the vector self-energy:

$$\frac{\delta \rho_v}{\delta \bar{\psi}} = \frac{j_\mu \gamma^\mu}{\rho_v}\psi \qquad\qquad \frac{\partial \mathcal{L}}{\partial \rho_v} \Rightarrow \frac{\partial g_\sigma}{\partial \rho_v}, \frac{\partial g_\omega}{\partial \rho_v}, \frac{\partial g_\rho}{\partial \rho_v}$$

$$\left[\gamma^\mu (i\partial_\mu - \Sigma_\mu) - (m - \Sigma)\right]\psi = 0$$

nucleon self-energies:
$$
\begin{aligned}
&\Sigma = g_\sigma \sigma \\
&\Sigma_\mu = g_\omega \omega_\mu + g_\rho \vec{\tau} \cdot \vec{\rho}_\mu + e\frac{(1-\tau_3)}{2}A_\mu + \Sigma_\mu^R
\end{aligned}
$$

inclusion of the rearrangment self-energy:

$$\Sigma_\mu^R = \frac{j_\mu}{\rho_v}\left(\frac{\partial g_\omega}{\partial \rho_v}\bar{\psi}\gamma^\nu \psi \omega_\nu + \frac{\partial g_\rho}{\partial \rho_v}\bar{\psi}\gamma^\nu \vec{\tau}\psi \cdot \vec{\rho}_\nu + \frac{\partial g_\sigma}{\partial \rho_v}\bar{\psi}\psi\sigma\right)$$

Essential for:

a) energy-momentum conservation $\partial_\mu T^{\mu\nu} = 0$

b) thermodynamic consistency of the model $\rho_B^2 \frac{\partial}{\partial \rho_B}\left(\frac{\varepsilon}{\rho_B}\right) = \frac{1}{3}\sum_{i=1}^{3} T^{ii}$

requires equality of the pressure obtained from the thermodynamic definition and from the energy-momentum tensor ($\boldsymbol{\varepsilon = T^{00}}$, $\boldsymbol{\rho B = (2/3\pi^2)\, k_F^3}$)

E. PARAMETERIZATION OF THE DENSITY DEPENDENCE

MICROSCOPIC: Dirac-Brueckner calculations of nucleon self-energies in symmetric and asymmetric nuclear matter

PHENOMENOLOGIC:
$$g_i(\rho) = g_i(\rho_{\rm sat}) f_i(x) \qquad f_i(x) = a_i \frac{1+b_i(x+d_i)^2}{1+c_i(x+d_i)^2} \qquad i = \sigma, \omega$$
$$g_\rho(\rho) = g_\rho(\rho_{\rm sat})\, \exp\left[-a_\rho(x-1)\right] \qquad x = \rho/\rho_{\rm sat}$$

Density dependence of the couplings of σ-, ω- and ρ-meson

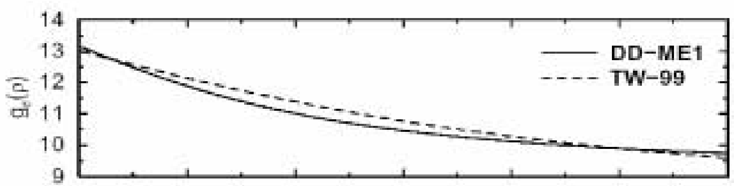

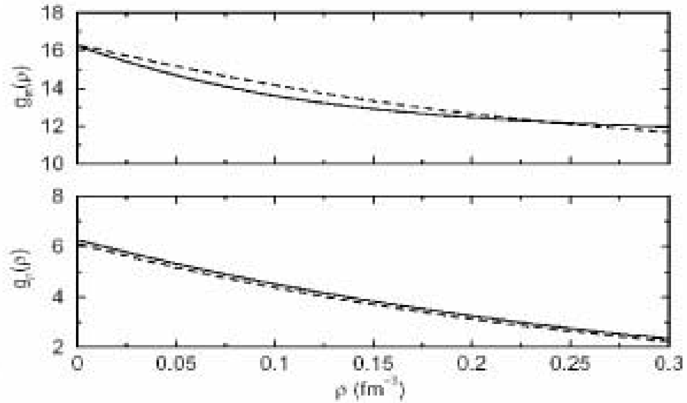

NUCLEAR MATTER EQUATION OF STATE: Binding energy per nucleon for symmetric nuclear matter as a function of the baryon density

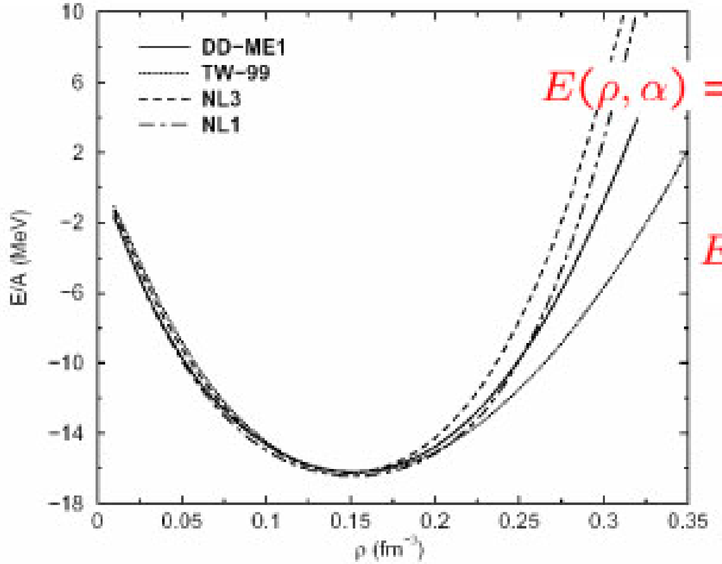

$$E(\rho,\alpha) = E(\rho,0) + S_2(\rho)\alpha^2 + S_4(\rho)\alpha^4 + \cdots$$

$$\alpha \equiv \frac{N-Z}{N+Z}$$

$$E(\rho,0) = -a_v + \frac{K_0}{18\rho_{\mathrm{sat}}^2}\,(\rho-\rho_{\mathrm{sat}})^2 + \ldots$$

ASYMMETRIC ENERGY

$$S_2(\rho) = a_4 + \frac{p_0}{\rho_{\mathrm{sat}}^2}\,(\rho-\rho_{\mathrm{sat}}) + \frac{\Delta K_0}{18\rho_{\mathrm{sat}}^2}\,(\rho-\rho_{\mathrm{sat}})^2 + \cdots$$

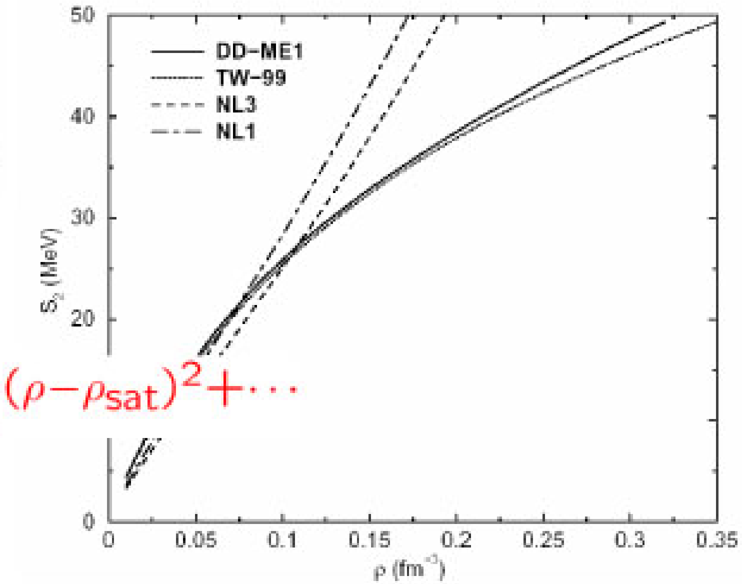

F. GROUND-STATE PROPERTIES OF FINITE NUCLEI

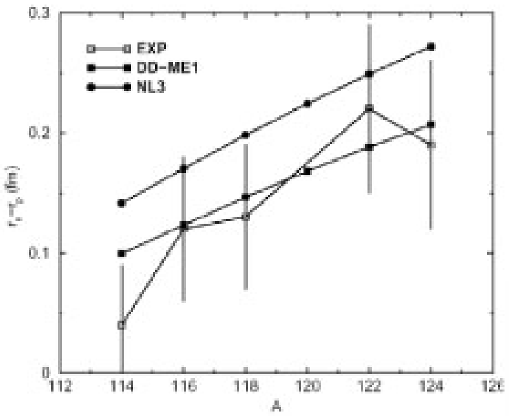

Differences between neutron and proton radii of ground-state distributions of Sn isotopes

Binding energies, charge isotope shifts and quadrupole deformations of Gd, Dy and Er isotopes

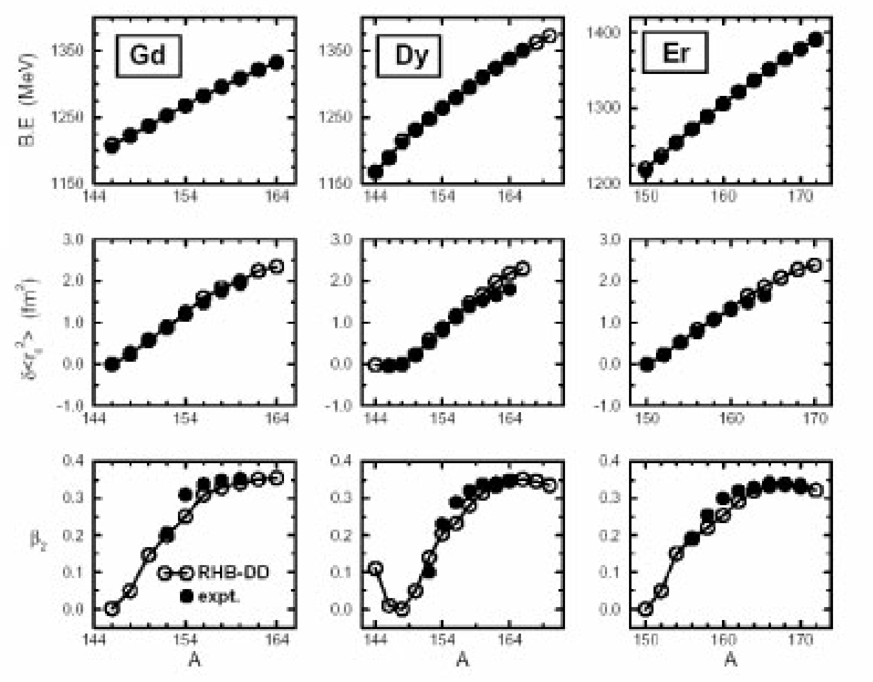

Charge isotope shifts in even-A Pb isotopes

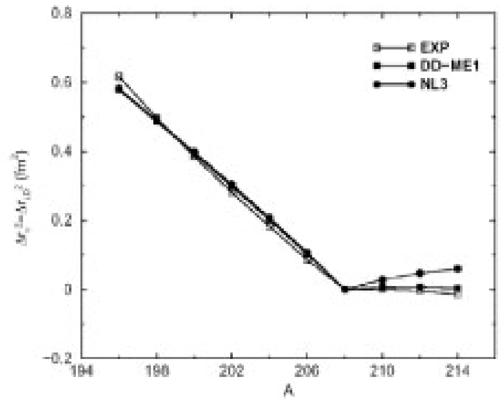

3. RELATIVISTIC POINT-COUPLING MODELS

Is the explicit meson-exchange representation of QHD necessary for a quantitative description of finite nuclei ?

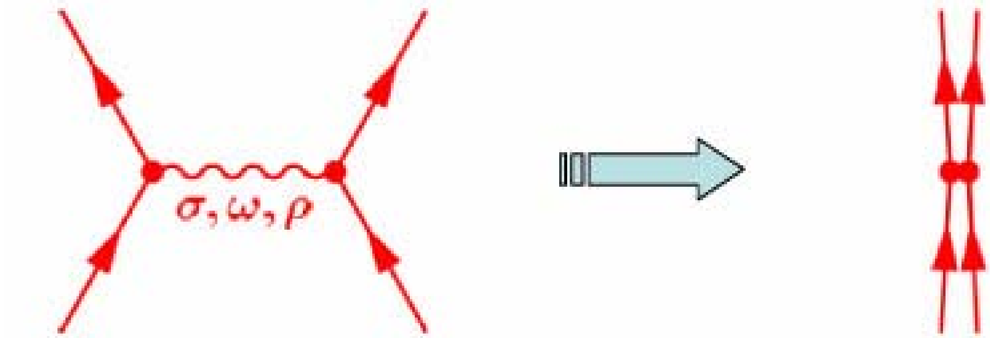

FINITE RANGE   CONTACT INTERACTION

A. Lagrangian

Elementary building blocks of the point-coupling vertices are two-fermion terms of the general type

$$\bar{\psi}\mathcal{O}_\tau\Gamma\psi \qquad \mathcal{O}_\tau \in \{1, \tau_i\} \qquad \Gamma \in \{1, \gamma_\mu, \gamma_5, \gamma_5\gamma_\mu, \sigma_{\mu\nu}\}$$

10 building blocks characterized by their transformation character in isospin and spacetime; interactions $\longrightarrow$ products of the elementary building blocks to a given order, and derivative terms in the Lagrangian simulate to some extent the effect of finite range

Four-fermion vertices:

isoscalar-scalar: $(\bar\psi\psi)^2$

isovector-scalar: $(\bar\psi\vec\tau\psi)\cdot(\bar\psi\vec\tau\psi)$

isoscalar-vector: $(\bar\psi\gamma_\mu\psi)(\bar\psi\gamma^\mu\psi)$

isovector-vector: $(\bar\psi\vec\tau\gamma_\mu\psi)\cdot(\bar\psi\vec\tau\gamma^\mu\psi)$

higher-order terms: $(\bar\psi\psi)^3 \quad (\bar\psi\psi)^4 \quad [(\bar\psi\gamma_\mu\psi)(\bar\psi\gamma^\mu\psi)]^2$

Lagragian of the point-coupling model:

$$
\begin{aligned}
\mathcal{L} &= \mathcal{L}^{\mathrm{free}} + \mathcal{L}^{\mathrm{4f}} + \mathcal{L}^{\mathrm{hot}} + \mathcal{L}^{\mathrm{der}} + \mathcal{L}^{\mathrm{em}} \\
\mathcal{L}^{\mathrm{free}} &= \bar\psi(\mathrm{i}\gamma_\mu\partial^\mu - m)\psi \\
\mathcal{L}^{\mathrm{4f}} &= -\frac{1}{2}\alpha_{\mathrm{S}}(\bar\psi\psi)(\bar\psi\psi) - \frac{1}{2}\alpha_{\mathrm{V}}(\bar\psi\gamma_\mu\psi)(\bar\psi\gamma^\mu\psi) \\
&\quad -\frac{1}{2}\alpha_{\mathrm{TS}}(\bar\psi\vec\tau\psi)\cdot(\bar\psi\vec\tau\psi) - \frac{1}{2}\alpha_{\mathrm{TV}}(\bar\psi\vec\tau\gamma_\mu\psi)\cdot(\bar\psi\vec\tau\gamma^\mu\psi) \\
\mathcal{L}^{\mathrm{hot}} &= -\frac{1}{3}\beta_{\mathrm{S}}(\bar\psi\psi)^3 - \frac{1}{4}\gamma_{\mathrm{S}}(\bar\psi\psi)^4 - \frac{1}{4}\gamma_{\mathrm{V}}[(\bar\psi\gamma_\mu\psi)(\bar\psi\gamma^\mu\psi)]^2 \\
\mathcal{L}^{\mathrm{der}} &= -\frac{1}{2}\delta_{\mathrm{S}}(\partial_\nu\bar\psi\psi)(\partial^\nu\bar\psi\psi) - \frac{1}{2}\delta_{\mathrm{V}}(\partial_\nu\bar\psi\gamma_\mu\psi)(\partial^\nu\bar\psi\gamma^\mu\psi) \\
&\quad -\frac{1}{2}\delta_{\mathrm{TS}}(\partial_\nu\bar\psi\vec\tau\psi)\cdot(\partial^\nu\bar\psi\vec\tau\psi) \\
&\quad -\frac{1}{2}\delta_{\mathrm{TV}}(\partial_\nu\bar\psi\vec\tau\gamma_\mu\psi)\cdot(\partial^\nu\bar\psi\vec\tau\gamma^\mu\psi) \\
\mathcal{L}^{\mathrm{em}} &= -eA_\mu\bar\psi[(1-\tau_3)/2]\gamma^\mu\psi - \frac{1}{4}F_{\mu\nu}F^{\mu\nu}
\end{aligned}
$$

Interaction terms in the Lagrangian are expressed in terms of the local densities (mean-field and no-sea approximations):

isoscalar-scalar:

$$\rho_S(\vec{r}) = \sum_\alpha \bar{\phi}_\alpha(\vec{r})\phi_\alpha(\vec{r})$$

isoscalar-vector:

$$\rho_V(\vec{r}) = \sum_\alpha \bar{\phi}_\alpha(\vec{r})\gamma_0\phi_\alpha(\vec{r})$$

isovector-scalar:

$$\rho_{TS}(\vec{r}) = \sum_\alpha \bar{\phi}_\alpha(\vec{r})\tau_3\phi_\alpha(\vec{r})$$

isovector-vector:

$$\rho_{TV}(\vec{r}) = \sum_\alpha \bar{\phi}_\alpha(\vec{r})\tau_3\gamma_0\phi_\alpha(\vec{r})$$

B. Equations of Motion

$$\begin{aligned}\gamma_0\varepsilon_\alpha\phi_\alpha \;=\; & (i\vec{\gamma}\cdot\vec{\partial} + m + V_S + V_V\gamma_0 + V_{TS}\tau_3 \\ & + V_{TV}\tau_3\gamma_0 + V_C\frac{1-\tau_3}{2}\gamma_0)\phi_\alpha\end{aligned}$$

$$V_S = \alpha_S\rho_S + \beta_S\rho_S^2 + \gamma_S\rho_S^3 + \delta_S\Delta\rho_S \qquad V_{TS} = \alpha_{TS}\rho_{TS} + \delta_{TS}\Delta\rho_{TS}$$

$$V_V = \alpha_V\rho_V + \gamma_V\rho_V^3 + \delta_V\Delta\rho_V \qquad V_{TV} = \alpha_{TV}\rho_{TV} + \delta_{TV}\Delta\rho_{TV}$$

C. Relation to meson-exchange finite range models

$$(-\Delta + m_\sigma^2)\sigma = -g_\sigma\rho_S \qquad \Rightarrow \qquad V_\sigma = g_\sigma\sigma$$

$$\frac{-g_\sigma^2}{-\Delta + m_\sigma^2}\rho_S \approx \underbrace{\frac{-g_\sigma^2}{m_\sigma^2}}_{\alpha_S}\rho_S + \underbrace{\frac{-g_\sigma^2}{m_\sigma^4}}_{\delta_S}\Delta\rho_S \Rightarrow$$

$$m_\sigma^2 = \alpha_S/\delta_S$$

$$g_\sigma^2 = -\alpha_S^2/\delta_S$$

Bulk properties of nuclear matter: point-coupling and meson-exchange interactions

	PC–F1	PC–LA	NL-Z2	NL3
ρ_0 (fm^{-3})	0.151	0.148	0.151	0.148
E/A (MeV)	-16.17	-16.126	-16.07	-16.24
m^*/m	0.61	0.575	0.583	0.595
K (MeV)	270	264	172	272
a_{sym} (MeV)	37.8	37.194	39.0	37.4

Deviation of the calculated energies from the experimental values: Ca, Ni, Sn and Pb isotopic chains

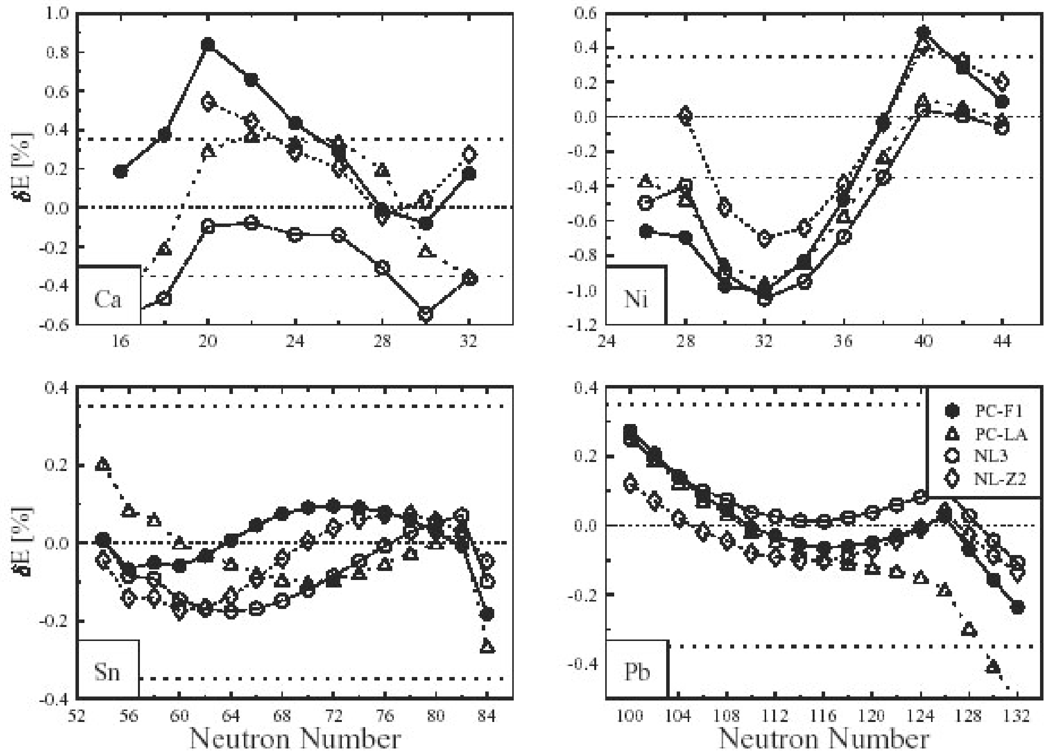

4. Applications

A. Proton-rich nuclei and the proton drip-line

characterized by exotic ground-state decay modes such as the direct emission of charged particles and β-decays with large Q-values; many proton-rich nuclei play an important role in the process of nucleosynthesis by rapid-proton capture

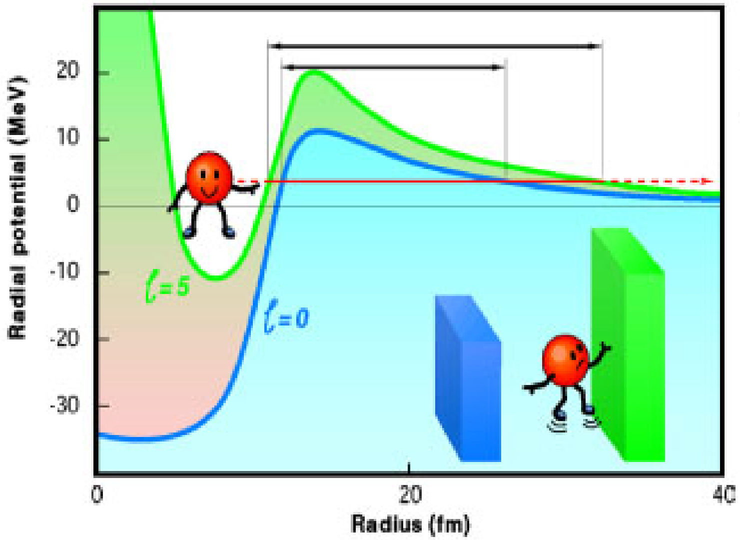

RHB calculation of proton-rich nuclei (NL3+D1S interaction)

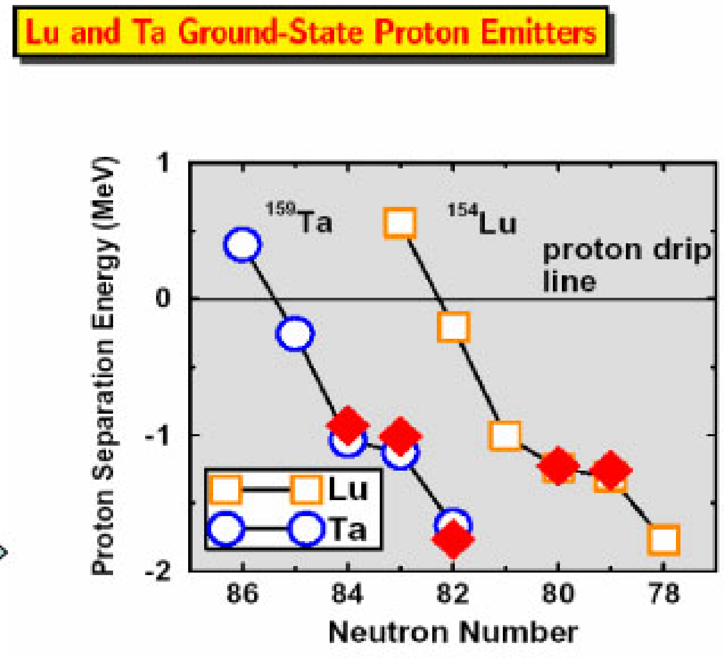

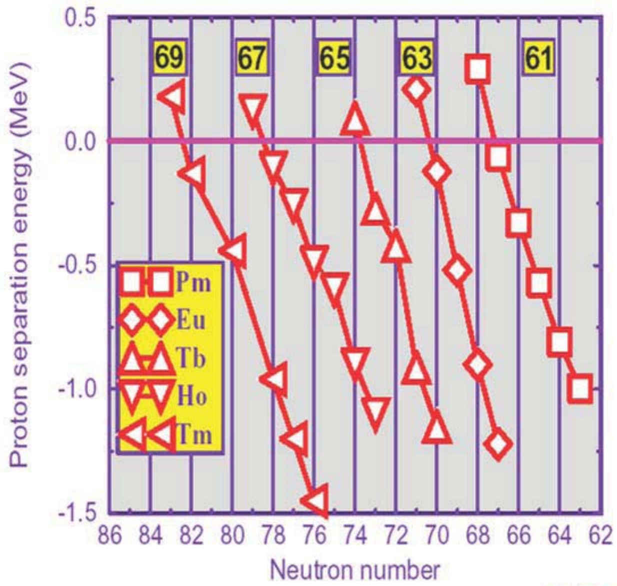

DEFORMED PROTON EMITTERS

separation energy

deformation

odd-proton orbital

spectroscopic factor

	N	S_p	β_2	p-orbital	u^2	E_p *exp.*
^{124}Pm	63	-1.00	0.35	$5/2^-[532]$	0.72	
^{125}Pm	64	-0.81	0.35	$5/2^-[532]$	0.74	
^{130}Eu	67	-1.22	0.34	$5/2^-[532]$	0.44	
^{131}Eu	68	-0.90	0.35	$5/2^+[413]$	0.44	0.950(8)
^{135}Tb	70	-1.15	0.34	$3/2^+[411]$	0.62	
^{136}Tb	71	-0.90	0.32	$3/2^+[411]$	0.65	
^{140}Ho	73	-1.10	0.31	$7/2^-[523]$	0.61	
^{141}Ho	74	-0.90	0.32	$7/2^-[523]$	0.64	1.169(8)
^{145}Tm	76	-1.43	0.23	$7/2^-[523]$	0.47	1.728(10)
^{146}Tm	77	-1.20	-0.21	$7/2^-[523]$	0.50	1.120(10)
^{147}Tm	78	-0.96	-0.19	$7/2^-[523]$	0.55	1.054(19)

Ground-state properties of probable proton-emitters; results of RHB model calculations (NL3+D1S interaction) are compared with experimental data

The proton drip-line in the sub-uranium region

Possible ground-state proton emitters in this mass region?

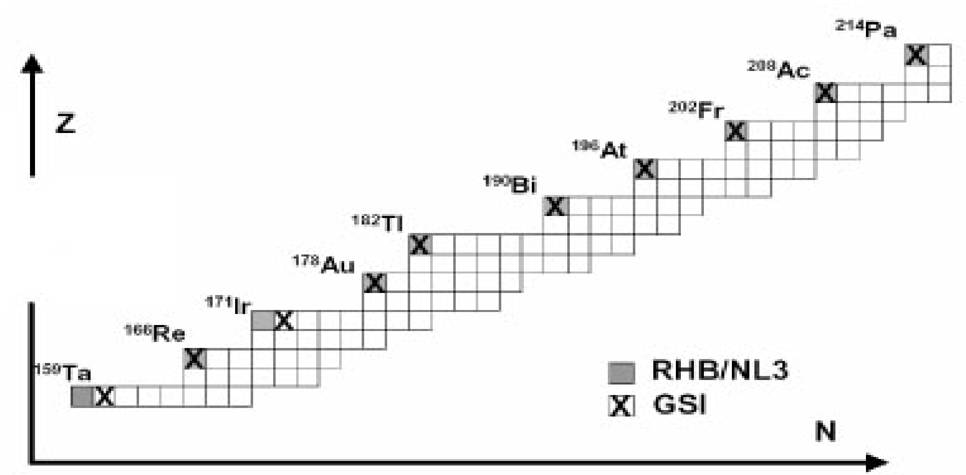

The proton drip-line in the region of superheavy elements

How far is the proton-drip line from the experimentally known superheavy nuclei?

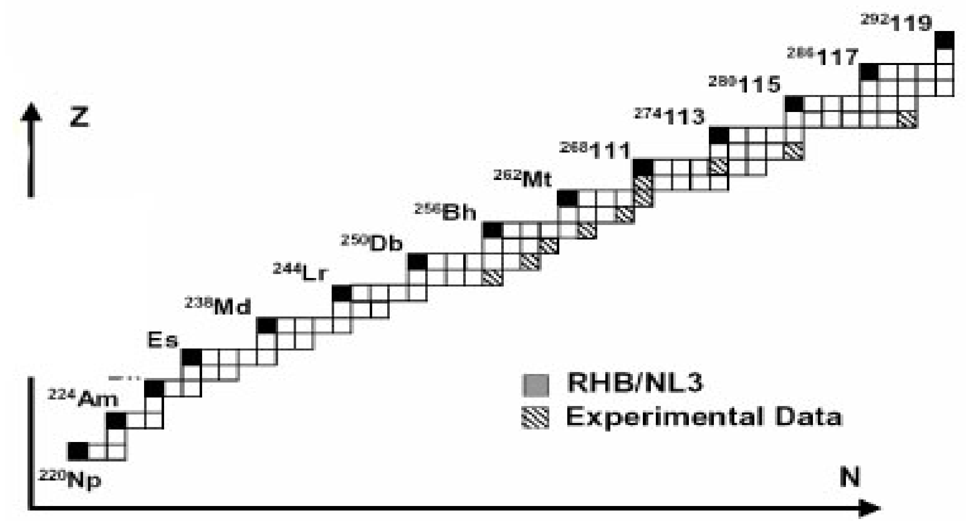

Shape coexistence in the deformed N = 28 region

RHB description of neutron rich N = 28 nuclei; NL3+D1S effective interaction.

Strong suppression of the spherical N = 28 shell gap.

1f7/2 ➡ fp core breaking ⇨ Shape coexistence

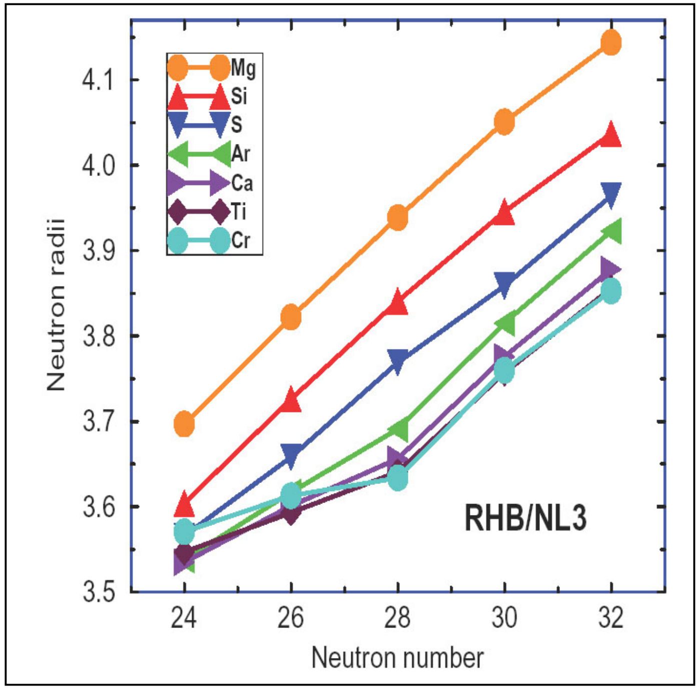

Ground-state quadrupole deformation

Average neutron pairing gaps

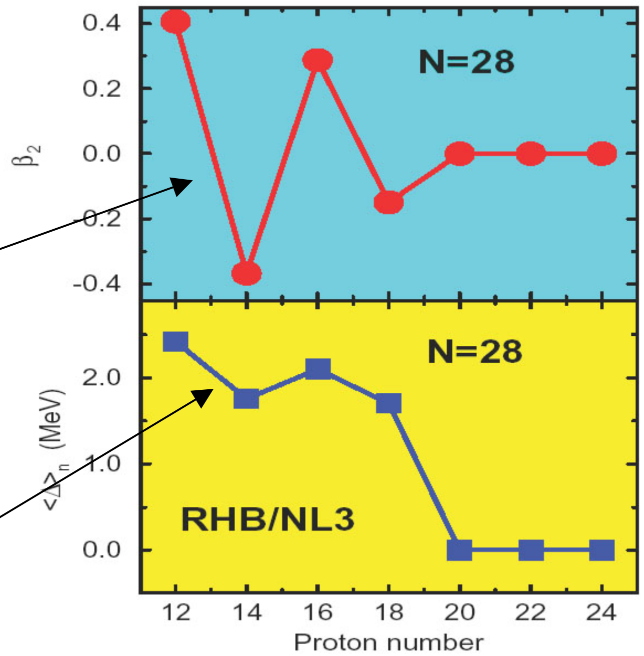

Neutron single-particle levels for ^{42}Si, ^{44}S and ^{46}Ar as functions of the quadrupole deformation. Energies in the canonical basis correspond to ground-state RHB solutions with constrained quadrupole deformation.

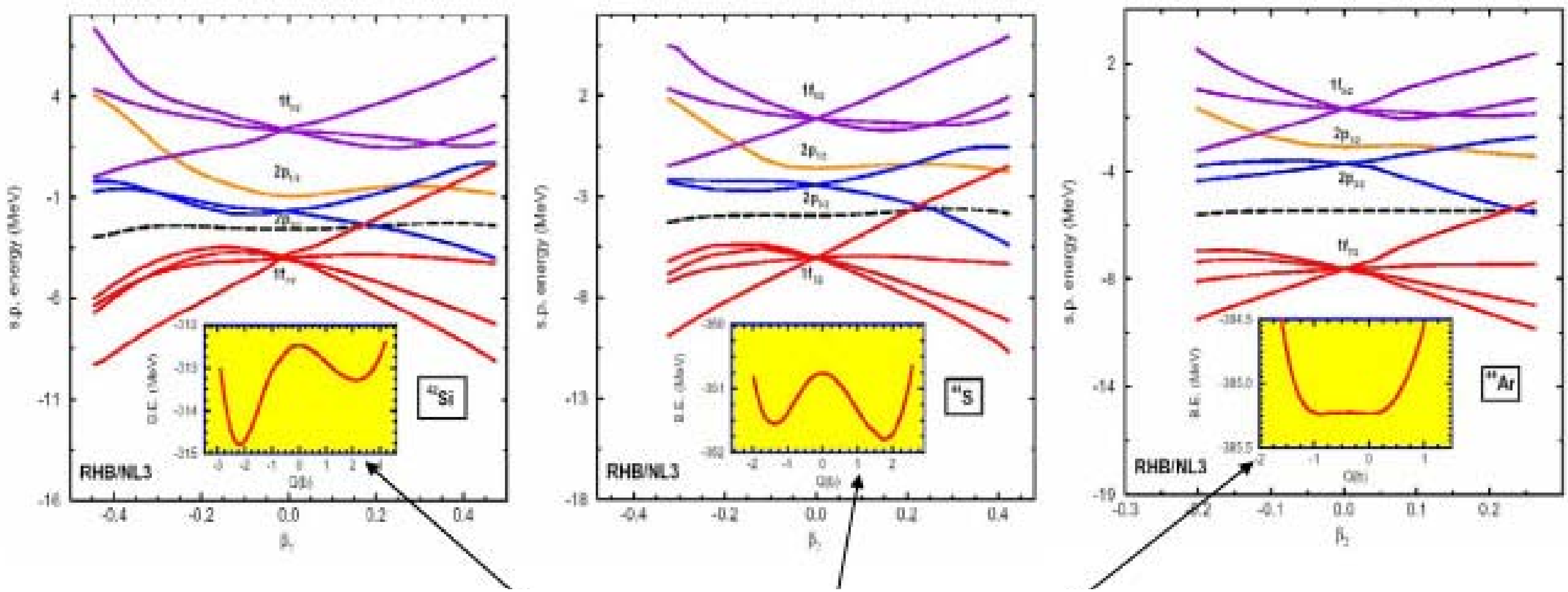

Total binding energy curves

SHAPE COEXISTENCE

Evolution of the shell structure, shell gaps and magicity with neutron number

B. Parity-violating elastic electron scattering and neutron density distributions

Elastic scattering of longitudinally-polarized electrons provides a direct measurement of the neutron distribution

Elastic electron scattering on a spin-zero nucleus:

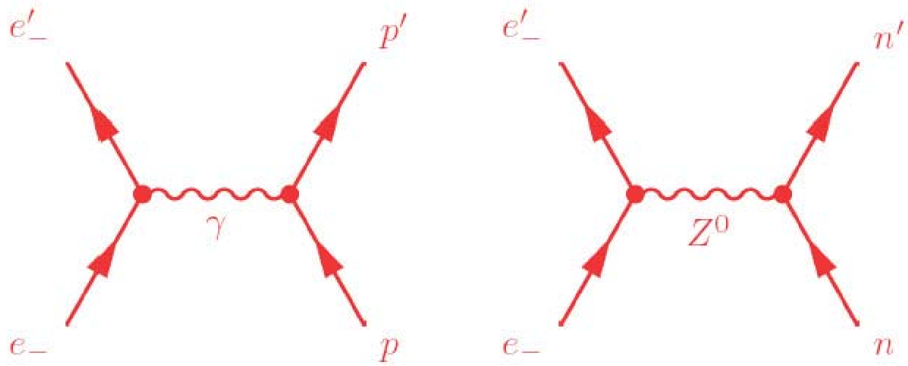

potential: $\hat{V}(r) = V(r) + \gamma_5 \frac{G_F}{2^{3/2}} \rho_W(r)$

weak-charge density:

$$\rho_W(r) = \int d^3r' G_E(|\mathbf{r}-\mathbf{r}'|)[-\rho_n(r') + (1-4\sin^2\Theta_W)\rho_p(r')]$$

in the limit of vanishing electron mass: $[\alpha \cdot \mathbf{p} + V_\pm(r)]\Psi_\pm = E\Psi_\pm$

$$\Psi_\pm = \frac{1}{2}(1 \pm \gamma_5)\Psi \qquad V_\pm(r) = V(r) \pm \frac{G_F}{2^{3/2}}\rho_W(r)$$

Helicity asymmetry: $$A_l = \frac{d\sigma_+/d\Omega \; - \; d\sigma_-/d\Omega}{d\sigma_+/d\Omega \; + \; d\sigma_-/d\Omega}$$

where +(-) refers to the elastic scattering on the potential $V_{\pm}(r)$. This difference arises from the interference of one-photon and Z^0 exchange between the electron and nucleus.

asymmetry parameter $\mathbf{A_l}$ ➡ a direct measurement of the Fourier transform of the neutron density

$$F(q) = \frac{4\pi}{q} \int dr \; r^2 j_0(qr) \rho_n(r)$$

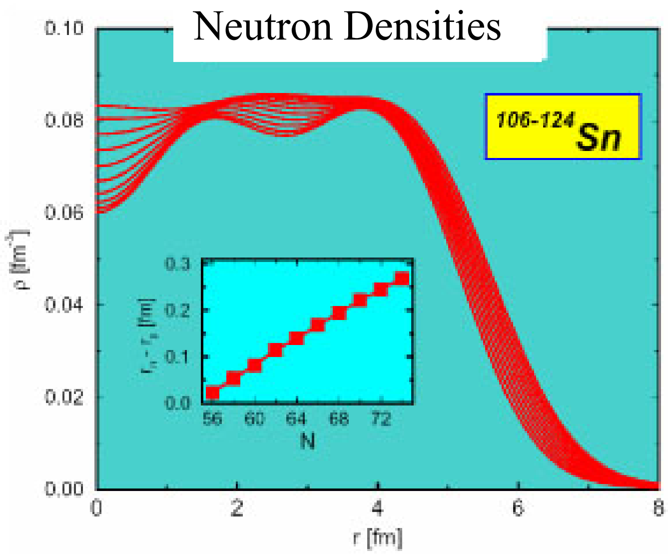

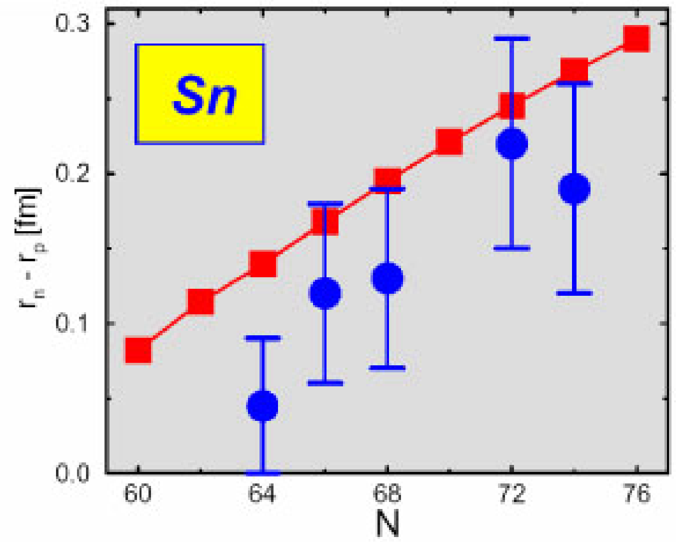

Parity-violating asymmetry parameters A_l for elastic scattering from $^{106\text{-}124}$Sn at 850 MeV

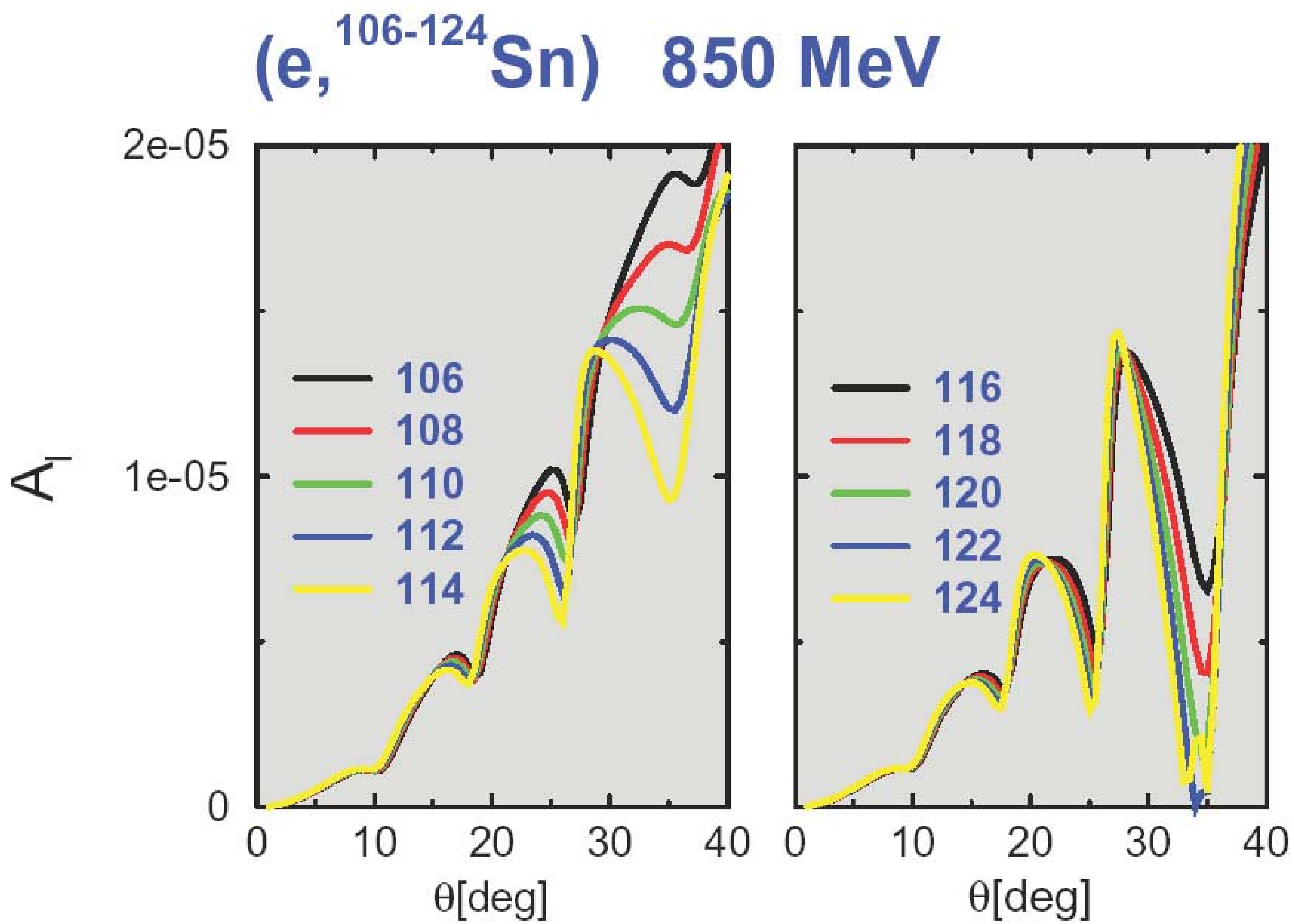

Asymmetry parameters A_l and Fourier transforms of neutron densities, as functions of the momentum transfer q, for (e, $^{106-114}$Sn) at 850 MeV

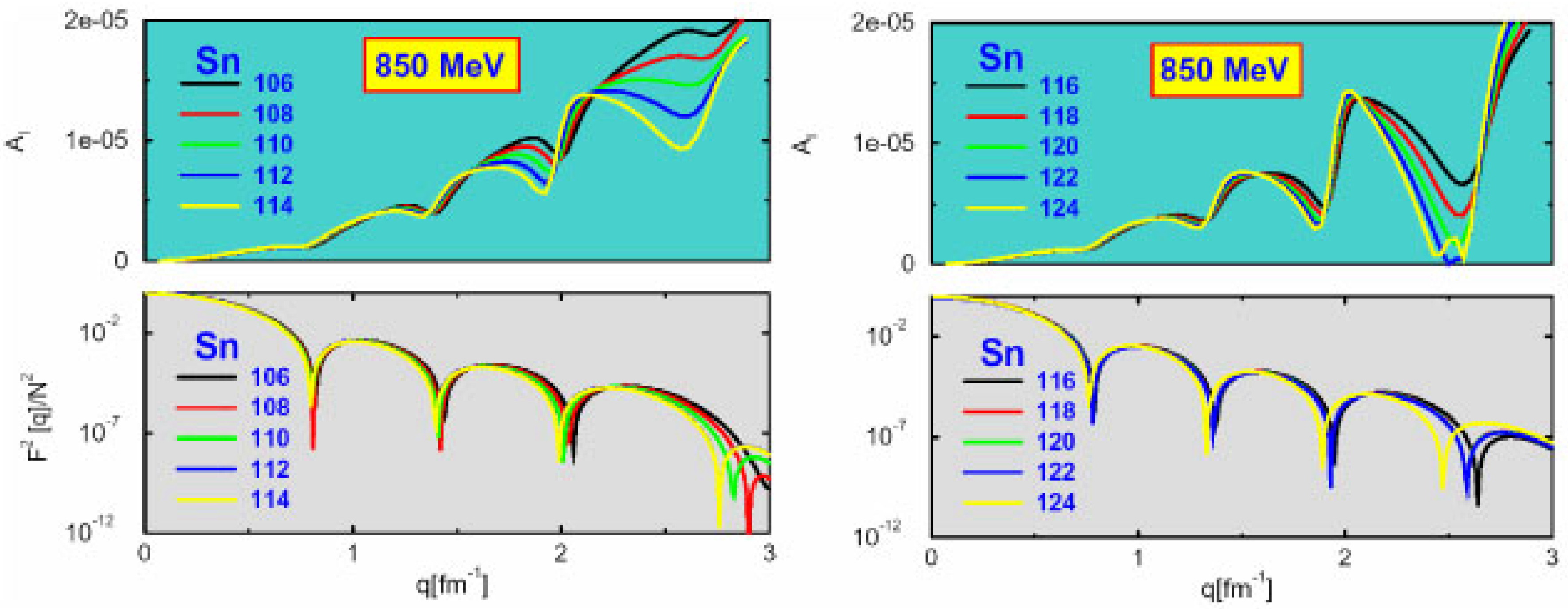

Differences between the asymmetries can be directly related to the form factors

C. Relativistic quasiparticle random phase approximation

1. Giant resonances in EXOTIC nuclei → evolution of low-lying dipole strength in nuclei with large neutron excess – **PYGMY RESONANCES**

2. EXOTIC giant resonances in nuclei – **TOROIDAL DIPOLE RESONANCE**

RQRPA → formulated in the canonical basis of the relativistic Hartree-Bogoliubov model; NL3 mean-field plus Gogny D1S pairing interactions

$$\begin{pmatrix} A^J & B^J \\ B^{*J} & A^{*J} \end{pmatrix} \begin{pmatrix} X^{\nu,JM}_{kk'} \\ Y^{\nu,JM}_{kk'} \end{pmatrix} = \omega_\nu \begin{pmatrix} 1 & 0 \\ 0 & -1 \end{pmatrix} \begin{pmatrix} X^{\nu,JM}_{kk'} \\ Y^{\nu,JM}_{kk'} \end{pmatrix}$$

RQRPA equations:

$$\begin{aligned}
A^J_{kk'll'} &= H^{11(J)}_{kl}\delta_{k'l'} - H^{11(J)}_{k'l}\delta_{kl'} - H^{11(J)}_{kl'}\delta_{k'l} + H^{11(J)}_{k'l'}\delta_{kl} \\
&\quad + \frac{1}{2}(\xi^+_{kk'}\xi^+_{ll'} + \xi^-_{kk'}\xi^-_{ll'})V^{ppJ}_{kk'll'} + \zeta_{kk'll'}\tilde{V}^{phJ}_{kl'k'l} \\
B^J_{kk'll'} &= \frac{1}{2}(\xi^+_{kk'}\xi^+_{ll'} - \xi^-_{kk'}\xi^-_{ll'})V^{ppJ}_{kk'll'} \\
&\quad + \zeta_{kk'll'}(-1)^{j_l - j_{l'} + J}\tilde{V}^{phJ}_{klk'l'} \\
H^{11}_{kl} &= (u_k u_l - v_k v_l)h^D_{kl} - (u_k v_l + v_k u_l)\Delta_{kl}
\end{aligned}$$

Evolution of isovector dipole strength in Sn isotopes

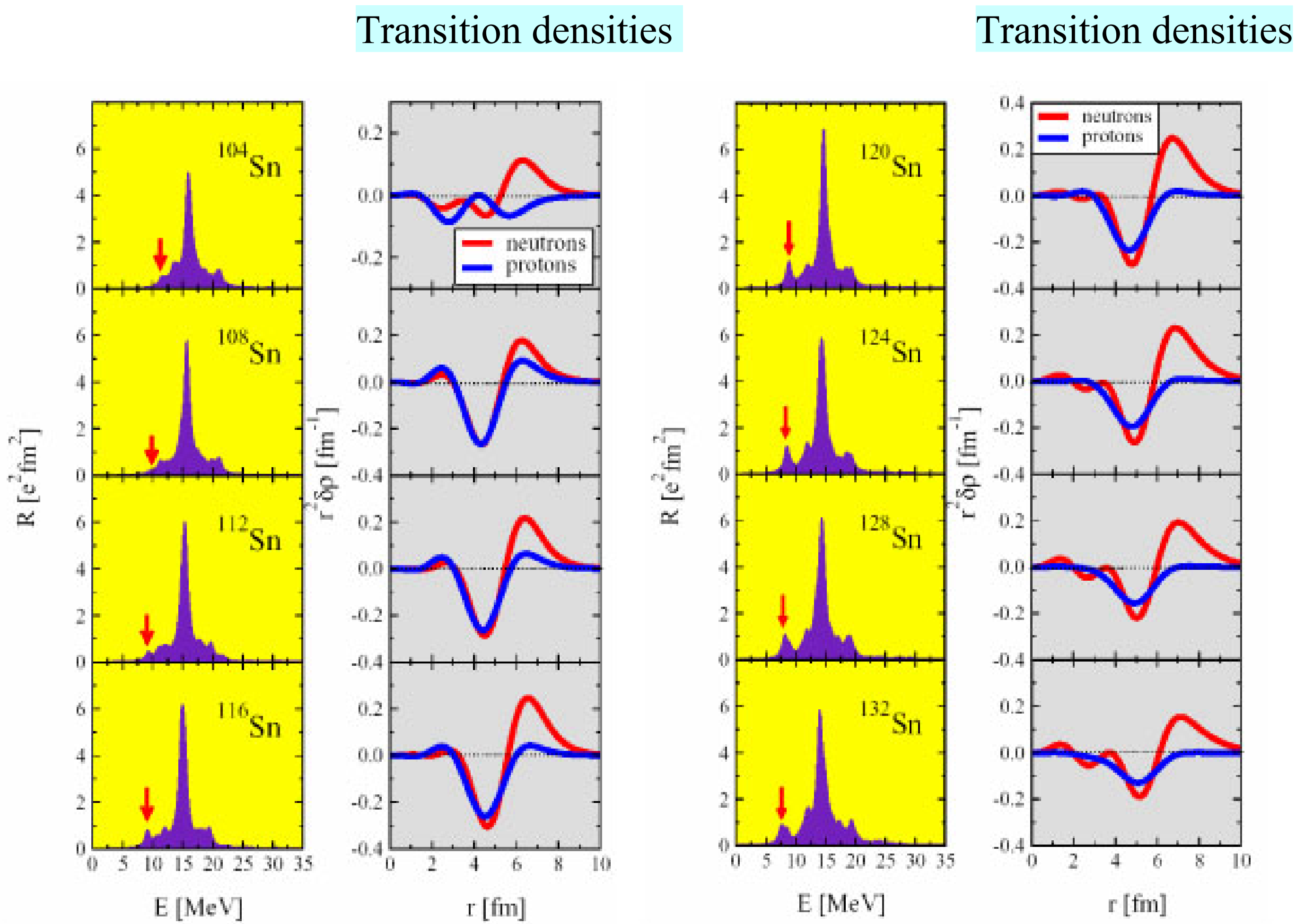

Evolution of isovector dipole strength in neutron-rich nuclei:

Low-lying dipole strength in light nuclei → non-resonant independent single-particle excitations of loosely bound nucleons

Heavier nuclei → among several single-particle transitions, a single collective dipole state is found below 10 MeV

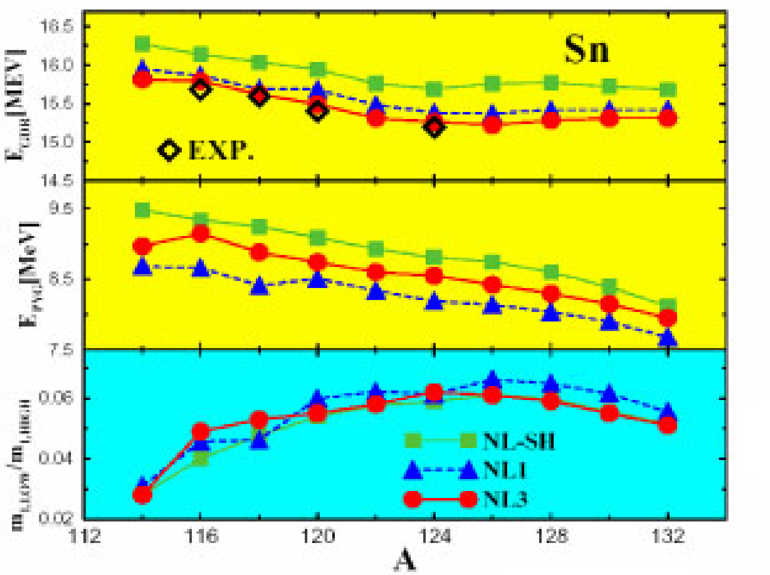

Mass dependence of GDR and pygmy dipole states in Sn isotopes; evolution of low-lying strengths

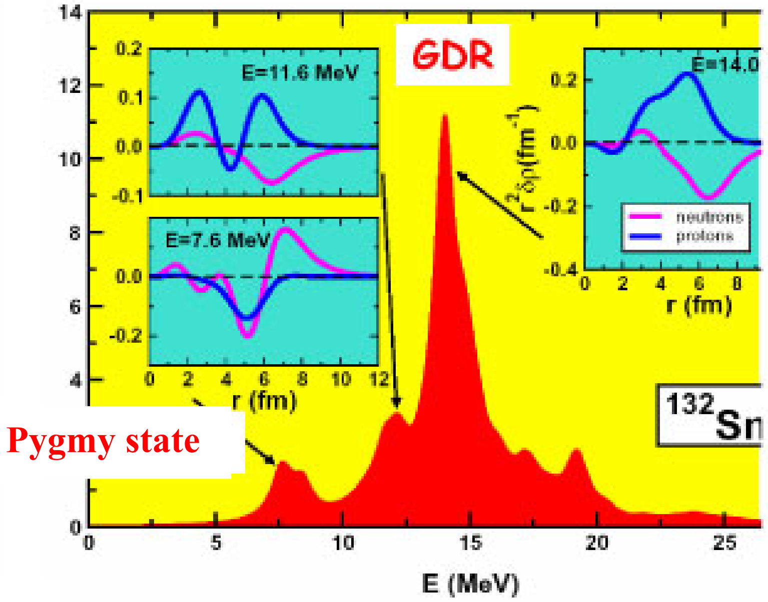

Isovector dipole strength in ^{132}Sn
Proton and neutron transition densities

Toroidal Giant Dipole Resonances

Multipole expansion of a four-current distribution:

charge moments
magnetic moments
electric transverse moments $\longrightarrow$ toroidal moments

Toroidal dipole moment: poloidal currents on a torus

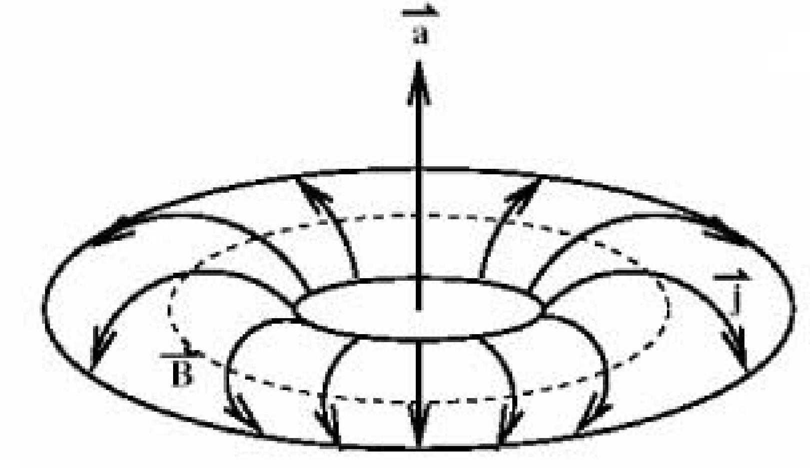

isoscalar toroidal dipole operator

$$\hat{T}_{1\mu}^{T=0} \sim \int [r^2 \left(\vec{Y}^*_{10\mu} + \frac{\sqrt{2}}{5} \vec{Y}^*_{12\mu} \right) - \langle r^2 \rangle_0 \vec{Y}^*_{10\mu}] \cdot \vec{J}(\vec{r}) d^3 r$$

Toroidal dipole strength distributions

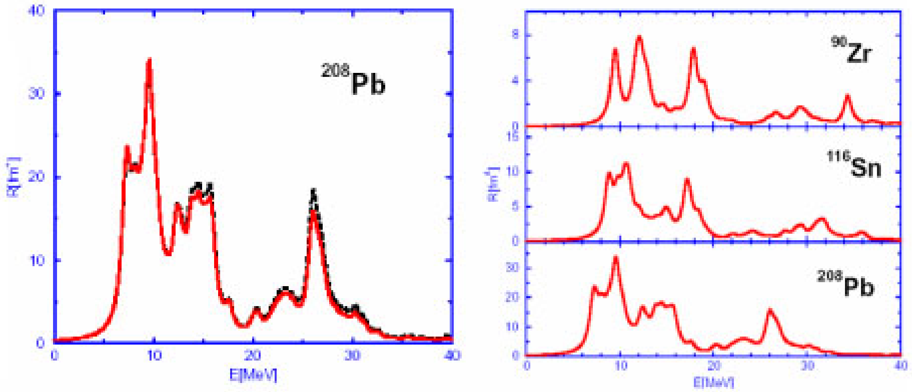

Velocity distributions in ^{116}Sn

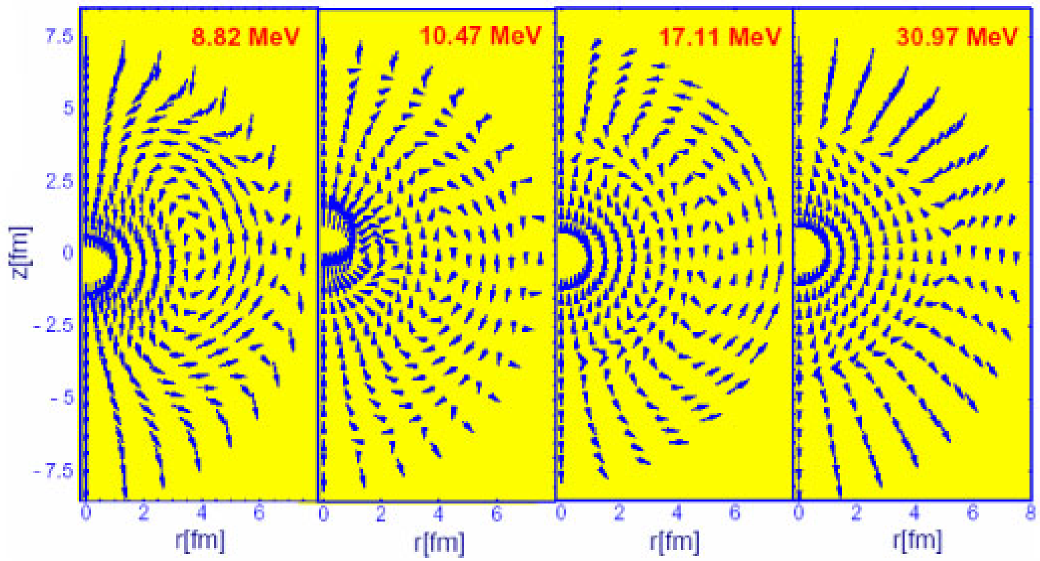

Nuclear Theory

Geometrical Symmetries in Nuclei

A. K. Jain

Indian Institute of Technology Roorkee

E-mail: ajainfph@iitr.ernet.in

Geometrical Symmetries in Nuclei[1]

Ashok Kumar Jain

Department of Physics

Indian Institute of Technology Roorkee

India

[1] These lectures are dedicated to my son NamaN, a beautiful soul.

Introduction

Symmetries in nature, art and architecture fascinate us. We are charmed by objects which are symmetric, and therefore beautiful. Most of these symmetries are geometric in nature, and are related to the external appearance. However, we do come across many other types of symmetries in physics that are quite different from the purely geometric, or spatial symmetries.

The theorem of Emmy Noether enunciates that each continuous symmetry is related to a conserved quantity, or a constant of motion. Accordingly, we have constants related to symmetries of translation, rotation and reflection in space and time. Thus, invariance under the time translation leads to the conservation of the total energy of a closed system. Likewise, invariance under space translation and rotation leads to the conservation of linear momentum and angular momentum, respectively. Besides the continuous symmetries, we also come across discrete symmetries like reflection, or inversion of space that leads to conservation of parity. Time reversal invariance can also be added to this list, as manifested by Kramer's degeneracy in single nucleon orbits. Most common among the discrete symmetries are the point-group symmetries used widely in the classification of crystal structure. These symmetries have also found useful application in molecules and nuclei.

Besides these, we have dynamical symmetries and the fundamental gauge symmetries in nature. However, complex systems like atoms, molecules and nuclei have their own set of symmetries which can be geometrical as well as dynamical, and emerge from the complexity of the system. Certain algebraic symmetries related to the various group structures such as U(5), SU(3) and SO(6) have also been identified in complex systems such as nuclei. These result in a characteristic set of patterns of energy levels, and inter related transition patterns. A more recent development along a similar line is the observation of simple behavior in systems at the critical point of quantum phase transitions. This behavior has been interpreted as the occurrence of a dynamical symmetry such as X (5) in ^{152}Sm. Systems lying at the critical point of first and second order phase transitions are being closely scrutinized for similar behaviour. However, we shall not discuss these kinds of symmetries.

Mean Field and Spontaneous Symmetry Breaking

The concepts of mean field and spontaneous breaking of the symmetries of mean field play an important role in explaining the observed band structures. The fundamental nucleon-nucleon interaction can be taken to be a two body force, and should be invariant under all the basic transformations like translation, rotation and inversion in space and time. However, a collection of nucleons as a nucleus give rise to a mean field, and may break one or more of these symmetries even though the fundamental N-N interaction has no such effect. Such symmetry breaking is termed as spontaneous breaking of symmetry, and is crucial in understanding a large variety of characteristic pattern of levels observed in experiments. However, as we shall see, additional varieties of patterns are predicted, and are waiting to be observed.

If nuclei also obeyed the basic symmetries of the N-N interaction, we would miss much of the richness in their band structure. Spontaneous breaking of one or more of these symmetries leads to a rich band structure, and enables us to classify and label the levels into various bands and infer information about the nature of the mean field. For example, the energy levels of ^{168}Er shown in the column on the left of Fig. 1 begin to look meaningful and systematic when classified into bands as on the right hand side.

Symmetry, Unitary Transformation, Degeneracy and Multiplets

A symmetry in quantum mechanics can be represented by a group of unitary transformations Û in the Hilbert space. Operator Q represents an observable, and transforms as

$$Q \;\rightarrow\; u^{\dagger} Q u$$

under the unitary transformation u. Since $u^{\dagger} = u^{-1}$ for unitary transformations, invariance of Q under u implies that

$$Q = u^{-1} Q u$$

$$\text{and } [u, Q] = 0 ,$$

which is a well known result from quantum mechanics. If the unitary operator happens to arise from the Hamiltonian of the quantum system, the operator Q leads to a conserved quantity. Under such circumstances, the unitary operator defined by H is $e^{-i\,t\,H}$, and

$$e^{itH} Q e^{-itH} = Q \text{ for all } t.$$

Thus, a commutation of Q with $u = e^{itH}$ also implies a commutation of Q with H, and Q is conserved.

Note that H is the generator of time translation because

$$\Psi^{'} = e^{itH}\Psi = (1 + itH)\Psi$$

represents a new state obtained by translation in time. Likewise,

$$\Psi^{'} = e^{i\theta J_z}\Psi = (1 + i\theta J_z)\Psi$$

represents a new state obtained by rotation by θ about the z–axis. J_z is the z–component of the angular momentum operator, and is the generator of rotation about the z-axis. If J_z is an invariant operator, we have

$$[H, J_z] = 0 .$$

Also, if $H\Psi = E\Psi$, we have

$$H\Psi^{'} = H(1 + i\theta J_z)\Psi = E\Psi^{'} .$$

This expression means that either Ψ is an eigenstate of both H and J_z, or the eigenvalue E has a degeneracy. Thus, both Ψ and $\Psi^{'}$ are eigenstates of H with the same energy eigenvalue E, leading to the concept of degeneracy and multiplets. An energy eigenstate can have n-fold degeneracy if n-fold rotation of Ψ about the z–axis leaves Ψ invariant. An interaction or deformation that violates this symmetry will lift the degeneracy and a multiplet will emerge.

As a simple example, consider a single particle moving in a spherically symmetric central potential and carrying angular momentum $\vec{j}$; the energy of this particle does not depend on j_z, and has $(2j+1)$-

fold degeneracy, where j is the angular momentum quantum number. However, a slight deformation of the potential splits the degeneracy of the j-multiplet, and a characteristic level pattern is obtained. Such symmetry breaking is witnessed when going from solutions of the spherical shell model to the deformed shell model, or the Nilsson model, as shown in Fig. 2. If the potential has an axial symmetry about the Z-axis, J_z is the only conserved quantity and the corresponding quantum number Ω can be used to label the state.

Discrete Symmetries in Nuclei

Most commonly encountered discrete symmetries in rotating nuclei correspond to parity P, rotation by π about the body-fixed x, y, z axes, $R_x(\pi)$, $R_y(\pi,)$, $R_z(\pi)$, time reversal T, and $TR_x(\pi)$, $TR_y(\pi)$ and $TR_z(\pi)$. All of these symmetries are two fold discrete symmetries, and breaking them causes a doubling of states. Dobaczewski et al. (2000) have carried out a detailed classification of the mean field solutions according to the discrete symmetries of a double point group denoted by D_{2h} (Landau and Lifshitz, 1956), and this includes all the symmetries listed above. We can enunciate the following simple rules to work out the consequences of these symmetries on a rotational band consisting of levels with angular momentum quantum numbers $I, I+1, I+2,$ etc:

1. When P is broken, we observe a parity doubling of states; a sequence such as $I^+, I+1^+, I+2^+$, ... turns into $I^{\pm}, I+1^{\pm}, I+2^{\pm}$, ... [see Fig. 3(a)].

2. When $R_x(\pi)$ is broken, states of both signatures occur; two sequences $I, I+2,$ ...etc. and $I+1, I+3,$ ...etc. having different signatures and are shifted in energy with respect to each other, to merge into one sequence like $I, I+1, I+2, I+3$ ... etc. [see Fig. 3(b)].

3. A doubling of states of the allowed angular momentum occurs when $R_y(\pi)$ T is broken. Sequence $I, I+2, I+4,$ ... etc. becomes $2(I), 2(I+2), 2(I+4),$ ..., with each state occurring twice (Chiral doubling) [see Fig. 3(c)].

4. When $P=R_x(\pi)$, the two signature partners will have different parity. Thus states of alternate parity occur, and we obtain a sequence like $I^+, I+1^-, I+2^+$, ... etc. [see Fig. 3(d)].

Since all these symmetries have a two-fold degeneracy, a breaking of each of them individually doubles the number of states, and Frauendorf (2001) has listed the consequences that are relevant for the two-body rotating Hamiltonian $H=T+V-\omega\vec{j}_x$, as reproduced in Table I. All the possibilities presented in this table can be determined by using these rules either alone or in combination.

Table I: Consequences of spontaneous breaking of one or more of the discrete symmetries of the rotating mean field.

Symmetry No.	**P**	$R_x(\pi)$	$R_y(\pi)T$	*1Level sequence*
1	S	S	S	$I^+, (I+2)^+, (I+4)^+$..............
2	S	D	S	$I^+, (I+1)^+, (I+2)^+$.............
3	S	D	D	$2I^+, 2(I+1)^+, 2(I+2)^+$..........
4	S	S	D	$2I^+, 2(I+2)^+, 2(I+4)^+$..........
5	S	D	$R_x(\pi)$	$I^+, (I+1)^+, (I+2)^+$.............
6	D	S	S	$I^\pm, (I+2)^\pm, (I+4)^\pm$.........
7	D	D	S	$I^\pm, (I+1)^\pm, (I+2)^\pm$......
8	D	S	D	$2I^\pm, 2(I+2)^\pm, 2(I+4)^\pm$..........
9	D	D	$R_x(\pi)$	$I^\pm, (I+1)^\pm, (I+2)^\pm$........
10	$R_x(\pi)$	D	S	$I^+, (I+1)^-, (I+2)^+$........
11	$R_x(\pi)$	D	D	$2I^+, 2(I+1)^-, 2(I+2)^+$........
12	$R_y(\pi)T$	S	D	$I^\pm, (I+2)^\pm, (I+4)^\pm$...........
13	$R_y(\pi)T$	D	D	$I^\pm, (I+1)^\pm, (I+2)^\pm$..........
14	$R_x(\pi)$	D	$R_x(\pi)$	$I^+, (I+1)^-, (I+2)^+$.........
15	D	D	D	$2I^\pm$,2 $(I+1)^\pm$,2 $(I+2)^\pm$..........

x is the axis of rotation

D denotes that the mean field changes under the corresponding operation, and S means the mean field remains the same; when another operation is shown, the two are identical

Last column shows the spectrum arising for a given set of conserved/broken symmetries

Although only positive parity is shown in rows 1-5, parity can also be negative (taken from Frauendorf (2001))

Nuclear Shapes

Some basic ideas of nuclear shapes need to be considered before proceeding further. The surface of an arbitrarily deformed body can be expressed by the radius vector along the polar angles θ and ϕ as

$$R(\theta,\phi) = R_0[1+\sum_{\lambda,\mu}\alpha_{\lambda,\mu}Y^*{}_{\lambda\mu}(\theta,\phi)]$$

where R_0 is the radius of an equivalent volume sphere. Terms $\lambda = 0, 1, 2, 3, 4$ etc. correspond to the monopole, dipole, quadrupole, octupole, hexadecapole etc shapes, and generally we obtain 2^{λ}-pole deformation for a given λ. These spherical harmonics have definite geometrical symmetries, and may occur in the mean field of the nucleus. Monopole shape oscillation may occur only at very high excitations in nuclei due to the incompressible nature of nuclear matter. The dipole term corresponds simply to a translation of the nucleus and does not have any physical significance. Therefore, the lowest order term of importance is the $\lambda = 2$ quadrupole term. Higher-order terms play a role in specific mass regions of nuclei, but $\lambda = 2$ is the most widespread and globally occurring shape in nuclei.

A permanent non-spherical shape gives rise to the possibility of observing rotational motion. Under these circumstances, the nuclear surface is more conveniently considered in the body-fixed frame rather than the space-fixed frame. The nuclear surface in the body-fixed frame can also be described by the similar relationship:

$$R(\theta,\phi) = R_0[1+\sum a_{\lambda,\mu}Y^*{}_{\lambda\mu}(\theta,\phi)]$$

where $a_{\lambda\mu}$ have been introduced as the new time-independent parameters in the body-fixed frame, which coincides with the principal axes. Parameters $a_{\lambda\mu}$ are related to $\alpha_{\lambda\mu}$:

$$a_{\lambda\mu} = \sum_{\mu'} D^{\lambda}_{\mu'\mu}(\Omega)\alpha_{\lambda\mu'}$$

The $Y_{2\mu}$ term corresponding to $\lambda = 2$ has five components labeled by $\mu = \pm 2, \pm 1, 0;$ $\mu = 0$ component corresponds to the situation where full rotational symmetry is maintained about one of the three principal axes (say the z-axis) and the other two axes (x- and y-) are equal. Such a shape is called a spheroid. For $x = y < z$, a prolate spheroid is obtained; and for $x = y > z$, an oblate spheroid is derived. The prolate spheroid is found to be the most common shape in nuclei, although the oblate shape is also known to occur near the magic numbers.

The next most commonly observed shape is $\lambda = 4$ hexadecapole shape, which is generally superposed on the quadrupole shape, and is only found with small amplitude. A small $\lambda = 3$ octupole shape is now believed to occur in certain pockets of nuclei, and is also superimposed on the quadrupole shape. Furthermore, much of the experimental evidence favours the occurrence of $\mu = 0$ component of the various multipoles. However, attention has now focused on $\mu \neq 0$ components of the various multipoles and their consequences, corresponding to the introduction of non-axial or axially-asymmetric degrees of freedom. Some common nuclear shapes corresponding to the various multipoles are shown in Fig. 4, while Fig. 5 depicts some extraordinary, or exotic shapes.

Observation of one or more of these varied shapes in nuclei has become a distinct possibility with recent enhancements in our experimental capabilities. While the ground state configurations of nuclei may not support all of these shapes, we now have the possibility of observing high-spin configurations, non-yrast configurations and configurations with abnormal N/Z ratio (nuclei some considerable distance away from the line of stability) which may support one or more of these novel shapes.

Each of these shapes is obtained by distinct symmetry breaking of the mean field, and therefore leaves a characteristic impression on the level pattern due to the lifting of degeneracy. Such operations leave these geometrical shapes invariant when coupled with the time-reversal and space-inversion (parity) operators, and provide a fertile ground for observing nuclear levels with fascinating patterns.

An additional new dimension to the whole scenario has been provided by the realization that rotation is also possible about an axis other than one of the principal axes. This phenomenon is particularly true for the tri-axial shapes where rotation about a tilted axis has successfully explained observed features and phenomena such as magnetic and chiral rotations. Such behaviour leads to additional types of symmetry breakings and ensuing consequences.

Collective Hamiltonian

The collective Hamiltonian for an irrotational flow of fluid can be written as (Bohr and Mottelson (1975); Pal (1982)):

$$H = T + V = \frac{1}{2}\sum_{\lambda,\mu}[B_\lambda \left|\dot{\alpha}_{\lambda\mu}\right|^2 + C_\lambda \left|\alpha_{\lambda\mu}\right|^2],$$

where

$$B_\lambda = \lambda^{-1}\rho_0 R_o^5 = \frac{3}{4\pi}\lambda^{-1} MAR_0^2$$

$$C_\lambda = C_\lambda^5 + C_\lambda^c = R_0^2 S(\lambda-1)(\lambda-2) - \frac{3}{2\pi}\frac{(Ze)^2}{R_0}.\frac{\lambda-1}{2\lambda+1},$$

and ρ_0 is the equilibrium density of nuclear matter. Note that the space-fixed frame and parameters have been used to give a classical Hamiltonian of a vibrator for each (λ, μ) mode, with a classical frequency of vibration given by $\omega_\lambda = \left(\frac{C_\lambda}{B_\lambda}\right)^{\frac{1}{2}}$. Transformation of this Hamiltonian to a body-fixed principal axes frame assumes a particularly simple form given by

$$H = T_{vib} + T_{rot} + V = \frac{1}{2}\sum_{\lambda\mu} B_\lambda \left|\dot{a}_{\lambda\mu}\right|^2 + \frac{1}{2}\sum_{K=1}^{3} \Im_k\, \omega_k^2 + \frac{1}{2}\sum_{\lambda\mu} C_\lambda \left|a_{\lambda\mu}\right|^2.$$

This equation is written in term of parameters $a_{\lambda\mu}$ defined in the body-fixed frame. The first and last terms represent the energies of a vibrator, and the second term corresponds to a rotator with $\Im_k (k = x, y, z)$ as the three components of the moment of inertia in the body-fixed frame. The pure vibrator Hamiltonian in the space-fixed frame becomes a vibrator plus a rotator Hamiltonian in the body-fixed frame.

Quadrupole motion $(\lambda = 2)$:

Consider only $\lambda = 2$ terms:

$$H = \frac{1}{2}B(\dot{\beta}^2 + \beta^2\dot{\gamma}^2) + \frac{1}{2}\sum_k \Im_k \omega_k^2 + \frac{1}{2}C\beta^2,$$

where β, γ parameters have been used, and

$$a_{20} = \beta\cos\gamma\ ,\ a_{22} = a_{2-2} = \frac{1}{\sqrt{2}}\beta\ Sin\gamma\ ,\ a_{21} = a_{2-1} = 0$$

$$\Im_k = 4B\beta^2 Sin^2\left(\gamma - k\frac{2\pi}{3}\right),$$

$$B = \frac{1}{2}\rho_0 R_0^5\,.$$

Quantization of this Hamiltonian leads to the Schrödinger equation:

$$\left[-\frac{\hbar^2}{2B}\left(\frac{1}{\beta^4}\frac{\partial}{\partial\beta}\beta^4\frac{\partial}{\partial\beta} + \frac{1}{\beta^2 Sin3\gamma}\frac{\partial}{\partial\gamma}Sin3\gamma\frac{\partial}{\partial\gamma}\right)\right.$$
$$\left. + \sum_k \frac{\hbar^2}{2\Im_k}R_k^2 + \frac{1}{2}C\beta^2\right]\psi(\beta,\gamma,\theta_1,\theta_2,\theta_3) = E\psi(\beta,\gamma,\theta_1,\theta_2,\theta_3).$$

which is separable in β- and γ-coordinates:

$$\Psi(\beta,\gamma,\theta_1,\theta_2,\theta_3) = f(\beta)\Phi(\gamma,\theta_1,\theta_2,\theta_3),$$

where $f(\beta)$ satisfies the β-equation:

$$\left(-\frac{\hbar^2}{2B}\frac{1}{\beta^4}\frac{d}{d\beta}\beta^4\frac{d}{d\beta} + \frac{1}{2}C\beta^2 + \frac{\Lambda\hbar^2}{2B}\frac{1}{\beta^2}\right)f(\beta) = Ef(\beta),$$

and $\Phi(\gamma, \theta_1, \theta_2, \theta_3)$ satisfies the rotor plus γ-motion equation:

$$\left(-\frac{1}{\sin 3\gamma}\frac{\partial}{\partial\gamma}Sin3\gamma\frac{\partial}{\partial\gamma} + \frac{1}{4}\sum_k \frac{R_k^2}{\sin^2\left(\gamma - k\frac{2\pi}{3}\right)}\right)\Phi(\gamma,\theta_1,\theta_2,\theta_3) = \Lambda\Phi(\gamma,\theta_1,\theta_2,\theta_3)\,.$$

If the nucleus is rigid for γ-vibration, only the rotational part is left in the rotor plus γ-motion equation, and we obtain:

$$\frac{1}{4}\sum \frac{R_k^2}{Sin^2\left(\gamma - k\frac{2\pi}{3}\right)}\Phi(\theta_1,\theta_2,\theta_3) = \Lambda\Phi(\theta_1\theta_2\theta_3).$$

The operators $R_k, (k \equiv x, y, z)$ are the components of the rotational angular momentum operator $\hat{R}$ along the body-fixed axes *x*, *y*, and *z*. Components of $\hat{R}$ along the space-fixed axes are donated by X, Y, Z, and

$$\left[R_X, R_Y\right] = iR_Z, ...etc$$

but

$$\left[R_x, R_y\right] = -iR_z, ...etc$$

Also, $\Phi(\theta_1\theta_2\theta_3)$ can be shown to be simply the function $D^I_{MK}(\theta_1\theta_2\theta_3)$, and these terms satisfy the eigenvalue equations:

$$\hat{R}^2 D^I_{MK} = I(I+1)D^I_{MK},$$
$$R_Z D^I_{MK} = MD^I_{MK},$$
$$R_z D^I_{MK} = KD^I_{MK}.$$

Spheroidal Shapes

When the ellipsoidal body has an axis of symmetry along one of the principal axes, a spheroid is obtained. Let the *z*-axis be the symmetry axis perpendicular to the *x*- and *y*-axis, and therefore $\gamma = 0$ and

$$\Im_x = \Im_y, \Im_z = 0,$$

as a consequence of the general rule that there cannot be any rotation about an axis of symmetry. The equation in $\hat{R}$ reduces to

.

$$\frac{1}{3}\left(R_x^2 + R_y^2\right)\Phi(\theta_1\ \theta_2\ \theta_3) = \frac{1}{3}\left(\hat{R}^2 - R^2\right)\Phi(\theta_1\ \theta_2\ \theta_3)$$
$$= \frac{1}{3}\left[I(I+1) - K^2\right]D^I_{MK}(\theta_1\ \theta_2\ \theta_3)$$

$\Im_x \neq \Im_y \neq \Im_z$ for a general ellipsoid, and the coefficients of R_x^2 and R_y^2 are not equal. We can write $R_x^2 = \frac{1}{4}(R_+ + R_-)^2$ and $R_y^2 = -\frac{1}{4}(R_+ - R_-)^2$, where $R_\pm = R_x \pm iR_y$, leading to terms of the type $R_+ R_+$, $R_- R_-$ and $(R_+ R_- + R_- R_+)$. The last operator leaves D^I_{MK} unchanged, while $R_+ R_+$ and $R_- R_-$ change D^I_{MK} to D^I_{MK-2} and D^I_{MK+2}, respectively. Therefore, the eigen functions, become a mixture of D^I_{MK}, with *K* differing by ± *2*.

The equation for rotor plus *γ*-motion can also be solved by using the D^I_{MK} functions, with eigen functions of the type:

$$\Phi^I{}_M(\gamma,\theta_1\ \theta_2\ \theta_3)=\sum_k g_K^I(\gamma)D_{MK}^I(\theta_1\ \theta_2\ \theta_3).$$

where K differ by ± *2*. This equation corresponds to rotor plus γ-motion and is difficult to solve because a chain of coupled differential equations are created.

Constraints on K-values

$\alpha_{2\mu}$ are the shape parameters in space-fixed frame, and define the shape uniquely. When we transform to the body-fixed axes and introduce the parameter $a_{2\mu}$ or *(β,γ) (θ1 θ2 θ3)*, the labeling of the body-fixed frame becomes arbitrary. Body-fixed axes (which coincide with the principal axes of the body) can be chosen in many ways. Restricting to right-handed frames only, there are 24 different ways to choose the body-frame (Pal, 1982), and we obtain different $(\beta, \gamma, \theta_1, \theta_2, \theta_3)$ values for each such choice. However, any change of body-frame which does not change the values of α_μ should leave the wave function invariant, as ensured by considering the effect of the rotation operators R_1, R_2 and R_3 on the wave function (Fig. 6).

All 24 frames can be obtained by application of one or more of the three rotation operators:

$$R_1(0,\pi,0), R_2\left(0,0,\frac{\pi}{2}\right), R_3\left(\frac{\pi}{2},\frac{\pi}{2},\pi\right)$$

where $R(\theta_1,\theta_2,\theta_3)$ denotes an operator consisting of

$$R(\theta_1,\theta_2,\theta_3)=e^{-i\theta_1 J_z}e^{-i\theta_2 J_y}e^{-i\theta_3 J_z}.$$

A combination of these operators can give the 24 different sets of body-fixed axes, which give different $(\beta, \gamma, \theta_1, \theta_2, \theta_3)$ for the same values of a_μ. Therefore, we demand that the wave function remain invariant under these three operations. The three operators affect the functions as follows, while β remains unaffected in all cases.

(i) $R_1^y(0,\pi,0)$: $\gamma\to\gamma$, $\theta_1\to\theta_1$, $\theta_2\to\theta_2+\pi$, $\theta_3\to-\theta_3$

hence

$$\begin{aligned}&\sum_K g_K^I(\gamma)D_{MK}^I(\theta_1,\theta_2,\theta_3)\\ &=\sum_{K'} g_{K'}^I(\gamma)D_{MK'}^I(\theta_1,\theta_2+\pi,-\theta_3)\\ &=\sum_{K'} g_{K'}^I(\gamma)D_{M-K'}^I(\theta_1,\theta_2,\theta_3)(-1)^{I+K'}\end{aligned}$$

and equating the coefficients of D_{MK}^I on both sides,

$$g_K^I(\gamma)=g_{-K}^I(\gamma)(-1)^{I-K}$$

(ii) $R_2^z\left(0,0,\frac{\pi}{2}\right)$: $\gamma\to-\gamma$, $\theta_1\to\theta_1$, $\theta_2\to\theta_2$, $\theta_3\to\theta_3+\frac{\pi}{2}$

hence

$$\sum_K g_K^I(\gamma) D_{MK}^I(\theta_1,\theta_2,\theta_3)$$
$$= \sum_{K'} g_{K'}^I(\gamma) D_{MK'}^I\left(\theta_1,\theta_2,\theta_3+\frac{\pi}{2}\right)$$
$$= \sum_{K'} g_{K'}^I(-\gamma) D_{MK'}^I(\theta_1,\theta_2,\theta_3) i^{K'}$$

and equating the coefficients

$$g_K^I(\gamma) = i^K g_K^I(-\gamma).$$

Using this relationship again to replace $g_K^I(-\gamma)$ gives

$$g_K^I(\gamma) = (-1)^K g_K^I(\gamma),$$

restricting K to even-integer values only. Combining the two equations from (i) and (ii), we obtain

$$g_K^I(\gamma) = (-1)^I g_{-K}^I(\gamma),$$

with K as even integers only.

(iii) $R_3\left(\frac{\pi}{2},\frac{\pi}{2},\pi\right): \gamma \to \gamma - \frac{4\pi}{3},\ \theta_1 \to \theta_1 + \frac{\pi}{2},\ \theta_2 \to \theta_2 + \frac{\pi}{2},\ \theta_3 \to \theta_3 + \pi$

therefore

$$\sum_K g_K^I(\gamma) D_{MK}^I(\theta_1,\theta_2,\theta_3)$$
$$= \sum_{KK'} g_{K'}^I(\gamma - 120^0) D_{KK'}^I\left(\frac{\pi}{2},\frac{\pi}{2},\pi\right) D_{MK}^I(\theta_1,\theta_2,\theta_3)$$

and equating the coefficients gives

$$g_K^I(\gamma) = \sum_{K'} g_{K'}^I(\gamma - 120^0) D_{KK'}^I\left(\frac{\pi}{2},\frac{\pi}{2},\pi\right)$$

Incorporating the relationship from (ii), the wave function remains invariant if written as

$$\Phi^I{}_M(\gamma,\theta_1,\theta_2,\theta_3) = \sum_K g_K^I(\gamma)\left[D_{MK}^I + (-1)^I D_{M-K}^I\right],$$

with K restricted to even integers only.

Axial Symmetry – Symmetric Top

If γ-motion is frozen, $g_K^I(\gamma)$ becomes independent of γ, and K $(= \Omega)$ is a good quantum number for a spheroidal shape (Fig. 7). The summation on K disappears, and therefore:

$$\Phi_{MK}^I(\theta_1,\theta_2,\theta_3) = g_K^I\left[D_{MK}^I + (-1)^I D_{M-K}^I\right]$$

$$= \sqrt{\frac{2I+1}{16\pi^2}}\left[D_{MK}^I + (-1)^I D_{M-K}^I\right]$$

where the normalization condition has been used (remember that K is allowed to have even-integer values only).

Only even integer values of I are allowed for $K = 0$, or the wave function vanishes. Therefore,

$$\Phi_{MK=0}^I = \sqrt{\frac{2I+1}{8\pi^2}}D_{MK=0}^I$$

and only $K = 0$ is allowed in the case of spheroidal symmetry. Consider the action of $R_2(0, 0, \phi)$ for rotation by an arbitrary angle ϕ about the z-axis, which is also the symmetry axis:

$$g_K^I(\gamma) = e^{iK\phi} g_K^I(\gamma) = e^{iK(\frac{\pi}{2}+\phi')} g_K^I(\gamma) \quad = e^{iK\phi'} g_K^I(-\gamma)$$

to give

$$g_K^I(\gamma) = e^{i2K\phi'} g_K^I(\gamma)$$

Since this relationship must be valid for any value of ϕ, only $K = 0$ applies.

Even-even Nuclei: *K = 0* Ground State Band, *β*-bands and *γ*-bands

When the axially-symmetric deformed nucleus acquires small oscillations in β and γ, the total energy E of the nucleus can be written as

$$E = \hbar\omega_\beta\left(N_\beta + \frac{5}{2}\right) + \hbar\omega_\gamma$$

$$\left(2n_\gamma + \frac{1}{2}K + 1\right) + \frac{\hbar^2}{2\Im}\left[I(I+1) - K^2\right]$$

where

$$\omega_\beta = \sqrt{\frac{C}{B}}, N_\beta = 2n_\beta + I - 1,$$

$$\omega_\gamma = \sqrt{\frac{C_\gamma}{B}}, N_\gamma = 2n_\gamma + \frac{1}{2}K.$$

The lowest lying band corresponds to no β-phonon $(N_\beta = 0)$, and no γ-phonon $(N_\gamma = 0,\ n_\gamma = 0,\ K = 0)$ excitation. Since $K = 0$ allows only even angular momentum states, we obtain $K = 0$, $I = 0, 2, 4 \ldots$, all of even parity for the ground rotational band.

Another rotational band arises for $N_\beta = 0$, $N_\gamma = 1$ (one γ-phonon), i.e., $n_\gamma = 0$, $K = 2$, and this $K = 2$ γ-band can have any integer $I = 2, 3, 4\ldots$ etc.

$K = 0$ β-band arises for $N_\beta = 1$, $N_\gamma = 0$ and since $K = 0$, $I = 0, 2, 4 \ldots$ and positive parity. Higher phonon excitations can be constructed by taking more than one β- or/and γ-phonons, and the various possible bands based on $\lambda = 2$ phonon excitations are shown in Fig. 8 (along with an example of these bands in Fig. 9). We also show an example of octupole phonon-excitation and a subsequent band.

Intrinsic Wave Function

The total wave function of a nucleus is most conveniently written as the product of an intrinsic and a rotational component. Odd-A and odd-odd nuclei require the intrinsic wave function which also contains the parity information.

Signature Quantum Number

An important consequence of introducing the intrinsic wave function is the emergence of signature quantum number for a spheroidal shape. Let z be the symmetry and quantization axis. As a consequence of the spheroidal shape, the nucleus has a reflection symmetry in the x-y plane. The total wave-function

$$\Psi^I_{MK} = \chi_\Omega D^I_{MK}$$

must remain invariant under a transformation $R_x(\pi)$ acting on the intrinsic coordinates, and $R_e(\pi)$ acting on the collective coordinates such that

$$R_x(\pi) = R_e(\pi) .$$

For axial symmetry, $K = \Omega$ and χ_Ω becomes χ_K, where $\chi_K = \sum_J C_J \chi_{JK}$.

The intrinsic state for $K = 0$ will re-evolve when operated twice by $R_x(\pi)$, and therefore:

$$R_x(\pi)\chi_{K=0} = r\chi_{K=0} ,$$
$$R_x^2(\pi)\chi_{K=0} = r^2\chi_{K=0} ,$$

so that

$$r^2 = 1 \quad \text{and} \quad r = \pm 1 .$$

One may also write these expressions as

$$R_x(\pi)\chi_{K=0} = e^{-i\pi J_x}\chi_{K=0} = e^{-i\pi\alpha}\chi_{K=0}$$

which leads to $\alpha = 0$ and $\alpha = 1$ corresponding to $r = +1$ and $r = -1$, respectively. Both α and r are referred to as the signature quantum number.

$$R_e(\pi)D^I_{MK=0} = e^{-i\pi I}Y^I_M = (-1)^I Y^I_M .$$

and $r = (-1)^I$.

The $K = 0$ rotational band is divided into two domains:

$$\alpha = 0, \; r = +1, \quad I = 0, 2, 4..........$$
$$\alpha = 1, \; r = -1, \quad I = 1, 3, 5.............$$

An example of $\alpha = 0$, $K = 0$ band is shown in Fig. 9; $K = 0$ band in an odd-odd nucleus has both $\alpha = 0$ and $\alpha = 1$ signatures.

For $K \neq 0$, the intrinsic states are two-fold degenerate as a consequence of the invariance with respect to 180^0 rotation about the x (or y) axis. This operation has the same effect as the time reversal operator in which the time reversed state is denoted by $\overline{K}$ and has a negative eigenvalue of j_z, so that

$$\chi_{\overline{K}} = R_x^{-1} \chi_K .$$

Since $\chi_K = \sum_j C_j \chi_{jK}$, we have

$$\chi_{\overline{K}} = e^{i\pi j_x} . \chi_K = \sum_j (-1)^{j+K} . \chi_{j-K}$$

The effect of $R_e(\pi)$ on D^I_{MK} is given by

$$R_e D^I_{MK} = e^{-i\pi I} D^I_{MK} = (-1)^{I+K} D^I_{M-K} .$$

A rotationally-invariant wave function can be constructed:

$$\Psi^I_{MK} = \frac{1}{\sqrt{2}} \left(1 + R^{-1}{}_x R_e\right) \left(\frac{2I+1}{8\pi^2}\right)^{\frac{1}{2}} \chi_K D^I_{MK}$$
$$= \left(\frac{2I+1}{16\pi^2}\right)^{\frac{1}{2}} \left[\chi_K D^I_{MK} + (-1)^{I+K} \chi_{\overline{K}} D^I_{M-K}\right]$$

For odd-A nuclei:

$$R_x^2 \chi_K = (-1)^{2j} \chi_{K,}$$

where $2j$ is odd.

$$R_x = e^{-i\pi j_x} = e^{-i\pi\alpha}$$

implies that $\alpha = \frac{1}{2}$ for $r = -i$, and $\alpha = -\frac{1}{2}$ for $r = +i$. Similarly,

$$R_e = e^{-i\pi I}$$

implies that $I = \frac{1}{2}$ for $r_e = -i$, and $I = \frac{3}{2}$ for $r_e = +i$.

Also $R_x^{-1} R_e = 1$ requires that

$$I = \frac{1}{2}, \frac{5}{2}, \frac{9}{2}.........., \text{ for } \alpha = \frac{1}{2}, \; r = -i,$$

and

$$I = \frac{3}{2}, \frac{7}{2}, \frac{11}{2}..........., \text{ for } \alpha = -\frac{1}{2}, \; r = +i .$$

Generally:

$$I = (\alpha + even\ number).$$

The favoured signature levels decreases in energy, whereas the unfavoured signature levels are elevated corresponding to the situation shown in the first row of Table I. An example of bands with $\alpha = 1/2$ and $\alpha = -1/2$ signatures is shown in Fig.10, based on $i_{13/2}$ orbital with $K = ½$ in which the $\langle ½ | j_+ | -½ \rangle$ matrix element (defines the decoupling parameter) plays an important role in lowering the energies of the favoured signature levels (decoupling effect). The decoupling effect is so strong that the levels *13/2, 17/2 ...* are the lowest, although *K* is very small, leading to the well known observation of decoupled bands. When the signature is no longer a good quantum number (i.e., R_x (π) is not a conserving operation), we get only one sequence of levels such as $I = \frac{1}{2}, \frac{3}{2}, \frac{5}{2}, \frac{7}{2}$......... etc., which corresponds to the second row of Table I.

At higher rotational frequencies, the Coriolis force becomes important and leads to significant *K*-mixing. Therefore, the time reversal as well as the full D_2-symmetry are broken. The only good quantum numbers that survive at high spins are signature α and parity π.

Parity

If the intrinsic Hamiltonian preserves parity, the corresponding wave function has fixed parity. Since parity operator *P* commutes with j_z:

$$P\chi_k = \pi\chi_k, \ \ \pi = \pm 1,$$

and all states in a given band have the same parity π. $K = 0$ bands can occur with π and α quantum numbers independent of each other; and therefore $K=0$ bands may have

$$I = 0^+, 2^+, 4^+ \text{.........}, \alpha = 0,$$

$$\text{or } I = 0^-, 2^-, 4^- \text{...........}, \alpha = 0, \text{ and}$$

$$I = 1^-, 3^-, 5^- \text{..............}, \ \alpha = 1,$$

$$\text{or } I = 1^+, 3^+, 5^+ \text{................}, \alpha = 1.$$

Ground rotational bands of even-even nuclei are known to exhibit

$$I = 0^+, 2^+, 4^+ \text{..........}, \alpha = 0 \ \text{band},$$

and octupole vibrational bands of even-even nuclei display

$$I = 1^-, 3^-, 5^- \text{........}, \ \alpha = 1 \ \text{band}.$$

Parity and Time-reversal Violating Terms

Under the parity operation $\widehat{P}$, $\vec{r} \to -\vec{r}$ and $\vec{p} \to -\vec{p}$, but spin $\vec{s}$ and time *t* remain unchanged. A Hamiltonian that contains terms such as $\vec{r}.\vec{s}$ or $\vec{s}.\vec{p}$ violates parity. Similarly, under the time-reversal operation $\widehat{T}$, $t \to -t$, $\vec{p} \to -\vec{p}$ and $\vec{s} \to -\vec{s}$, but $\vec{r}$ remain unchanged. When present in the Hamiltonian, terms like $\vec{r}.\vec{p}$ and $\vec{r}.\vec{s}$ violate time-reversal invariance, leading to a doublet structure in the spectrum as both $\widehat{P}$ and $\widehat{T}$ correspond to two-fold discrete symmetry. A connection between rotational motion and $\hat{P}$ and $\hat{T}$-violating Hamiltonian occurs if the system, while violating $\hat{R}_x(\pi)$ symmetry, preserves the $\hat{R}_x\hat{P}$ or $\hat{R}_x\hat{T}$ symmetry (see Table I).

Ellipsoid with D_2 Symmetry – Asymmetric Top

A general ellipsoid does not have axial symmetry, but has full D_2-symmetry, i.e., the system is invariant with respect to the three rotations by 180^0 about each of the three principal axes (tri-axial shape). The nucleus has a finite γ-deformation different from 0^0 or multiples of $2\pi/3$. Even if the γ-motion is frozen, K is not a good quantum number, and the wave function may be of the form:

$$\Phi^I_M(\gamma,\theta_1,\theta_2,\theta_3) = \sum_K g^I_K \left[D^I_{MK} + (-1)^I D^I_{M-K}\right].$$

Since K is allowed to have only even-integer values, values $K = 2, 4$ …… can be adopted; $K = 0$ is not allowed as axial symmetry has been lost. Parity and signature are still good quantum numbers as $P = 1$ and $R_x(\pi) = 1$. Besides these two operations, $R_y(\pi)\ T$ is also conserved (assuming rotation about the x-axis, which is also the long axis of the ellipsoid). A typical rotational band may have I = 2, 4, 6 ……, corresponding to the first row of Table I. This situation is shown in the upper panel of Fig. 11.

Odd-Multipole Shapes: Simplex Quantum Number

An odd-multipole shape such as Y_{30} (octupole deformation) has an axial symmetry, say about the long axis, violating the $\hat{R}_x(\pi)$ and $\hat{P}$ symmetry, but preserving $\hat{R}_x\hat{P}$. The reflection symmetry is broken and two degenerate states with identical shapes arise, corresponding to the two minima in the octupole deformation energy (Fig. 12), i.e., 9th row of Table I. Operation $\hat{R}_x\hat{P}$ corresponds to a reflection in a plane containing the symmetry axis, denoted by

$$\hat{S} = \hat{P}\hat{R}_x^{-1},$$

where $\hat{S}$ acts on the intrinsic variables.

$K = 0$ band: intrinsic states with $K = 0$ are eigenstates of $\hat{S}$ as well as $\hat{T}$, in which

$$\hat{S}\chi_{K=0} = s\chi_{K=0} = e^{-i\sigma\pi}\chi_{K=0}.$$

Since $\hat{P} = \hat{S}\hat{R}_x$ and $\hat{R}_x D^I_{MK=0} = (-1)^I D^I_{MK=0}$, we obtain

$$\pi = s(-1)^I,$$

where π is the eigenvalue of $\hat{P}$. Hence, the $K = 0$ band can be classified as

$$I^\pi = 0^+, 1^-, 2^+, 3^- \ldots\ldots\ldots, s = +1,$$

$$\text{or } I^\pi = 0^-, 1^+, 2^-, 3^+ \ldots\ldots\ldots\ldots, s = -1.$$

For $K \neq 0$, intrinsic states have a two-fold degeneracy with respect to $\hat{T}$ (Kramer's degeneracy), and the band is classified as

$$I = \frac{1}{2}^-, \frac{3}{2}^+, \frac{5}{2}^- \ldots\ldots\ldots\ldots, s = -i,$$

$$\text{or } I=\frac{1}{2}^{+},\frac{3}{2}^{-},\frac{5}{2}^{+}\ldots\ldots\ldots\ldots\ldots, s=+i\,,$$

where only levels with $I \geq K$ occur. Since $\hat{S}\chi_K = \chi_{\bar{K}}$, the positive and negative parity states with the same spin are degenerate, giving rise to the phenomenon of parity doublets.

Examples of Octupole Deformed Nuclei

Shell effects play a major role in stabilizing a given configuration towards a particular nuclear shape. Nuclei lying in a narrow range beyond ^{208}Pb and to a lesser extent the nuclei in the neutron-excess light rare-earths have been found to be prone to octupole deformation of the Y_{30} type. As shown in Fig. 13, appropriate orbitals with $\Delta l = 3$ are observed to be very close together and near the Fermi energy for nuclei just beyond ^{208}Pb. For example, $1j_{15/2}$ and $2g_{9/2}$ neutron orbitals are 1.42 MeV apart in ^{209}Pb, while $1i_{13/2}$ and $2f_{7/2}$ proton orbitals are 1.70 MeV apart in ^{209}Bi. The corresponding orbitals in the rare-earth are $1i_{13/2}$ and $2f_{7/2}$ neutron orbitals and $1h_{11/2}$ and $2d_{5/2}$ proton orbitals, and for the lighter nuclei the $1g_{9/2}$ and $2p_{3/2}$ orbitals come close together near particle number 34. An early review of the experimental systematics that support the octupole deformation appears in Jain et al. (1990), and a detailed account of theory and experiment related to the octupole shapes can be found in Butler and Nazarewicz (1996).

As noted earlier, parity doublets arise of the type $I^{\pi} = 0^{\pm}, 1^{\pm}, 2^{\pm}\ldots\ldots$ in even-even, and $I^{\pi} = \frac{1}{2}^{\pm}, \frac{3}{2}^{\pm}, \frac{5}{2}^{\pm}\ldots.$ in odd-A nuclei. These parity doublet (PD) bands split into two, if the barrier separating the two octupole minima has a finite height. Due to tunneling between the two mirror octupole shapes, the two bands of opposite parity are displaced in energy with respect to each other, and the even spins are energetically favoured (Fig. 14). A similar situation exists for odd-A nuclei, that is also shown in Fig. 14. Consider *K = 1/2* bands in which the rotational band is further modified by the octupole decoupling parameter $a^{*} = a.\,p$, so that

$$E = E_0 + A\left[I(I+1) + a^{*}(-1)^{I+\frac{1}{2}}(I+\frac{1}{2}) \right],$$

and obviously $a^{*}(p=+1) = -a^{*}(p=-1)$. Thus, the decoupling parameters for *K = 1/2* bands have opposite sign, but nearly same absolute value. The possibility of tunneling along with octupole decoupling further complicates the energies of the *K = 1/2* band as shown in Fig. 14.

An example of a spectrum where PD bands have been observed is given in Fig. 15 (level scheme of ^{225}Ra taken from Gasparo et al. (2000)). The first interpretation of ^{225}Ra in terms of octupole deformation was provided by Sheline et al. (1989), and the experimental studies of Gasparo et al. (2000) further confirm this interpretation in which 5 PD bands can be identified in the observed spectrum. Each pair of PD bands has been assigned a labelling $K(\langle s_z \rangle, \langle \pi \rangle)$, and for *K = 1/2* bands $\langle -j_+ \rangle$, the octupole decoupling parameter. Value of $\langle \hat{\pi} \rangle$ indicates the degree of parity mixing in the single particle states.

Density Distribution – Two Planes of Symmetry

Axial-symmetry is lost when shapes like $Y_{3\mu}$, $\mu \neq 0$ are considered. The density distribution has only two independent planes of symmetry for μ even, and rotation is possible about the long axis. As well as $R_x(\pi) = 1$, $R_y(\pi)T = P$, and parity doublets of even or odd angular momenta arise. Therefore, we expect a level pattern such as $I = 2^{\pm}, 4^{\pm}$.... etc., or $I = 1^{\pm}, 3^{\pm}, 5^{\pm}$.........etc.
(row 12 in Table I, and the top panel of Fig. 16).

If the axis of rotation is perpendicular to one of the symmetry planes and the rotation axis is denoted as the *x*-axis, we have $\hat{R}_x(\pi) = \hat{P}$ and $\hat{R}_y(\pi)T = \hat{P}$ in which signature is not a good quantum number. A pair of parity doublet bands is obtained such as for axial symmetry: $I = 4^+, 5^-, 6^+$........ and $I = 4^-, 5^+, 6^-$........... (as given in row 13 of Table I). This situation is also shown in the middle panel of Fig. 16, and is discussed below as tetrahedral symmetry.

Density Distribution - Only One Plane of Symmetry

Further symmetry reductions occur if only one plane of symmetry is supported by the nuclear shape; under such circumstances one may also have odd μ components. Fig. 16 depicts such a shape in which rotation is possible along the long axis as well as any one of the short axes. Signature is not a good quantum number in either case, and both even and odd spins will be found in the rotational sequence. Parity is also not conserved, and therefore both parities will occur. When rotation is about the long axis, $\hat{R}_y(\pi)T = \hat{P}$ and four distinct situations can be obtained by the application of $\hat{R}_x(\pi)$ and $\hat{P}$. A sequence such as $I^{\pi} = 4^{\pm}, 5^{\pm}, 6^{\pm}$......... is obtained that represents the situation shown as row 12 of Table I, and is depicted in the top panel of Fig. 17. However, when rotation is about one of the short axes, $\hat{R}_x(\pi) = \hat{P}$, four distinct situations occur through the application of $\hat{R}_x(\pi)$ and $\hat{R}_y(\pi)T$, with the derivation of two nearly-degenerate sequences such as $I^{\pi} = (8^+)^2, (9^-)^2, (10^+)^2$........ The two $\Delta I = 1$ degenerate sequences with alternating parity represent bands that are chiral partners (one left-handed and the other right handed), as defined by row 11 of Table I and in the bottom panel of Fig. 17.

Tetrahedral and Triangle Symmetries in Nuclei

As suggested by Li and Dudek (1994), there is a possibility of observing a four-fold degeneracy in the level patterns of a number of *N ~ 136* isotones. This symmetry arises as a consequence of the $\lambda = 3$, $\mu \neq 0$ components in the nuclear shape (see preceeding sections). A tetrahedral symmetry is expected in particular to break both the spherical symmetry and the symmetry by inversion. More specifically, a deformation of $Y_{32}(\theta, \phi)$ is related to the T_d^D symmetry group because of two 2-dimensional and one 4-dimensional irreducible representations. Therefore, three families of multiplets exist: two are doubly degenerate and one is quadruply degenerate.

Theoretical spectra of single particle states as a function of the deformation parameter a_{32} (coefficient of the Y_{32} term) reveal strongly increasing gaps at *Z = 32*, $\Delta E > 2MeV$, at *Z = 40* with $\Delta E \approx 3MeV$, and a huge gap at *Z = 56, 58* with $\Delta E \approx 4MeV$ (Fig. 18). Calculations reveal strong tetrahedral-symmetry effects at N, Z = 16, 20, 32, 40, 56-58, 70, 90-94 for both neutrons/protons, and 136/142 for neutrons only. These minima in tetrahedral shapes coincide with oblate and/or prolate minima in energy. A ten-dimensional minimization in energy for $\beta, \gamma, a_{3\mu}(\mu = 0, 1, 2, 3)$, and $a_{4\mu}(\mu = 0, 1, 2, 3, 4)$ shapes leads to tetrahedral equilibrium shapes of $a_{32} = 0.13, 0.13, 0.15$ and 0.11 for ${}^{80}_{40}Zr_{40}$, ${}^{108}_{40}Zr_{68}$, ${}^{160}_{70}Yb_{40}$ and ${}^{242}_{100}Fm_{142}$, respectively. The tetrahedral nuclei also obey the simplex symmetry and lead to parity-doublet bands, but with one important difference: since these nuclei will not have any significant dipole moment, typical E1 transitions of axial octupole nuclei will be absent. We compare the rotational spectrum of an axial-octupole nucleus with a tetrahedral rotor in Fig. 19. A pear-shaped octupole nucleus has considerable dipole moment and hence strong E1 and E2 transitions. On the other hand, a tetrahedral "pyramid" shape rotor with some quadrupole shape has zero dipole moment, and the lowest multipole transitions will be pure E2 type. However, only E3 transitions will be seen in the ideal case of a pure tetrahedral rotor.

Recent calculations of Yamagami et al (2000) suggest the possibility of exotic shapes that break the reflection and axial symmetries in proton rich $N = Z$ nuclei: ${}^{64}Ge$, ${}^{68}Se$, ${}^{72}Kr$, ${}^{76}Sr$, ${}^{80}Zr$ and ${}^{84}Mo$. In particular, the oblate ground state of ${}^{68}Se$ is very soft against Y_{33} triangular deformation, and the low-lying spherical minimum co-existing with the prolate ground state in ${}^{80}Zr$ is extremely soft against the Y_{32} tetrahedral deformation. The Y_{33} triangular deformation has only one plane of symmetry and a rotational spectrum that differs significantly from the Y_{32} tetrahedral shape. There are no known examples of Y_{32} and Y_{33} symmetries so far, although their experimental discovery is a distinct possibility.

Rotation About an Axis Other than the Principal Axis - Tilted Axis Cranking

So far we have considered situations where rotation is always about one of the principal axes of the body. Riemann had pointed out the possibility of having ellipsoidal shapes of equilibrium when the vorticity of internal motion of a non-rigid system leads to uniform rotation about an axis different from the principal axes of the density distribution. Nuclear configurations can occur that support rotation about an axis lying in one of the principal planes (planar-tilted axis cranking), or rotation about an axis lying out of the three principal planes (aplanar-tilted axis cranking).

Consider the effect of planar- and aplanar-tilted axis of rotation for a tri-axial shape. Parity P and $\hat{R}_y(\pi)T$ are conserved for rotation about an axis lying in one of the principal planes. Signature is not a good quantum number; and therefore all spins will be seen with the same parity (e.g., a sequence like $I^\pi = 4^+, 5^+, 6^+......$, corresponding to row 2 of Table I, as shown in the middle panel of Fig. 11).

A further doubling of states occurs if the axis of rotation is out of all the principal planes (aplanar TAC), in which only parity is conserved. Four distinct situations are obtained by the operation of $R_x(\pi)$ and $R_y(\pi)T$ to give a rotational sequence of the type $I^\pi = (4^+)^2, (5^+)^2, (6^+)^2......$, where each spin occurs twice and is almost degenerate. This situation is defined as row 3 of Table I, and is depicted in the bottom panel of Fig 11.

Consider odd-multipole shapes such as octupole shape in which planar TAC gives rise to a situation, where $R_y(\pi)T = P$. Parity is no longer an invariant operation, and we obtain four distinct situations by the application of $R_x(\pi)$ and P. Two nearly degenerate rotational sequences emerge of $I^\pi = 4^\pm, 5^\pm, 6^\pm.....$ (identical to the situation specified in row 13 of Table I, and shown in the bottom panel of Fig. 16).

Magnetic Rotation – Magnetic Top

Recent studies have shown that the isotropy of the mean field can be broken in a way other than through an anisotropic charge density distribution. The new kind of anisotropy arises from the net magnetic dipole moment instead of net electric quadrupole moment. Such a situation arises when a higher-lying high-j neutron particle (hole) combines with a high-j proton hole (neutron) at right angles to each other. Therefore, the resultant angular momentum about which the nucleus appears to rotate makes an angle with the principal axes (Fig. 20). Magnetic effects of current anisotropy dominate when the deformation is small. As shown in Fig. 20, a net magnetic dipole moment is generated, and implies current anisotropy. Higher angular momentum states are generated by the closing of the neutron and the proton blades as in a pair of shears, hence the term "shears mechanism" (Frauendorf, 1993). As a consequence, we obtain a "rotation" band, $R_x(\pi)$ symmetry is broken and signature is no longer a good quantum number. A $\Delta I = 1$ band is formed as shown in the example of ^{134}Ce (Fig. 21); consecutive levels of band B5 in ^{134}Ce are connected by strong M1 transitions, with the M1 intensity decreasing as the shears close (Fig. 22) as a result of a decrease in the dipole moment with increasing spin. The first example of MR band would appear to be that of ^{83}Kr, as reported recently by Malik et al., (2004), although a large number of such cases have been discovered that are spread within the A = 80, 110, 130, 190 mass regions (Amita et al., 2000).

Chiral Bands

An aplanar tilt is possible in which the axis of rotation does not coincide with any of the three principal axes, nor lie in any of the principal planes. Such a situation is best visualized in a triaxial odd-odd nucleus. If the configuration is such that the odd-proton alignment is along the short axis, the odd-neutron alignment is along the long axis, and the rotational contribution is along the intermediate axis, we obtain three angular momenta perpendicular to each other and the resultant angular momentum acquires an aplanar tilt. Note that the rotation has been taken along the intermediate axis because the moment of inertia about this axis is maximum and the rotational energy is minimum. While parity is still conserved, such an arrangement breaks the $R_y(\pi)T$ symmetry. The two situations shown in the upper part of this panel have a right-handed sense of rotation; while on the other hand, the two situations shown in the lower part have a left-handed sense of rotation. This breakage of symmetry doubles the number of levels, and we should observe two pairs of identical $\Delta I = 1$ bands with the same parity that are termed chiral bands.

The bands in real nuclei will be shifted in energy because of tunneling between the right-handed and left-handed states. However, the existence of triaxiality and an optimum quadrupole deformation play an important role in breaking chiral symmetry. Dimitrov et al. (2000) presented the first results of an aplanar TAC calculation which support the existence of chiral bands in ^{134}Pr, although recent observations of a chiral pair of bands in an odd-A nucleus ^{135}Nd (Zhu et al. (2003)) have confirmed that chiral rotation is a purely geometric phenomenon and not confined to odd-odd systems alone. The level scheme of ^{135}Nd is shown in Fig. 23, where the A and B bands become chiral partners at higher rotational frequencies. The triaxial shapes shown in the upper part of the figure are labeled by l, s and i-axes which stand for long, short and intermediate axes, respectively. Expressed in the order s-i-l, these axes form a "right-handed" system in the ellipsoid on the left and a "left-handed" system in the ellipsoid on the right to give a chiral doublet. Bands A and B are shown in the level scheme, and come very close to and interlaced with each other at a rotational frequency of about 0.45 MeV. Since the two bands are based on the same configuration $\left[\pi h_{11/2}^{2}, \nu h_{11/2}^{-1}\right]$, there are a significant number of linking transitions. Fig. 24 shows a pair of such bands in ^{135}Ce, which is an odd-A nucleus (Lakshmi et al, unpublished). We observe a two-way connection between the pair of bands for the first time, confirming that the pair of bands have the same configuration. These studies also indicate that the chiral bands are purely a geometrical phenomenon arising out of the special situation of the three vectors.

Conclusions

The basics of geometrical symmetries and their consequences in nuclei have been discussed. Connections between the various shapes and band structures were emphasized, and unusual shapes were also considered. Recent discoveries such as the magnetic rotation and chiral rotation were noted, which involve rotation about a tilted axis rather than the usual principal axis. Efforts have been made to develop a simple guide that will be useful to experimentalists.

Acknowledgements

Financial support from the IAEA,Vienna; DST (Government. of India); and DAE (Government. of India) is gratefully acknowledged.

Bibliography

General References:

A. Bohr and B.R. Mottelson, Nuclear Structure, Vol.1, Single Particle Motion, and Vol.2, Nuclear Deformations, Benjamin (1969 and 1975).

M.K. Pal, Theory of Nuclear Structure, East-West Press (1982).

P. Ring and P. Schuck, The Nuclear Many Body Problem, Springer (1980).

K. Heyde, Basic Ideas and Concepts in Nuclear Physics, 2nd Edition, IOP Publishing (1999).

L.D. Landau and E.M. Lifshitz, Quantum Mechanics, Vol. 3 of Course of Theoretical Physics, Pergamon Press (1956).

Table of Isotopes, Eighth Edition, Wiley (1996).

Symmetries:

W. Greiner and J.A. Maruhn, Nuclear Models, Springer (1989).

J. Dobaczewski, J. Dudek, S.G. Rohozinski and T.R. Werner, Phys. Rev. **C62**, (2000) 014310 and 014311.

P. Van Isacker, Rep. Prog. Phys. **62** (1999) 1661.

S. Frauendorf, Rev. Mod. Phys. **73** (2001) 463.

Reflection Asymmetric Shapes:

P.A. Butler and W. Nazarewicz, Rev. Mod. Phys. **68** (1996) 349.

A.K. Jain, R.K. Sheline, P.C. Sood and K. Jain, Rev. Mod. Phys. **62** (1990) 393.

R.K. Sheline, A.K. Jain, K. Jain and I. Ragnarsson, Phys. Lett. **B219** (1989) 47.

J. Gasparo, G. Ardisson, V. Barci and R.K. Sheilne, Phys. Rev. **C62** (2000) 064305.

Tetrahedral and Triangular Shapes:

X. Li and J. Dudek, Phys. Rev. **C49** (1994) R1250.

S. Takami, K. Yabana and M. Matsuo, Phys. Lett. **B431** (1998) 242.

M. Yamagami, K. Matsuyanagi and M. Matsuo, Nucl. Phys. **A672** (2000) 123.

Magnetic Rotation:

S. Frauendorf, Nucl. Phys. **A557** (1993) 259c.

R.M. Clark and A.O. Macchiavelli, Ann. Rev. Nucl. Part. Sci. **50** (2000) 1.

Amita, A.K. Jain and B. Singh, At. Data Nucl. Data Tables **74** (2000) 283; revision to be published (2003).

A.K. Jain and Amita, Pramana - J. Phys. **57** (2001) 611.

S.S. Malik, P. Agarwal and A.K. Jain, Nucl. Phys. **A732** (2004) 13.

S. Lakshmi, H.C. Jain, P.K. Joshi, Amita, P. Agarwal, A.K. Jain and S.S. Malik, Phys. Rev. **C66** (2002) 041303(R) .

S. Lakshmi, H.C. Jain, P.K. Joshi, A.K. Jain and S.S. Malik, Phys. Rev. **C69** (2004) 43194.

Chiral Bands:

V.I. Dimitrov, S. Frauendorf and F. Donau, Phys. Rev. Lett. **84** (2000) 5732.

D.J. Hartley et al., Phys. Rev. **C64** (2001) 031304(R).

S. Zhu et al., Phys. Rev. Lett. **91** (2003) 132501.

S. Lakshmi, H.C. Jain, P.K. Joshi and A.K. Jain, unpublished.

Critical Point Symmetries:

R.F. Casten and N.V. Zamfir, Phys. Rev. Lett. **87** (2001) 052503 .

F. Iachello, Phys. Rev. Lett. **91** (2003) 132502.

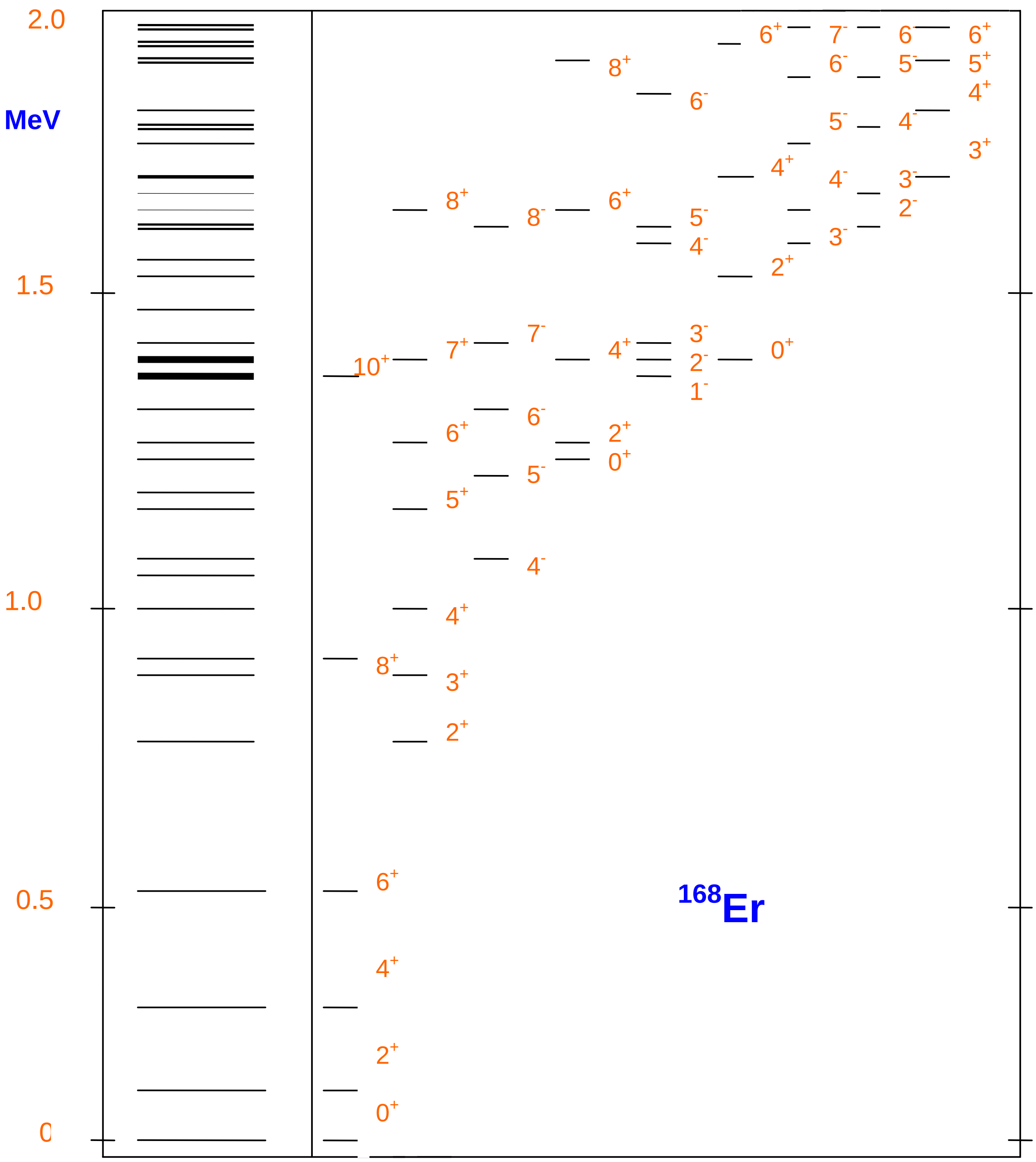

Fig. 1: Level energies shown in the left-hand column exhibit more systematic patterns when grouped into bands.

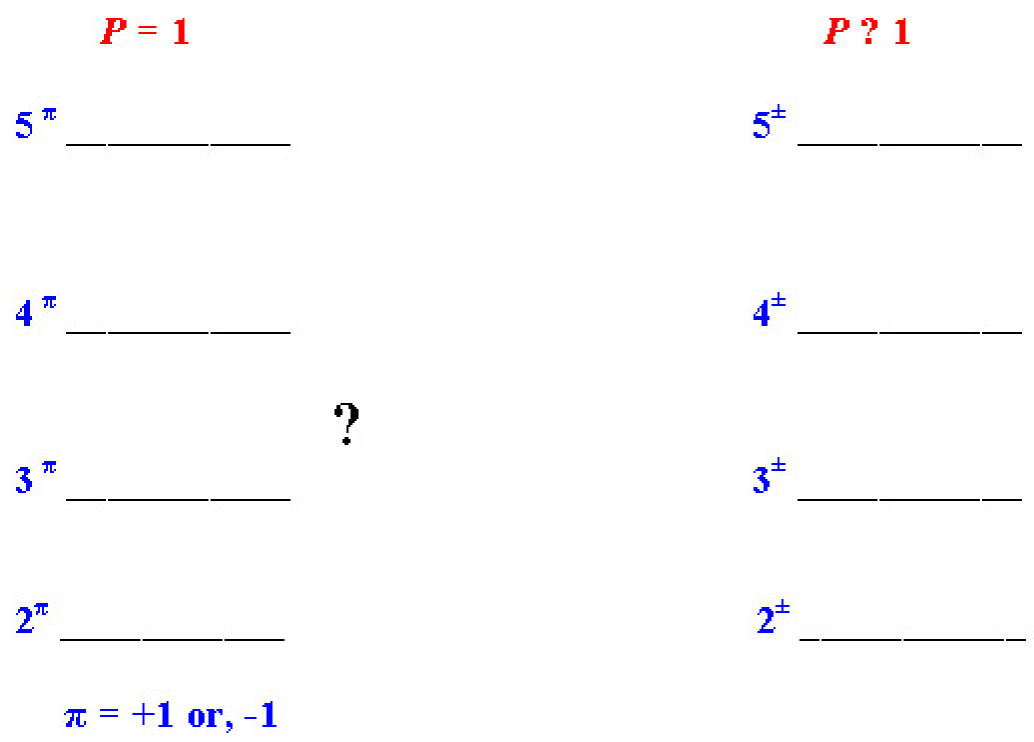

Fig. 2: As deformation increases, the shell model levels evolve into Nilsson model levels, signifying the loss of spherical symmetry.

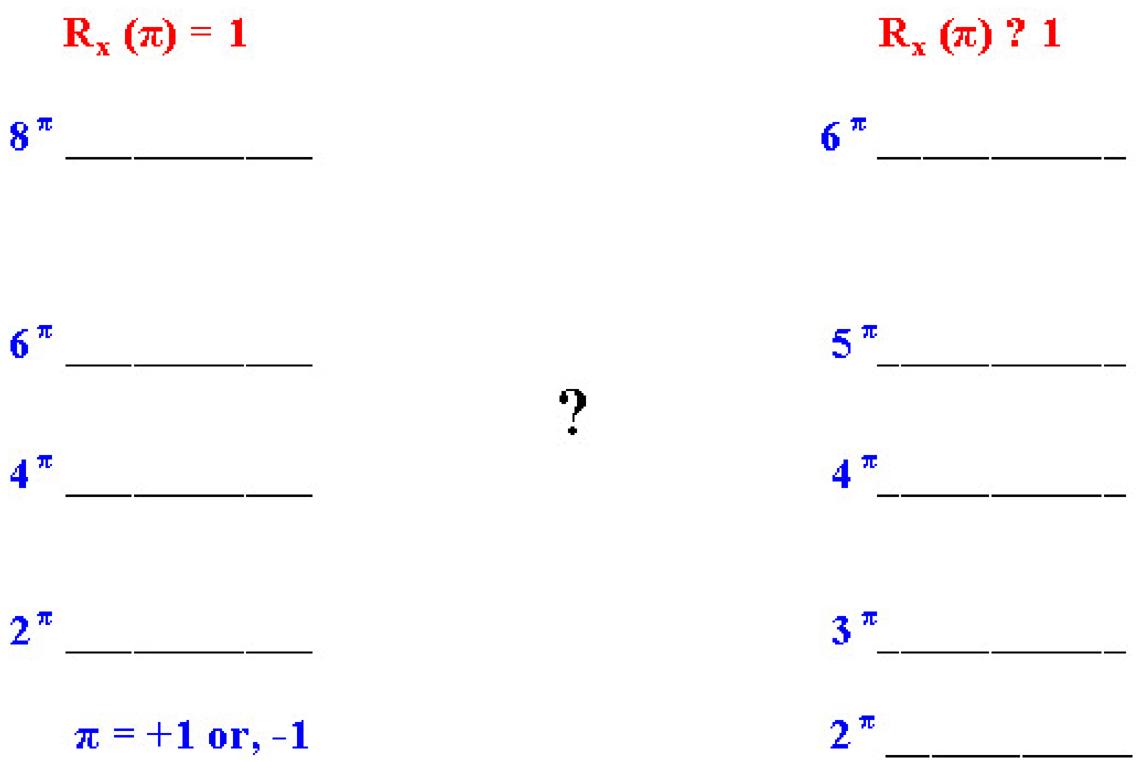

Fig. 3(a): Effect of symmetry breaking due to parity.

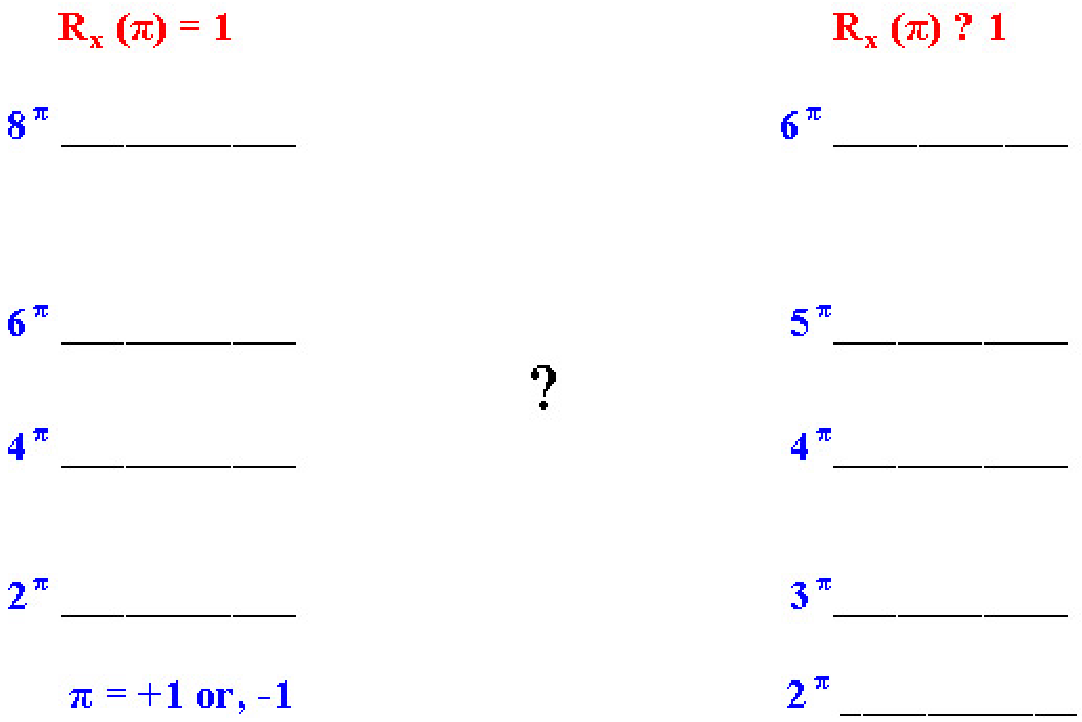

Fig. 3(b): Effect of symmetry breaking due to rotation by π about the x-axis $R_x(\pi)$ on a band (signature symmetry breaking).

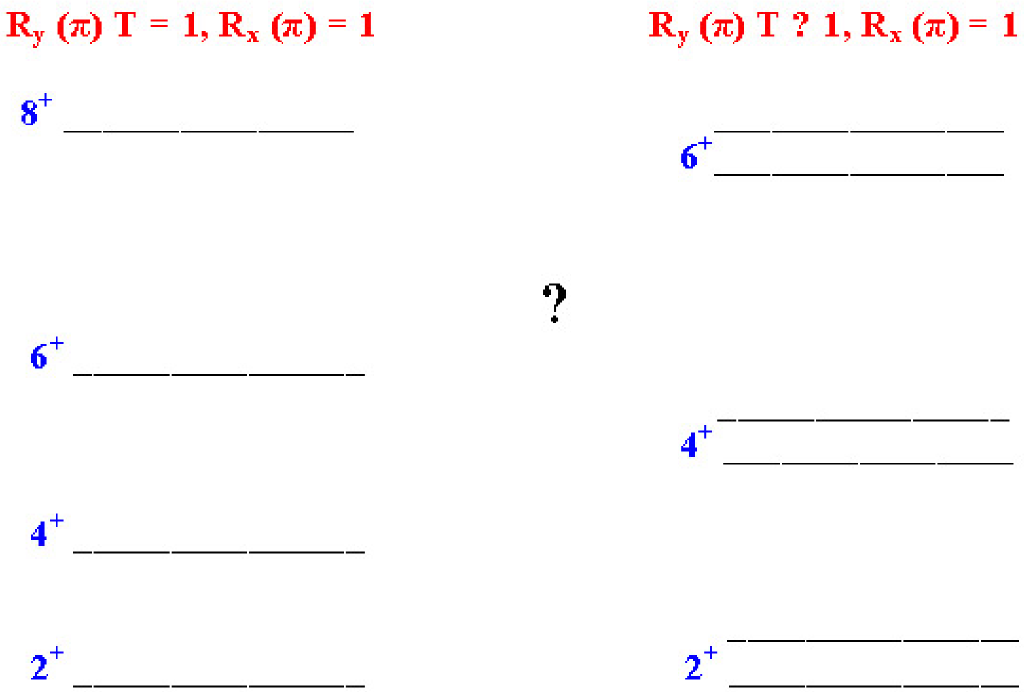

Fig. 3(c-1): Effect of symmetry breaking of $R_y(\pi)T$ on a band with a broken signature; T is the time reversal operator.

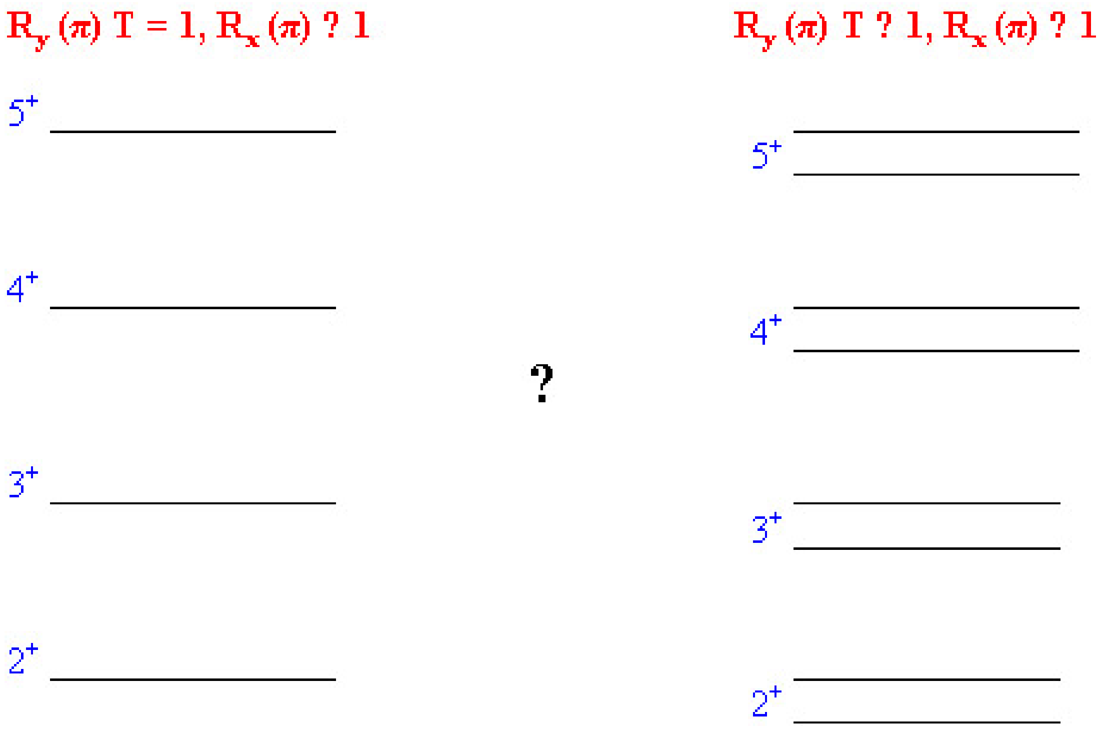

Fig. 3(c-2): Same as Fig 3(c-1), but for a band with a good signature.

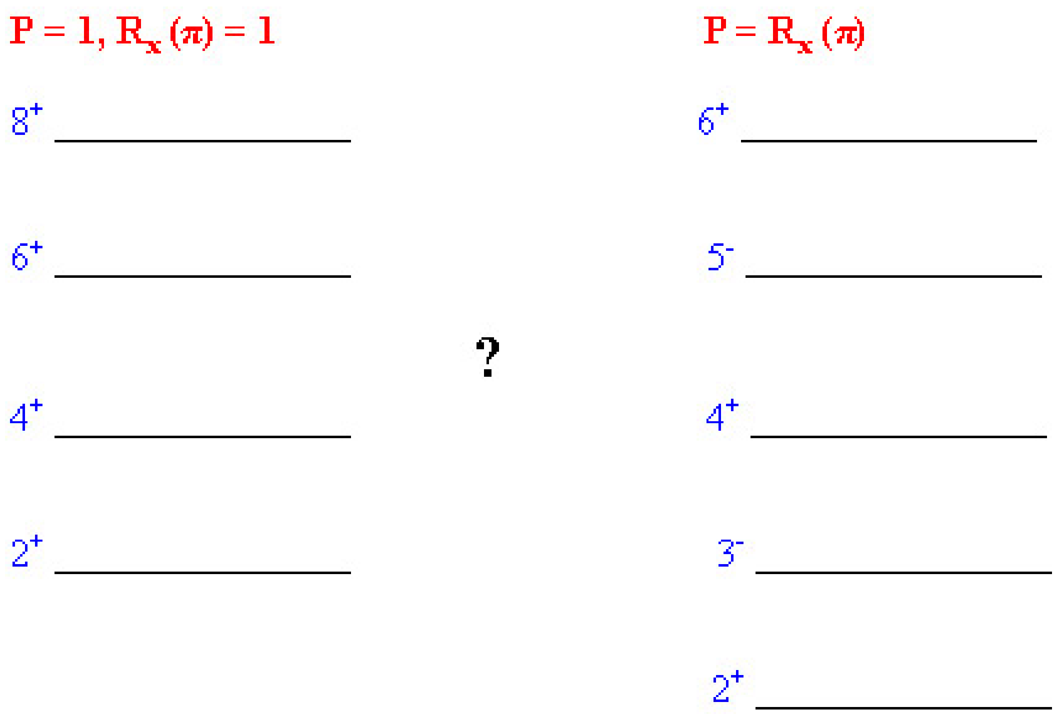

Fig. 3(d): Effect on a band when both parity P and signature $R_x(\pi)$ are broken, but $P = R_x(\pi)$.

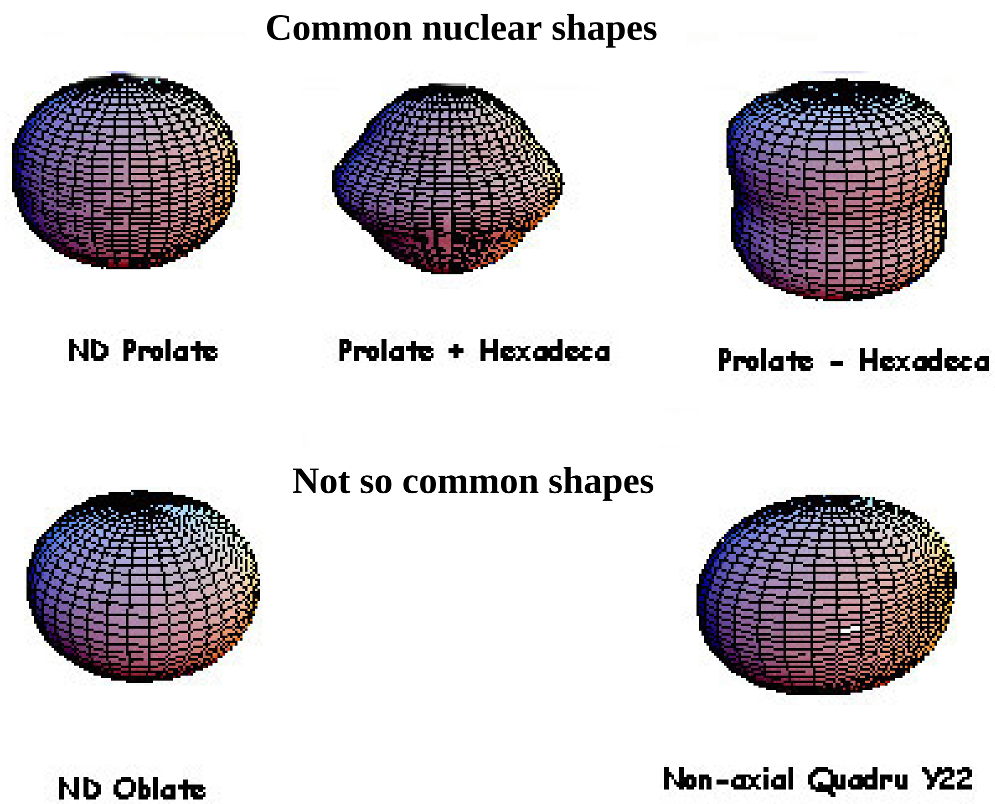

Fig. 4: Nuclear shapes with axial symmetry.

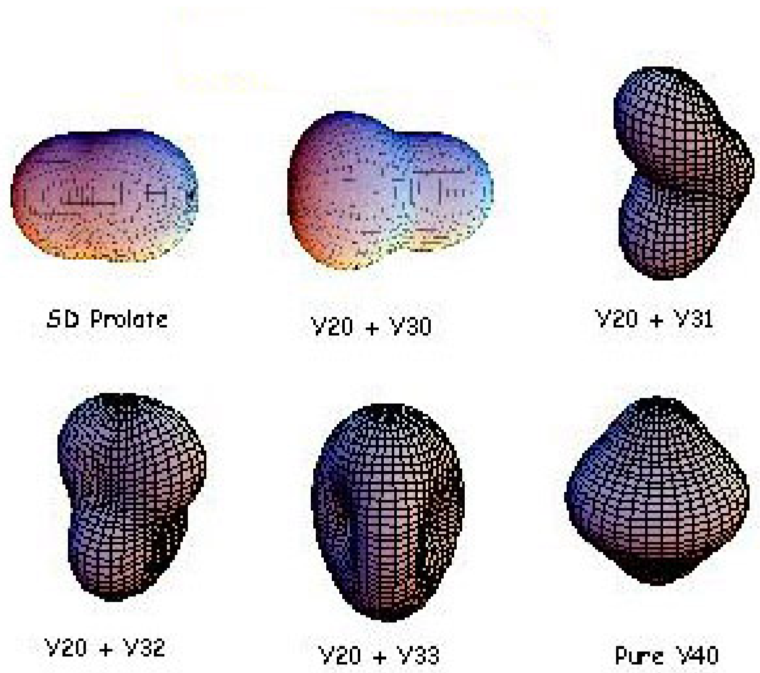

Fig. 5: Exotic nuclear shapes.

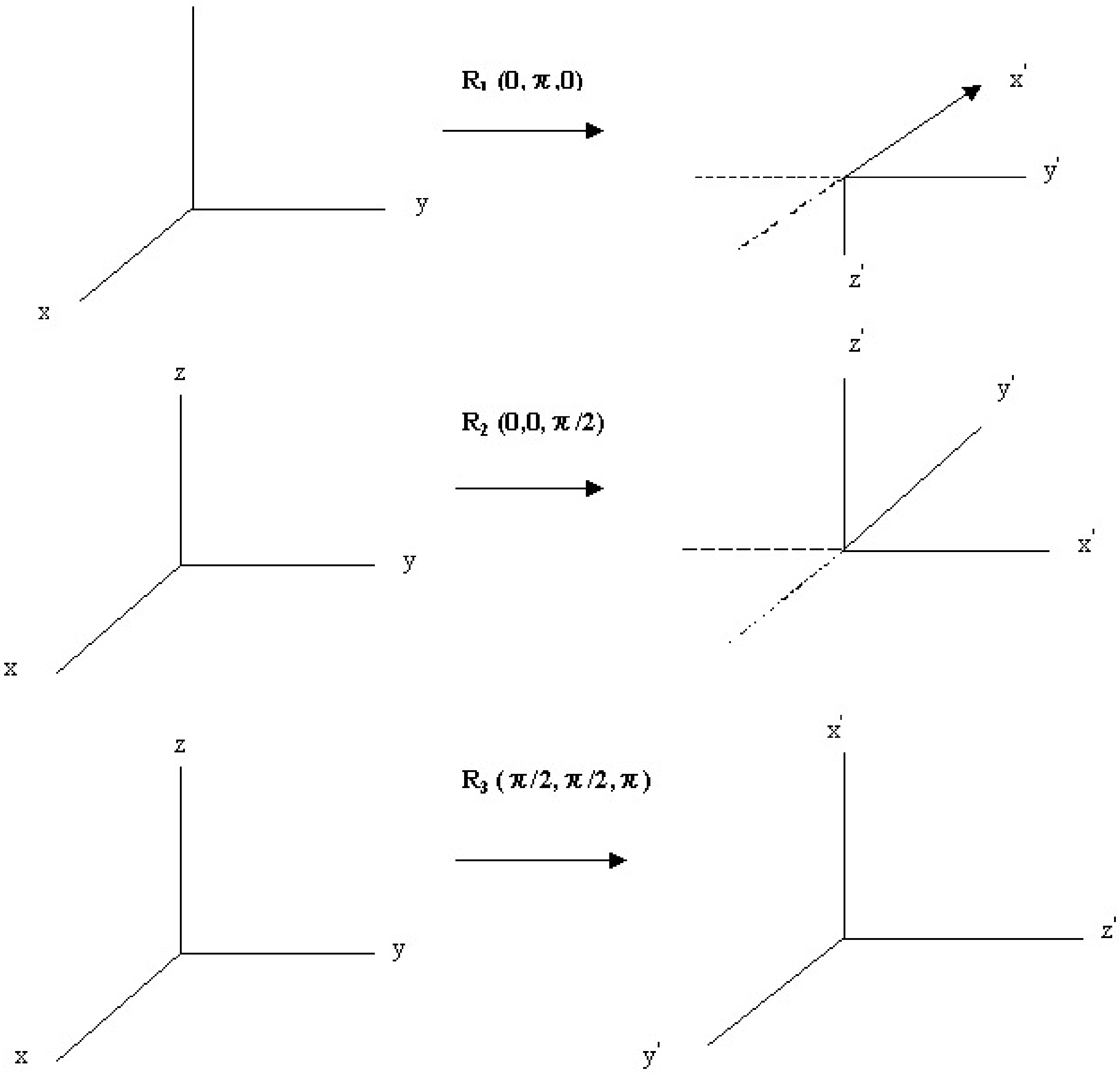

Fig. 6: Effect of the three rotation operators R_1, R_2, R_3 on a frame of reference.

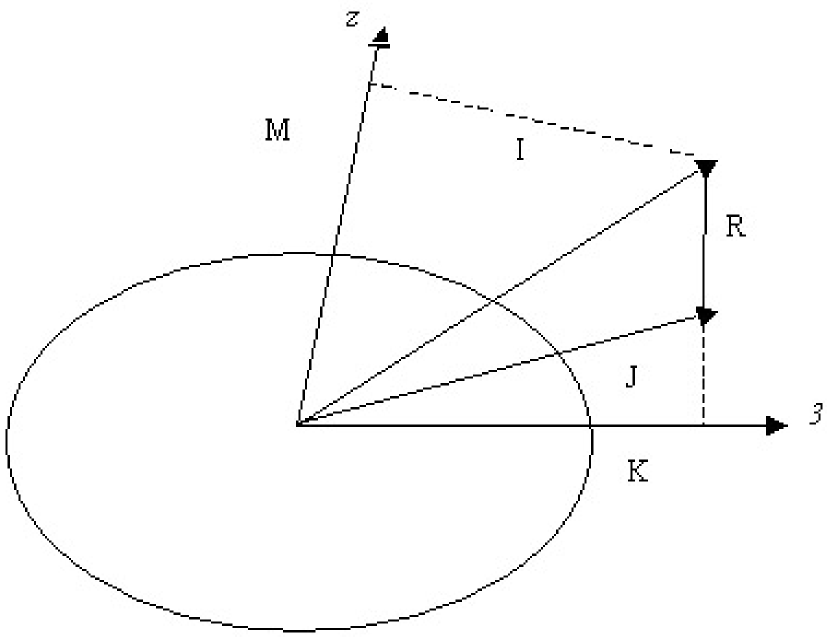

Fig. 7: Projections of the total angular momentum I on the space-fixed z-axis and the body- fixed 3-axis.

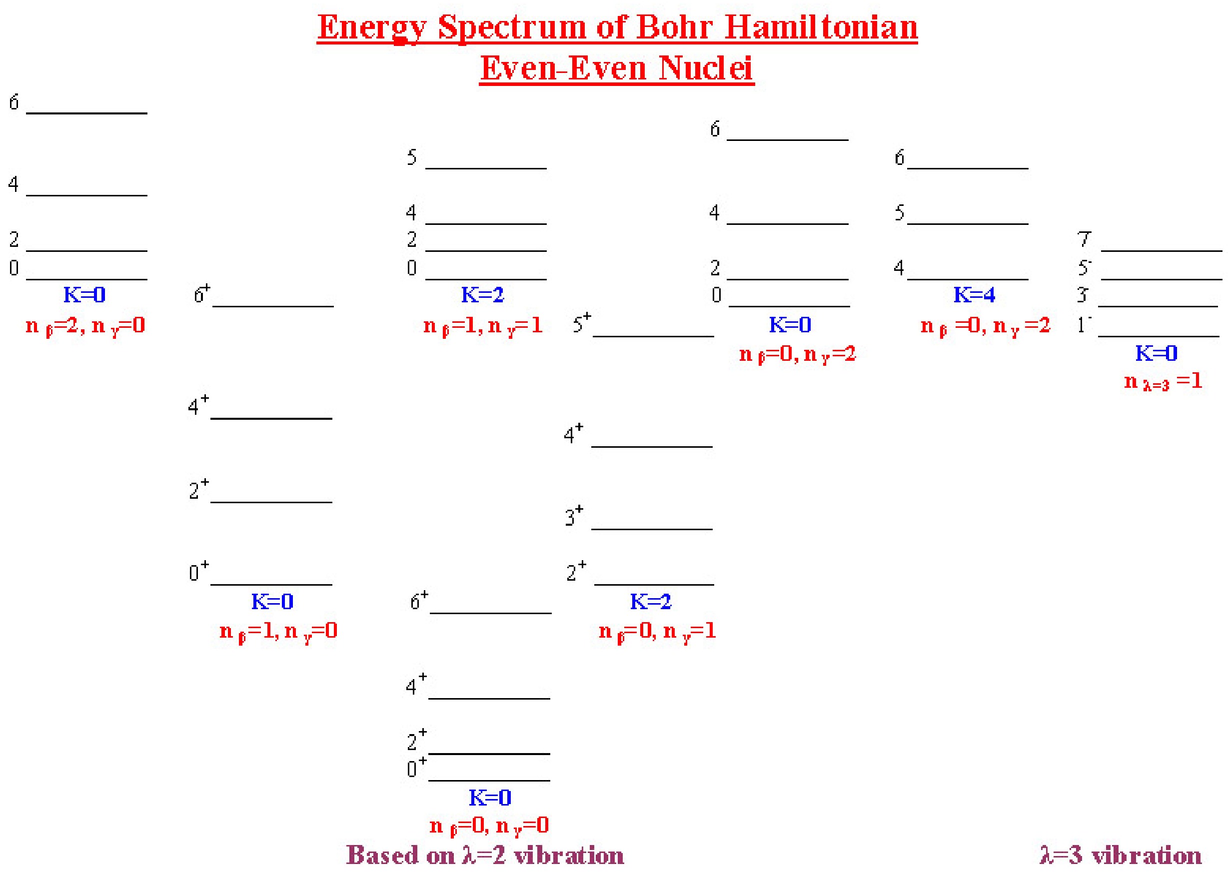

Fig. 8: Band structure of an even-even nucleus resulting from the quantization of a Bohr Hamiltonian for quadrupole shapes; one octupole band is also shown on the extreme right.

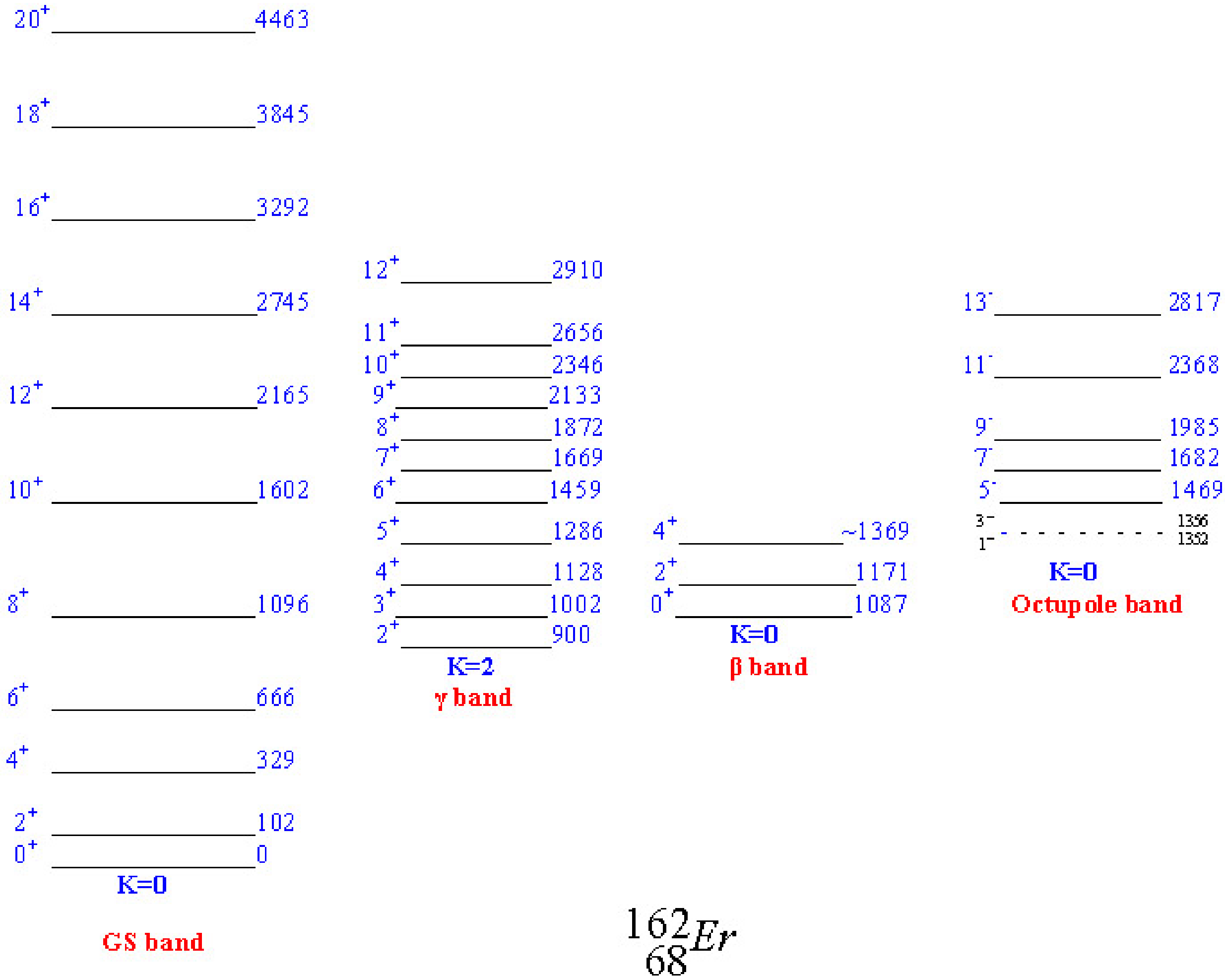

Fig. 9: Observed band structure in an even-even nucleus (^{162}Er) classified according to Fig. 8.

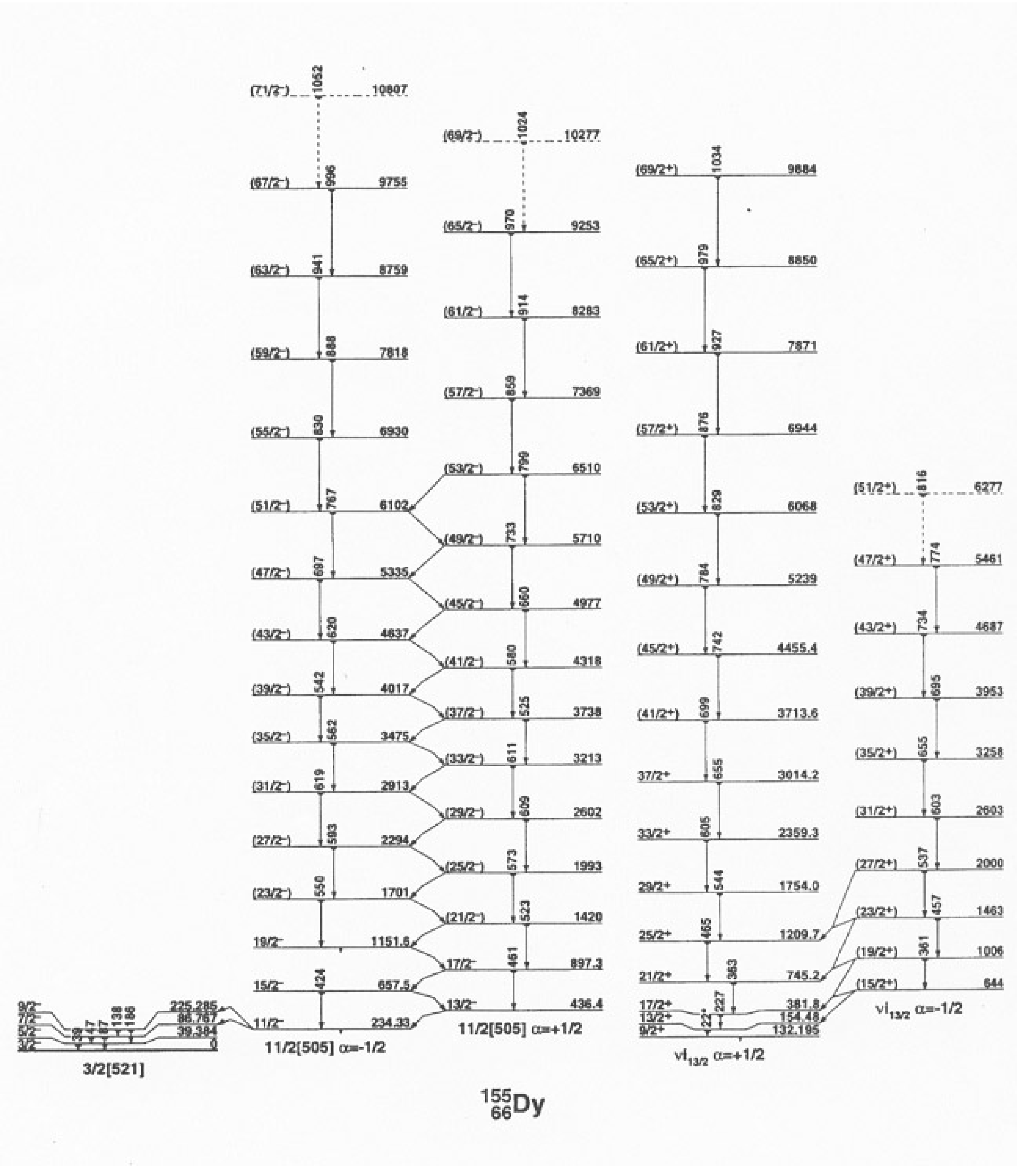

Fig. 10: Observed band structure in an odd-A nucleus (^{155}Dy) taken from the Table of Isotopes (bands are labeled by the signature quantum numbers).

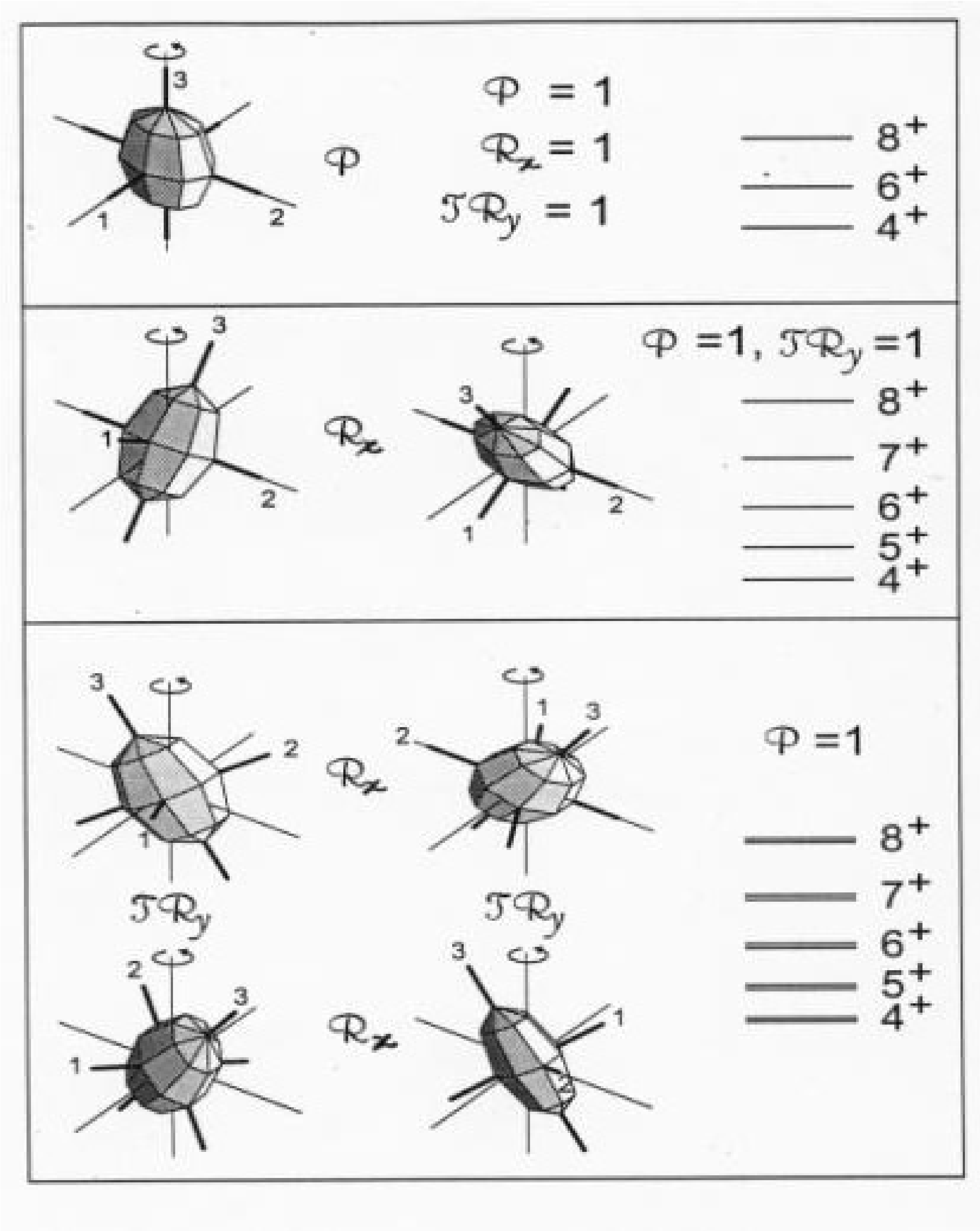

Fig. 11: Effect of planar (top and middle panel) and aplanar (bottom panel) axis of rotation on the rotational band of a tri-axial shape (Frauendorf, 2000).

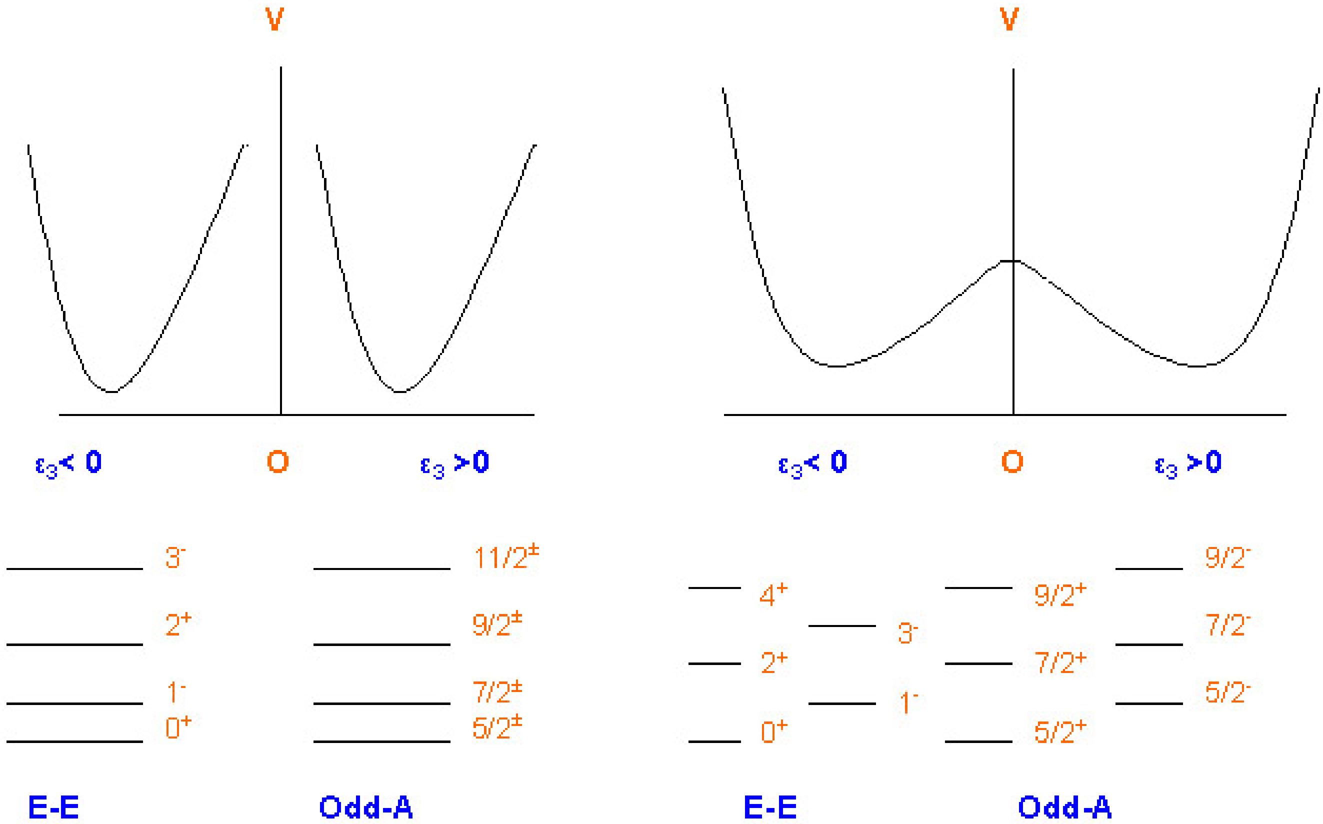

Fig. 12: Presence of an axially symmetric octupole shape leads to the breaking of parity: if the barrier in octupole degree of freedom is too high, the states do not mix and a band structure is obtained (as on the left); while mixing leads to a splitting of parity doublets for a finite barrier height.

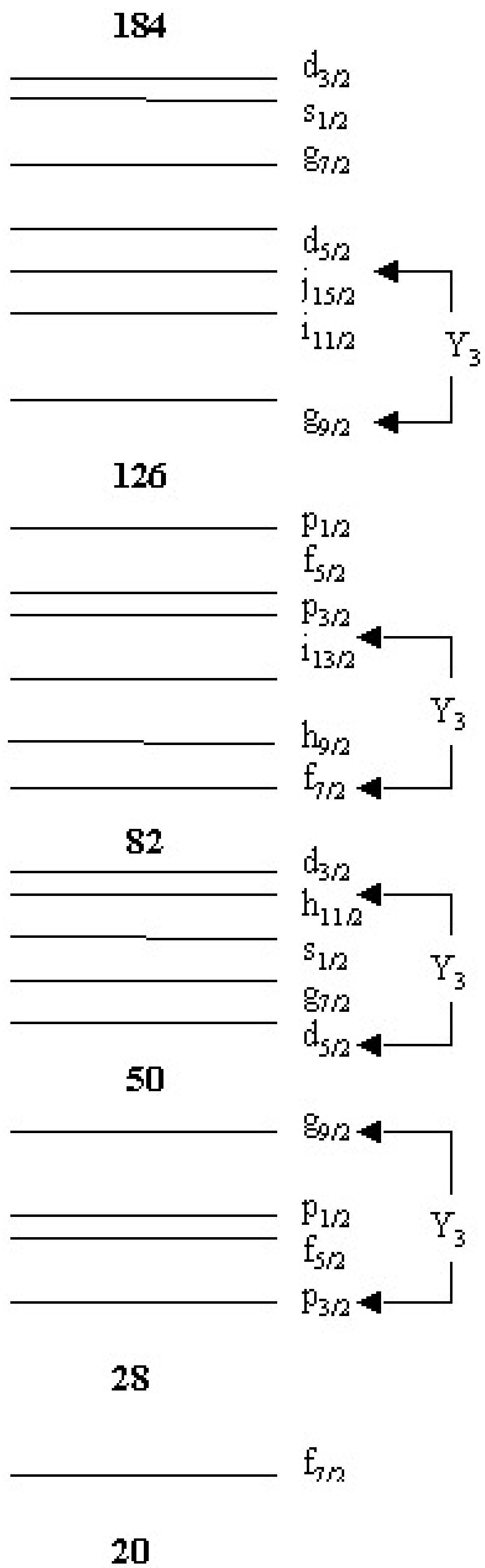

Fig. 13: Spherical single-particle states that show the proximity of levels differing in angular momentum by 3 units.

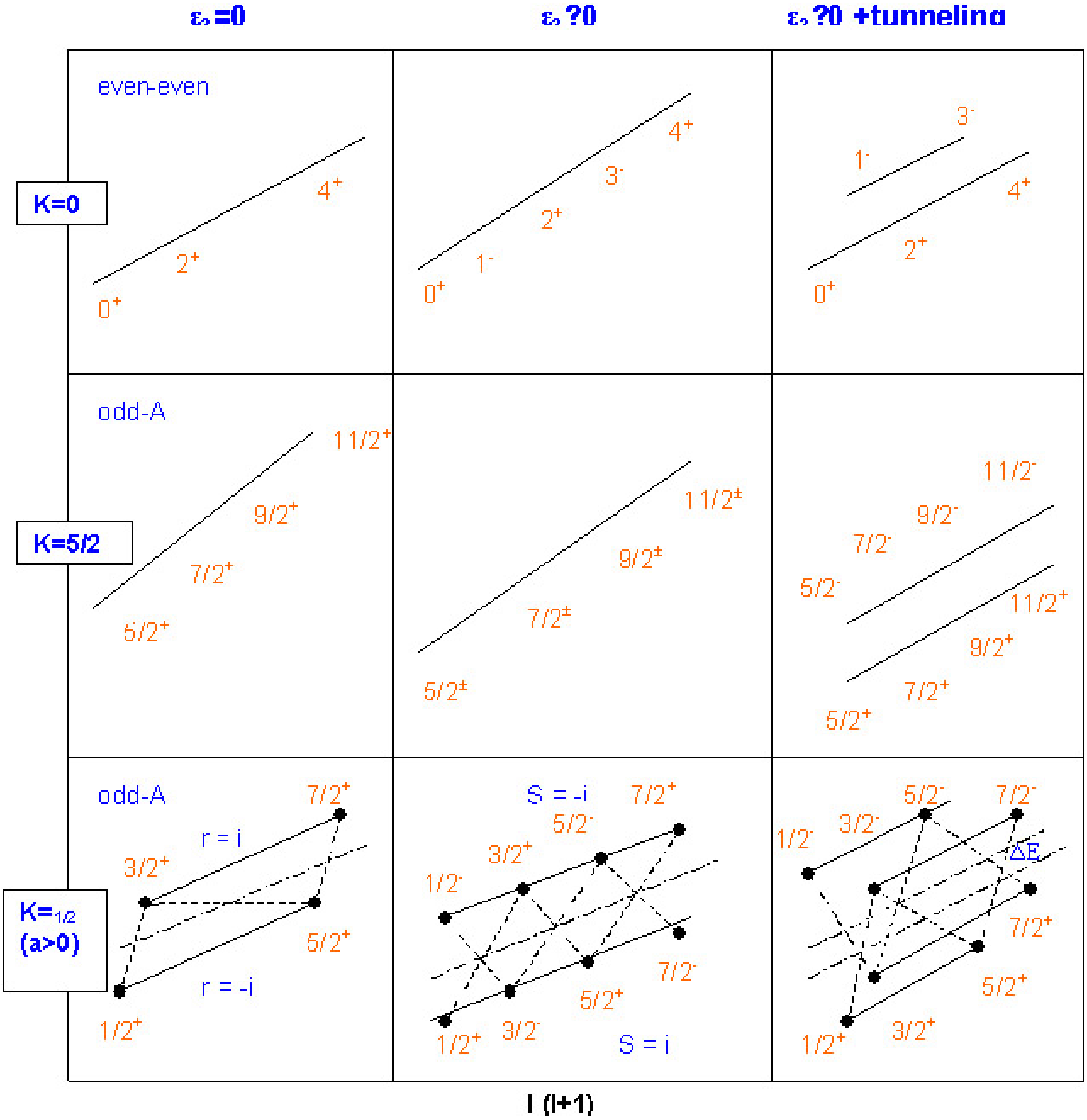

Fig. 14: Energy (on the vertical axis) vs. I(I+1) for various even-even (top), odd-A (middle), and K = 1/2 odd-A (bottom) bands in the absence and presence of octupole shape.

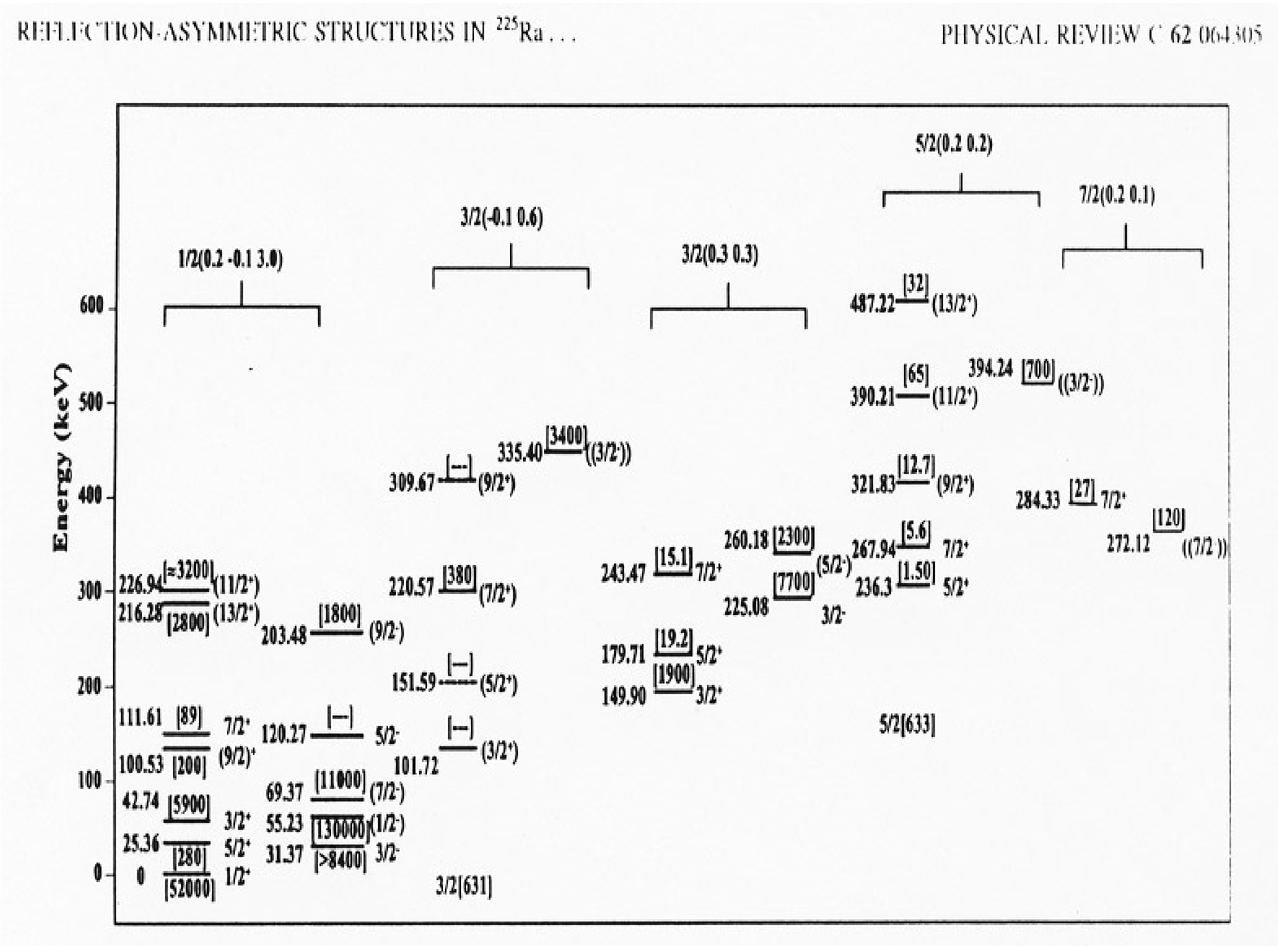

Fig. 15: Experimental data for ^{225}Ra, showing the classification of bands into parity doublets (Gasparo et al., 2000).

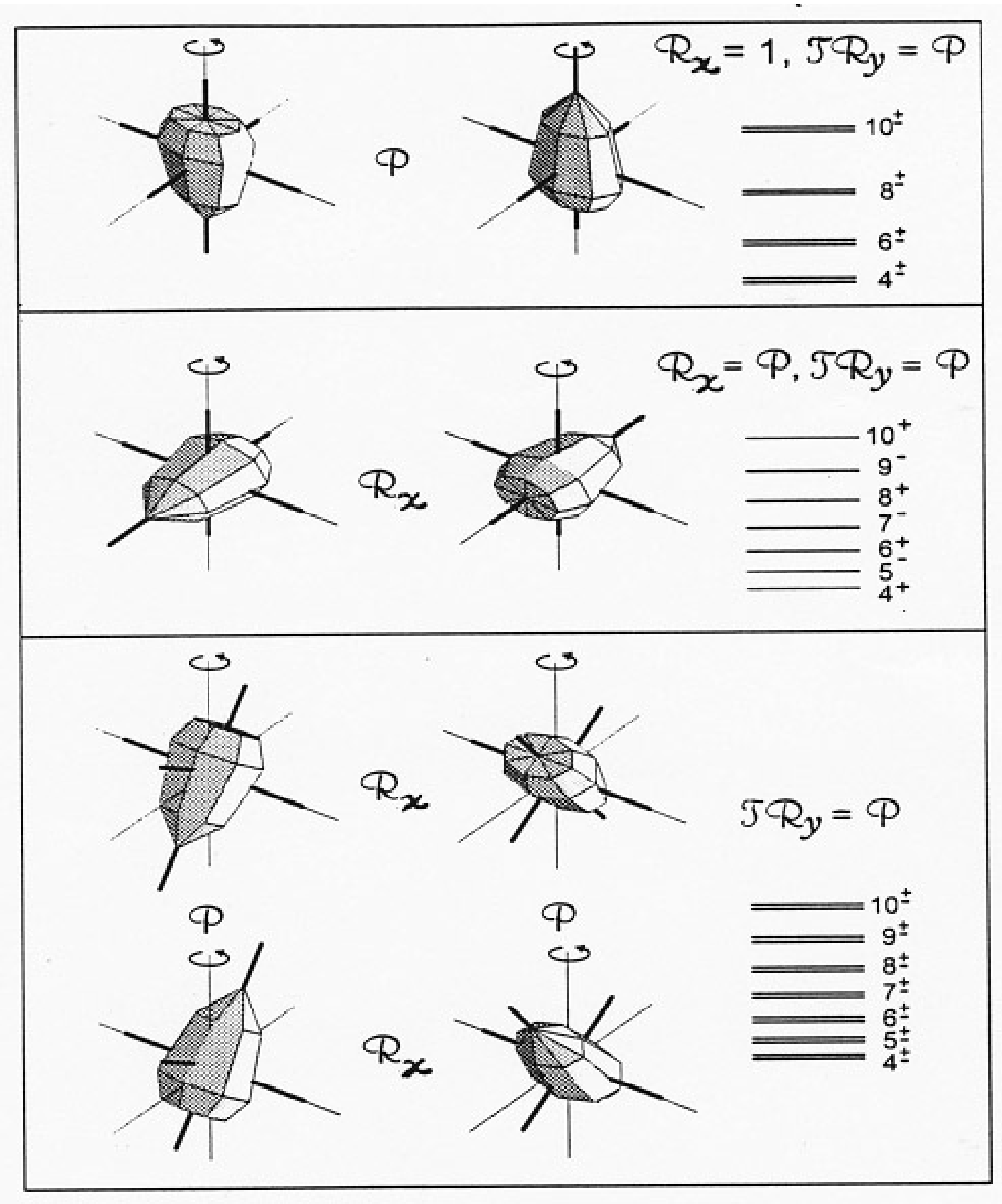

Fig. 16: Effect of planar (top and middle panel) and aplanar (bottom panel) axis of rotation on the rotational band of an axial octupole shape, in which the density distribution has two planes of symmetry (Frauendorf, 2000).

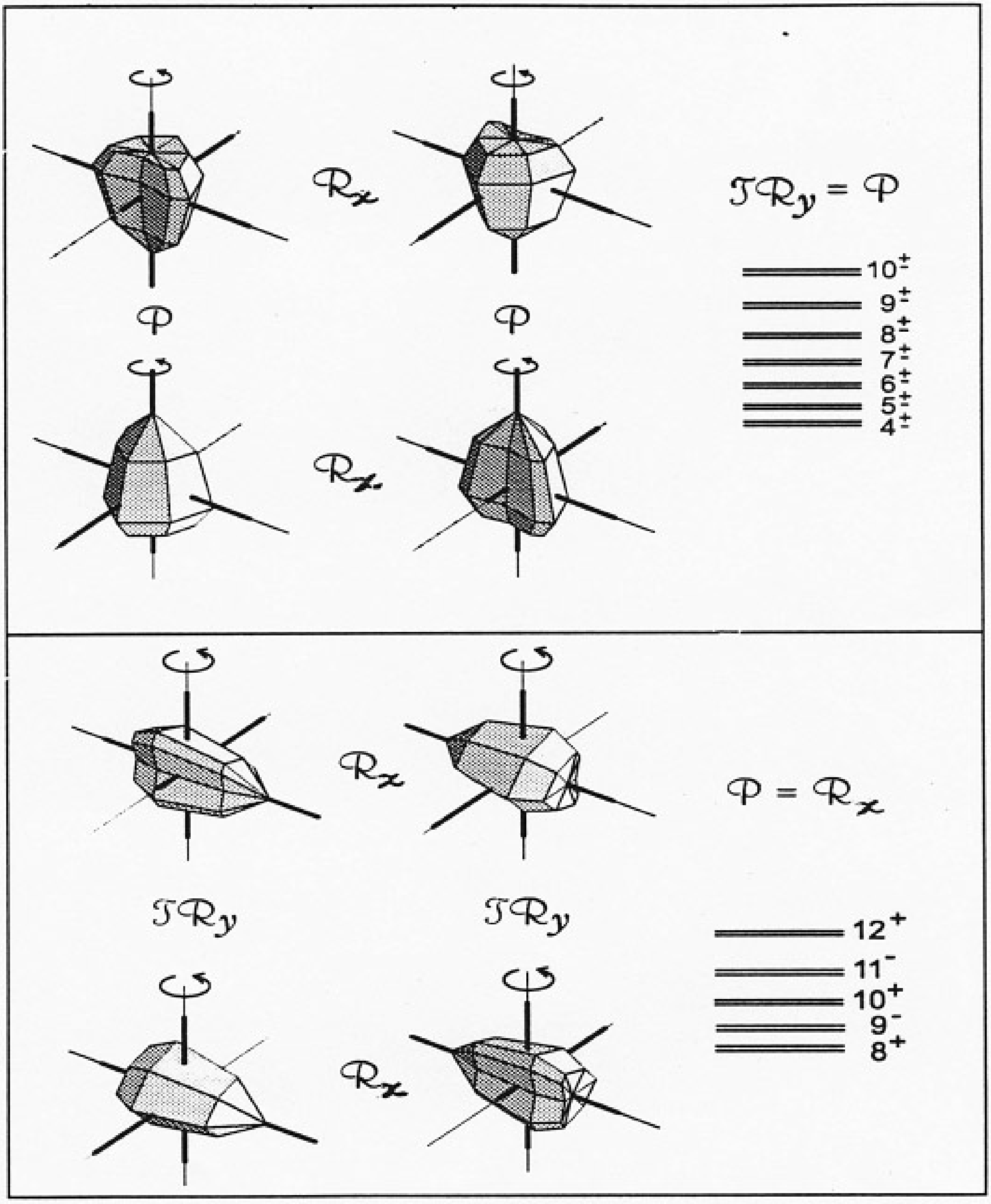

Fig. 17: Effect of planar axis of rotation on the rotational band of a shape that has only one plane of symmetry (Frauendorf, 2000).

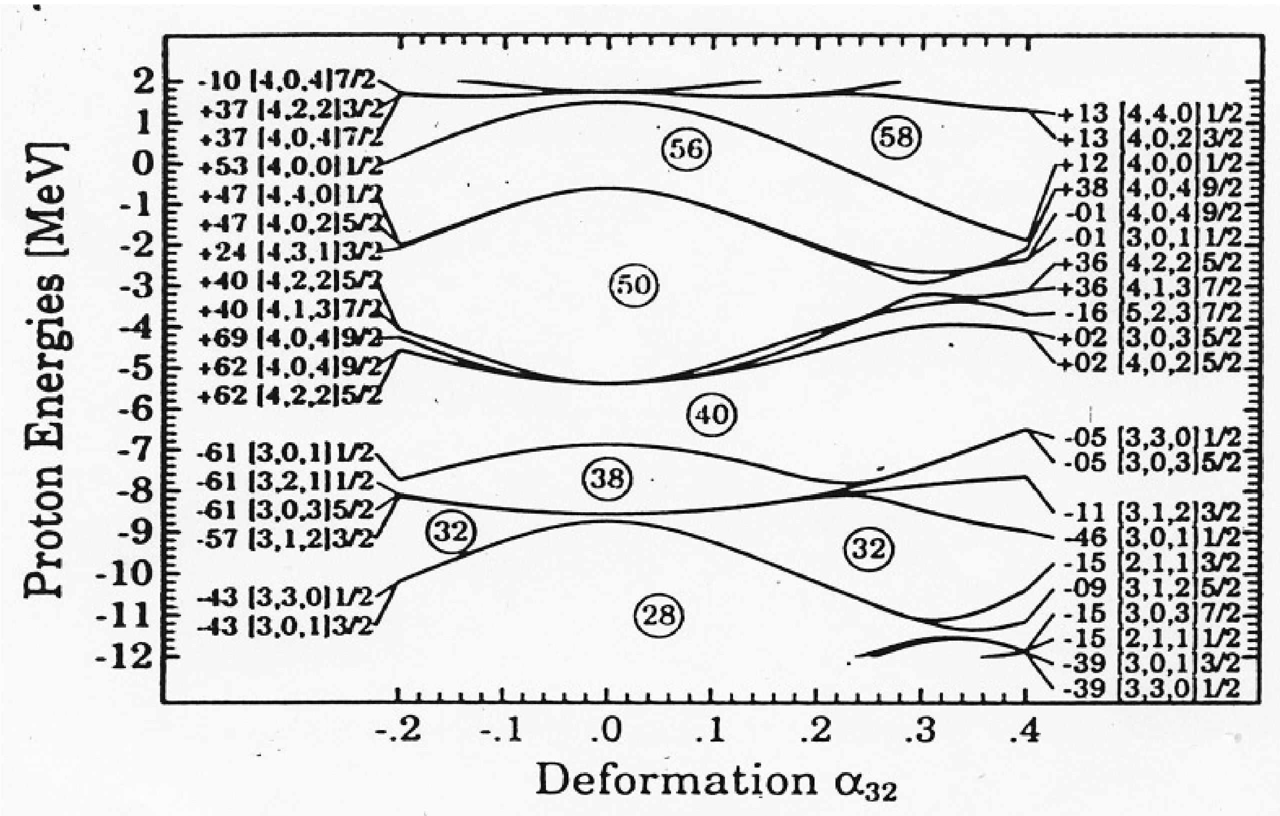

Fig. 18: Theoretical spectrum of single particle states as a function of the parameter $a_{32,}$ which is the coefficient of Y_{32} term; large gaps signify the magic numbers for this shape.

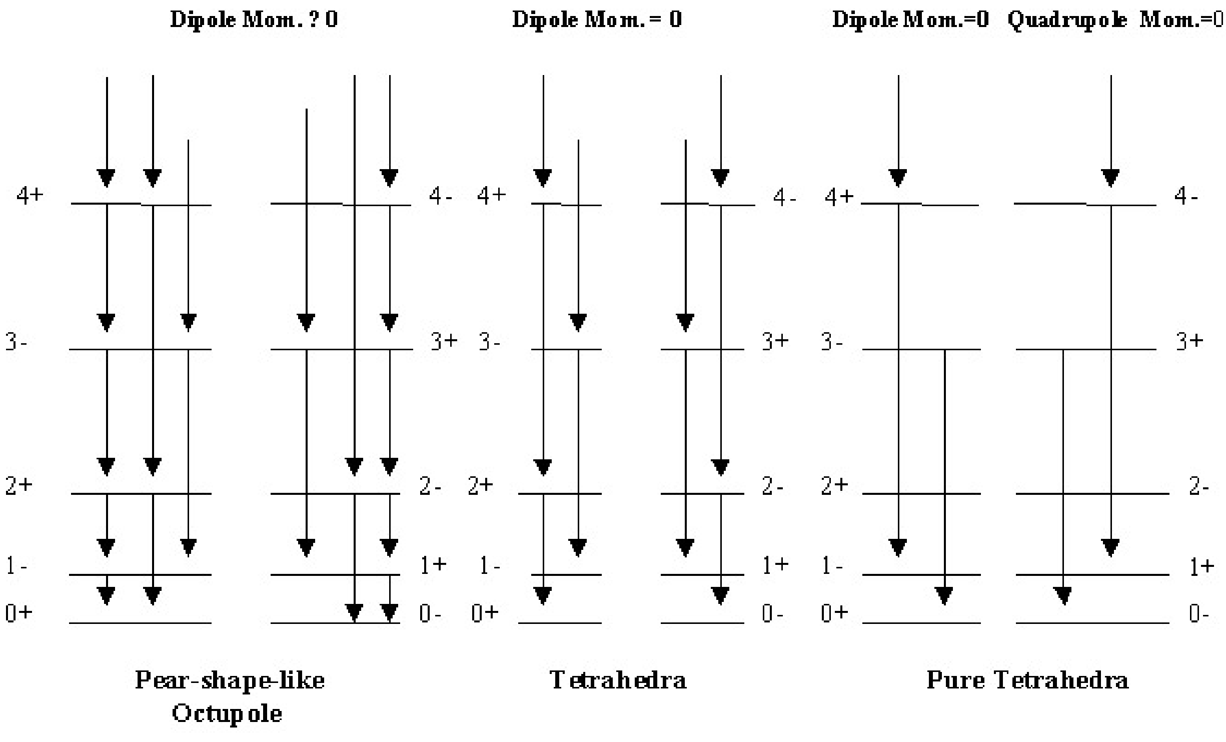

Fig. 19: Rotational spectrum of an axial octupole nucleus (left), quadrupole plus tetrahedral rotor (middle), and a pure tetrahedral rotor (right).

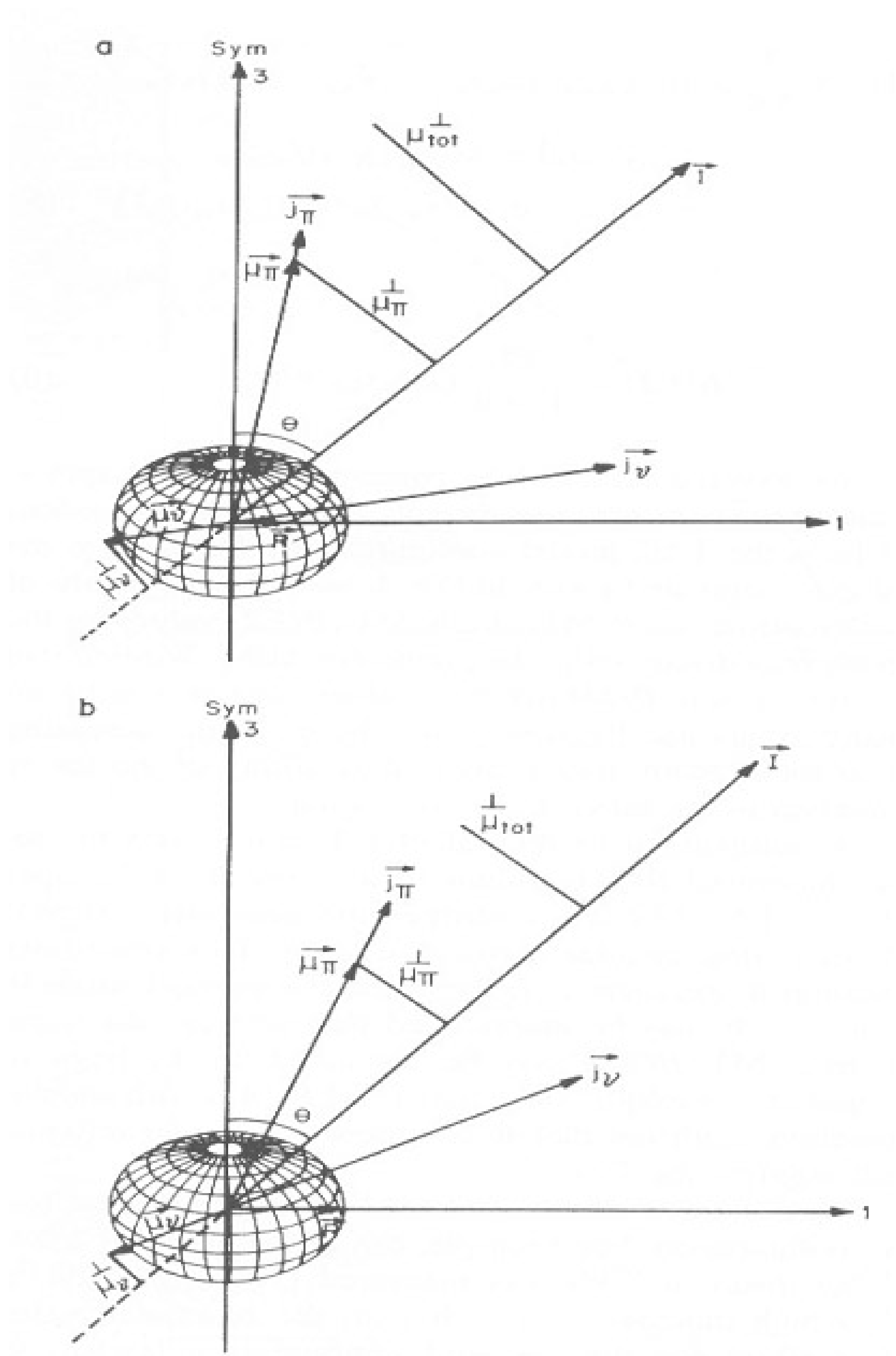

Fig. 20: Coupling scheme of shears mechanism for a small oblate-shaped nucleus at (a) small rotational frequency and (b) large rotational frequency (Amita et al., 2000).

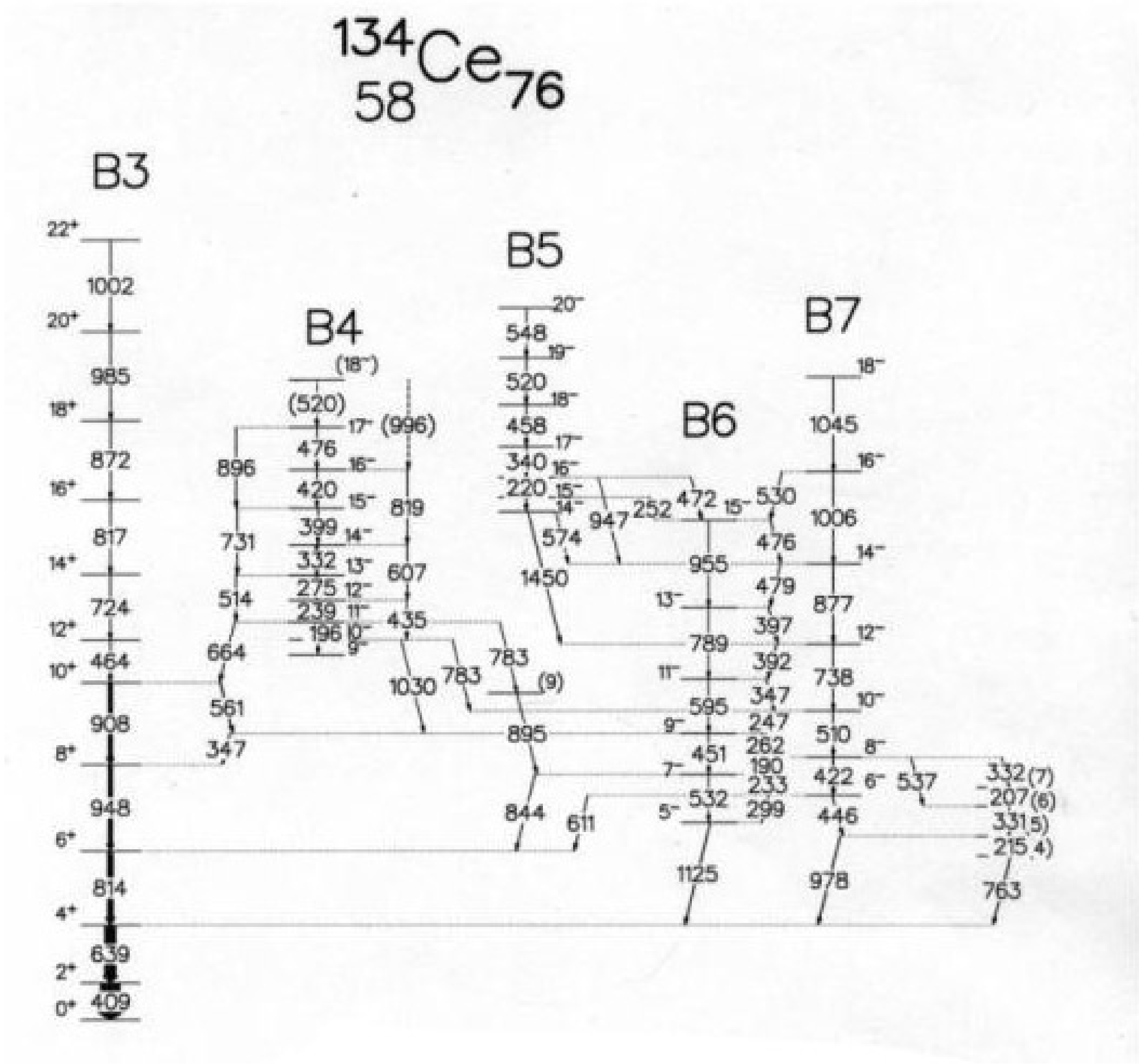

Fig. 21: Partial level scheme of ^{134}Ce that indicates the magnetic rotation band B5 (Lakshmi et al., 2004).

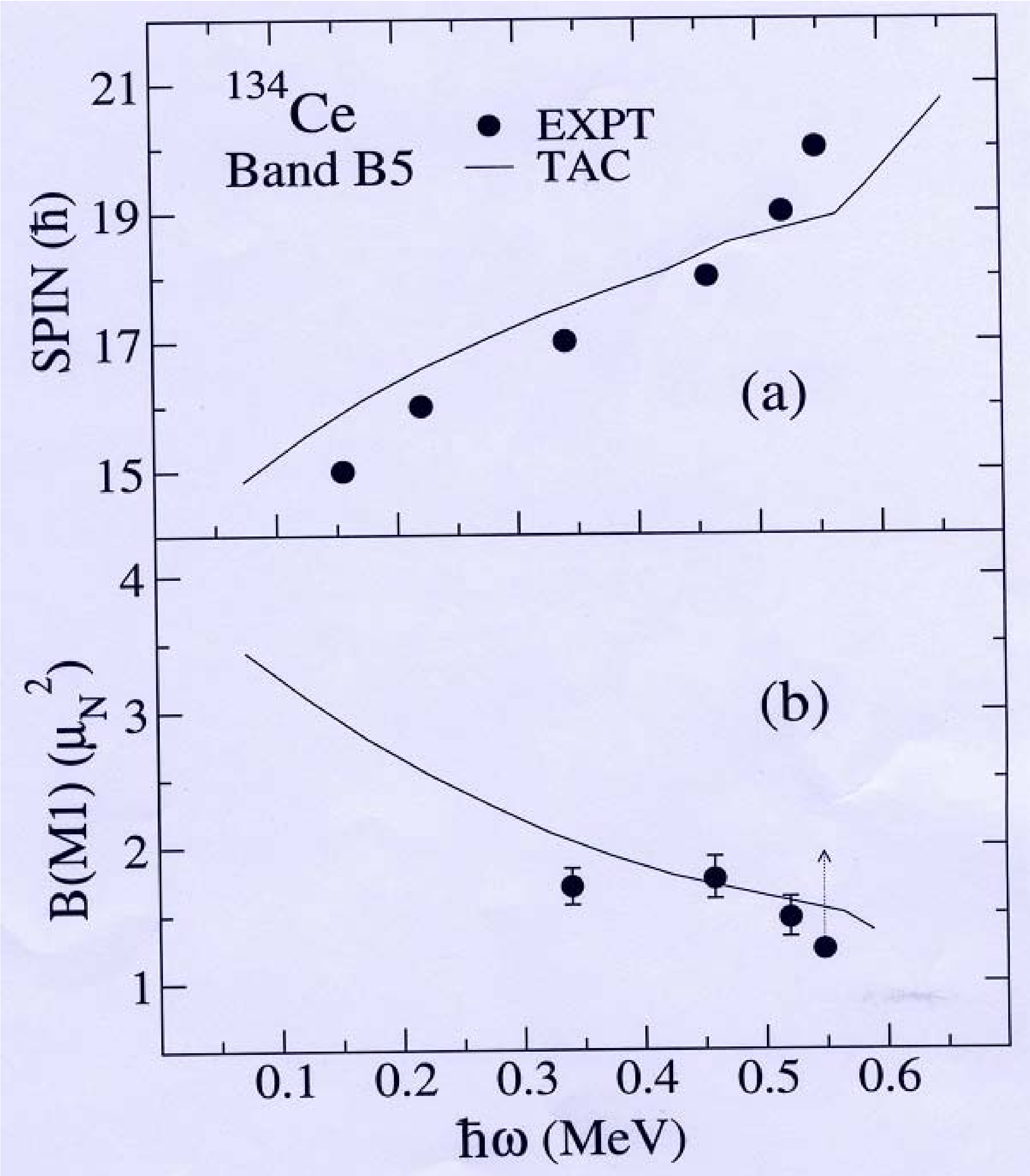

Fig. 22: Experimental plots of angular momentum vs. rotational frequency (top) and B(M1) vs. rotational frequency (bottom) as compared with the TAC calculations (Lakshmi et al., 2004).

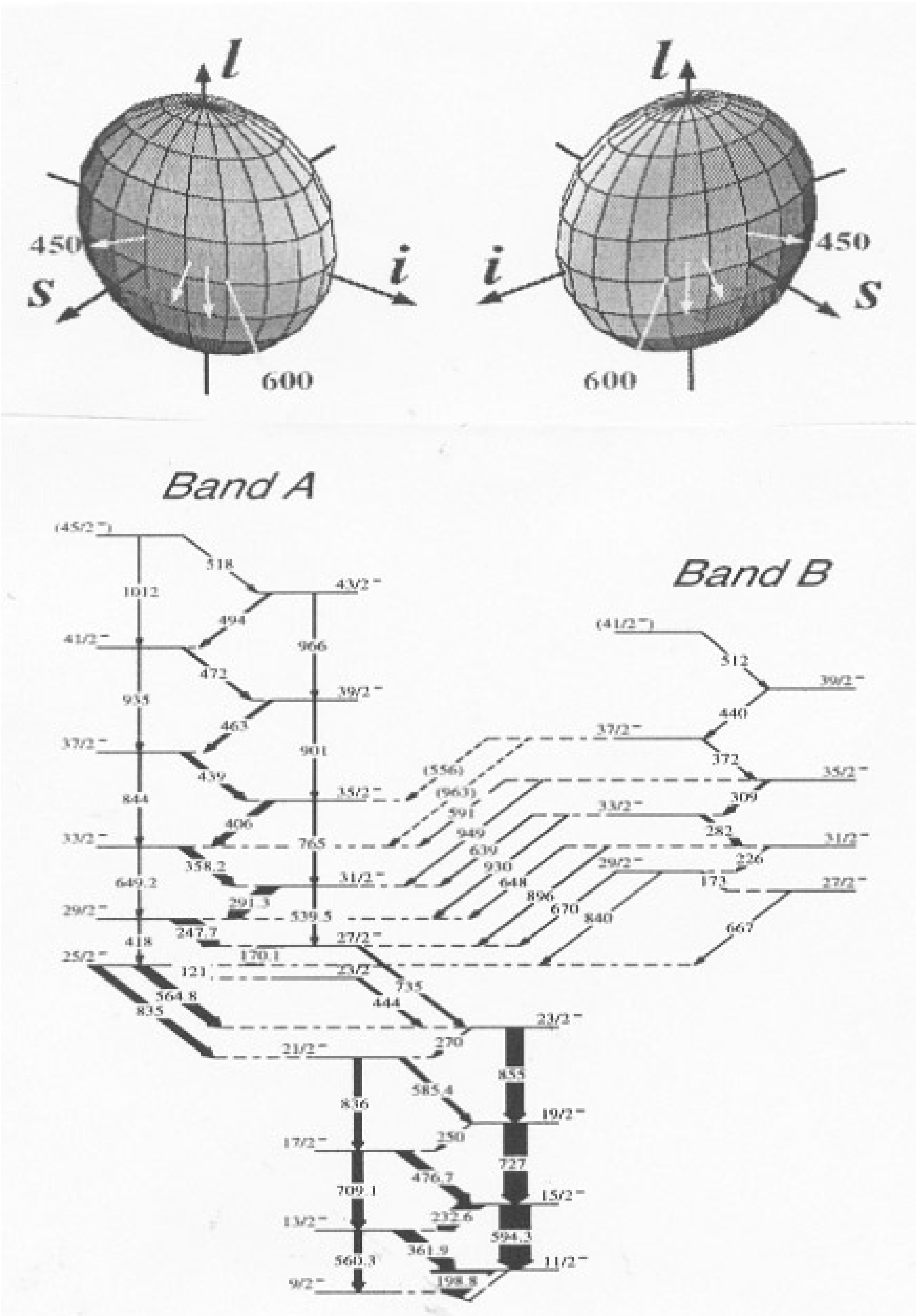

Fig. 23: Chiral pattern of bands observed in ^{135}Nd (Zhu et al., 2003).

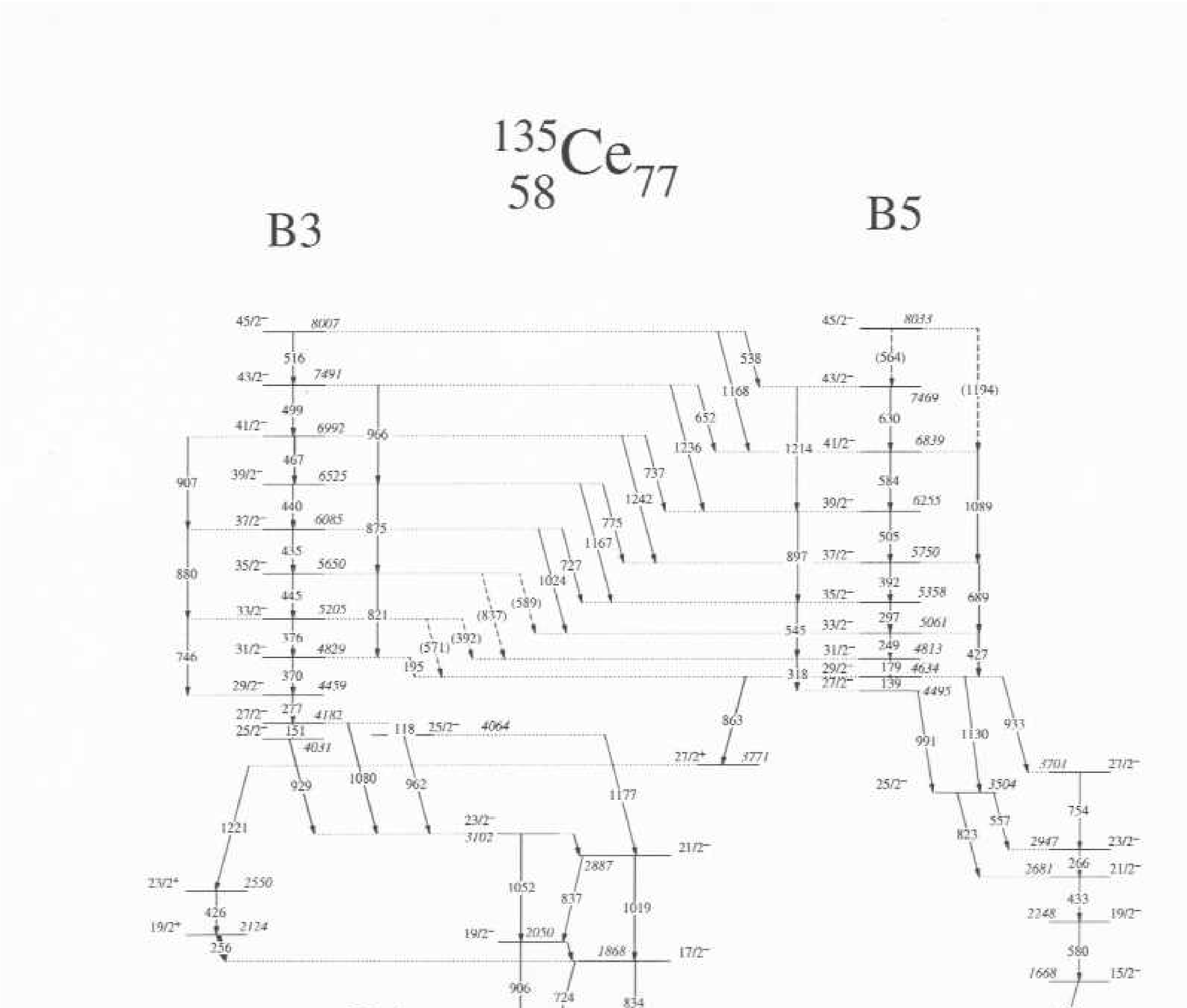

Fig. 24: Possible example of chiral pair of bands in ^{135}Ce (Lakshmi et al., private communication.)

Experimental nuclear spectroscopy:

Introduction

P. von Brentano

IKP University
Cologne, Germany

E-mail: brentano@ikp.uni-koeln.de

Recommended reading: Experimental nuclear spectroscopy is a broad subject.

Excellent books:

R.F. Casten: Nuclear Structure from a Simple Perspective
Oxford Studies in Nuclear Physics, 23
Second edition, Oxford University Press (OUP)
ISBN: 0198507240

A. Bohr and B. R. Mottelson: Nuclear Structure
Publisher: World Scientific Pub Co.
1st edition (January 15, 1998)
ISBN: 9810231970

H. Ejiri and M. J. A. de Voigt: Gamma-ray and Electron Spectroscopy in Nuclear Physics
Oxford Studies in Nuclear Physics, 11
Clarendon Press, Oxford (1989)
ISBN: 0198517238

H. Morinaga and T. Yamazaki: In-beam Gamma Spectroscopy
ISBN**:** 0720402972

D. N. Poenaru and W. Greiner: Experimental Techniques in Nuclear Physics
Publisher: Walter De Gruyter Inc
Published Date: 6 January 1997
ISBN: 3110144670

R. Bock: Heavy Ion Collisions, Vols. 1-3
Elsevier Science & Technology Books
ISBN:0720407389

Experimental nuclear spectroscopy:

Introduction

States, energies, widths, electromagnetic transitions

Observables, quantum numbers

Example levels in ^{124}Xe vs IBA

Nuclear shapes rigid or soft?

Much new knowledge has been obtained in recent times; "conventional" shape parameters β and γ that apply to nuclei with a rigid shape have been generalized to parameters called Q-invariants and K-invariants, and are also applicable to nuclei with a soft shape.

States : energies, widths, lifetimes and electromagnetic transitions

Quasi-stationary state $\Psi_0(t)$ – modelling an excited nuclear state – has a complex energy:

$$\varepsilon_0 = E_0 \ - \ (i/2)\,\Gamma_0$$

where E_0 is the energy of the state, and Γ_0 is the width of the state.
Width is related to the lifetime of the state by the relationship:

$$\tau_0 = (h/2\pi)$$

Energy of the state can be measured most directly from the mass of the state (e.g., in an ion trap). Generally, measure energy differences in reactions, and not energies. Width Γ_0 of the state can be measured from the lifetime.

Lifetime τ_0 can be obtained from the exponential decay of the state

$$|\,\psi_0(t)\,|^2 = \mathrm{A} * exp(-\mathrm{t}/\tau)$$

Given the lifetime τ_0 or the partial lifetimes τ_{0k}, one can obtain the electromagnetic transition probabilities $B(E, M, \lambda)$ – crucial observables

Experimental nuclear spectroscopy:

Observables, Quantum numbers:

Beside the Hamiltonian and energy E_0, there are a number of other important observables and quantum numbers, e.g., ,

$H,\ I^2,\ I_z,\ \sigma^2,\ T_z$

$P,\ T^2,\ K = I_3,\quad F^2$

where the observables and the corresponding quantum numbers in the second row are less well defind than those in the first row

An interesting question is whether a given state ψ_0 with an energy E_0 also has the other good quantum number numbers, e.g., parity π. Yes, if the following is true:

[H, P] = 0, and ψ_0 is not degenerate

Then, $H\psi_0 = E_0*\psi_0$ and $HP\psi_0 = E_0*P\psi_0$

Thus, $P\psi_0$ and ψ_0 are degenerate states with the same energy E_0, and therefore are identical states, i.e., $P\psi_0 = \lambda\ \psi_0$. A somewhat delicate point if one remembers that the various magnetic sub-states are degenerate in energy for $B = 0$.

Thus, in nuclear structure physics, most of the given observables have good or at least approximately good quantum numbers.

Crucial aim of nuclear structure physics: measure the additional quantum numbers for many nuclear states as well as the energies and partial lifetimes.

Undertake a critical evaluation, and compile and make this information easily accessible.

Experimental nuclear spectroscopy:

Example: levels in ^{124}Xe vs IBA

This level scheme is from the Cologne group: experiments provide a rather "complete" low-spin level scheme, with many spin multiplets, e.g., four 4^+ states.

Such data allow a very stringent test of theoretical models (IBA-1 proposed by Arima and Iacchello).

Provides the Hamiltonian that can be checked. Also "extra" levels with unknown spins and parities, and theoretical levels not used in the comparison. This "incomplete" information is very useful and should always be given.

Often theoretical papers show only the levels – authors do not appear to realize how much of the "testing" value of their data is lost in such "comparisons".

Experimental nuclear spectroscopy:

Nuclear shapes: rigid or soft?

Crucial and fundamental parameters of the nucleus are the radius R_0 and the Bohr parameters β and γ, which descibe the quadrupole shape of the nuclear surface. These parameters are to some extent model dependent.

The most used simple model is the rigid axial rotor model of Bohr and Mottelson, and the generalization of the model to a triaxial shape by Davidov and Fillipov (see later).

The shape parameters β and γ are widely used. However, there is a problem: even in the "body-fixed" reference system, many nuclei have no fixed values of γ and β.

Thus, the values of β and γ found in the literature are effectively the parameters β_{eff} and γ_{eff}, although rarely admitted by the authors. Both β_{eff} and γ_{eff} shape parameters are model dependent. Kumar and Cline have suggested a rather clean way of introducing these effective parameters by using the concept of Q-invariants. Relative Q-invariants called K-invariants were introduced by the Cologne-Dubna group. Unfortunately, these invariants are defined by sum rules, and we have to undertake some extapolation – can be safely done by suitable nuclear models (e.g., Interacting Boson model 1 introduced by Arima and Iacchello, or the proton-neutron version IBA-2 as introduced by Iacchello, Arima, Otsuka and Talmi).

Shape parameters for the nucleus:

a) β and γ shape parameters for nuclei that have a rigid shape in the intrinsic system

b) β_{eff} and γ_{eff} shape parameters for nuclei that have a soft (vibrating) rigid shape in the intrinsic system

Values of the Q-invariant and K-invariant parameters for the dynamic symmetries of the interacting Boson model.

Data comparisons

Experimental progress has been made by improving the accuracy of measurements of the lifetimes of nuclear states. Problem of unknown side feeding in fusion reactions has been solved by suitable data and novel analysis methods (particularly the work of the Dewald group in Cologne). Thus, reliable lifetimes are now available from fusion reactions, allowing the determination of the shapes of collective excitations in nuclei.

Experimental nuclear spectroscopy:

Lifetimes from Döppler-shifted spectra of RDDS (recoil distance Döppler-shifted data).

Qualitative arguments:

Method, and example of ^{158}Er

Results for *Xe* isotopes

Three setups for low-spin spectroscopy at FN-Tandem, Cologne and in Lexington.

Comparison of spectra

Inelastic neutron scattering

Lifetimes from (n, n´t**γ)** data of Lexington

Lifetimes of highly-excited states from NRF at S-Dalinac, Darmstadt, and Dynamitron, Stuttgart

Nuclear Resonance Fluorescence (NRF)

resonant inelastic photon scattering

$A(\gamma, \gamma')A*$

Resonance reaction:

$$A + \gamma \rightarrow A**(E, I) \rightarrow \gamma + A*$$

Experimental nuclear spectroscopy:

Nuclear Shapes

P. von Brentano

IKP University
Cologne, Germany

E-mail: brentano@ikp.uni-koeln.de

Shape parameters for the nucleus:

a) β and γ shape parameters for nuclei that have a rigid shape in the intrinsic system

b) Shape parameters β_{eff} and γ_{eff} for nuclei that have a soft (vibrating) shape in the intrinsic system

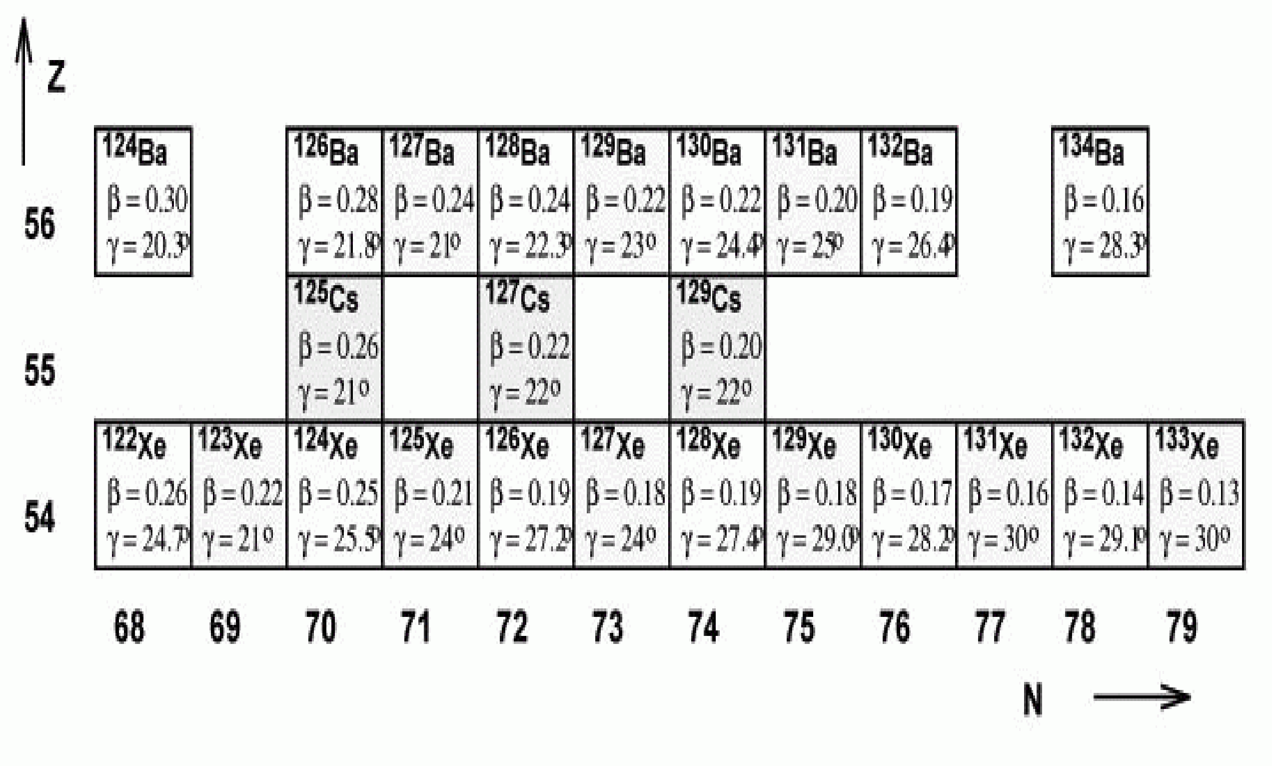
Z
56
55
54
124Ba β = 0.30 γ = 20.3°
126Ba β = 0.28 γ = 21.8°
127Ba β = 0.24 γ = 21°
128Ba β = 0.24 γ = 22.3°
129Ba β = 0.22 γ = 23°
130Ba β = 0.22 γ = 24.4°
131Ba β = 0.20 γ = 25°
132Ba β = 0.19 γ = 26.4°
134Ba β = 0.16 γ = 28.3°
125Cs β = 0.26 γ = 21°
127Cs β = 0.22 γ = 22°
129Cs β = 0.20 γ = 22°
122Xe β = 0.26 γ = 24.7°
123Xe β = 0.22 γ = 21°
124Xe β = 0.25 γ = 25.5°
125Xe β = 0.21 γ = 24°
126Xe β = 0.19 γ = 27.2°
127Xe β = 0.18 γ = 24°
128Xe β = 0.19 γ = 27.4°
129Xe β = 0.18 γ = 29.0°
130Xe β = 0.17 γ = 28.2°
131Xe β = 0.16 γ = 30°
132Xe β = 0.14 γ = 29.1°
133Xe β = 0.13 γ = 30°
68 69 70 71 72 73 74 75 76 77 78 79
N

^{124}Xe

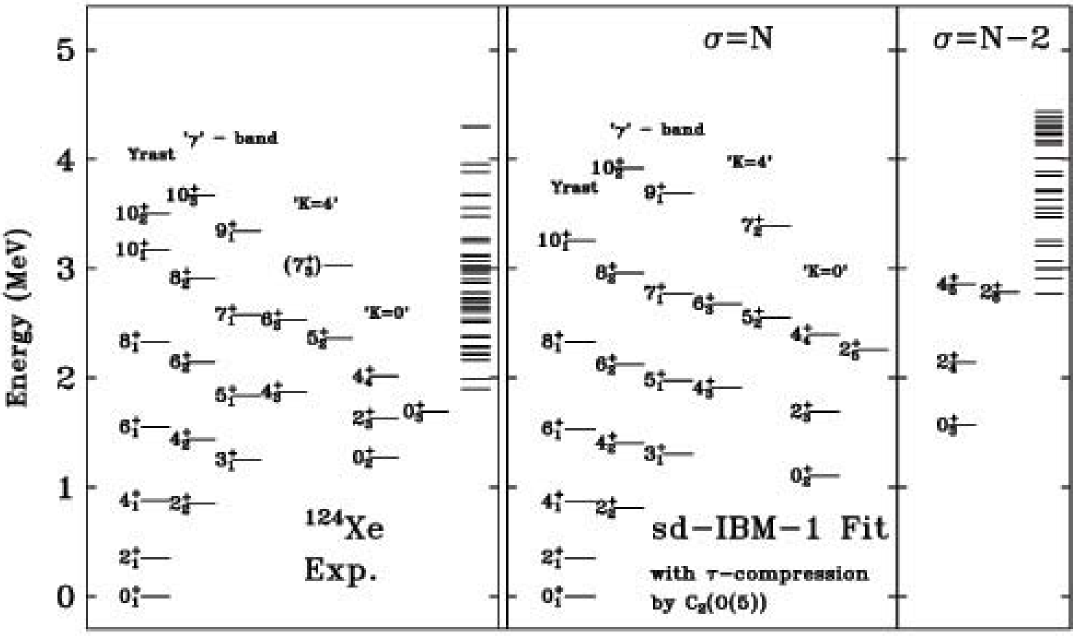

$$\begin{aligned}\mathbf{H}_{\tau-\mathbf{ECQF}} &= \epsilon \mathbf{n_d} + \lambda \mathbf{LL} + \kappa \mathbf{Q}^{\chi}\mathbf{Q}^{\chi} + \beta \mathbf{C_2}(\mathbf{O}(\mathbf{5})) \\ &= \kappa \left(\frac{\epsilon}{\kappa}\mathbf{n_d} + \frac{\tilde{\lambda}}{\kappa}\mathbf{LL} + \mathbf{Q}^{\chi}\mathbf{Q}^{\chi} + \mathbf{4}\frac{\beta}{\kappa}\mathbf{T}^{(\mathbf{3})}\mathbf{T}^{(\mathbf{3})} \right)\end{aligned}$$

$$\epsilon/\kappa = -20.9\ ,\ \chi = -0.257\ ,\ \beta/\kappa = 0.563\ ,\ \lambda/\kappa = -0.284$$
$$\kappa = -34.91 keV\ ,\ e_b = 0.14224 e^2 b^2$$

V.Werner et al., Nucl. Phys. **A693** (2001) 451

Investigation of nuclear deformation

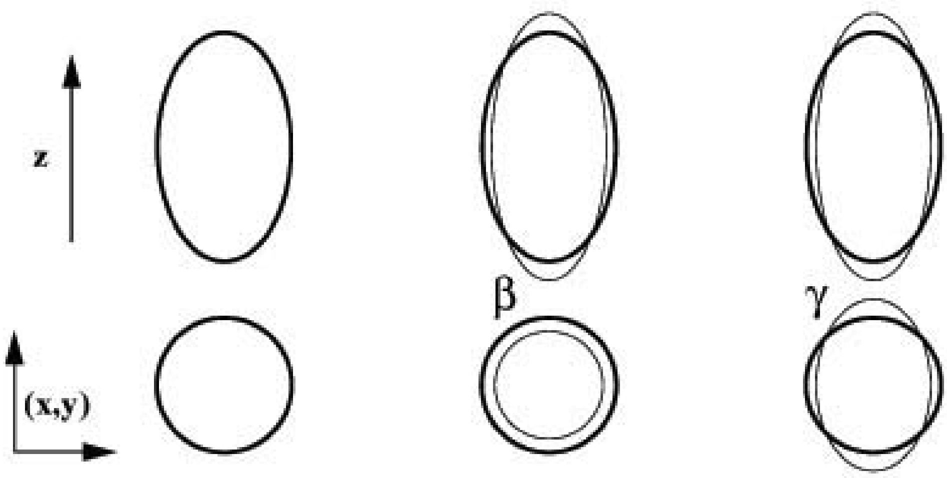

geometrical model → rigid β and γ

cannot describe γ - soft nuclei

→ **adopt to quantities that can describe non-rigid deformations**

→ **make them model-independent**

One approach is:

Quadrupole-Shape-Invariants

K. Kumar, Phys. Rev. Lett **28** (1972) 249
D. Cline, Ann. Rev. Nucl. Part. Sci. **36** (1968) 683

Investigation of nuclear deformation

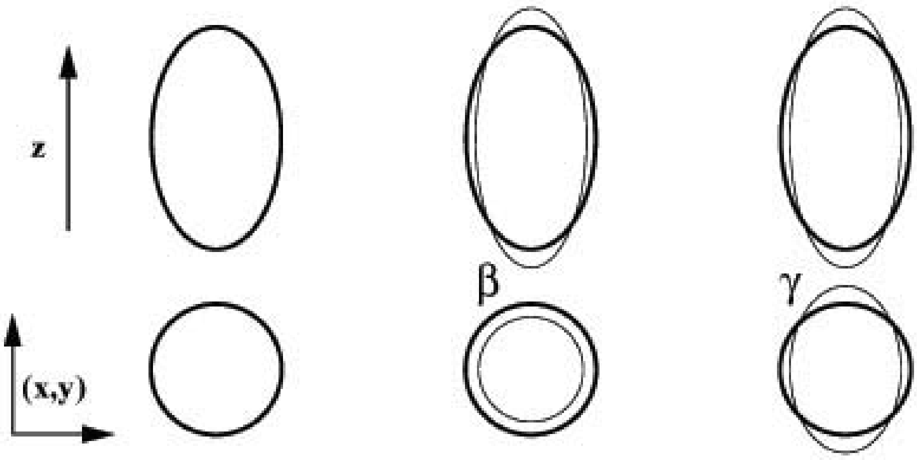

$$\mathbf{R}_\lambda = R\left(1+\beta\sqrt{\frac{5}{4\pi}}cos\left(\gamma-\frac{2\pi}{3}\lambda\right)\right) \qquad \lambda = 1,2,3$$

$$\mathbf{Q_0} = \frac{3ZR^2\beta}{\sqrt{5\pi}}$$

$\mathbf{D^J_{MK}}$ = generalized spherical functions defining the unitary transformation from a coordinate system fixed in space to a coordinate system fixed to the nucleus

$$\hat{\mathbf{Q}}_{2\mu} = eQ_0\left(D^2_{\mu 0}cos\gamma + \frac{D^2_{\mu 2}+D^2_{\mu,-2}}{\sqrt{2}}sin\gamma\right)$$

Davydov and Filippov, Nucl. Phys. **8** (1958) 237

Simple E2-relations in the Q-phonon scheme

V. Werner, P. von Brentano, R. V. Jolos

Quadrupole shape invariants

- What are shape invariants?
- Relation to nuclear deformation

Method of obtaining relationships between E2 matrix elements

- Use various couplings of E2 operators
- Use Q−phonon scheme
- Check validity in IBM−1
- Check with data

Q–Invariants Definitions

$$\mathbf{q_2} = \langle 0_1^+|(\mathbf{Q}\cdot\mathbf{Q})|0_1^+\rangle = \sum_{\mathbf{j}} \mathbf{B}(\mathbf{E2}; 0_1^+ \cdot \mathbf{2j}^+)$$

$$\mathbf{q_3} = \sqrt{\frac{35}{2}}\ |\langle 0_1^+|[\mathbf{QQQ}]^{(0)}|0_1^+\rangle|$$

$$\mathbf{q_4} = \langle 0_1^+|(\mathbf{Q}\cdot\mathbf{Q})\ (\mathbf{Q}\cdot\mathbf{Q})|0_1^+\rangle$$

$$\mathbf{q_5} = \sqrt{\frac{35}{2}}\ |\langle 0_1^+|(\mathbf{Q}\cdot\mathbf{Q})\ [\mathbf{QQQ}]^{(0)}|0_1^+\rangle|$$

$$\mathbf{q_6} = \frac{35}{2}\ \langle 0_1^+|[\mathbf{QQQ}]^{(0)}\ [\mathbf{QQQ}]^{(0)}|0_1^+\rangle$$

$$\boxed{\mathbf{K_n} = \frac{\mathbf{q_n}}{\mathbf{q_2^{n/2}}} \qquad \text{for} \quad n \in \{3,4,5,6\}}$$

Geometrical Interpretation

$$\mathbf{q_2} = \left(\frac{\mathbf{3ZeR^2}}{\mathbf{4}\pi}\right)^{\mathbf{2}} \langle\beta^{\mathbf{2}}\rangle \equiv \left(\frac{\mathbf{3ZeR^2}}{\mathbf{4}\pi}\right)^{\mathbf{2}} \beta_{\text{eff}}{}^{\mathbf{2}}$$

$$\mathbf{K_3} = \frac{\langle\beta^{\mathbf{3}}\cos\mathbf{3}\gamma\rangle}{\langle\beta^{\mathbf{2}}\rangle^{\mathbf{3/2}}} \equiv \cos\mathbf{3}\gamma_{\text{eff}}$$

$$\mathbf{K_4} = \frac{\langle\beta^{\mathbf{4}}\rangle}{\langle\beta^{\mathbf{2}}\rangle^{\mathbf{2}}}$$

$$\mathbf{K_5} = \frac{\langle\beta^{\mathbf{5}}\cos\mathbf{3}\gamma\rangle}{\langle\beta^{\mathbf{2}}\rangle^{\mathbf{5/2}}}$$

$$\mathbf{K_6} = \frac{\langle\beta^{\mathbf{6}}\cos^{\mathbf{2}}\mathbf{3}\gamma\rangle}{\langle\beta^{\mathbf{2}}\rangle^{\mathbf{3}}}$$

Fluctuations:

$$\boxed{\begin{aligned}\sigma_\beta &= \frac{\langle\beta^{\mathbf{4}}\rangle - \langle\beta^{\mathbf{2}}\rangle^{\mathbf{2}}}{\langle\beta^{\mathbf{2}}\rangle^{\mathbf{2}}} = \mathbf{K_4 - 1}\\ \sigma_\gamma &= \frac{\langle\beta^{\mathbf{6}}\cos^{\mathbf{2}}\mathbf{3}\gamma\rangle - \langle\beta^{\mathbf{3}}\cos\mathbf{3}\gamma\rangle^{\mathbf{2}}}{\langle\beta^{\mathbf{2}}\rangle^{\mathbf{3}}} = \mathbf{K_6 - K_3{}^2}\end{aligned}}$$

Various Couplings of the 4th order moment

decouple via Wigner-Eckart and insert 1s (ones)

$$\mathbf{q}_4^{(0)} = \langle 0_1^+ | \overbrace{(\mathbf{Q}\cdot\mathbf{Q})}^{\overset{1}{\sum_i |2_i^+\rangle\langle 2_i^+|}} \underbrace{\;\;}_{\sum_j |0_j^+\rangle\langle 0_j^+|} \overbrace{(\mathbf{Q}\cdot\mathbf{Q})}^{\overset{1}{\sum_k |2_k^+\rangle\langle 2_k^+|}} | 0_1^+ \rangle$$

$$\mathbf{q}_4^{(2)} = \langle 0_1^+ | \left[\overbrace{[\mathbf{Q}\mathbf{Q}]^{(2)}}^{\sum_i |2_i^+\rangle\langle 2_i^+|} \underbrace{\;\;}_{\sum_j |2_j^+\rangle\langle 2_j^+|} \overbrace{[\mathbf{Q}\mathbf{Q}]^{(2)}}^{\sum_k |2_k^+\rangle\langle 2_k^+|} \right]^{(0)} | 0_1^+ \rangle$$

$$\mathbf{q}_4^{(4)} = \langle 0_1^+ | \left[\overbrace{[\mathbf{Q}\mathbf{Q}]^{(4)}}^{\sum_i |2_i^+\rangle\langle 2_i^+|} \underbrace{\;\;}_{\sum_j |4_j^+\rangle\langle 4_j^+|} \overbrace{[\mathbf{Q}\mathbf{Q}]^{(4)}}^{\sum_k |2_k^+\rangle\langle 2_k^+|} \right]^{(0)} | 0_1^+ \rangle$$

Aim: $\mathbf{q}_4^{(0)} \propto \mathbf{q}_4^{(2)} \propto \mathbf{q}_4^{(4)}$

Selection rules of the Q-phonon scheme

$$q_4^{(0)} = \sum_{i,j,k} \langle 0_1^+ || Q || 2_i^+ \rangle \langle 2_i^+ || Q || 0_j^+ \rangle \langle 0_j^+ || Q || 2_k^+ \rangle \langle 2_k^+ || Q || 0_1^+ \rangle$$

$$q_4^{(2)} = \frac{1}{5\sqrt{5}} \sum_{i,j,k} \langle 0_1^+ || Q || 2_i^+ \rangle \langle 2_i^+ || Q || 2_j^+ \rangle \langle 2_j^+ || Q || 2_k^+ \rangle \langle 2_k^+ || Q || 0_1^+ \rangle$$

$$q_4^{(4)} = \frac{1}{15} \sum_{i,j,k} \langle 0_1^+ || Q || 2_i^+ \rangle \langle 2_i^+ || Q || 4_j^+ \rangle \langle 4_j^+ || Q || 2_k^+ \rangle \langle 2_k^+ || Q || 0_1^+ \rangle$$

$$|2_1^+ \propto Q \; |0_1^+\rangle$$

$$|J_1^+\rangle \propto (QQ)^{(J)} \; |0_1^+\rangle \propto (Q \; |2_1^+\rangle)^{(J)} \qquad \textbf{(J=0,2,4)}$$

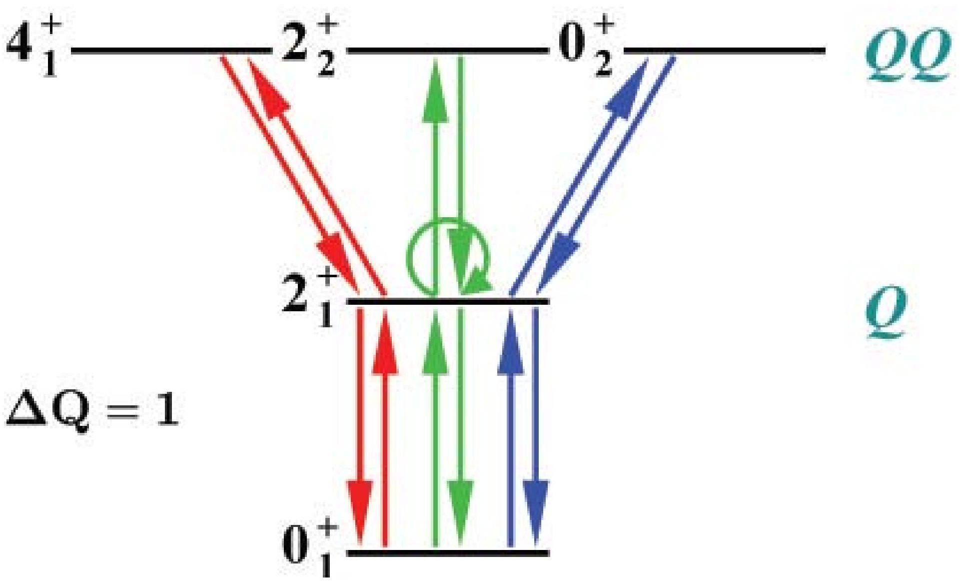

G. Siems et al., Phys. Lett. **B320** (1994) 1
T. Otsuka, K.–H. Kim, Phys. Rev. **C50** (1994) 1768

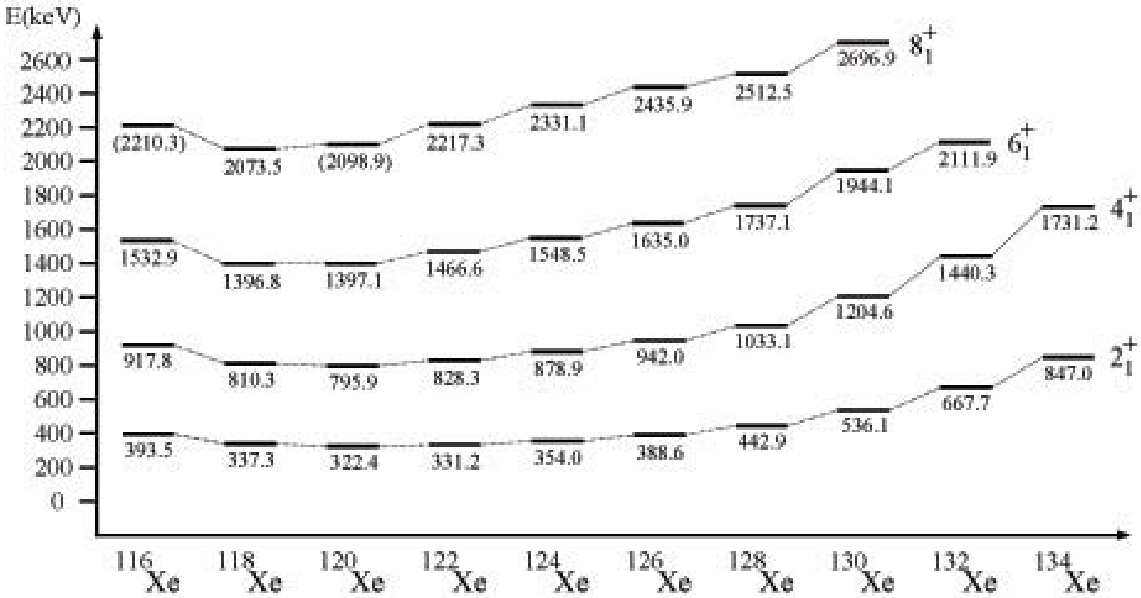
E(keV)
2600
2400
2200
2000
1800
1600
1400
1200
1000
800
600
400
200
0
(2210.3)
2073.5
(2098.9)
2217.3
2331.1
2435.9
2512.5
2696.9
8_1^+
1532.9
1396.8
1397.1
1466.6
1548.5
1635.0
1737.1
1944.1
2111.9
6_1^+
917.8
810.3
795.9
828.3
878.9
942.0
1033.1
1204.6
1440.3
1731.2
4_1^+
393.5
337.3
322.4
331.2
354.0
388.6
442.9
536.1
667.7
847.0
2_1^+
^{116}Xe
^{118}Xe
^{120}Xe
^{122}Xe
^{124}Xe
^{126}Xe
^{128}Xe
^{130}Xe
^{132}Xe
^{134}Xe

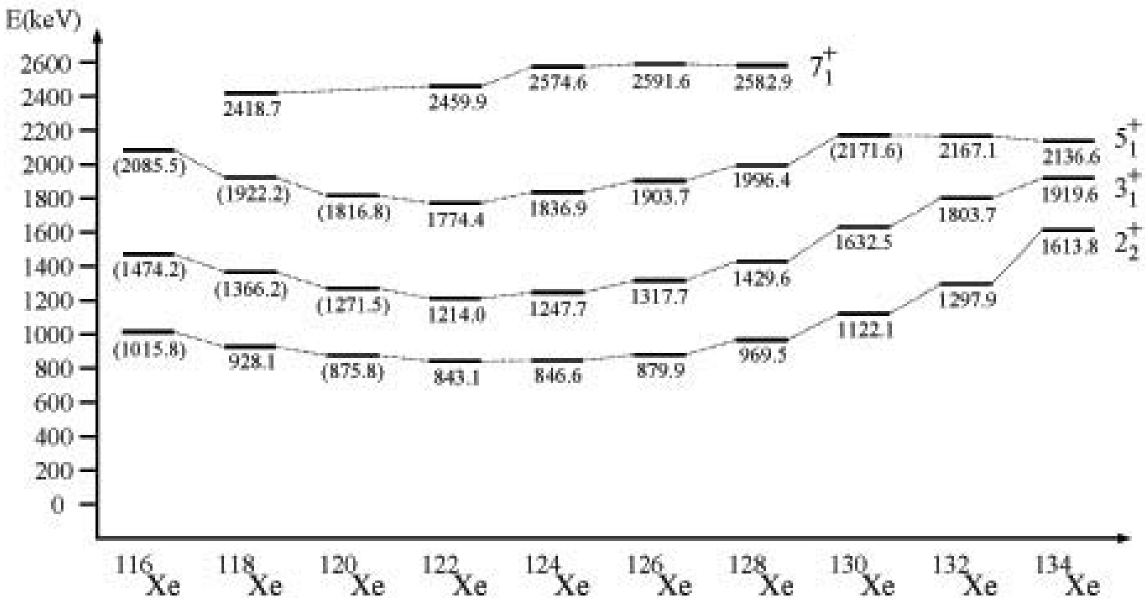
E(keV)
2600
2400
2200
2000
1800
1600
1400
1200
1000
800
600
400
200
0
2418.7
2459.9
2574.6
2591.6
2582.9
7_1^+
(2085.5)
(1922.2)
(1816.8)
1774.4
1836.9
1903.7
1996.4
(2171.6)
2167.1
2136.6
5_1^+
1919.6
3_1^+
(1474.2)
(1366.2)
(1271.5)
1214.0
1247.7
1317.7
1429.6
1632.5
1803.7
1613.8
2_2^+
(1015.8)
928.1
(875.8)
843.1
846.6
879.9
969.5
1122.1
1297.9
^{116}Xe
^{118}Xe
^{120}Xe
^{122}Xe
^{124}Xe
^{126}Xe
^{128}Xe
^{130}Xe
^{132}Xe
^{134}Xe

Values of Q-invariants and K-parameters for the dynamical symmetries of the Interacting Boson model

Comparison with data

Shape Invariants in the IBA limits

$$K_3 = \cos 3\gamma_{\text{eff}} \qquad \beta^2_{2,\text{eff}} = \left(\frac{4\pi}{3eZR_0^2}\right)^2 \cdot q_2$$

	SU(3)	O(6)	U(5)
$\gamma_{\text{eff}} = \frac{1}{3}\arccos K_3$	0 °	30 °	30 °
$K_3 = \frac{q_3}{q_2^{3/2}}$	1	0	0
$K_4 = \frac{q_4}{q_2^2}$	1	1	1.4
$K_5 = \frac{q_5}{q_2^{5/2}}$	1	0	0
$K_6 = \frac{q_6}{q_2^3}$	1	0.32	0.68
$\sigma_4 = \frac{q_4 - q_2^2}{q_2^2} = K_4 - 1$	0	0	0.4
$\sigma_5 = \frac{q_5 - q_2 \cdot q_3}{q_2^{5/2}} = K_5 - K_3$	1	0	0
$\sigma_6 = \frac{q_6 - q_3^2}{q_2^3} = K_6 - K_3^2$	0	0.32	0.68

sd – IBA - 1 parameters

$$\mathbf{H_{CQF}} = \kappa \mathbf{Q}^{\chi} \cdot \mathbf{Q}^{\chi}$$

$\Longrightarrow$ one structure parameter χ

$$\begin{aligned}\mathbf{H_{ECQF}} &= \varepsilon \mathbf{n_d} + \kappa \mathbf{Q}^{\chi} \cdot \mathbf{Q}^{\chi} \\ &= \kappa \left(\frac{\varepsilon}{\kappa} \mathbf{n_d} + \mathbf{Q}^{\chi} \cdot \mathbf{Q}^{\chi} \right)\end{aligned}$$

$\Longrightarrow$ two structure parameter $(\varepsilon/\kappa, \chi)$

	SU(3)	O(6)	U(5)
ε/κ	0	0	$-\infty$
χ	$-\sqrt{7}/2$	0	0

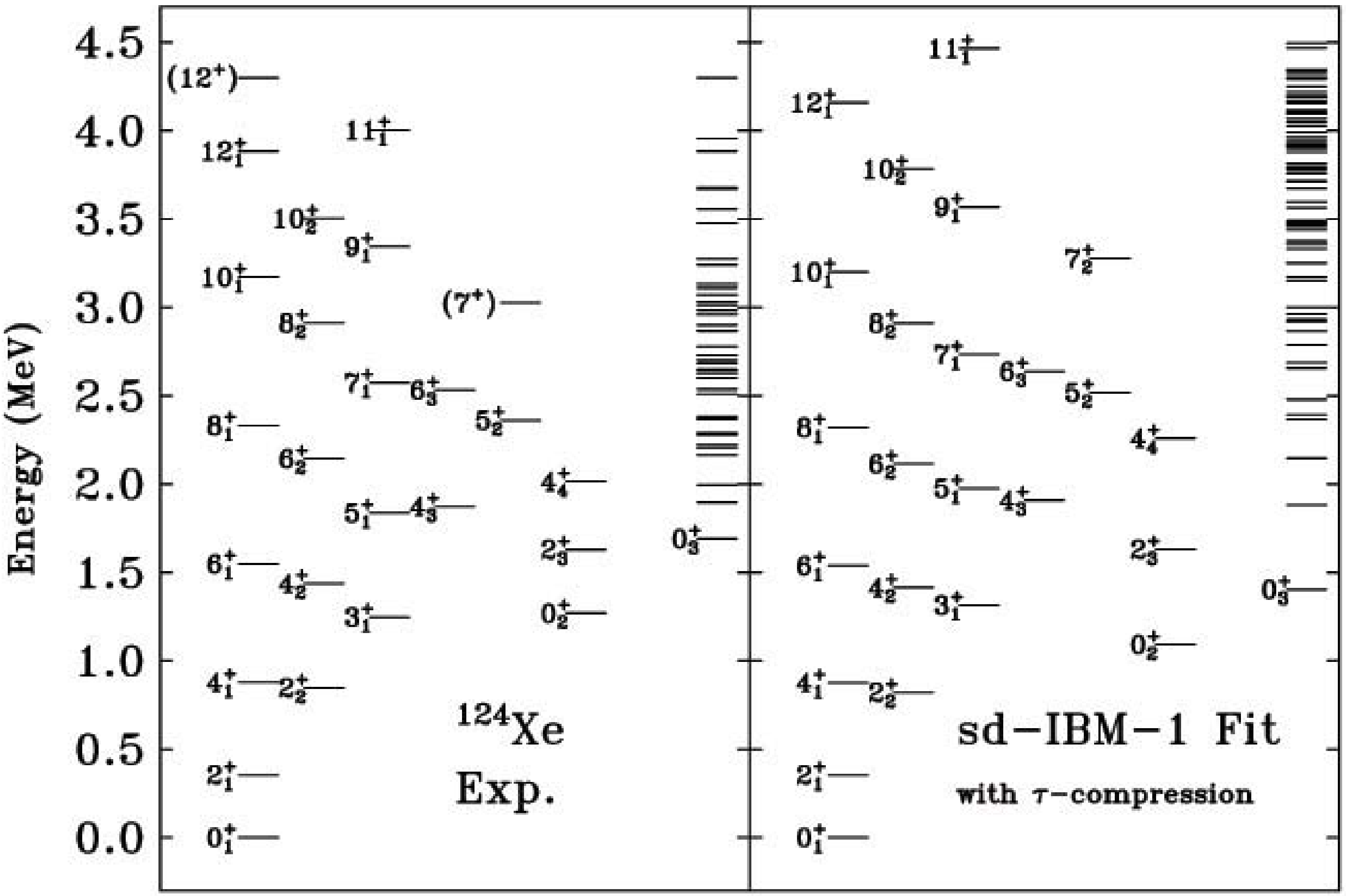

Energy (MeV)
4.5
4.0
3.5
3.0
2.5
2.0
1.5
1.0
0.5
0.0
124Xe
Exp.
sd-IBM-1 Fit
with τ-compression

Calculated B(E2) - ratios

^{124}Xe

$Q_i \to$	Q_f	$I_i \to I_f$	exp.	τ-ECQF	ECQF	CQF	[1]
$QQ \to$	Q	$2_2^+ \to 2_1^+$	100	100	100	100	100
$QQ \not\to$		$2_2^+ \to 0_1^+$	2.4(4)	2.4	2.4	2.4	2.2
$QQQ \to$	QQ	$3_1^+ \to 2_2^+$	100*	100	100	100	100
$QQQ \to$	QQ	$3_1^+ \to 4_1^+$	32(6)*	32	33	36	30
$QQQ \not\to$	Q	$3_1^+ \to 2_1^+$	3.0(4)*	2.9	3.4	3.3	3.2
$QQQ \to$	QQ	$4_2^+ \to 2_2^+$	100	100	100	100	100
$QQQ \to$	QQ	$4_2^+ \to 4_1^+$	49(7)	69	69	75	64
$QQQ \not\to$	Q	$4_2^+ \to 2_1^+$	0.10(5)	0.53	0.08	0.03	0.18
$QQQQ \to$	QQQ	$5_1^+ \to 3_1^+$	100	100	100	100	100
$QQQQ \to$	QQQ	$5_1^+ \to 6_1^+$	71(36)*	37	37	41	33
$QQQQ \to$	QQQ	$5_1^+ \to 4_2^+$	95(17)	46	45	45	44
$QQQQ \not\to$	QQ	$5_1^+ \to 4_1^+$	1.9(3)	1.6	1.5	1.3	1.6
$QQQ \to$	QQ	$0_2^+ \to 2_2^+$	100	100	100	100	100
$QQQ \not\to$	Q	$0_2^+ \to 2_1^+$	21(9)	21	21	1.5	81
$QQQQ \to$	QQQ	$2_3^+ \to 0_2^+$	100	100	100	100	100
$QQQQ \not\to$	QQ	$2_3^+ \to 2_2^+$	2.7(17)*	4.2	6.8	0.05	20.6
$QQQQ \not\to$	QQ	$2_3^+ \to 4_1^+$	4.9(29)	10.8	14.7	0.75	31.4
$QQQQ \not\to$	Q	$2_3^+ \to 2_1^+$	0.4(2)*	0.001	0.06	0.0001	0.007
$QQQQ \not\to$		$2_3^+ \to 0_1^+$	0.26(15)	0.007	0.8	0.12	0.64
$QQQQ \to$	QQQ	$2_3^+ \to 3_1^+$	–	68	42	120	44
$QQQQ \to$	QQQ	$4_3^+ \to 4_2^+$	100*	100	100	100	100
$QQQQ \to$	QQQ	$4_3^+ \to 3_1^+$	23.9(7)	112	116	112	140
$QQQQ \to$	QQQ	$4_3^+ \to 6_1^+$	–	2.2	2.3	2.1	5.7
$QQQQ \not\to$	QQ	$4_3^+ \to 4_1^+$	0.08(18)	0.48	0.87	0.82	0.98
$QQQQ \not\to$	QQ	$4_3^+ \to 2_2^+$	4.3(13)	1.85	1.07	0.73	1.57

[1] calculated with fit parameters from
W.-T. Chou, N.V. Zamfir, R.F. Casten, Phys. Rev. **C56** (1997) 829

Calculated shape invariants

^{124}Xe

$$F_2 = \frac{B(E2;0_1^+ \to 2_1^+)}{q_2} \qquad q_2 = \sum_j B(E2;0 \to 2_j^+)$$

	τ–ECQF	ECQF	CQF	[1]
q_2	1.542	1.546(5)	1.543	1.541
F_2	0.98	0.97	0.98	0.98
K_3	0.26	0.32(4)	0.22	0.39
K_4	1.031	1.043(13)	1.000	1.107
K_5	0.29	0.36(5)	0.22	0.51
K_6	0.35	0.39(3)	0.30	0.53
β_{eff}	0.269	0.269(1)	0.269	0.269
γ_{eff}	25.0°	23.9(9)°	25.7°	22.3°
σ_4	0.031	0.043(13)	0.0	0.107
σ_5	0.03	0.04(6)	0.0	0.12
σ_6	0.28	0.29(4)	0.25	0.37

[1] calculated with fit parameters from
W.-T. Chou, N.V. Zamfir, R.F. Casten, Phys. Rev. **C56** (1997) 829

Calculated shape invariants in the O(6) - region

$$\mathbf{R_2^{SU(3)}} = \frac{\mathbf{q_2^{fit}}}{\mathbf{q_2(SU(3))}} \qquad \mathbf{R_2^{O(6)}} = \frac{\mathbf{q_2^{fit}}}{\mathbf{q_2(O(6))}} \qquad \mathbf{R_2^{U(5)}} = \frac{\mathbf{q_2^{fit}}}{\mathbf{q_2(U(5))}}$$

	^{124}Xe	^{126}Xe	^{132}Ce	O(6)
N_B	8	7	8	∞
e_B	0.130	0.120	0.150	
q_2	1.542	1.082	2.020	
F_2	0.98	0.98	0.94	1
$R_2^{SU(3)}$	0.60	0.63	0.60	
$R_2^{O(6)}$	0.95	0.98	0.96	
$R_2^{U(5)}$	2.21	2.10	2.23	
K_3	0.258	0.200	0.282	0
K_4	1.031	1.016	1.029	1
K_5	0.285	0.211	0.283	0
K_6	0.345	0.300	0.334	0.32
β_{eff}	0.269	0.223	0.275	
γ_{eff}	25.0°	27.7°	24.5°	30°
σ_4	0.031	0.016	0.029	0
σ_5	0.027	0.091	0.001	0
σ_6	0.278	0.286	0.254	0.32

Approximations for K_4

$$K_4 = \frac{\langle 0_1^+|(Q\cdot Q)\ (Q\cdot Q)|0_1^+\rangle}{\langle 0_1^+|(Q\cdot Q)|0_1^+\rangle} \propto \frac{\langle 0_1^+|(QQ)^{(4)}\ (QQ)^{(4)}|0_1^+\rangle}{\langle 0_1^+|(Q\cdot Q)|0_1^+\rangle^2}$$

$$\longrightarrow \qquad K_4^{\mathrm{appr}} = \frac{7}{10}\,\frac{B(E2;4_1^+\to 2_1^+)}{B(E2;2_1^+\to 0_1^+)}$$

$$K_4 = \frac{\langle 0_1^+|(Q\cdot Q)\ (Q\cdot Q)|0_1^+\rangle}{\langle 0_1^+|(Q\cdot Q)|0_1^+\rangle} \propto \frac{\langle 0_1^+|(QQ)^{(2)}\ (QQ)^{(2)}|0_1^+\rangle}{\langle 0_1^+|(Q\cdot Q)|0_1^+\rangle^2}$$

$$\longrightarrow \qquad K_4 \approx \frac{7}{10}\left[\frac{\frac{35}{32\pi}Q_{2_1^+}^2 + B(E2;2_2^+\to 2_1^+)}{B(E2;2_1^+\to 0_1^+)}\right]$$

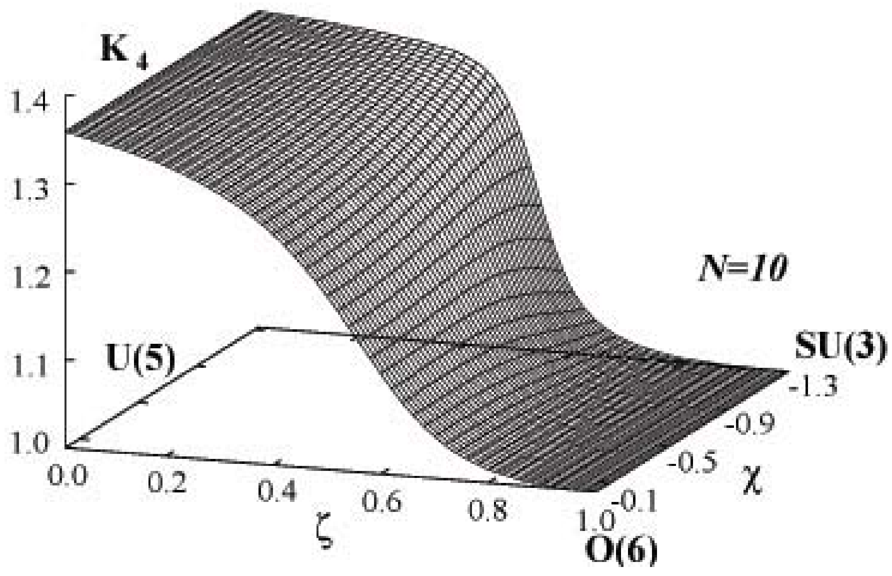

Quality of the K_4 relation

$$K_4 = \frac{\langle 0_1^+ | (Q\cdot Q)\ (Q\cdot Q) | 0_1^+ \rangle}{\langle 0_1^+ | (Q\cdot Q) | 0_1^+ \rangle}$$

$$K_4^{\mathrm{appr}} = \frac{7}{10}\ \frac{B(E2;4_1^+ \to 2_1^+)}{B(E2;2_1^+ \to 0_1^+)}$$

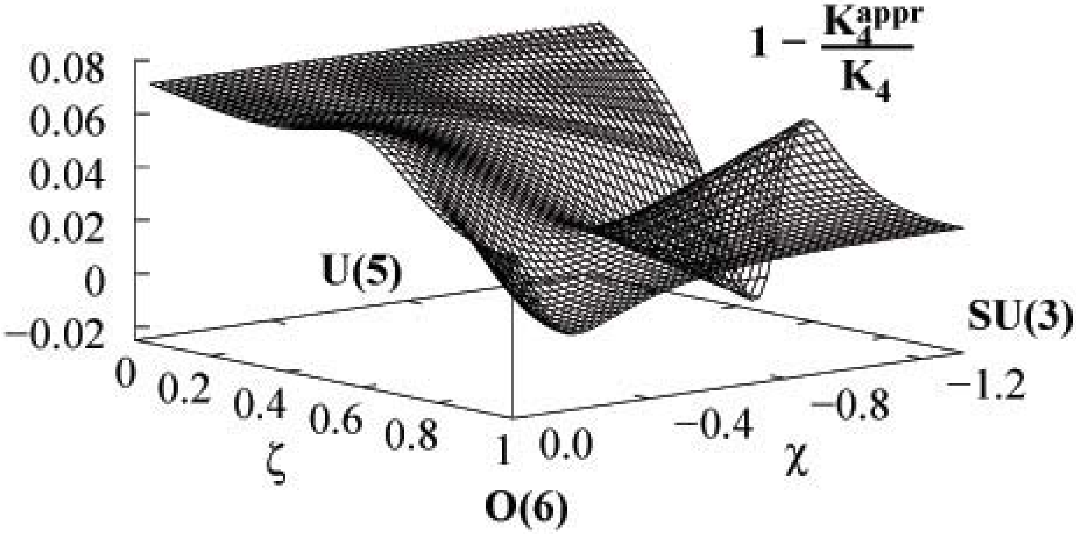

Summary

- Shape invariants give model-independent access to nuclear deformation

- Able to derive relations between matrix elements of low−lying states

- Validity of approximations was checked in IBM−1

- Important knowledge about basic observables: lifetimes of

$$\mathbf{2_1^+,\ 4_1^+,\ 2_\gamma^+}$$

V. Werner et al., Phys. Lett. **B521** (2001) 146

Relationship between quadrupole moment and two B(E2) values

Q-phonon model

Relative, energy-reduced γ intensities I_γ/E_γ^5 [arbitrary units] for $^{124\text{-}126}$Xe in comparison to the sd-IBM-1 prediction in the consistent Q-formalism. The first four columns specify the transitions: The dominant Q-phonon configurations [7, 8, 12, 19] and spins of the involved levels are given.

Transition			^{124}Xe		^{126}Xe	
'Ψ_i' $\to$	'Ψ_f'	$I_i \to I_f$	Expt.	IBM-1	IBM-1	Expt.
QQ $\to$	Q	$2_2^+ \to 2_1^+$	100	100	100	100
QQ $\not\to$		$2_2^+ \to 0_1^+$	2.4(4)	2.4	1.6	1.5(4)
QQQ $\to$	QQ	$3_1^+ \to 2_2^+$	100*	100	100	100
QQQ $\to$	QQ	$3_1^+ \to 4_1^+$	32(6)*	32	35	34(2)
QQQ $\not\to$	Q	$3_1^+ \to 2_1^+$	3.0(4)*	2.9	2.0	2.0(15)
QQQ $\to$	QQ	$4_2^+ \to 2_2^+$	100	100	100	100
QQQ $\to$	QQ	$4_2^+ \to 4_1^+$	49(7)	69	75	76(22)
QQQ $\not\to$	Q	$4_2^+ \to 2_1^+$	0.10(5)	0.53	0.5	0.4(1)
QQQQ $\to$	QQQ	$5_1^+ \to 3_1^+$	100	100		
QQQQ $\to$	QQQ	$5_1^+ \to 6_1^+$	71(36)*	37		
QQQQ $\to$	QQQ	$5_1^+ \to 4_2^+$	95(17)	46		
QQQQ $\not\to$	QQ	$5_1^+ \to 4_1^+$	1.9(3)	1.6		
QQQ $\to$	QQ	$0_2^+ \to 2_2^+$	100	100	100	100
QQQ $\not\to$	Q	$0_2^+ \to 2_1^+$	21(9)	21	7.9	7.7(22)
QQQQ $\to$	QQQ	$2_3^+ \to 0_2^+$	100	100	100	100
QQQQ $\not\to$	QQ	$2_3^+ \to 2_2^+$	2.7(17)*	4.2	1.0	2.2(10)*
QQQQ $\not\to$	QQ	$2_3^+ \to 4_1^+$	4.9(29)	10.8	4.5	2.0(8)
QQQQ $\not\to$	Q	$2_3^+ \to 2_1^+$	0.4(2)*	0.001	0.01	0.14(6)*
QQQQ $\not\to$		$2_3^+ \to 0_1^+$	0.26(15)	0.007	0.007	0.13(4)
QQQQ $\to$	QQQ	$2_3^+ \to 3_1^+$	–	68	94	67(25)*
QQQQ $\to$	QQQ	$4_3^+ \to 4_2^+$	100*	100	100	100*
QQQQ $\to$	QQQ	$4_3^+ \to 3_1^+$	23.9(7)	112	111	43.0(13)*
QQQQ $\not\to$	QQ	$4_3^+ \to 4_1^+$	0.08(18)	0.48	0.3	4.5(14)*
QQQQ $\not\to$	QQ	$4_3^+ \to 2_2^+$	4.3(13)	1.85	1.3	2.8(9)

Test with data - 1st relationship

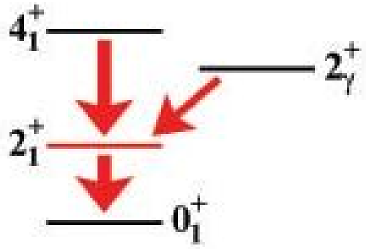

$$\underbrace{\mathbf{B}(\mathbf{E2};\mathbf{2}_1^+\to\mathbf{2}_1^+)}_{(\mathbf{Q}^2_{2_1^+})}+\underbrace{\mathbf{B}(\mathbf{E2};\mathbf{2}_2^+\to\mathbf{2}_1^+)}_{(\gamma-\mathbf{band})}=\underbrace{\mathbf{B}(\mathbf{E2};\mathbf{4}_1^+\to\mathbf{2}_1^+)}_{(\mathbf{yrast}-\mathbf{band})}$$

	$\mathbf{B}(\mathbf{E2};\mathbf{2}_1^+\to\mathbf{2}_1^+)$ [$\mathbf{e}^2\mathbf{b}^2$]	$\mathbf{B}(\mathbf{E2};\mathbf{2}_2^+\to\mathbf{2}_1^+)$ [$\mathbf{e}^2\mathbf{b}^2$]	(1) + (2) [$\mathbf{e}^2\mathbf{b}^2$]	$\mathbf{B}(\mathbf{E2};\mathbf{4}_1^+\to\mathbf{2}_1^+)$ [$\mathbf{e}^2\mathbf{b}^2$]
^{156}Gd	1.296(54)	0.017(1)	1.314(54)	1.312(25)
^{160}Gd	1.51(6)	0.030(2)	1.54(6)	1.47(2)
^{164}Dy	1.43(28)	0.043(4)	1.48(28)	1.45(7)
^{186}Os	0.61^{+9}_{-15}	0.16^{+2}_{-1}	0.77^{+9}_{-15}	0.85^{+4}_{-4}
^{196}Pt	0.08(6)	0.32(2)	0.40(6)	0.41(6)
^{106}Pd	0.10(2)	0.12(1)	0.22(2)	0.21(2)
^{114}Cd	0.05(2)	0.093(6)	0.14(2)	0.20(2)

Test with data - 2nd relationship

$$\frac{10}{7}\left(\mathrm{B(E2;}\,2_1^+ \rightarrow 0_1^+) + \mathrm{B(E2;}\,2_1^+ \rightarrow 0_{QQ}^+)\right) = \mathrm{B(E2;}\,4_1^+ \rightarrow 2_1^+)$$

	$\mathrm{B(E2;}\,2_1^+ \rightarrow 0_1^+)$ [e^2b^2]	$\mathrm{B(E2;}\,2_1^+ \rightarrow 0_{QQ}^+)$ [e^2b^2]	$10/7 \cdot [(1)+(2)]$ [e^2b^2]	$\mathrm{B(E2;}\,4_1^+ \rightarrow 2_1^+)$ [e^2b^2]
^{156}Gd	0.933(25)	n.o.	1.332(36)	1.312(25)
^{160}Gd	1.05(1)	n.o.	1.50(1)	1.47(2)
^{164}Dy	1.114(16)	n.o.	1.591(23)	1.45(7)
^{186}Os	0.56(1)	0.008(4)	0.81(1)	0.85(4)
^{196}Pt	0.264(11)	0.004(2)	0.38(1)	0.41(6)
^{106}Pd	0.13(2)	0.027(4)	0.23(2)	0.21(2)
^{114}Cd	0.102(6)	0.090(5)	0.27(1)	0.20(2)

Predictive power for various nuclei

$$\mathbf{Q}^2_{2_1^+} = \frac{32\pi}{35}\left(\mathbf{B}(\mathbf{E2}; 4_1^+ \to 2_1^+) - \mathbf{B}(\mathbf{E2}; 2_2^+ \to 2_1^+)\right)$$

$$\mathbf{B}(\mathbf{E2}; 0^+_{\mathbf{QQ}} \to 2_1^+) = \frac{7}{2}\,\mathbf{B}(\mathbf{E2}; 4_1^+ \to 2_1^+) - 5\ \mathbf{B}(\mathbf{E2}; 2_1^+ \to 0_1^+)$$

	$Q^2_{2_1^+}$(exp.) [e^2b^2]	$Q^2_{2_1^+}$(rel.) [e^2b^2]	$B(E2; 0^+_{QQ} \to 2_1^+)$(exp.) [$e^2b^2$]	$B(E2; 0^+_{QQ} \to 2_1^+)$(rel.) [$e^2b^2$]
^{156}Gd	3.72(15)	3.72(7)	n.o.	< 0.08
^{160}Gd	4.33(17)	4.14(6)	n.o.	(< -0.02)
^{164}Dy	4.12(81)	4.04(20)	n.o.	(< -0.2)
^{186}Os	1.76^{+26}_{-44}	1.98(13)	0.040(20)	0.18(15)
^{196}Pt	0.24(18)	0.26(18)	0.02(1)	0.12(21)
^{106}Pd	0.30(6)	0.26(6)	0.14(2)	0.09(12)
^{114}Cd	0.13(6)	0.31(6)	0.090(5)	0.19(8)

Q-phonon scheme

$$|2_1^+\rangle \propto \mathbf{Q}\ |0_1^+\rangle$$

$$|\mathbf{J}^+\rangle \propto (\mathbf{QQ})^{(\mathbf{J})}\ |0_1^+\rangle \propto (\mathbf{Q}\ |2_1^+\rangle)^{(\mathbf{J})}$$

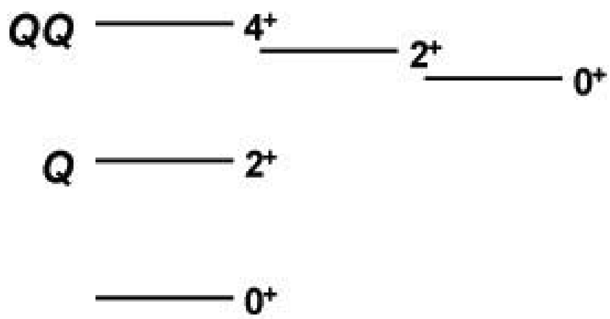

E2 transitions: $\Delta Q = 1$

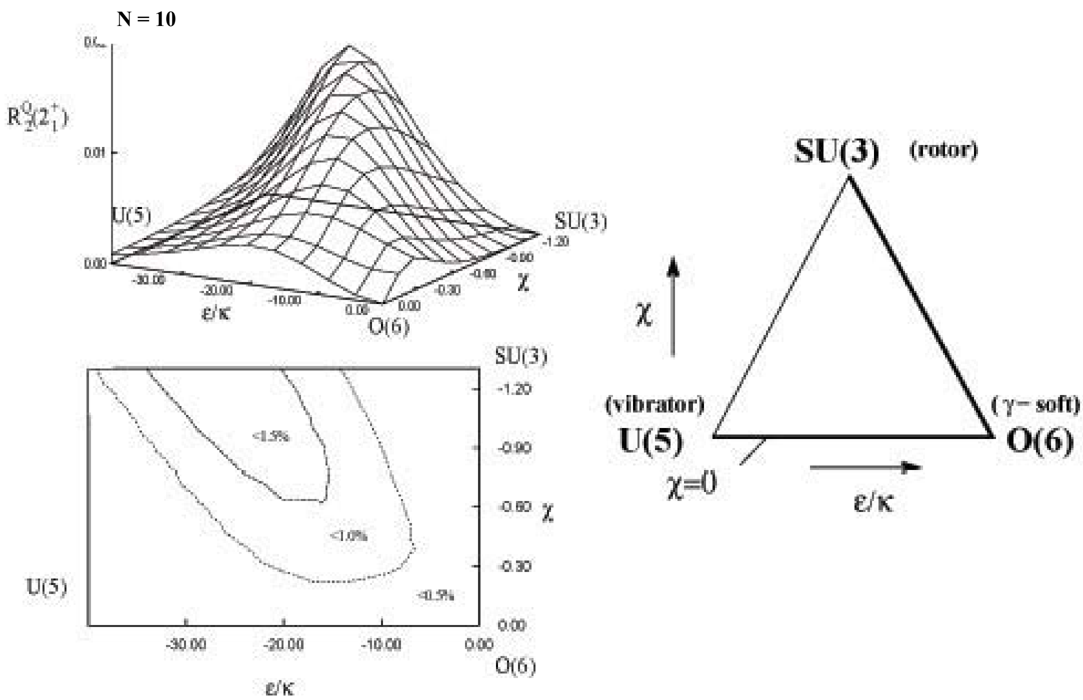

N. Pietralla et al., Phys. Rev. **C57** (1998) 150

^{124}Xe

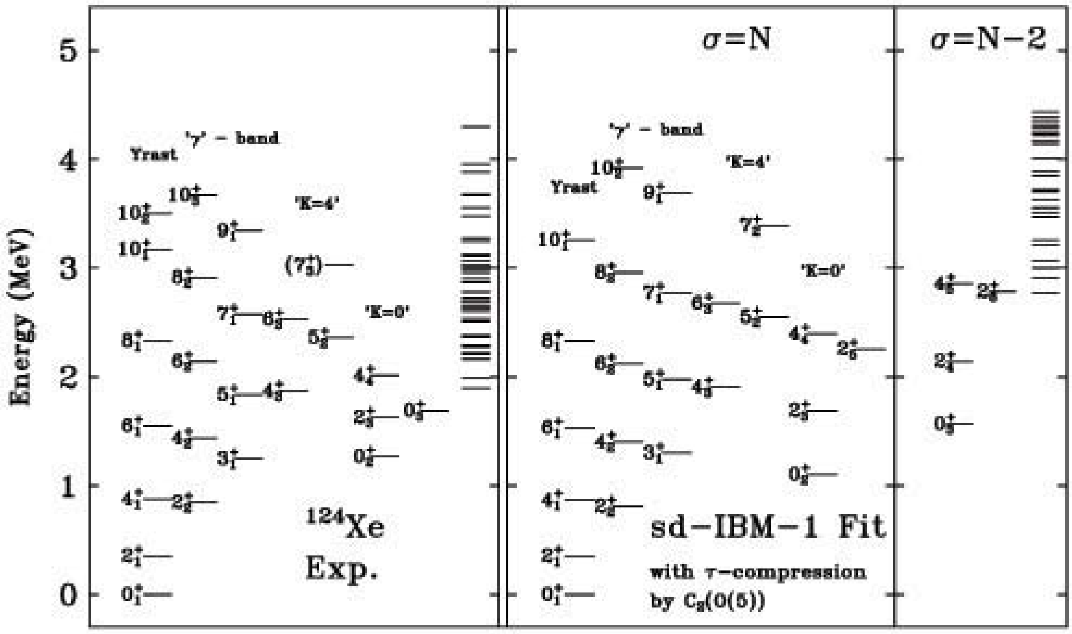

$$\mathbf{H}_{\tau-\mathbf{ECQF}} = \epsilon \mathbf{n_d} + \lambda \mathbf{LL} + \kappa \mathbf{Q}^{\chi}\mathbf{Q}^{\chi} + \beta \mathbf{C_2}(\mathbf{O}(\mathbf{5}))$$
$$= \kappa \left(\frac{\epsilon}{\kappa}\mathbf{n_d} + \frac{\tilde{\lambda}}{\kappa}\mathbf{LL} + \mathbf{Q}^{\chi}\mathbf{Q}^{\chi} + \mathbf{4}\frac{\beta}{\kappa}\mathbf{T}^{(\mathbf{3})}\mathbf{T}^{(\mathbf{3})} \right)$$

$$\epsilon/\kappa = -20.9 \ , \ \chi = -0.257 \ , \ \beta/\kappa = 0.563 \ , \ \lambda/\kappa = -0.284$$
$$\kappa = -34.91keV \ , \ e_b = 0.14224e^2b^2$$

V. Werner et al., Nucl. Phys. **A693** (2001) 451

^{124}Xe

ΔQ	$I_i \rightarrow I_f$	^{124}Xe exp.	^{124}Xe IBM	^{134}Ce exp.	^{134}Ce IBM	^{190}Os exp.	^{190}Os IBM
1	$2_2^+ \rightarrow 2_1^+$	100	100	100	100	100	100
2	$2_2^+ \rightarrow 0_1^+$	2.4(4)	2.4	5.4	5.4	17.9(6)	18.1
1	$3_1^+ \rightarrow 2_2^+$	100*	100	54.5	100	100	100
1	$3_1^+ \rightarrow 4_1^+$	32(6)*	32	100	30.4	45(7)	16
2	$3_1^+ \rightarrow 2_1^+$	3.0(4)*	2.9	4	6	7.1(6)	10.2
1	$4_2^+ \rightarrow 2_2^+$	100	100	100	100	100	100
1	$4_2^+ \rightarrow 4_1^+$	49(7)	69	55	63	57(6)	41
2	$4_2^+ \rightarrow 2_1^+$	0.10(5)	0.53	0.6	2.0	1.29(5)	3.0
1	$5_1^+ \rightarrow 3_1^+$	100	100	100 (5_2^+)	100	100	100
1	$5_1^+ \rightarrow 6_1^+$	71(36)*	35	–	35	–	21
1	$5_1^+ \rightarrow 4_2^+$	95(17)	46	–	48	–	58
2	$5_1^+ \rightarrow 4_1^+$	1.9(3)	2.2	≤ 7.5	4.3	5(2)	8
1	$0_2^+ \rightarrow 2_2^+$	100	100	100	100	100	100
2	$0_2^+ \rightarrow 2_1^+$	21(9)	21	≤ 2.7	2.7	9.9(18)	9.7
	$2_3^+ \rightarrow 0_2^+$	100	100	100	100	100	100
	$2_3^+ \rightarrow 3_1^+$	–	117	–	117	27(5)	101
	$2_3^+ \rightarrow 2_2^+$	2.7(17)*	2.9	≤ 32	0.3	–	0.06
	$2_3^+ \rightarrow 4_1^+$	4.9(29)	12.5	–	2.0	–	5.8
	$2_3^+ \rightarrow 2_1^+$	0.4(2)*	0.001	0.7	0.0003	0.6(2)	0.04
	$2_3^+ \rightarrow 0_1^+$	0.26(15)	0.19	0.5	0.04	0.19(2)	0.34
	$4_3^+ \rightarrow 4_2^+$	100*	100	100	100	52(18)*	105
	$4_3^+ \rightarrow 3_1^+$	23.9(7)	114	120(70)	104	100	100
	$4_3^+ \rightarrow 6_1^+$	–	2.2	–	1.8	–	1.8
	$4_3^+ \rightarrow 4_1^+$	0.08(18)	0.69	13(8)	0.52	0.31(3)*	0.52
	$4_3^+ \rightarrow 2_2^+$	4.3(13)	2.45	4(2)	7	27.8(13)	26.3
	$4_3^+ \rightarrow 2_1^+$	–	0.01	0.05(3)	0.01	0.004(1)*	0.08

Experimental nuclear spectroscopy:

Measurement of lifetimes

P. von Brentano

IKP University
Cologne, Germany

E-mail: brentano@ikp.uni-koeln.de

RDDS Method

Recoil **D**istance **D**öppler-**S**hift
→ lifetimes in ps range

$$\boxed{E_{Flight} \approx E_{Stop}\left(1 + \frac{v}{c}\cos\theta\right)}$$

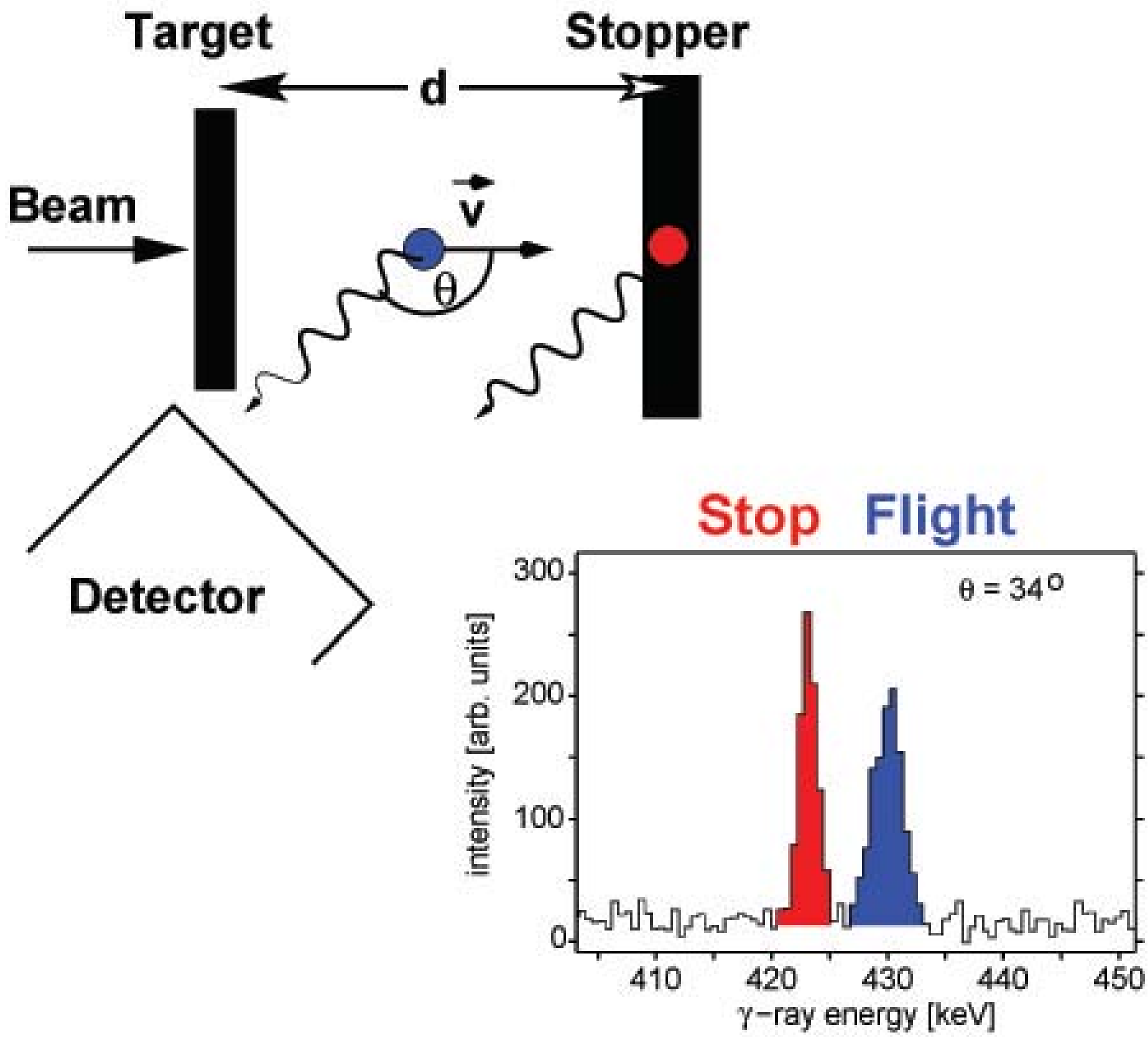

^{46}V: EUROBALL Experiment

RDDS-lifetime measurement with Köln Plunger
at Euroball IV, Strasbourg

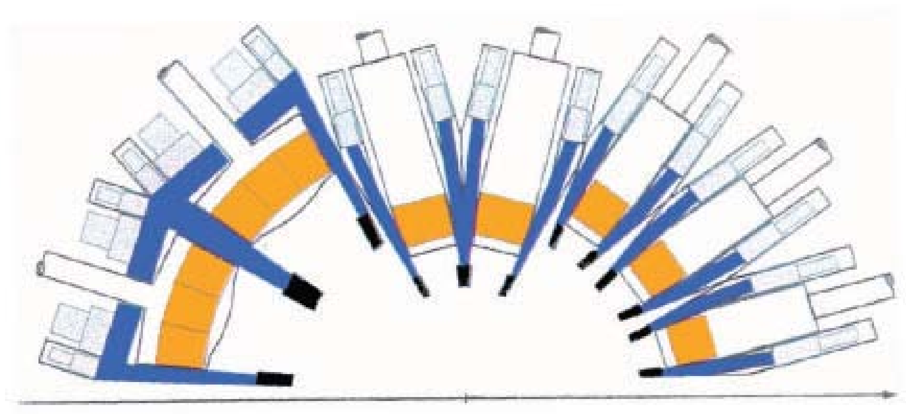

- ^{24}Mg(^{28}Si, αpn)^{46}V at 110 MeV
  ⇒ $v/c = 4.5\%$
- 17 target-to-stopper distances between 1 and 7750 µm
- 3 x 10^9 γγ-events

Analysis of γγ-coincidence data using the **Differential Decay Curve Method**

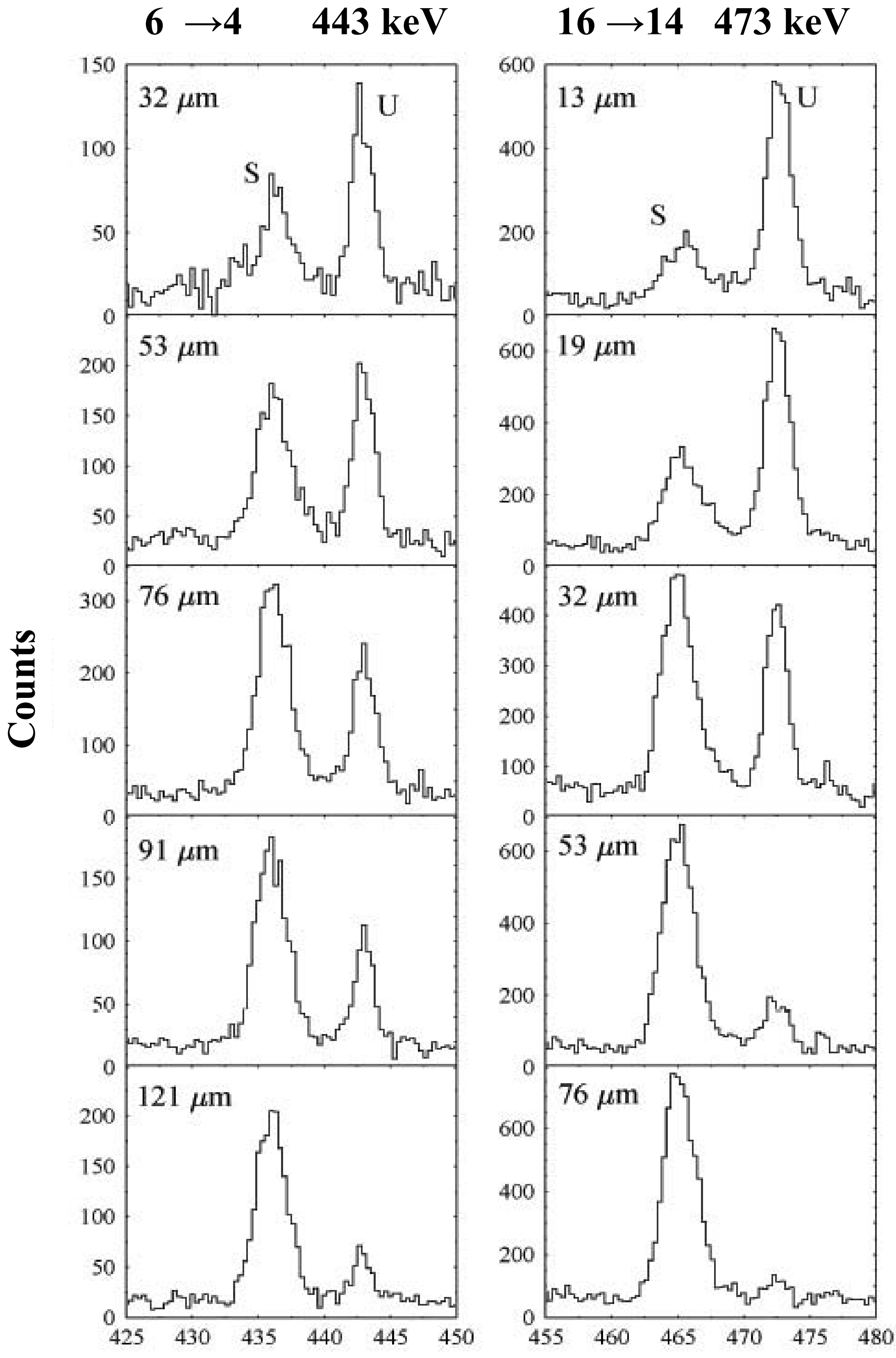
6 →4 443 keV
16 →14 473 keV
Counts
32 μm
53 μm
76 μm
91 μm
121 μm
13 μm
19 μm
32 μm
53 μm
76 μm
S
U

Gamma-ray energy [keV]

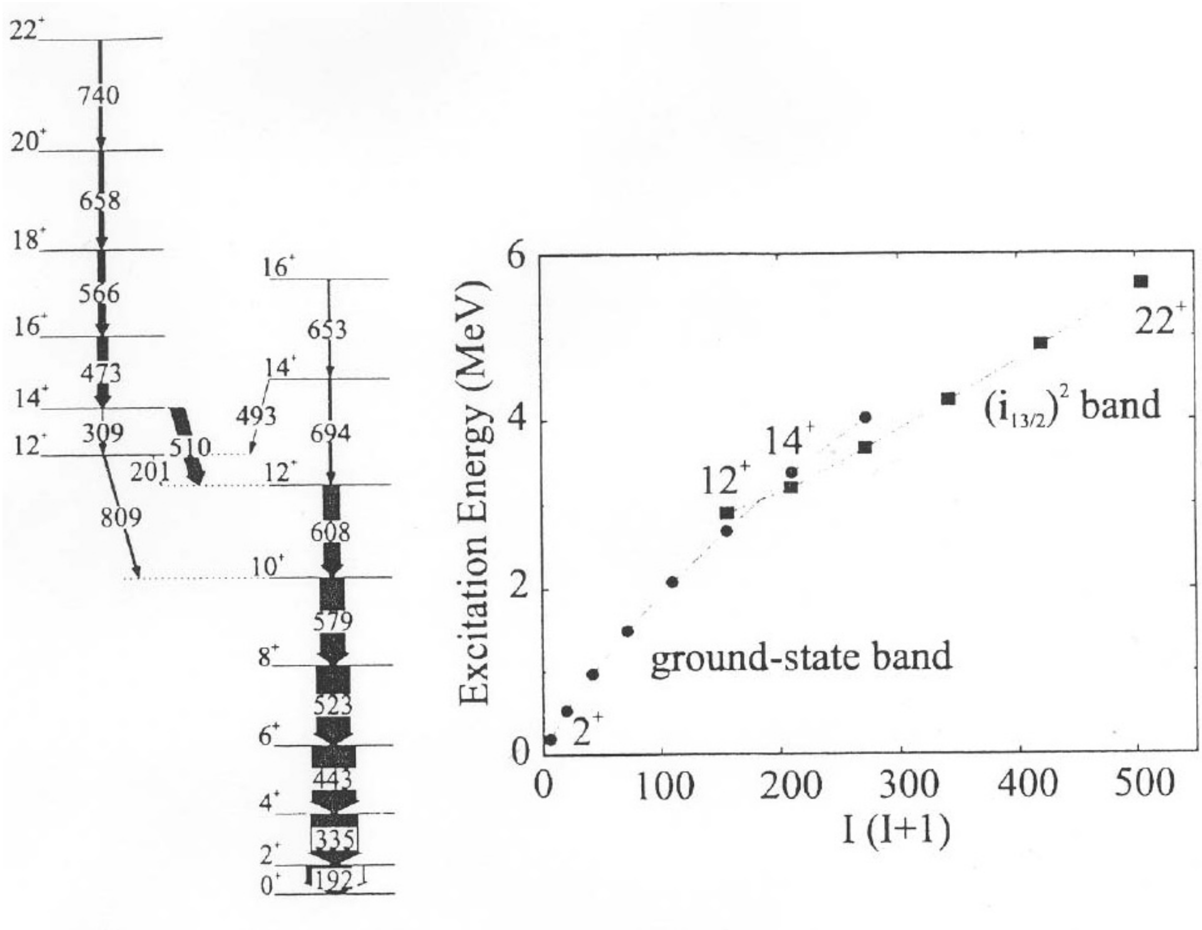

Lifetimes from Döppler-shifted Spectra using RDDS data

Quantitative analysis of ^{158}Er

Recoil Distance Döppler Shift Data

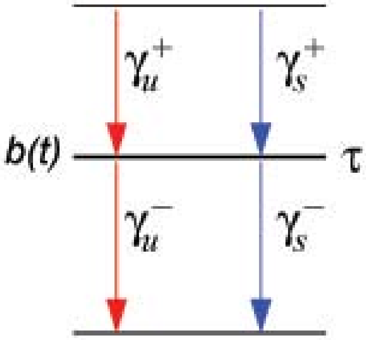

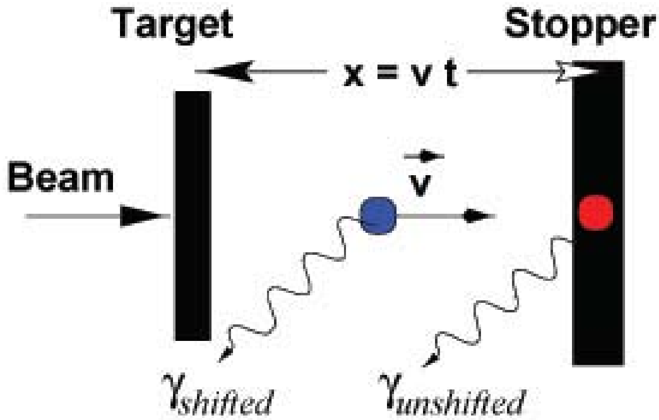

$$\#\gamma_u^+(t)\Big|_t^\infty = B_u^+(t),$$

$$\#\gamma_u^-(t)\Big|_t^\infty = B_u^-(t)$$

$$B_u^+(t) + b(t) = B_u^-(t)$$

$$B_u^-(t) = \int_t^\infty \frac{1}{\tau}\, b(t)dt \quad \Rightarrow \quad \dot{B}_u^-(t) = -\frac{1}{\tau}\, b(t)$$

$$\Rightarrow \quad \boxed{\dot{B}_u^- = -\tfrac{1}{\tau}\left(B_u^- - B_u^+\right)}$$

Lifetimes from γγ-coincidences

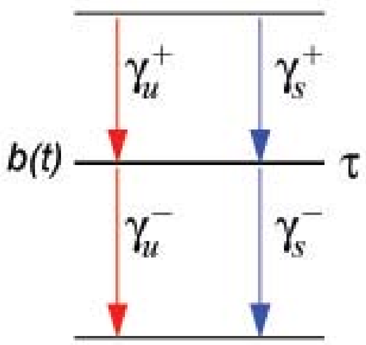

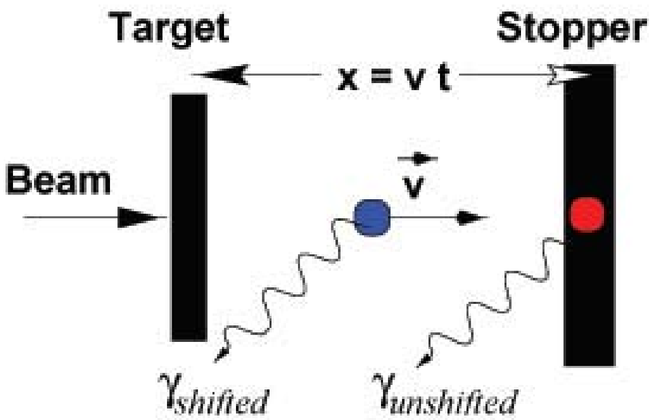

$$\{\gamma_1, \gamma_2\} := \#\gamma_2 \text{ in coincidence with } \gamma_1$$

$$B_u^+ = \{\gamma_u^+, \gamma_{u+s}^-\} = \{\gamma_u^+, \gamma_u^-\} + \underbrace{\{\gamma_u^+, \gamma_s^-\}}_{=0}$$

$$B_u^- = \{\gamma_{u+s}^+, \gamma_u^-\} = \{\gamma_u^+, \gamma_u^-\} + \{\gamma_s^+, \gamma_u^-\}$$

$$\{\gamma_{u+s}^+, \gamma_{u-s}^+\}^\bullet = 0 \qquad \Rightarrow \qquad \dot{B}_u^- = -\{\gamma_s^+, \gamma_s^-\}^\bullet$$

$$\dot{B}_u^- = -\frac{1}{\tau}\left(B_u^- - B_u^+\right) \Rightarrow \boxed{\{\gamma_s^+, \gamma_s^-\}^\bullet = \frac{1}{\tau}\{\gamma_s^+, \gamma_u^-\}}$$

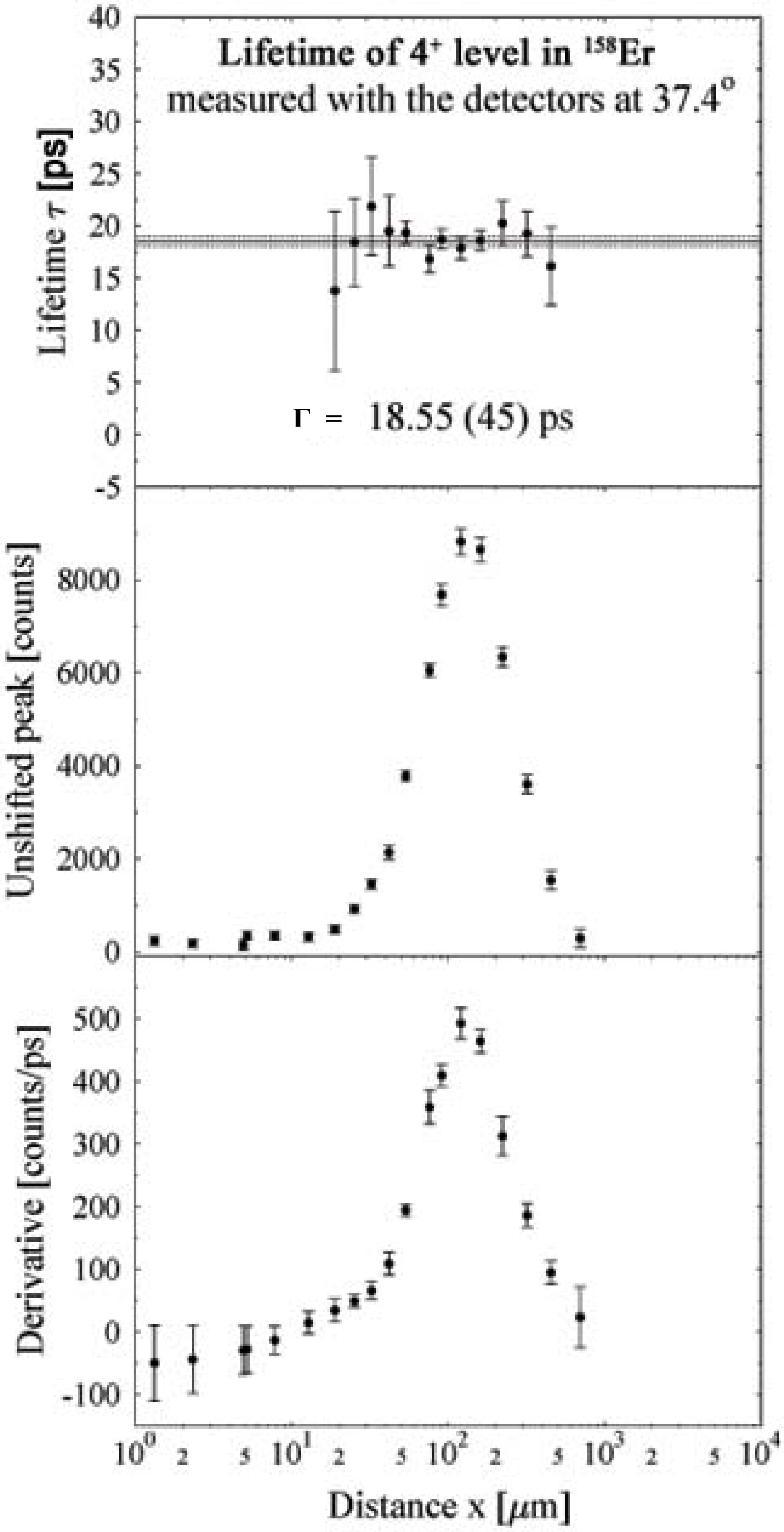

Lifetime of 4+ level in 158Er
measured with the detectors at 37.4°
Lifetime τ [ps]
Γ = 18.55 (45) ps
Unshifted peak [counts]
Derivative [counts/ps]
Distance x [μm]

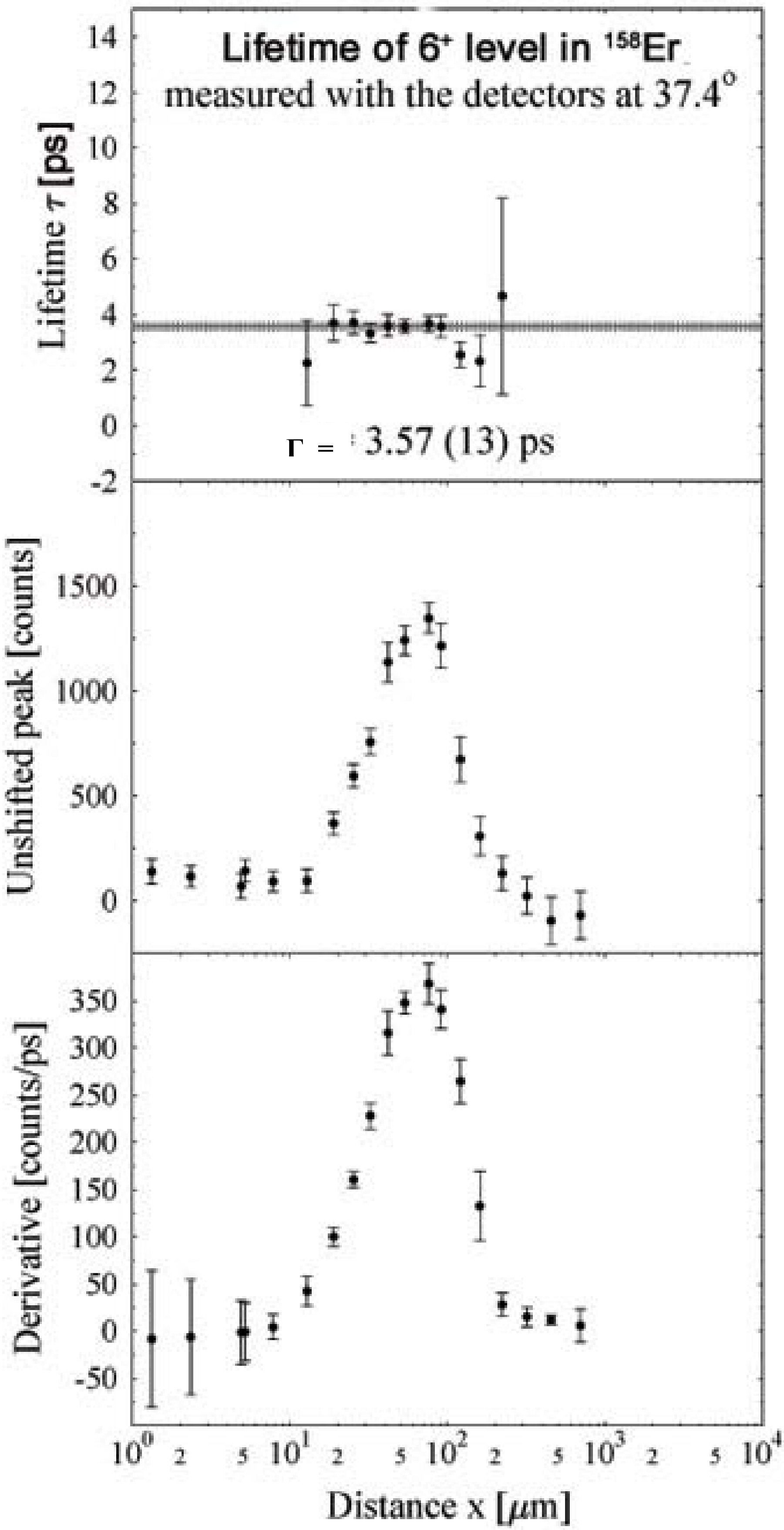

Lifetime of 6+ level in 158Er
measured with the detectors at 37.4°
Lifetime τ [ps]
Γ = 3.57 (13) ps
Unshifted peak [counts]
Derivative [counts/ps]
Distance x [μm]

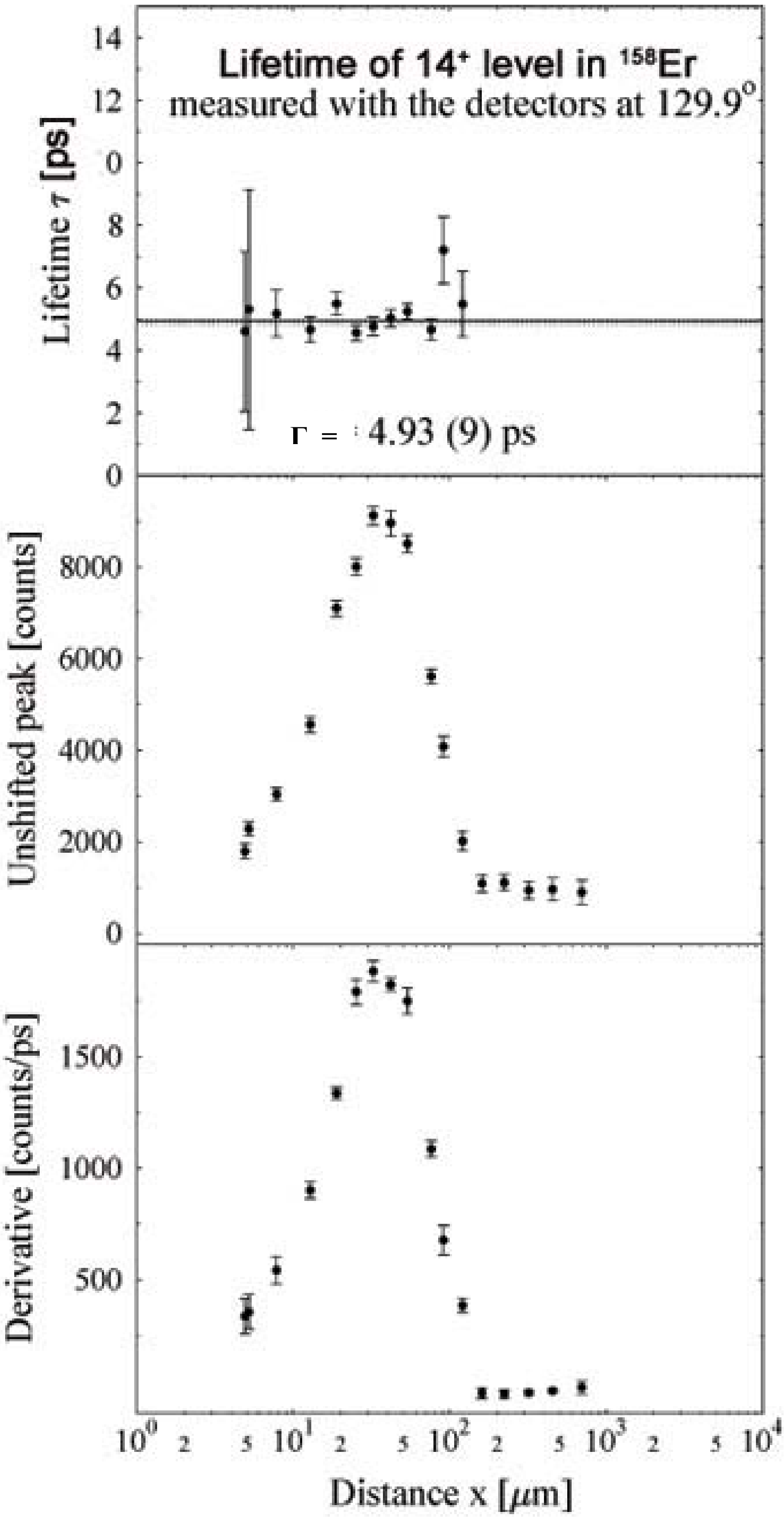
Lifetime of 14⁺ level in ¹⁵⁸Er
measured with the detectors at 129.9°
Lifetime τ [ps]
τ = 4.93 (9) ps
Unshifted peak [counts]
Derivative [counts/ps]
Distance x [μm]

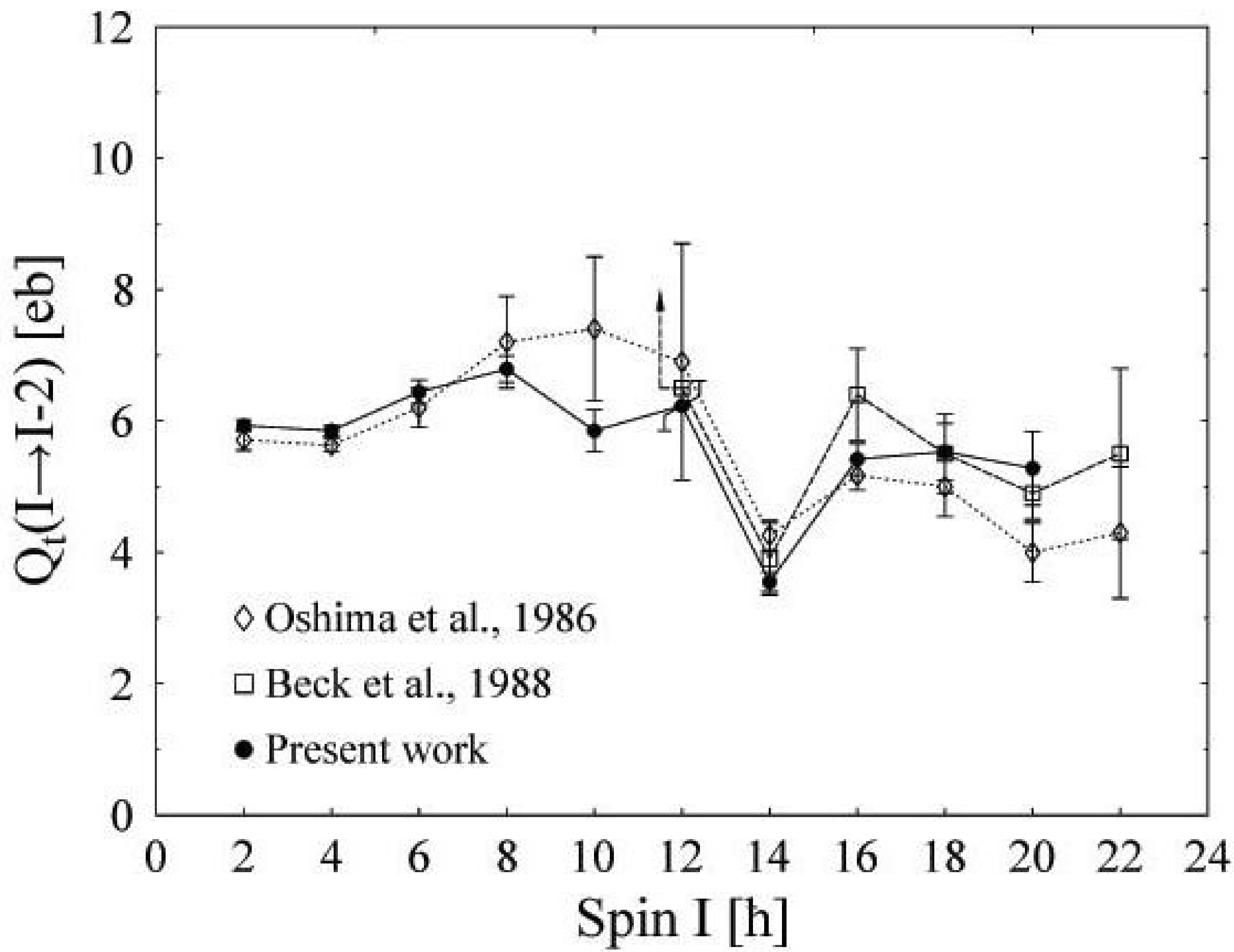

$Q_t(I \to I\text{-}2)$ [eb]
Spin I [ħ]
◊ Oshima et al., 1986
□ Beck et al., 1988
● Present work
0
2
4
6
8
10
12
14
16
18
20
22
24

Lifetimes from Döppler-shifted Spectra using RDDS data

Quantitative analysis of *Xe* isotopes

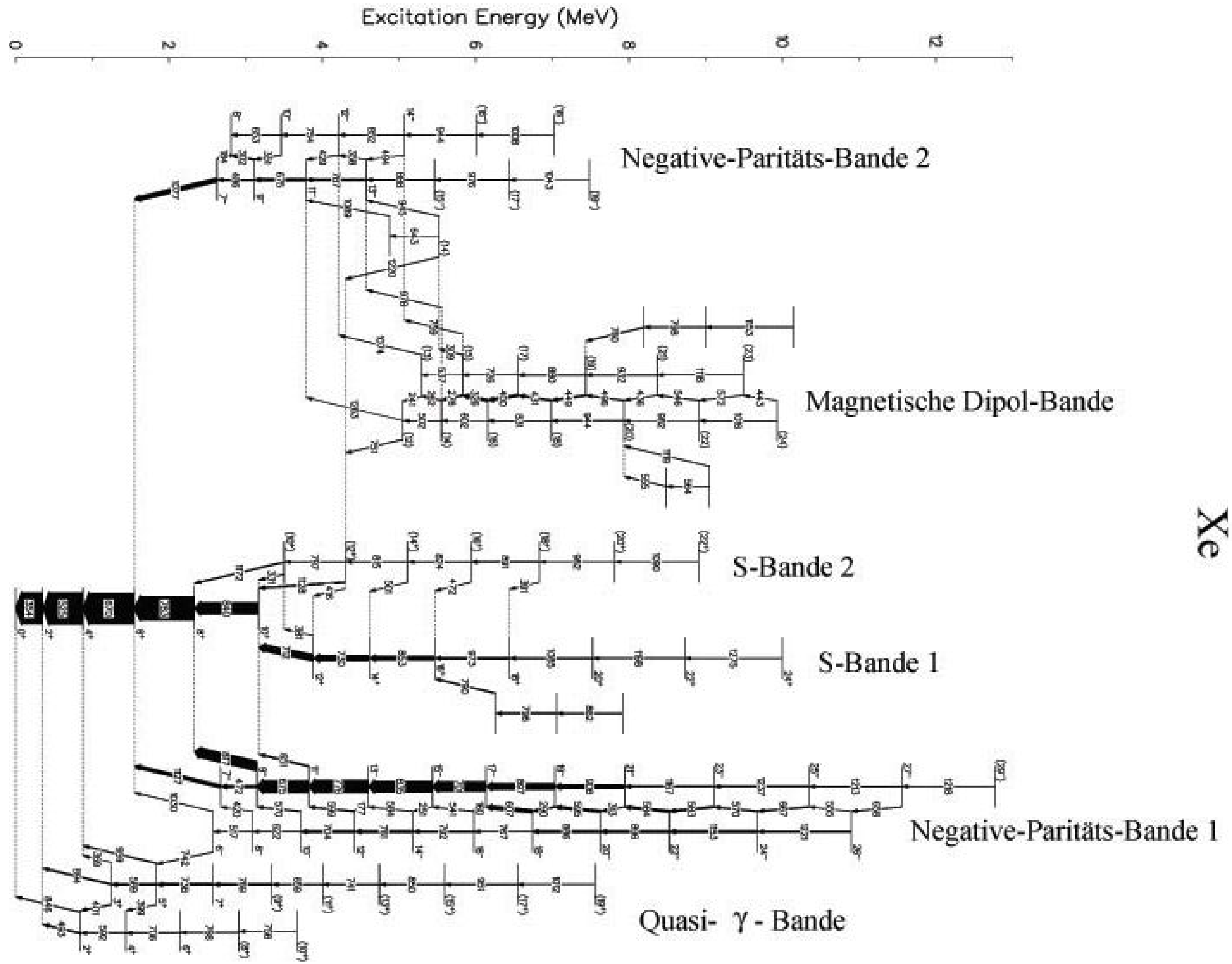
Excitation Energy (MeV)
Negative-Paritäts-Bande 2
Magnetische Dipol-Bande
S-Bande 2
S-Bande 1
Negative-Paritäts-Bande 1
Quasi- γ - Bande

^{124}Xe

^{124}Xe Lifetimes (τ)

E_{lev} $[keV]$	I^{π} $[\hbar]$	$\overline{\tau}(\Delta\overline{\tau})$ $[ps]$	$\overline{\tau}_c(\Delta\overline{\tau}_c)$ $[ps]$
354	2^+	67.5(17)	67.5(17)
879	4^+	8.19(23)	8.19(23)
1549	6^+	1.82(17)	1.86(16)
2331	8^+	1.03(39)	1.15(35)
3172	10^+	2.49(33)	2.51(32)
3883	12^+	2.13(37)	2.16(36)
4299	12^+	> 2.5	> 2.5
5552.7	(15)	0.89(8)	1.02(8)
5828.3	(16)	1.84(13)	1.88(12)
6154.8	(17)	1.75(8)	1.80(8)
6554.6	(18)	0.40(8)	0.56(9)

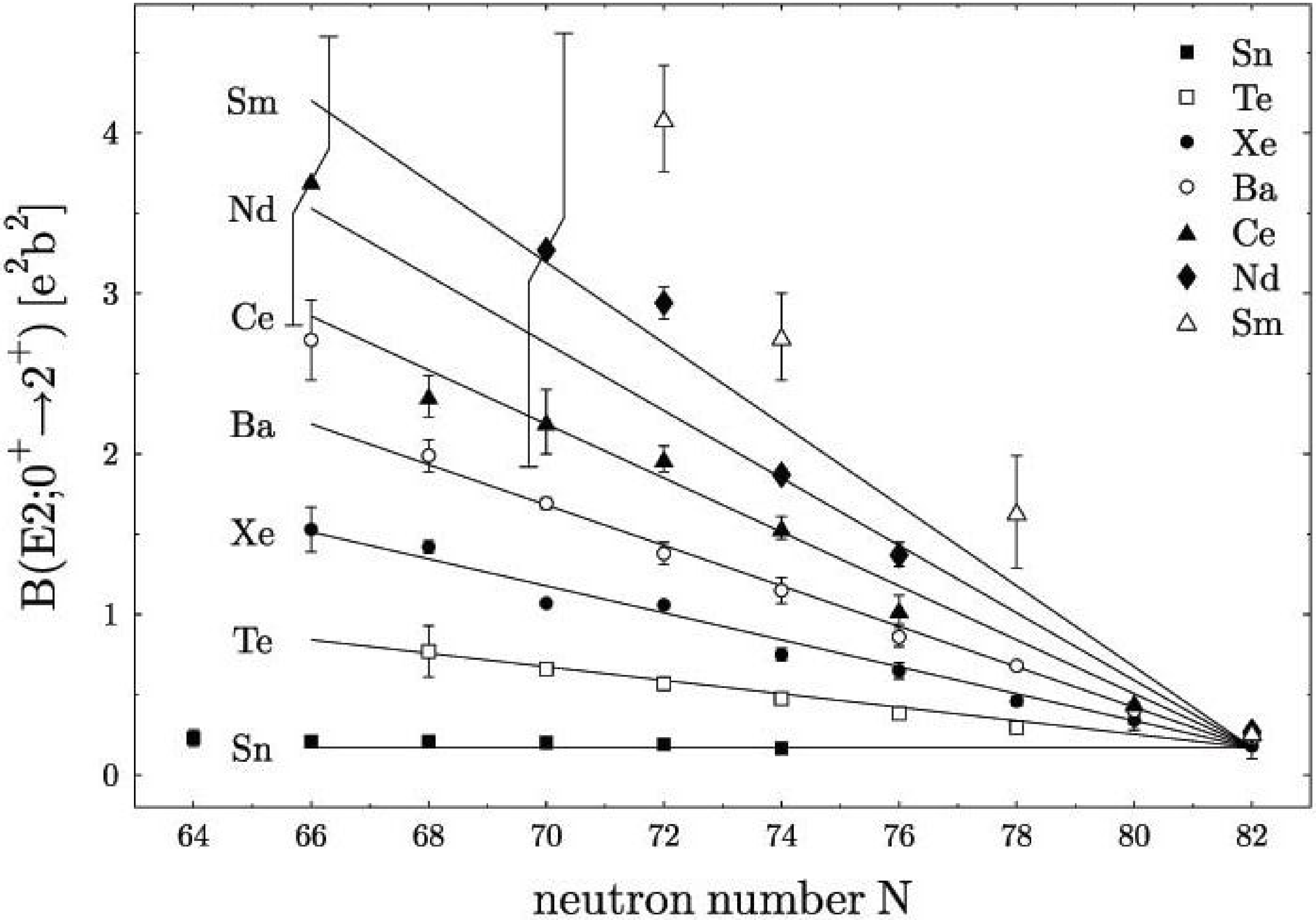

B(E2;0+→2+) [e²b²]
neutron number N
0
1
2
3
4
64
66
68
70
72
74
76
78
80
82
Sm
Nd
Ce
Ba
Xe
Te
Sn
Sn
Te
Xe
Ba
Ce
Nd
Sm

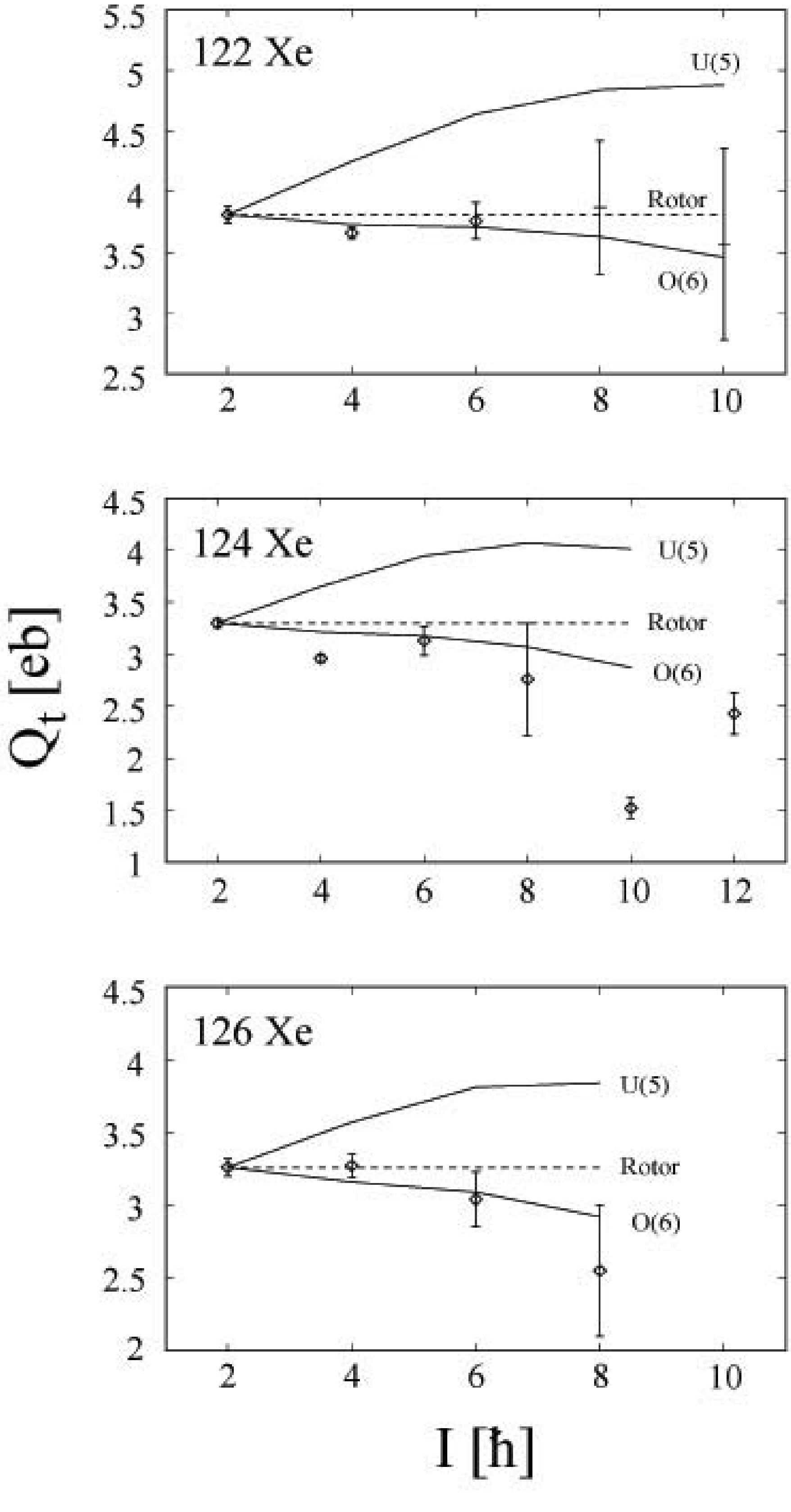
122 Xe
124 Xe
126 Xe
U(5)
Rotor
O(6)
Q_t [eb]
I [ħ]

Lifetimes of highly excited states from NRF: S-Dalinac, Darmstadt and Dynamitron, Stuttgart

NRF = Nuclear resonance fluorescence

NRF = Resonant inelastic photon scattering

NRF = $A(\gamma,\gamma)A*$

Resonance reaction:

$A + \gamma \rightarrow A_{**}(E,I) \rightarrow \gamma + A_{*}$

Photon Scattering Technique
(Nuclear Resonance Fluorescence)

$\Pi\lambda$-strength

$\Delta J = 1,2$

high energy resolution

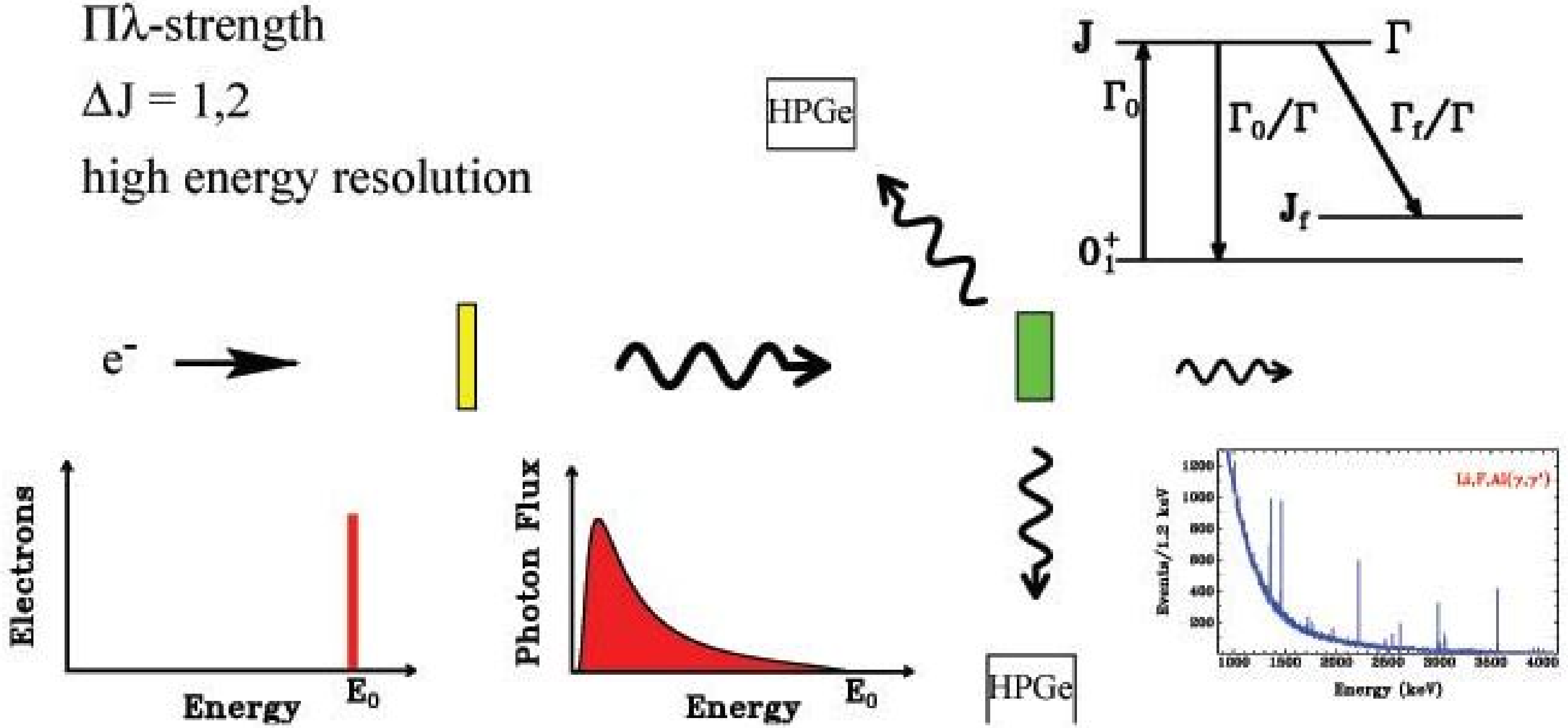

NRF – setup at the Stuttgart Dynamitron

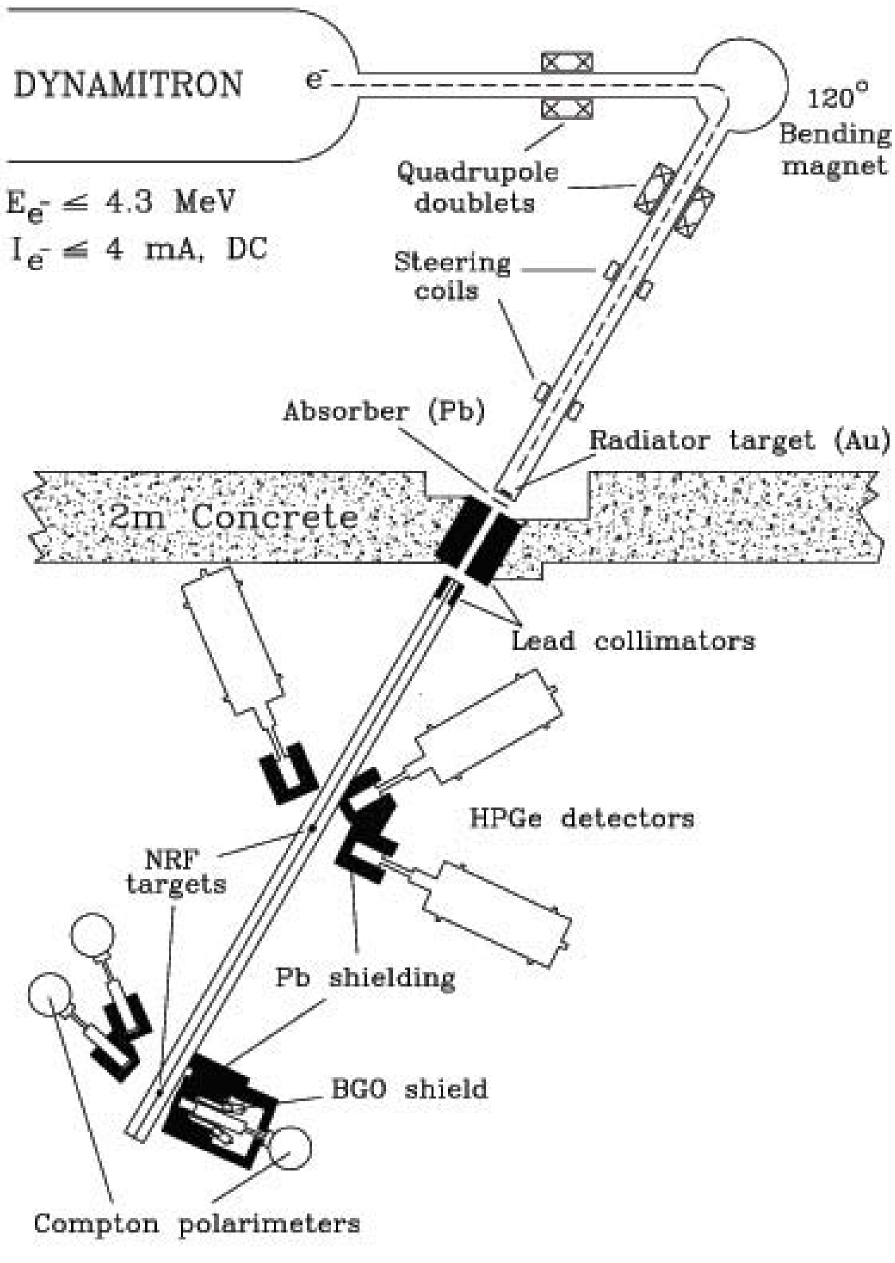

γ–ray spectra of ^{94}Mo From different experiments

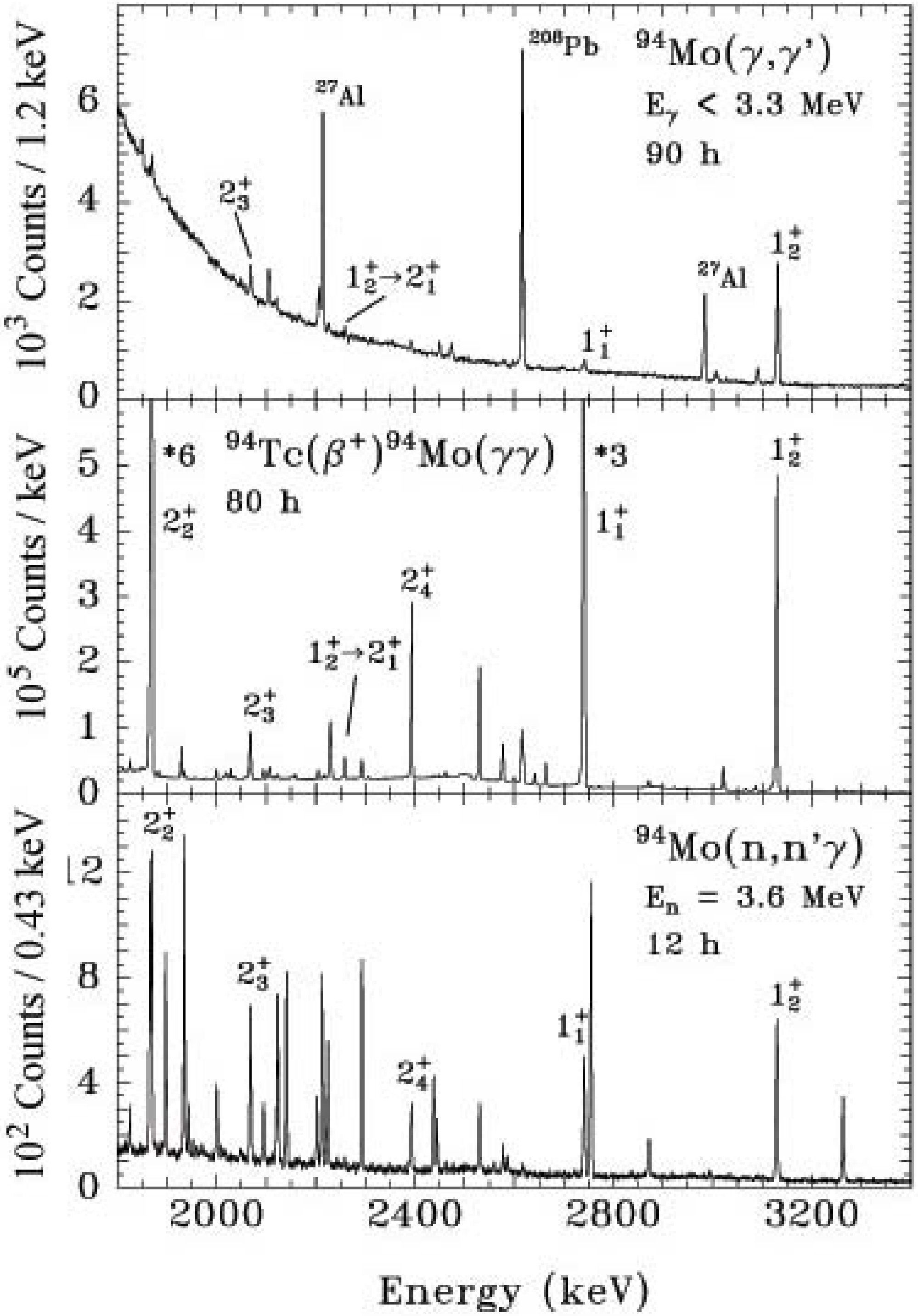

$^{92}Zr\ (\gamma, \gamma')$

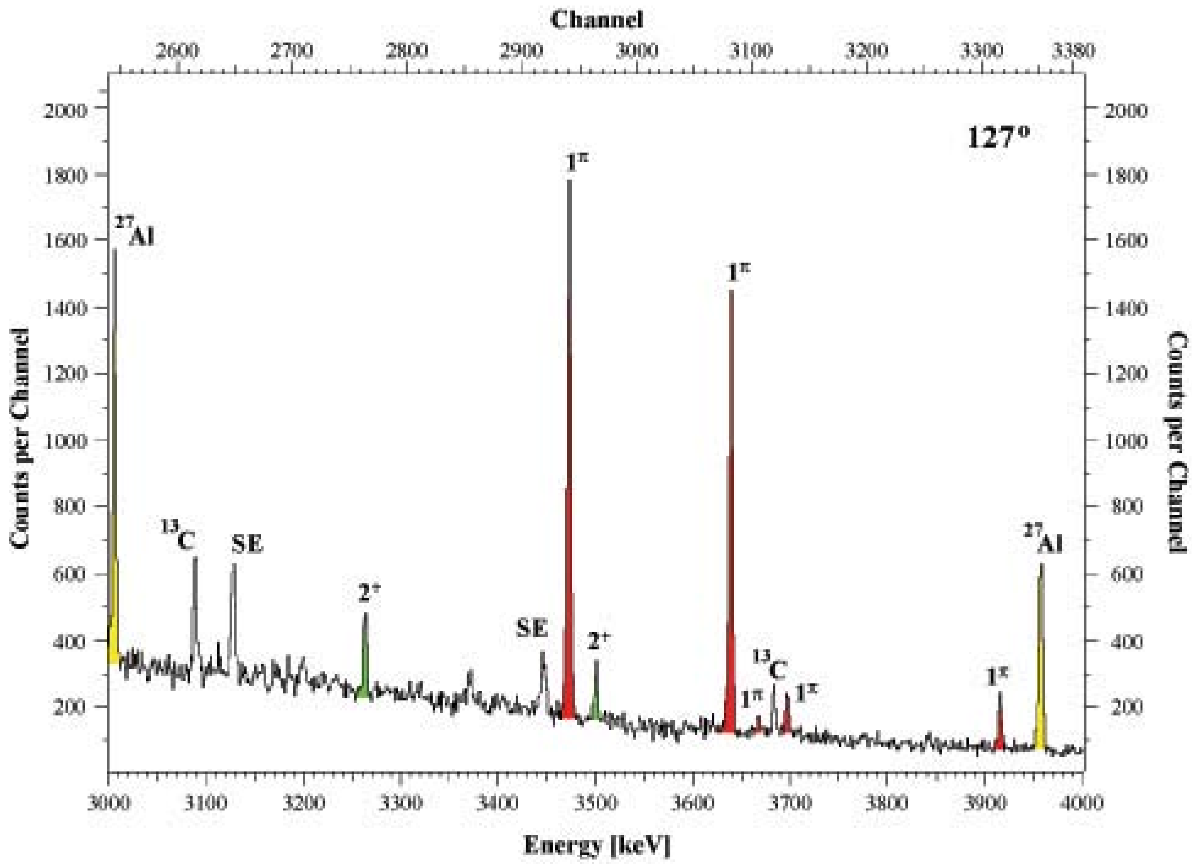

^{92}Zr (γ, γ´)

E_{Level} [keV]	J_i^π	J_f^π	$I_{s,0}$ [eV·b]	Γ_0 [meV]	Γ_f/Γ_0	δ	$B(\Pi\lambda)$	τ [fs]
				^{92}Zr				
1847.6(5)	2_2^+	0_1^+	2.4(3)	1.6(4)	1.0	E2	E2 3.7(8)[c]	118^{+33}_{-21}
		2_1^+			2.6(6)	$+0.032^{+22}_{-21}$	M1 0.46(15)[a]	
							E2 0.3(1)[c]	
3263.2(5)	2^+	0_1^+	3.1(2)	7.4(7)	1.0	E2	E2 1.0(1)[c]	20.6^{+22}_{-18}
		2_1^+			3.3(3)	-0.27^{+9}_{-5}	M1 0.16(2)[a]	
							E2 1.2(2)[c]	
3370(1)	$1^{(-)*}$	0_1^+	1.5(2)	1.45(17)	1.0	Π1	M1 0.0033(4)[a]	455^{+61}_{-48}
							E1 0.037(4)[b]	
3472.3(5)	1^{+*}	0_1^+	27.6(10)	45.2(18)	1.0	Π1	M1 0.094(4)[a]	9.3^{+4}_{-4}
							E1 1.04(4)[b]	
		2_1^+			0.37(2) (Π1)			
		0_2^+			0.19(2)	Π1	M1 0.08(1)[a]	
							E1 0.9(1)[b]	
3500.4(5)	2^+	0_1^+	2.7(2)	1.75(15)	1.0	E2	E2 0.17(1)[c]	376^{+35}_{-29}
3638.4(5)	1	0_1^+	37.0(13)	51.5(22)	1.0	Π1	M1 0.093(4)[a]	10.5^{+5}_{-4}
							E1 1.03(4)[b]	
		0_2^+			0.21(3)	Π1	M1 0.08(1)[a]	
							E1 0.9(1)[b]	
3667(1)	1	0_1^+	1.8(3)	2.1(3)	1.0	Π1	M1 0.0037(6)[a]	314^{+58}_{-43}
							E1 0.040(7)[b]	
3697.3(5)	1	0_1^+	4.2(4)	9.6(11)	1.0	Π1	M1 0.016(2)[a]	35.7^{+48}_{-38}
							E1 0.18(2)[b]	
		2_1^+			0.93(14) (Π1)			
3915.4(5)	1	0_1^+	11.8(14)	15.6(19)	1.0	Π1	M1 0.022(3)[a]	42.1^{+59}_{-46}
							E1 0.25(3)[b]	
				^{94}Zr				
2846.4(5)	1^-	0_1^+	113(7)	88(25)	1.0	E1	E1 3.7(11)[b]	6.7^{+26}_{-14}
		2_1^+			0.11(3)	E1	E1 1.3(5)[b]	

M1 [μ_N^2] E2 [W.u.] E1 [$10^{-3} e^2 fm^2$]

V. Werner et al., Phys. Lett. **B550** (2002) 140

M1 - systematics

1^+_{sc}

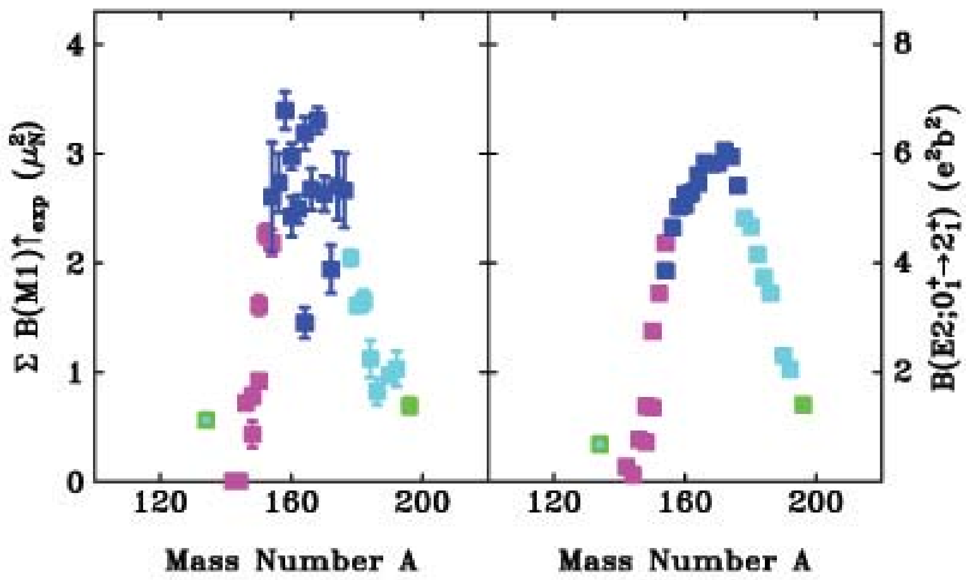

strong at mid-shell

strongly correlated to E2-strength

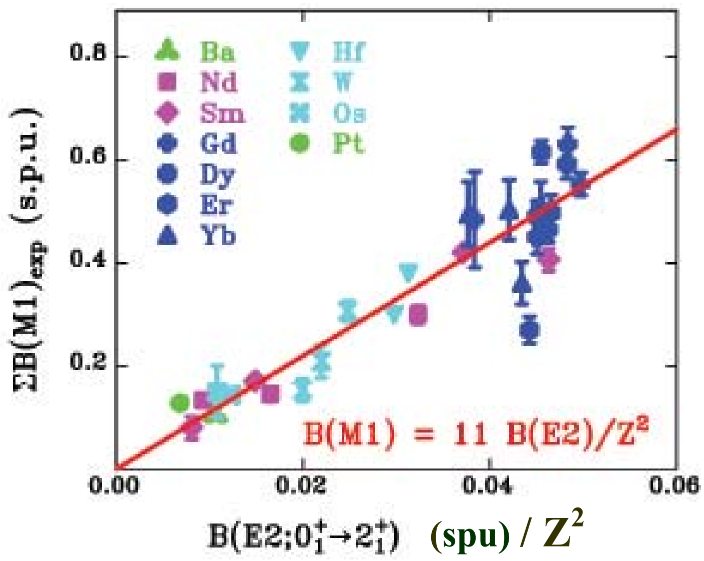

N. Pietralla et al., Phys.Rev. **C58** (1998) 184

Three setups for low-spin spectroscopy at FN-Tandem, Cologne and in Lexington

Comparison of spectra

Inelastic neutron scattering

Lifetimes from (n, n´γ) data measured at Lexington

Experimental setup at the Van de Graaff accelerator of the University of Kentucky

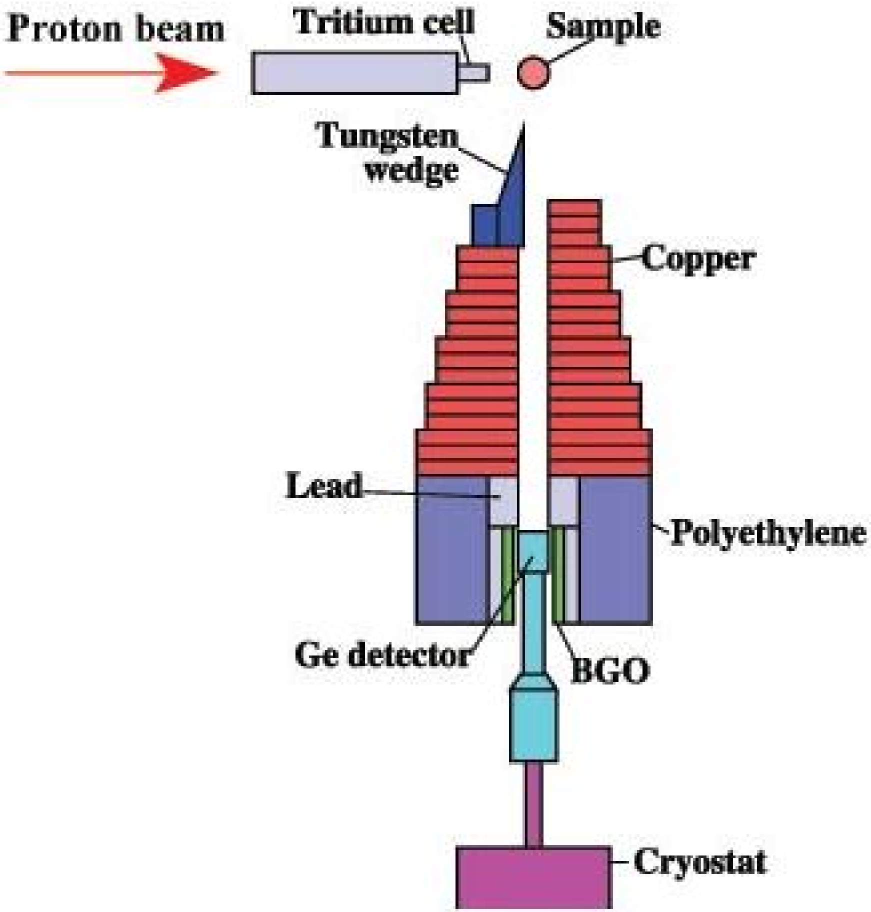

Angular distributions: J , δ, τ

Excitation function: level scheme, J

γγ-coincidence experiments at the Osiris spectrometer, Cologne

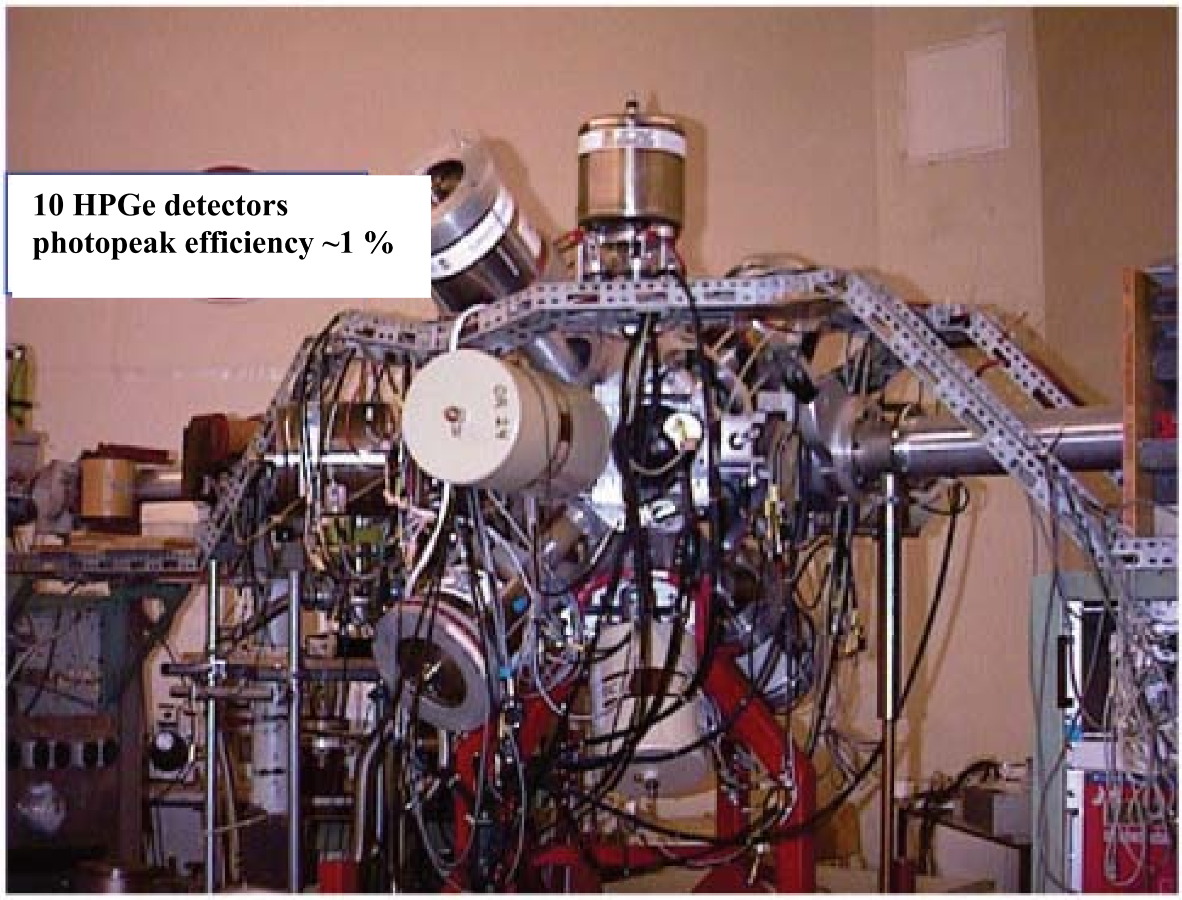

Observables

γ energies

branching ratios

multiple mixing ratios

effective lifetimes (Döppler shifts from in-beam experiments)

New HORUS spectrometer, Cologne

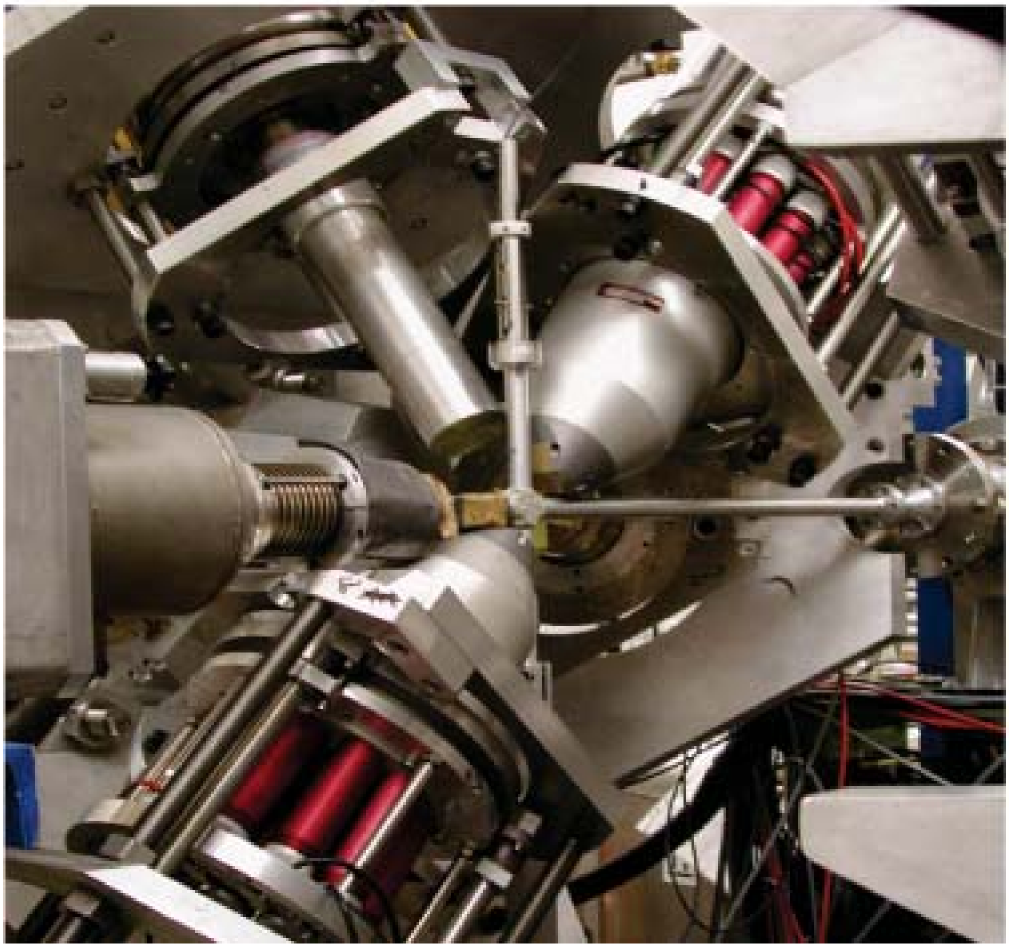

HORUS γγ coincidence

first experiments with the new HORUS spectrometer

- 9 HPGe detectors, 4 with anti-Compton shields
- 1 EUROBALL cluster detector
- Photopeak efficiency: about 2 %
- Up to 14 HPGe detectors can be mounted

γ-ray spectra of ^{94}Mo from different experiments

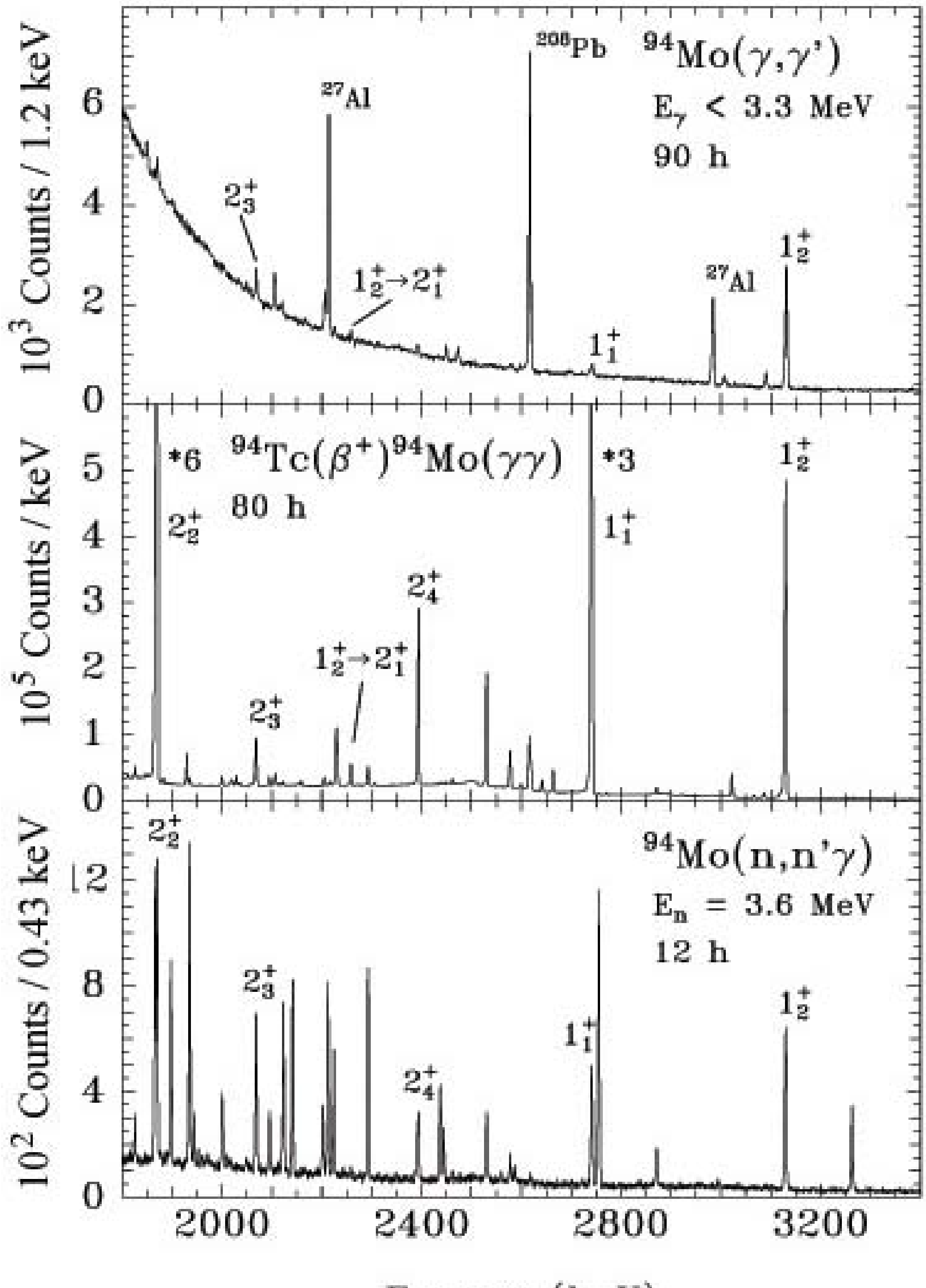

Lifetime determination from Döppler shifts

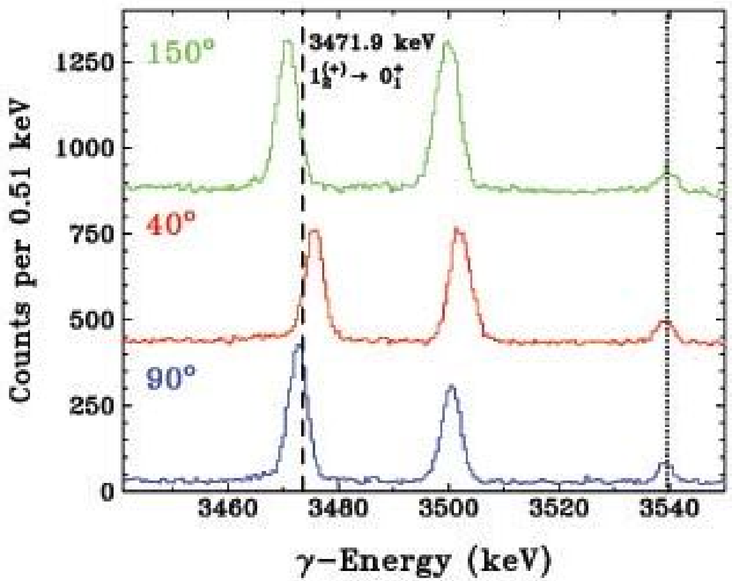

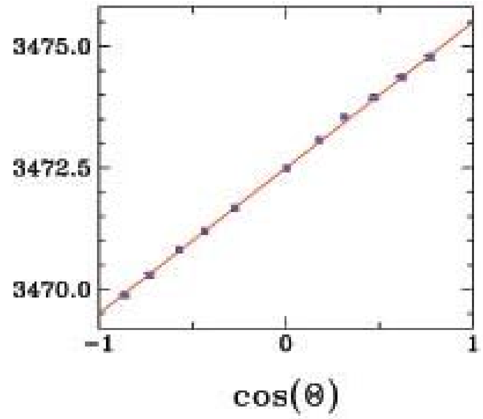

F(τ) = 0.884(6)
τ = 7.6(9) fs

$$E_\gamma(\theta) = E_0 \left(1 + F(\tau)\frac{v_{\rm cm}}{c}\right) \cos\theta$$

$F(\tau)$ Doppler shift attenuation factor
θ emission angle relative to the incident beam

One-phonon 2_1^+ metastable state

$^{94}Mo(n, n'\gamma)$

2_3^+

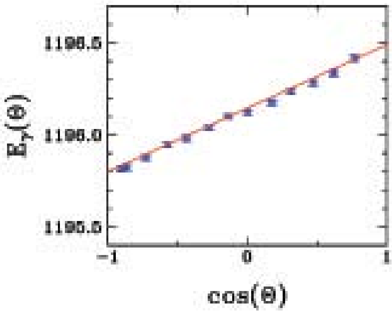

→ **τ = 50.8(43) fs**

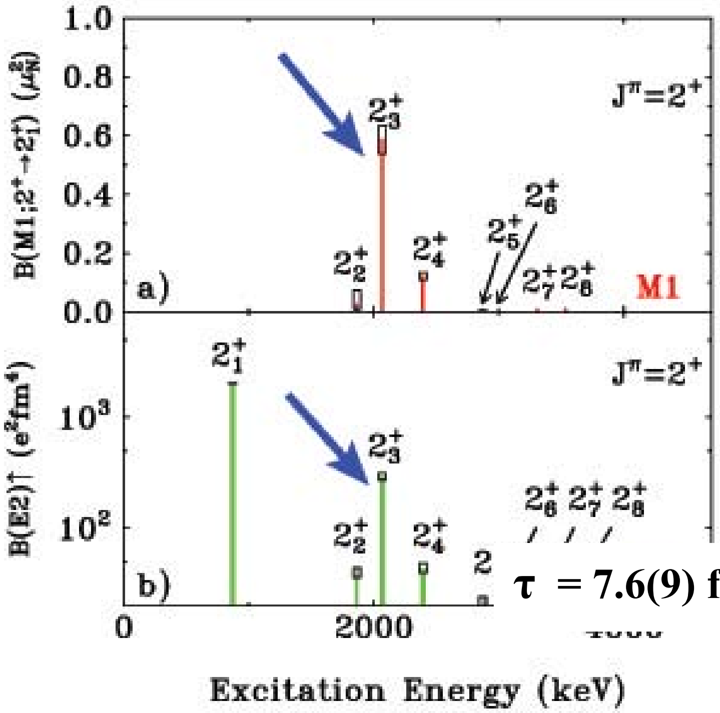

τ = 7.6(9) fs

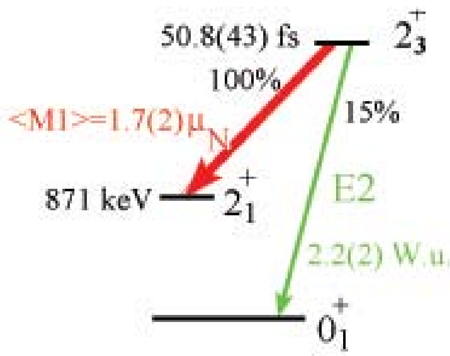

→ 2_3^+ identified as one-phonon metastable state

Statistical Analyses

Evaluation of Discrepant Data I

D. MacMahon

NPL, UK

E-mail: desmond.macmahon@npl.co.uk

Evaluation of Discrepant Data, I

Desmond MacMahon
National Physical Laboratory
Teddington, United Kingdom

Evaluation of Discrepant Data

- What is the half-life of ^{137}Cs?

- Look at the published data from experimental measurements

- For greater detail: T. D. MacMahon, A. Pearce, P. Harris, Convergence of Techniques for the Evaluation of Discrepant Data, Appl. Radiat. Isot. **60** (2004) 275-281

Measured Half-lives of Cs-137

Authors	Measured half-lives in days $t_{1/2}$	σ
Wiles & Tomlinson (1955a)	9715	146
Brown et al. (1955)	10957	146
Farrar et al. (1961)	11103	146
Fleishman et al. (1962)	10994	256
Gorbics et al. (1963)	10840	18
Rider et al. (1963)	10665	110
Lewis et al. (1965)	11220	47
Flynn et al. (1965)	10921	183
Flynn et al. (1965)	11286	256
Harbottle (1970)	11191	157
Emery et al. (1972)	11023	37
Dietz & Pachucki (1973)	11020.8	4.1
Corbett (1973)	11034	29
Gries & Steyn (1978)	10906	33
Houtermans et al. (1980)	11009	11
Martin & Taylor (1980)	10967.8	4.5
Gostely (1992)	10940.8	6.9
Unterweger (2002)	11018.3	9.5
Schrader (2004)	10970	20

Evaluation of Discrepant Data

- The measured data range from 9715 to 11286 days.
- What value are we going to use for practical applications?
- Simplest procedure is to take the unweighted mean.
- If x_i (for i = 1 to N) are the individual values of the half-life, the unweighted mean (x_u), and associated standard deviation (σ_u) are given by:

Unweighted Mean

$$x_u = \frac{\sum x_i}{N}$$

$$\sigma_u = \sqrt{\frac{\sum (x_i - x_u)^2}{N(N-1)}}$$

Unweighted Mean

- Gives the result: 10936 ± 75 days
- However, the unweighted mean is influenced by outliers in the data, in particular the first low value of 9715 days
- Secondly, the unweighted mean takes no account of different authors making measurements of different precision, so we effectively lose some of the information content of the listed data

Weighted Mean

- We can take into account the authors' quoted uncertainties σ_i, i = 1 to N, by weighting each value, using weights w_i to give the weighted mean, (x_w):

$$w_i = \frac{1}{\sigma_i^2}$$

$$x_w = \frac{\sum x_i w_i}{\sum w_i}$$

Weighted Mean

- Standard deviation of the weighted mean (σ_w) is given by:

$$\sigma_w = \sqrt{\frac{1}{\sum w_i}}$$

- And for the half-life of Cs-137, a value of 10988 ± 3 days results

Weighted Mean

- This result has a small uncertainty, but how reliable is the value?
- How do we know that all the data are consistent?
- We can look at the deviations of the individual data from the mean, compared to their individual uncertainties
- We can define a quantity 'chi-squared'

$$\chi_i^2 = \frac{(x_i - x_w)^2}{\sigma_i^2}$$

Weighted Mean

- We can also define a 'total chi-squared':

$$\chi^2 = \sum_i \chi_i^2$$

- 'Total chi-squared' should be equal to the number of degrees of freedom (i.e., to the number of data points minus one) in an ideal consistent data set

Weighted Mean

- So, we can define a 'reduced chi-squared':

$$\chi_R^2 = \frac{\chi^2}{N-1}$$

- which should be close to unity for a consistent data set.

Weighted Mean

- For the Cs-137 data under consideration, 'reduced chi-squared' is 18.6, indicating significant inconsistencies in the data
- We need to look at the data again
- Can we identify the most discrepant data?

Measured Half-lives of Cs-137

Authors		Measured half-lives in days	
		$t_{1/2}$	σ
Wiles & Tomlinson (1955a)		**9715**	**146**
Brown et al. (1955)		10957	146
Farrar et al. (1961)		11103	146
Fleishman et al. (1962)		10994	256
Gorbics et al. (1963)		10840	18
Rider et al. (1963)		10665	110
Lewis et al. (1965)		11220	47
Flynn et al. (1965)		10921	183
Flynn et al. (1965)		11286	256
Harbottle (1970)		11191	157
Emery et al. (1972)		11023	37
Dietz & Pachucki (1973)		11020.8	4.1
Corbett (1973)		11034	29
Gries & Steyn (1978)		10906	33
Houtermans et al. (1980)		11009	11
Martin & Taylor (1980)		10967.8	4.5
Gostely (1992)		10940.8	6.9
Unterweger (2002)		11018.3	9.5
Schrader (2004)		10970	20

Weighted Mean

- Highlighted values are the more discrepant
- Their values are far from the mean and their uncertainties are small
- In cases such as the Cs-137 half-life, the uncertainty (σ_w) ascribed to the weighted mean is far too small
- One way of taking into account the inconsistencies is to multiply the uncertainty of the weighted mean by the Birge ratio:

Weighted Mean

- Birge Ratio:

$$\sqrt{\frac{\chi^2}{N-1}} = \sqrt{\chi_R^2}$$

- This approach would increase the uncertainty of the weighted mean from 3 days to 13 for Cs-137, which would be more realistic.

Limitation of Relative Statistical Weights (LRSW)

- This procedure has been adopted by the IAEA in the Coordinated Research Programme on X-ray and gamma-ray standards
- A Relative Statistical Weight is defined as $\dfrac{w_i}{\sum w_i}$
- If the most precise value in a data set (value with the smallest uncertainty) has a relative weight greater than 0.5, the uncertainty is increased until the relative weight of this particular value has dropped to 0.5.

Limitation of Relative Statistical Weights (LRSW)

- Avoids any single value having too much influence in determining the weighted mean, although for Cs-137 there is no such value
- LRSW procedure compares the unweighted mean with the new weighted mean; if they overlap, i.e.,

$$\left| x_u - x_w \right| \quad \leq \quad \sigma_u + \sigma_w$$

the weighted mean is the adopted value

Limitation of Relative Statistical Weights (LRSW)

- If the weighted mean and the unweighted mean do not overlap, the data are inconsistent, and the unweighted mean is adopted
- Whichever mean is adopted, the associated uncertainty is increased if necessary, to cover the most precise value in the data set

Limitation of Relative Statistical Weights (LRSW)

- Cs-137 half-life:
- Unweighted Mean is 10936 ± 75 days
- Weighted Mean is 10988 ± 3 days
- These two means do overlap, so the weighted mean is adopted
- Most precise value in the data set is that of Dietz and Pachucki (1973) of 11020.8 ± 4.1 days
- Therefore, the uncertainty in the weighted mean is increased to 33 days to give 10988 ± 33 days

Median

- Individual values in a data set are listed in order of magnitude
- If there is an odd number of values, the middle value is the median
- If there is an even number of values, the median is the average of the two middle values
- Median has the advantage that this approach is very insensitive to outliers
- See also: J. W. Müller, Possible Advantages of a Robust Evaluation of Comparisons, J. Res. Nat. Inst. Stand. Technol. **105** (2000) 551-555; Erratum, *ibid.*, **105** (2000) 781.

Median

- We now need some way of attributing an uncertainty to the median
- First we have to determine the quantity 'median of the absolute deviations' or 'MAD'

$$MAD \quad = \quad med\ \{\left| x_i - \tilde{m} \right|\} \quad for\ i = 1, 2, 3 \,.....\, N$$

where $\tilde{m}$ *is the median value*

Median

- Uncertainty in the median can be expressed as:

$$\frac{1.9 \times MAD}{\sqrt{(N-1)}}$$

Median

- Median is 10970 ± 23 days for the Cs-137 half-life data presented
- As for the unweighted mean, the median does not use the uncertainties assigned by the authors, so again some information is lost
- However, the median is much less influenced by outliers than is the unweighted mean

Evaluation of Discrepant Data

- In summary, we have:

◆ Unweighted Mean:	10936 ± 75 days
◆ Weighted Mean:	10988 ± 3 days
◆ LRSW:	10988 ± 33 days
◆ Median:	10970 ± 23 days

Statistical Analyses:

Evaluation of Discrepant Data, II

D. MacMahon

NPL, UK

E-mail: desmond.macmahon@npl.co.uk

Evaluation of Discrepant Data, II

Desmond MacMahon
National Physical Laboratory
Teddington, United Kingdom

Evaluation of Discrepant Data

Cs-137 half-life:

- Unweighted Mean: 10936 ± 75 days
- Unweighted mean can be influenced by outliers and has a large uncertainty
- Weighted Mean: 10988 ± 3 days
- Weighted mean has an unrealistically low uncertainty due to the high quoted precision of one or two measurements; value of ‘chi-squared’ is very high, indicating inconsistencies in the data

Evaluation of Discrepant Data

Cs-137 half-life:

- LRSW: 10988 ± 33 days
- Limitation of Relative Statistical Weights has not increased the uncertainty of any value in the case of Cs-137, but has increased the overall uncertainty to include the most precise value
- Median: 10970 ± 23 days
- Median is not influenced by outliers, nor by particularly precise values; however, this approach ignores all the uncertainty information supplied with the measurements

Evaluation of Discrepant Data

- There are two other statistical procedures which attempt to:

  (i) identify the more discrepant data, and

  (ii) decrease the influence of these data by increasing their uncertainties
- These procedures are known as the Normalised Residuals technique and the Rajeval technique
- See also: M.U. Rajput, T. D. MacMahon, Techniques for Evaluating Discrepant Data, Nucl. Instrum. Meth. Phys. Res., **A312** (1992) 289-295.

Evaluation of Discrepant Data

- Normalised Residuals technique:

  A normalised residual for each value in a data set is defined as follows:

$$R_i = \sqrt{\frac{w_i\, W}{(W - w_i)}} \times (x_i - x_w)$$

$$where \quad x_w = \frac{\sum x_i\ w_i}{W}; \quad w_i = \frac{1}{\sigma_i^2}; \quad W = \sum w_i$$

Evaluation of Discrepant Data

- A limiting value (R_0) of the normalised residual for a set of N values is defined as:

$$R_0 = \sqrt{1.8 \ln N + 2.6} \quad for \quad 2 \le N \le 100$$

- If any value in the data set has $|R_i| > R_0$, the weight of the value with the largest R_i is reduced until the normalised residual is reduced to R_0
- This procedure is repeated until no normalised residual is greater than R_0

Evaluation of Discrepant Data

- Weighted mean is then re-calculated with the adjusted weight
- Result of applying this method to the Cs-137 data is shown in the next table, which shows only those values whose uncertainties have been adjusted

Author	Half-life (days)	Original Uncertainty	R_i **$R_0 = 2.8$**	Adjusted Uncertainty
Wiles 1955	9715	146	- 8.7	453
Gorbics 1963	10840	18	- 8.3	52
Rider 1963	10665	110	- 2.9	114
Lewis 1965	11220	47	4.9	88
Dietz 1973	11020.8	4.1	10.1	18.4
Martin 1980	10967.8	4.5	- 5.4	8.7
Gostely 1992	10940.8	6.9	- 7.4	16.4
Unterweger 2002	11018.3	9.5	3.3	15.5
New Weighted Mean	**10985**	**10**		

Rajeval Technique

- This technique is similar to the normalised residuals technique: only inflate the uncertainties of the more discrepant data, although a different statistical recipe is used
- Also has a preliminary population test which allows the rejection of highly discrepant data
- Normally makes more adjustments than the normalised residuals method, but the outcomes are usually very similar

Rajeval Technique

Initial Population Test:

outliers in the data set are detected by calculating the quantity y_i:

$$y_i = \frac{x_i - x_{ui}}{\sqrt{\sigma_i^2 + \sigma_{ui}^2}}$$

where x_{ui} is the unweighted mean of the whole data set excluding x_i, and σ_{ui} is the standard deviation associated with x_{ui}

Rajeval Technique

- Critical value of $|y_i|$ at 5% significance is 1.96
- At this stage, only values with $|y_i| > 3 \times 1.96 = 5.88$ are rejected
- Cs-137 half-life data: only the first value of 9715 ± 146 days is rejected, with a value of $|y_i| = 8.61$

Rajeval Technique

Standardised deviates Z_i are calculated in the next stage of the procedure

$$Z_i = \frac{x_i - x_w}{\sqrt{\sigma_i^2 - \sigma_w^2}} \quad where \quad \sigma_w = \sqrt{\frac{1}{W}}$$

Rajeval Technique

Probability integral for each Z_i

$$P(Z) \quad = \quad \int_{-\infty}^{Z} \frac{1}{\sqrt{2\pi}} \exp\left(\frac{-t^2}{2}\right) dt$$

is determined.

Rajeval Technique

- Absolute difference between P(Z) and 0.5 is a measure of the 'central deviation' (CD)
- Critical value of the central deviation (cv) can be determined by the expression:

$$cv \quad = \quad \left[(0.5)^{\frac{N}{N-1}} \right] \quad for\ N > 1$$

Rajeval Technique

If the central deviation (CD) of any value is greater than the critical value (cv), that value is regarded as discrepant, and the uncertainties of the discrepant values are adjusted to

$$\sigma_i' = \sqrt{\sigma_i^2 + \sigma_w^2}$$

Rajeval Technique

- An iteration procedure is adopted in which σ_w is recalculated each time and added in quadrature to the uncertainties of those values with CD > cv
- Iteration process is terminated when all CD < cv
- Cs-137 half-life data: one value is rejected by the initial population test, and 8 of the remaining 18 values have their uncertainties adjusted as shown in the next table

Author	Half-life (days)	Original Uncertainty	CD **cv = 0.480**	Adjusted Uncertainty
Gorbics 1963	10840	18	0.500	74
Rider 1963	10665	110	0.498	159
Lewis 1965	11220	47	0.500	125
Dietz 1973	11020.8	4.1	0.500	28
Corbett 1973	11034	29	0.443	34
Houtermans 1980	11009	11	0.473	22
Gostely 1992	10940.8	6.9	0.500	15
Unterweger 2002	11018.3	9.5	0.499	27
New Weighted Mean	**10970**	**4**		

Rajeval Technique

Compare Rajeval technique table with that for the Normalised Residuals technique; differences are seen to be:

1. Rajeval technique has rejected the Wiles and Tomlinson value

2. Normally the Rajeval technique makes larger adjustments to the uncertainties of discrepant data than does the Normalised Residuals technique, and has a lower final uncertainty

Evaluation of Discrepant Data

- We now have 6 methods of extracting a half-life from the measured data:

Evaluation Method	Half-life (days)	Uncertainty
Unweighted Mean	10936	75
Weighted Mean	10988	3
LRSW	10988	33
Median	10970	23
Normalised Residuals	10985	10
Rajeval	10970	4

Evaluation of Discrepant Data

- Already pointed out that the unweighted mean can be influenced by outliers, and therefore is to be avoided if possible.

- Weighted mean can be heavily influenced by discrepant data that have small quoted uncertainties, and would only be acceptable if the reduced chi-squared is small, i.e., close to unity. This criterion is certainly not the case for Cs-137 half-life, with a reduced chi-squared of 18.6

Evaluation of Discrepant Data

- Limitation of Relative Statistical Weights (LRSW) for Cs-137 half-life data still chooses the weighted mean, but inflates the associated uncertainty to cover the most precise value
- Therefore, both the LRSW value and associated uncertainty are heavily influenced by the most precise value of Dietz and Pachucki, which is identified as the most discrepant value in the data set by the Normalised Residuals and Rajeval techniques

Evaluation of Discrepant Data

- Median is a more reliable estimator - very insensitive to outliers and to discrepant data
- However, by not using the experimental uncertainties, the median approach is not making use of all the information available
- Normalised Residuals and Rajeval techniques have been developed to address the problems of other techniques and to maximise the use of all the experimental information available

Evaluation of Discrepant Data

- Normalised Residuals and Rajeval techniques use different statistical methods to reach the same objective: to identify discrepant data and to increase the uncertainties of such data to reduce their influence on the final weighted mean
- Author's opinion: best value for the half-life of Cs-137 would be that obtained by taking the mean of the Normalised Residuals and Rajeval values, together with the larger of the two uncertainties

Evaluation of Discrepant Data

Adopted half-life of Cs-137 would be

10977 ± 10 days

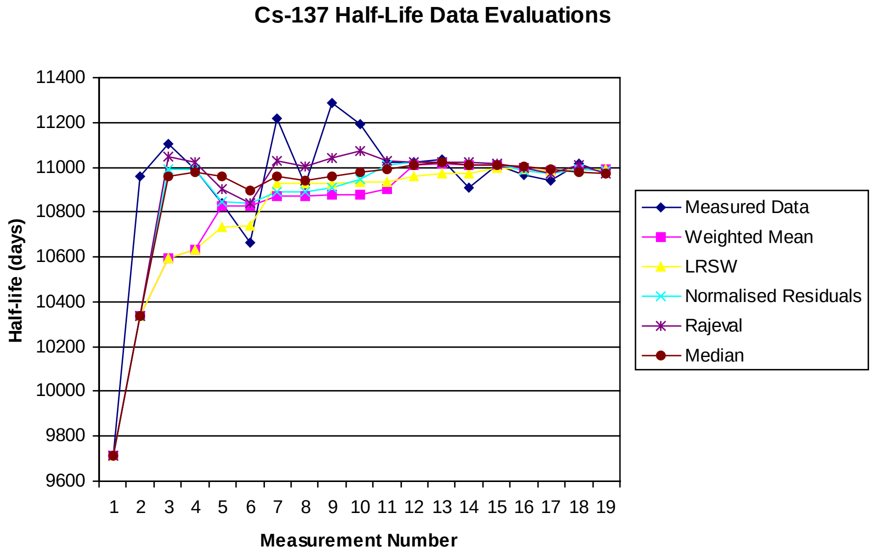

Evaluation of Discrepant Data

- ◆ The previous figure shows how the evaluation techniques behave as each new data point is added to the data set
- ◆ Left-hand portion of the plot shows that the weighted mean and LRSW values take much longer to recover from the first low and discrepant value than do the other techniques

Evaluation of Discrepant Data

- ◆ Next figure shows an expanded version of the second half of the previous figure, revealing in more detail how the different techniques behave as the number of data points reaches 19
- ◆ Taking into account the 19th point, the overall spread in the evaluation techniques is only 18 days or 0.16%

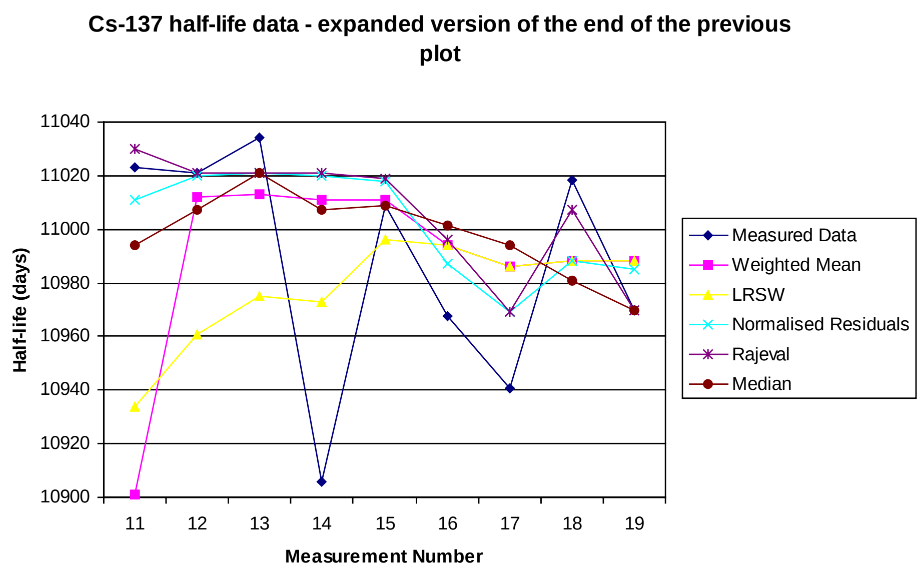

15 March 2005

DRAFT

Evaluation of Decay Data: Relevant IAEA Co-ordinated Research Projects

A. L. Nichols

International Atomic Energy Agency, Nuclear Data Section
Division of Physical and Chemical Sciences
Department of Nuclear Sciences and Applications
Wagramerstrasse 5, PO Box 100
A-1400 Vienna, Austria.

Presented to IAEA-ICTP Workshop on Nuclear Structure and Decay Data: Theory and Evaluation, 4 April 2005

Summary

Specific IAEA Co-ordinated Research Projects (CRPs) have been directed towards the generation of recommended high-quality decay data for a number of important applications. Decay-scheme data for specific radionuclides have required study and evaluation through an agreed set of procedures. The role of the IAEA Nuclear Data Section in creating these dedicated data files is described, and both the objectives and resulting decay data from these most relevant CRPs are also reviewed.

1. Introduction

Two primary aims of the IAEA Nuclear Data Section (NDS) are to develop and disseminate atomic and nuclear data in forms appropriate for a wide range of applications [1], as requested by IAEA Member States. Hence, NDS staff prepare and maintain a significant number of databases, including atomic and molecular data for fusion energy and plasma research that are accessible through a separate server [2]. NDS staff are also involved in technology transfer activities to assist scientists of developing countries in their use of these atomic and nuclear databases.

Data development within the NDS is conducted mainly through Co-ordinated Research Projects (CRPs). Usually these projects result in the production of a new (or significant upgrades of an existing) database; typically 5-12 scientific groups from different countries work together under IAEA contracts or agreements over a period of 3-4 years, maintaining contact throughout the course of the CRP. Examples of recent CRPs sponsored and organised by the NDS are listed in Table 1.

Following a brief description of the IAEA-NDS and how to gain access to their facilities and databases, the contents of this paper focus on those CRPs devoted over the previous 30 years to improving the recommended decay data used in both energy- and non-energy-based applications. Specific decay-data requirements were identified by users and consultants, and a suitable evaluation procedure was adopted to achieve the desired objectives. The reader should be warned that the decay data recommended by the CRP on X-ray and Gamma-ray Standards for Detector Calibration (1986-90) in 1991 will soon be

Table 1. Recent IAEA-NDS Co-ordinated Research Projects (CRPs).

Short Title	Duration	No. of Participants
Update of X-ray and Gamma-ray Decay Data Standards for Detector Calibration and Other Applications	1998-2002	11
RIPL-II: Input Parameter Testing	1998-2002	8
Prompt Gamma Activation Analysis	1999-2003	10
Standard Cross Sections	2002-06	9
RIPL-III: Parameters for Nuclear Reaction Applications – Non-energy Applications	2002-06	11
Nuclear Data for Th-U Fuel Cycle	2003-07	9
Cross Sections for Production of Therapeutic Radionuclides	2003-07	8
Updated Decay Data Library for Actinides	2005-09	approved
Reference Database for Ion Beam Analysis	2005-09	approved
Reference Database for Neutron Activation Analysis	2005-07 (?)	approved
Minor Actinide Neutron Reaction Data	2007-11 (?)	

replaced with a completely new set of recommended decay data at the conclusion of a recent CRP dedicated to the improvement and extension of this important database (see Section 4).

1.1 Nuclear data

Nuclear data are commonly categorized in terms of two main groups:

- **Nuclear reaction data:** Encompasses cross sections, angular and energy distributions of secondary particles, resonance parameters and related quantities. These libraries are complete for neutron-induced reactions up to 20 MeV; however, coverage at higher energies is less comprehensive. Although few evaluations exist for photonuclear and charged-particle induced reactions, some selected experimental data have been compiled in EXFOR.
- **Nuclear structure and decay data:** Atomic masses, half-lives, decay schemes, nuclear level properties, and energies and intensities of emitted particles and γ rays are included in these data. The major database is ENSDF, while related bibliographic data are contained in NSR. There are many other nuclear structure and decay data libraries, mostly derived from or related to ENSDF and including the *Table of Isotopes* [3], *Isotope Explorer* [4] and NUBASE [5].

The type of information given for both groupings can also be classified on the basis of bibliographic detail, experimental data and evaluated data.

- **Bibliographic data:** References with some description of the contents, but no numerical data. Examples are CINDA (Computer Index of Neutron Data) and NSR (Nuclear Science References).
- **Experimental data:** Results of individual measurements as reported by the authors. The most important example of a compiled library of experimental nuclear reaction data is EXFOR/CSISRS.
- **Evaluated data:** Recommended values are based on all available data from experiments and/or theory, derived from a critical analysis of the experimental data and their uncertainties, inter- and extrapolation, and/or nuclear model calculations. The resulting libraries are assembled in strictly defined formats such as ENDF-6

(international format for evaluated nuclear reaction data) or ENSDF (format of the Evaluated Nuclear Structure Data File). The main cross-section libraries in ENDF format also contain the relevant decay data needed in their main application(s).

1.2 Nuclear data centre networks

Both the collection and distribution of nuclear data are organised worldwide. Two international networks are coordinated by the IAEA to collect and distribute nuclear data (Table 2):

- Network of Nuclear Reaction Data Centres [6],
- Nuclear Structure and Decay Data Evaluators' Network [7].

The data centres participating in these nuclear data networks are involved in the various stages of data preparation between measurement and application (i.e., compilation, review, evaluation, processing and distribution).

Specialized data centres cooperate with the major centres in the various functions (particularly data compilation and evaluation). This sharing of the work on a worldwide basis is normally defined by their geographical location and data expertise, and is coordinated by the IAEA Nuclear Data Section.

Table 2. Nuclear Data Networks.

Nuclear Reaction Data Centres Network	Nuclear Structure and Decay Data Evaluators' Network
IAEA Nuclear Data Section, Vienna, Austria	**IAEA Nuclear Data Section,** Vienna, Austria
OECD, NEA Data Bank, Paris, France	**US National Nuclear Data Center,** Brookhaven, USA (maintains Master database)
US National Nuclear Data Center, Brookhaven, USA	**13 data evaluation centres:** Belgium, Canada, PRChina, France, Japan, Kuwait, the Netherlands, Russian Federation, UK and USA
Russian Federation Nuclear Data Centre, Obninsk, Russian Federation	**Data dissemination centres:** France, Sweden, USA, IAEA and OECD-NEA
9 co-operating specialised centres: PRChina, Hungary, Japan, Republic of Korea, Russian Federation and Ukraine	

1.3 Access to IAEA-NDS data libraries

The IAEA Nuclear Data Section holds a total of about 100 nuclear data libraries, representing enormous economic and scientific value. All libraries and the related documentation are available free of charge to scientists in IAEA Member States. An overview is given in the document *Index of Nuclear Data Libraries available from the* IAEA *Nuclear Data Section* [8], and brief descriptions of the contents and/or format of most libraries are published in the IAEA-NDS-report series [9].

The main method of distributing numerical nuclear data in the early 21st century is via the Internet, and therefore the IAEA Nuclear Data Section offers a variety of such electronic services. At the same time, conventional mail services have been maintained for the convenience of users with their varying needs and technical infrastructures (ie., sending customized retrievals or complete libraries as hardcopy, magnetic tape, CD-ROM and diskettes, as well as by e-mail). Users are also kept up to date about new data libraries and other developments through the *IAEA Nuclear Data Newsletter* [10].

- **Worldwide Web (WWW)**: The web page of IAEA Nuclear Data Services can be found at the web addresses (URL) *http://www-nds.iaea.org* (IAEA Vienna, Austria), *hhtp://www-nds.indcentre.org.in* (BARC, India), and *http://www-nds.ipen.br* (IPEN, Brazil). This page contains interactive access to the major databases as well as an overview of all nuclear data libraries and databases available from the IAEA *(IAEA Nuclear Data Guide)*, access to various reports, documents and manuals, nuclear data utility programs, and the *IAEA Nuclear Data Newsletter*.

- **Secure FTP:** IAEA Nuclear Data Section keeps several accounts for file transfers requiring no password (all accessible by the IP address *ndsalpha.iaea.org* using a secure client, such as sftp, scp, pscp or WinSCP3): ANONYMOUS contains several complete libraries, utility codes and documents for public use; FENDL2 and RIPL permit access to the respective data libraries; NDSOPEN is used for bilateral file exchange.

Hardcopy documents published by NDS include handbooks, research and meeting reports (INDC report series), data library documents (IAEA-NDS report series), and the *IAEA Nuclear Data Newsletter*. Most new reports are available electronically on the WWW in PDF format. NDS staff can be contacted by e-mail to request hardcopy documents, and other mail services and nuclear data related information [11].

1.4 Technology transfer

Technology transfer to developing countries is carried out in several ways by the NDS:

- Technical co-operation projects to provides online nuclear data services to countries with insufficient Internet connections to the NDS through the installation of mirror servers in Brazil and India.

- Nuclear data workshops are organized on a regular basis, and are usually held at the Abdus Salam International Centre for Theoretical Physics in Trieste, Italy. Regular topics have included “Nuclear Reaction Data and Nuclear Reactors: Physics, Design and Safety” (held every even year) and “Nuclear Data for Science and Technology” (held every odd year, with extensive changes in their content (varying from medical physics to materials analysis)). More appropriately, over the previous 3 years, a combination of IAEA and IAEA-ICTP workshops have been dedicated to Nuclear Structure and Decay Data: Theory and Evaluation.

2. Co-ordinated Research Project: Decay Data for the Transactinium Nuclides (IAEA Technical Reports Series No. 261, 1986)

Transactinium nuclides are important in the nuclear fuel cycles of both thermal and fast reactors, and have found increasing application in other fields. The IAEA convened an Advisory Group Meeting on Transactinium Isotope Nuclear Data (TND) at the Kernforschungszentrum Karlsruhe in 1975 [12]. Users and measurers were brought together to review the status and requirements of the nuclear data for transactinium nuclides relevant to fission reactor research and technology. One of the areas specifically addressed at this meeting was the status of the decay data for these nuclides; participants recommended that the IAEA implement a Co-ordinated Research Project to review, measure and evaluate the required transactinium decay data. Five groups experienced in decay data measurements agreed to participate in the work of this CRP, and met for the first time at IAEA, Vienna in 1978 [13]. Subsequent CRP meetings were held annually up to 1984 [14-19], in conjunction with two further IAEA Advisory Group Meetings in 1979 and 1984 [20, 21].

2.1 Actinide and transactinium nuclides

The accuracies requested for many of the data were quite high, especially the γ-ray emission probabilities that presented challenging experimental problems. Nevertheless, during the seven years of the CRP, some of these problems were solved, and a considerable amount of data was produced with the required accuracy (at least for the prominent transitions of most interest to the user). The work of the CRP not only helped improve the existing capabilities of the participating laboratories, but also encouraged the development of such capabilities at other laboratories. Together with the systematic production of highly accurately measured decay data, this interaction between laboratories represented one of the more significant long-term effects of the work.

CRP participants established the following guidelines for the assignment of uncertainties:

- total uncertainty to be based on 1σ random error plus one-third the linear sum of the systematic errors based on a statistical confidence-level of 68.3%;
- an uncertainty assigned to a mean value should not be smaller than the smallest uncertainty of the values used to calculate the mean;
- for those nuclides that are sufficiently long lived that their half-lives cannot simply be determined by following their decay, the half-lives are generally determined through the measurement of two quantities: number of atoms in the sample and sample activity; since the CRP participants believe that both these quantities cannot be determined reliably with accuracies better than 0.1%, they assigned a minimum uncertainty of 0.1% to these resulting half-lives.

2.2 Recommended transactinium decay data, 1985/86

The CRP highlighted a significant number of data requirements and succeeded in satisfying many of them. Examples of the recommended decay data and their literature sources are given in Appendix A. Improvements have subsequently been made in the quality of specific decay data for the transactinium nuclides, although several of the identified decay data needs remained unsatisfied.

The CRP accomplished a number of goals:

(a) Evaluated the accuracy requirements for decay data requested by users at the Advisory Group Meetings, and grouped them into three general categories:
   (i) those satisfied by available data;
   (ii) those which lie beyond the capabilities of measurement techniques (of 1985/6);
   (iii) those not satisfied, but are achievable with existing experimental capabilities.
(b) Assessed the status of the existing data in the light of these requirements, and maintained an awareness of new measurements.
(c) Identified and co-ordinated the measurement expertise in order to acquire the required data.
(d) Prepared a report that presented a critical evaluation of the data and summarized their status (IAEA Technical Reports Series No. 261, IAEA Vienna, Austria, 1986).

Table 3. Transactinium Isotope Decay Data: Requirements, Status and CRP Activities.

AEEW – UKAEA Atomic Energy Establishment, Winfrith, UK;
AERE – UKAEA Atomic Energy Research Establishment, Harwell, UK;
CBNM – CEC Central Bureau for Nuclear Measurements, Geel, Belgium;
INEL – Idaho National Engineering Laboratory, Idaho Falls, USA;
JAERI – Japan Atomic Energy Research Institute, Tokai-Mura, Japan;
LMRI – CEA Laboratoire de Métrologie des Rayonnements Ionisants, Saclay, France.

The label "+" refers to measurements or evaluations performed by laboratories that have contributed indirectly to the IAEA Co-ordinated Research Project.

Nuclide	Data type	Accuracy (%) (a) Required	Achieved	Needs	CRP activities Measurements	Evaluations	Comments
Th-228	$T_{1/2}$	1	0.1	Decay chain calculations (includes daughters)	–	CBNM	
	P_γ	2 (b)	2–5		CBNM, INEL	CBNM, LMRI	
Th-229	$T_{1/2}$	1	2	Mass determination in U-233 chain	–	–	CRP participants believe that the achieved accuracy of the half-life is adequate
	P_γ	2 (b)	1–3		INEL, +	INEL	
Th-230	$T_{1/2}$	1	0.4	Marine dating	+	+	
Th-232	$T_{1/2}$	not requested	0.4	Includes daughters	–	+	
	P_γ	not requested			–		
Th-233	$T_{1/2}$	1	0.5	Thorium cycle-decay heat	–	–	P_β and P_γ requirements are not satisfied. AERE measurement of P_γ planned
	P_β	2	unknown		–	–	
	P_γ	2	unknown		AERE	–	
Pa-231	$T_{1/2}$	1	0.3	Non-destructive assay	–	–	
	P_α	2	2–7		–	AEEW	
	P_γ	2	2–5		AERE	AEEW	
Pa-233	$T_{1/2}$	1	0.4	Decay heat and mass determination	–	–	
	P_β	2	unknown		–	–	Requirement for P_β is not satisfied
	P_γ	2	1		AERE, CBNM, INEL	INEL	
U-232	$T_{1/2}$	1	0.7	Shielding calculations (includes daughters)	AERE, +	+	$T_{1/2}$ requires confirmation. AERE measurement is planned
	P_α	2	1		–	–	
	P_γ	2	1–2		AERE, CBNM, INEL, +	CBNM	

Table 3 (cont.)

Nuclide	Data type	Accuracy (%) (a) Required	Achieved	Needs	CRP activities Measurements	Evaluations	Comments
U-233	$T_{1/2}$	0.5	0.1		+	+	
	$T_{1/2}$ (SF)	not requested		Thorium fuel cycle	+	–	
	P_α	2	1–2	and environmental	+	INEL	
	P_γ	2	1–2	studies	AERE, INEL	INEL	AERE measurement planned
	P_X (d)	5	unknown		–	–	P_X requirement not satisfied
U-234	$T_{1/2}$	0.3	0.1		+	AEEW	
	$T_{1/2}$ (SF)	not requested		Mass determination	+	–	
	P_α	1	0.03–1	and non-destructive	CBNM, JAERI, +	AEEW	
	P_γ	2	1–2	assay	CBNM	AEEW	
U-235	$T_{1/2}$	0.5	0.1		–	+	
	$T_{1/2}$ (SF)	not requested		Mass determination	+	–	The required accuracy of 3% for P_α is unlikely to be achieved
	P_α	3	5–12	and non-destructive	–	–	
	P_γ	1	1	assay	AERE, CBNM, INEL, +	CBNM	
U-236	$T_{1/2}$	1	0.1		–	+	
	$T_{1/2}$ (SF)	not requested	3	Mass determination	+	–	
	P_α	3	5–15	and non-destructive	–	–	P_α and P_γ requirements are not satisfied
	P_γ	3	10	assay	–	–	
U-237	P_γ	1	2–3	Non-destructive assay of Pu	AERE, INEL	LMRI	AERE measurement of P_γ in progress
U-238	$T_{1/2}$	1	0.1	Mass determination	–	+	Required accuracies for P_α, P_γ and P_X are unlikely to be achieved.
	$T_{1/2}$ (SF)	2	1.2	and non-destructive	+	+	
	P_α	3	5–20	assay; $T_{1/2}$ (SF) for	–	–	
	P_γ	3	13	geochronology;	AERE, +	–	AERE measurement of P_γ planned
	P_X (d)	3	unknown	P_X for environmental studies	–	–	
U-239	$T_{1/2}$	1	0.2		–	AEEW	
	P_β	2	2–20	Decay heat	+	AEEW	P_β requirement is not satisfied
	P_γ	2	2		+	AEEW	
Np-236	$T_{1/2}$	5	10		+	–	$T_{1/2}$ and P_β requirements not satisfied
	Branching ratio	5	2	U-232 production	–	–	
	P_β	2	unknown		–	–	
	P_γ	2	2		–	–	
Np-236m	$T_{1/2}$	5	2		–	–	
	Branching ratio	5	2	U-232 production	–	–	
Np-237	$T_{1/2}$	0.5	0.5		AERE/CBNM	–	Confirmatory measurement of $T_{1/2}$ is definitely required. New $T_{1/2}$ results are expected from AERE and CBNM in 1985. P_α and P_X requirements are not satisfied. Measurement of P_α is planned by CBNM
	P_α	1	20	Environmental studies	CBNM	–	
	P_γ	1	1–2	and mass	AERE, CBNM, +	INEL	
	P_X (d)	2	unknown	determination			

Table 3 (cont.)

Nuclide	Data type	Accuracy (%) (a) Required	Achieved	Needs	CRP activities Measurements	Evaluations	Comments
Np-238	$T_{1/2}$	2	0.1	Activation analysis of	–	–	
	P_γ	2	5	Np-237 and Am-242m determination	–	–	P_γ requirement is not satisfied
Np-239	$T_{1/2}$	1	0.2	Decay heat and	–	–	
	P_β	2	(c)	detector calibration	–	–	
	P_γ	1	1–2	standard	CBNM, +	CBNM	
Pu-236	$T_{1/2}$	1	3.0		–	+	$T_{1/2}$, P_α and P_γ
	P_α	2	1–3	U-232 production	–	–	requirements are not
	P_γ	3	30		–	–	satisfied
Pu-237	$T_{1/2}$	not requested	0.1		+	CBNM	
	P_X (d)	2	unknown	Environmental studies	–	–	P_X requirement is not satisfied
Pu-238	$T_{1/2}$	0.5	0.3		+	+	
	$T_{1/2}$ (SF)	2	4	Mass determination	–	+	$T_{1/2}$ (SF) requirement is
	P_α	1	<1	and non-destructive	CBNM, +	LMRI	not satisfied.
	P_γ	1	1–2	assay; P_X for detector calibration	CBNM, INEL, LMRI	LMRI	LMRI measurement of P_γ planned
	P_X (d)	2	2–3		–	–	
Pu-239	$T_{1/2}$	0.5	0.1		AERE, CBNM, +	CBNM	
	P_α	1	1–2	Mass determination,	+	JAERI	
	P_γ	1	<1	non-destructive	INEL, LMRI, +	JAERI	
	P_X(d)	3	3	assay and environmental studies	–	–	
Pu-240	$T_{1/2}$	0.5	0.1		+	CBNM/LMRI	
	$T_{1/2}$ (SF)	2	3	Mass determination,	CBNM	+	$T_{1/2}$(SF) requirement is
	P_α	1	1–2	non-destructive assay	+	LMRI	not satisfied.
	P_γ	1	1–2	and environmental	INEL, LMRI	LMRI	P_γ measurement planned
	P_X (d)	3	3	studies; $T_{1/2}$ (SF) for waste management	–	–	by LMRI
Pu-241	$T_{1/2}$	0.5	0.7	Mass determination	AERE, CBNM, +	CBNM	$T_{1/2}$ requirement is not
	$T_{1/2}$ (α)	1	0.8	and non-destructive	CBNM	–	satisfied (measurements in
	P_γ	1	1–2	assay	INEL, +	LMRI	progress)
Pu-242	$T_{1/2}$	1	0.3	Mass determination,	+	+	
	$T_{1/2}$ (SF)	5	1.5	non-destructive assay	–	+	
	P_α	5	<1	and environmental	–	–	
	P_γ	5	2–5	studies	CBNM	–	P_X requirement is not
	P_X (d)	3	unknown		–	–	satisfied
Am-241	$T_{1/2}$	0.2	0.1	Non-destructive assay	–	CBNM	
	P_α	not requested	1–2	and low energy gamma	+	CBNM	
	P_γ	0.5–1	1–10	emission standard.	CBNM, LMRI	CBNM	CBNM measurement of P_γ
	P_X (d)	2	3	0.5% accuracy requested for 59.5 keV gamma emission probability	–	–	in progress. P_X requirement not satisfied

Table 3 (cont.)

Nuclide	Data type	Accuracy (%) (a) Required	Achieved	Needs	CRP activities Measurements	Evaluations	Comments
Am-242	$T_{1/2}$	1	0.1	Cm-244 production and	–	y	
	Branching ratio	1	1	Am mass determination	–	–	
Am-242m	$T_{1/2}$	1	1.4	Cm-244 production	+	AEEW	$T_{1/2}$ requires confirmatory
	Branching ratio	1	0.03	and Am mass determination	–	AEEW	measurement. P_X requirements not satisfied
	P_X (d)	3	unknown		–	–	
Am-243	$T_{1/2}$	1	0.2	Mass determination,	+	CBNM	
	P_α	1	unknown	long term storage and	–	CBNM	P_α, P_γ and P_X
	P_γ	1	2	environmental studies	CBNM, +	CBNM	requirements are not
	P_X(d)	2	unknown		–	–	satisfied
Cm-242	$T_{1/2}$	0.2	0.04		AERE, JAERI, +	JAERI	
	$T_{1/2}$ (SF)	5	2	Non-destructive	JAERI, +	JAERI	
	P_γ	5	4–20	assay	–	–	
Cm-243	$T_{1/2}$	1	0.3		–	+	
	P_α	5	1–3	Non-destructive	–	–	
	P_γ	5	2–10	assay and environ-	–	–	
	P_X(d)	5	unknown	mental studies	–	–	P_X requirement is not satisfied
Cm-244	$T_{1/2}$	1	0.3		–	+	
	$T_{1/2}$ (SF)	3	0.4		–	+	
	P_α	3	<1	Non-destructive assay	+	LMRI	
	P_γ	3	2–10	and environmental	–	LMRI	P_γ requirement is not
	P_X (d)	3	3	studies	–	–	satisfied
Cm-245	$T_{1/2}$	1	1	Long term storage and	+	+	
	P_α	5	0.5–2	environmental studies	–	–	
	P_γ	5	10		–	–	P_γ and P_X requirements
	P_X (d)	5	unknown		–	–	are not satisfied
Cm-246	$T_{1/2}$	1	2	Long term storage and	–	+	$T_{1/2}$, P_α, P_γ and P_X
	P_α	3	1–5	environmental studies	–	–	requirements are not
	P_γ	3	unknown		–	–	satisfied
	P_X (d)	3	unknown		–	–	
Cm-248	$T_{1/2}$	2	1	Long term storage and	–	+	
	P_α	3	<1	environmental studies	–	–	P_γ and P_X requirements
	P_γ	3	unknown		–	–	are not satisfied
	P_X (d)	3	unknown		–	–	
Cf-250	$T_{1/2}$	0.2	0.7	Impurity in Cf-252	–	–	$T_{1/2}$ and $T_{1/2}$ (SF)
	$T_{1/2}$ (SF)	2	4	neutron standard	–	–	requirements are not satisfied
Cf-252	$T_{1/2}$	0.2	0.3	Neutron standard	LMRI	INEL	$T_{1/2}$ requirement is not
	$T_{1/2}$ (SF)	1	0.3		–	+	satisfied; discrepancies exist among measured half-lives

(a) Uncertainties for α, γ and X-ray emission probabilities: required and achieved accuracies apply to the major transitions only.
(b) Listed requirements represent those for the more prominent transitions from all members of the decay chain of these nuclides.
(c) β emission probabilities are inferred from the γ-ray emission probabilities.
(d) P_x refers to L-X-ray emission probabilities.

The CRP participants concluded that, despite the large body of accurate decay data produced by the laboratories up to 1985/86, much remained to be done. A number of the accuracy requirements were not met. The outstanding transactinium decay data requirements have indeed encouraged others to become involved in producing highly accurate data, and plans are currently being made by IAEA-NDS staff to establish a new CRP to re-evaluate these data and update the recommended database (see Section 2.3).

2.3 Future plans – Co-ordinated Research Project: Updated Decay Data Library for Actinides

The previous CRP on actinide decay data addressed the preparation of a database directly, and provided the catalyst for a series of new measurements that continued well into the 1990s. All of this new work and earlier data need to be re-compiled and evaluated to produce an updated set of recommended decay data to replace the current IAEA database (of 1985/86). Thus, the International Nuclear Data Committee (INDC) in their advice to the Nuclear Data Section on nuclear data issues for 2002 and 2004 had noted the need for further improvements to the actinide decay data files for a wide range of applications. Thus, an appropriate CRP will begin in late 2005, with the following aims:

- promotion of actinide decay data research and development;
- evaluation of actinide decay data - proposed actinides and associated decay chains include: ^{226}Ra and daughters (?), ^{232}Th and daughters (?), ^{231}Th, ^{231}Pa, ^{233}Pa, $^{232-237}$U, ^{239}U, ^{237}Np, ^{239}Np, $^{238-242}$Pu, ^{241}Am, ^{242m}Am, ^{243}Am, ^{242}Cm, ^{244}Cm and ^{252}Cf;
- assembly of recommended decay data files for the agreed set of actinides, and all recommended data to be added to the NDS home page.

3. Co-ordinated Research Project: X-ray and Gamma-ray Standards for Detector Calibration (IAEA-TECDOC-619, 1991)

The question of γ-ray detector efficiency calibration arose during the CRP on Transactinium Decay Data (Section 2) when the importance of reputable reference standards became apparent. Although a provisional compilation of calibration data was agreed upon for that work [22], a strong recommendation was made to prepare an internationally-accepted file of X- and γ-ray decay data of nuclides used to calibrate detector efficiencies [21]. Furthermore, the International Nuclear Data Committee (INDC) proposed a preparative meeting with experts associated with the International Committee for Radionuclide Metrology (ICRM) to pursue this aim. An IAEA Consultants' Meeting was held at the Centre d' Etudes Nucléaires de Grenoble in May 1985 to discuss the quality of all relevant data and define a suitable programme to resolve the various issues [23]. As a consequence of these discussions, a CRP on X-ray and Gamma-ray Standards for Detector Calibration was established in 1986 by the IAEA Nuclear Data Section. Participants in the programme were specialists in γ-ray spectroscopy, and the related areas of standards and data evaluation. Their objective was to produce a recommended set of decay parameters for selected radionuclides judged as the most important for the efficiency calibration of equipment used to detect and quantify X- and γ-ray emissions. CRP meetings were held in Rome (1987 [24]) and Braunschweig (1989 [25]) to monitor progress, promote the necessary measurements, determine an evaluation methodology, and agree upon the final recommended half-lives and X- and γ-ray emission probabilities.

Various factors, such as source preparation and source-detector geometry, may affect the quality of measurements made with intrinsic germanium and other γ-ray spectrometers. However, the accuracy of such measurements depends invariably upon the accuracy of the efficiency versus energy calibration curve, and hence upon the accuracy of the decay data for the radionuclides from which calibration standard sources are prepared. Both half-lives and X- and γ-ray emission probabilities need to be known to good accuracy. Participants were given the task of establishing a data file that would be internationally accepted. Valuable contributions were also provided by multinational intercomparison projects organised by the International Committee for Radionuclide Metrology (ICRM) and the Bureau International des Poids et Mesures (BIPM).

3.1 Calibrant Radionuclides

The objectives of the CRP were identified with the following steps:

a) selection of appropriate calibration nuclides,
b) assessment of the status of the existing data,
c) identification of data discrepancies and limitations,
d) stimulation of measurements to meet the data needs, and
e) evaluation and recommendation of improved calibration data.

Other considerations for the selection of radionuclides included: commonly used and readily available nuclides; nuclides used and offered as standards by national laboratories; multi-line nuclides for rapid calibrations; definition of a set of single-line nuclides to avoid the need for coincidence summing corrections; and choice of nuclides with accurately known emission probabilities.

Emission probability data for selected photons were evaluated and expressed as absolute probabilities of the emission per decay. A recommended list of 36 nuclides evolved from the CRP meetings (Table 4). After assessing the status of the existing data, the participants agreed to measure and/or evaluate data which were either discrepant or of inadequate accuracy. The laboratories contributing to this effort are listed in the columns marked "CRP activities" of Table 4.

An evaluation procedure was developed for the half-life data, which was also used, when appropriate, for the γ-ray emission probabilities. This methodology is described in detail in Ref. [26]. The recommended value consisted of the weighted average of the published values in which the weights were taken to be the inverse of the squares of the overall uncertainties. A set of data was self-consistent if the reduced-χ^2 value was approximately 1.0 or less. When the data in a set were inconsistent and there were three or more values, the method of limitation of the relative weight proposed by Zijp [27] was recommended. The sum of the individual weights was computed; if any one weight contributed over 50% of the total, the corresponding uncertainty was increased so that the contribution of the value to the sum of the weights would be less than 50%. The weighted average was then recalculated and used if the reduced-χ^2 value for this average was < 2. If the reduced-χ^2 was > 2, the weighted or unweighted mean was chosen according to whether or not the 1σ uncertainty on each mean value included the other term. The basis for the latter choice is that it may be unreasonable to use the weighted average if the data do not comprise a consistent set.

Table 4. Calibration Standards: Decay Parameters and CRP Activities.

AEA – UK Atomic Energy Authority, Winfrith Technology Centre, UK;
CBNM – CEC-JRC Central Bureau of Nuclear Measurements, Geel, Belgium;
Hiroshima University, Hiroshima, Japan;
INEL – Idaho National Engineering Laboratory, Idaho Falls, USA;
LMRI – CEA Laboratoire de Métrologie des Rayonnements Ionisants, Saclay, France;
NIST – US National Institute of Standards and Technology, Washington DC, USA;
NPL – National Physical Laboratory, Teddington, UK;
OMH – National Office of Measures, Budapest, Hungary;
PTB – Physikalisch-Technische Bundesanstalt, Braunschweig, German.

$T_{½}$ - half-life
P_X – X-ray emission probability
P_γ - γ-ray emission probability
α_t – total internal conversion coefficient

Radio-nuclide	Data Type	Uncertainty Achieved(%)$^+$	CRP activities		Comments
			Measurements	Evaluations	
^{22}Na	$T_{1/2}$	0.1	NIST	NPL/PTB	
	P_γ	0.015	-	NIST	
^{24}Na	$T_{1/2}$	0.03	-	NPL/PTB	
	P_γ	0.0015-0.005	-	NIST	
^{46}Sc	$T_{1/2}$	0.05	-	NPL/PTB	
	P_γ	0.0016	-	Hiroshima Univ.	
^{51}Cr	$T_{1/2}$	0.03	-	NPL/PTB	
	P_X	1.3	-	CBNM	
	P_γ	0.5	OMH	AEA	
^{54}Mn	$T_{1/2}$	0.13	NIST/NPL	NPL/PTB	
	P_X	3.1	-	CBNM	
	P_γ	0.0024	-	Hiroshima Univ.	
^{55}Fe	$T_{1/2}$	0.8	PTB	NPL/PTB	
	P_X	3.5	-	CBNM	

Table 4 (cont.)

Radio-nuclide	Data Type	Uncertainty Achieved(%)+	CRP activities		Comments
			Measurements	Evaluations	
^{56}Co	$T_{1/2}$	0.3	PTB/NPL	NPL/PTB	
	P_γ	0.007-0.4	-	Hiroshima Univ.	
^{57}Co	$T_{1/2}$	0.03	NIST/NPL	NPL/PTB	P_γ for 14.4 keV transition particularly uncertain
	P_x	0.7	-	CBNM	
	P_γ	0.2-1.5	PTB	OMH	
^{58}Co	$T_{1/2}$	0.1	NPL	NPL/PTB	
	P_x	3.8	-	CBNM	
	P_γ	0.01	-	OMH	
	α_t	3	-	LMRI	
^{60}Co	$T_{1/2}$	0.03	NIST/NPL	NPL/PTB	
	P_γ	0.006-0.02	-	NIST	
^{65}Zn	$T_{1/2}$	0.11	NPL	NPL/PTB	Few direct measurements of P_γ for 1115 keV transition
	P_x	2.3	-	CBNM	
	P_γ	0.5	NPL/PTB	AEA	
^{75}Se	$T_{1/2}$	0.2	NIST/NPL	NPL/PTB	Significant uncertainty in P_γ arises from quantifying direct population of ^{75}As ground state
	P_x	7.1	-	CBNM	
	P_γ *	0.3-1.2	LMRI/NIST/OMH/PTB	AEA	
	α_t	1-7	-	LMRI	
^{85}Sr	$T_{1/2}$	0.006	-	NPL/PTB	P_γ for 514 keV transition depends on a theoretical estimate of the branch to the ground state
	P_x	1.4	-	CBNM	
	P_γ	0.4	-	Hiroshima Univ.	
	α_t	12	-	Hiroshima Univ.	
^{88}Y	$T_{1/2}$	0.02	-	NPL/PTB	
	P_x	1.3	-	CBNM	
	P_γ	0.03-0.3	PTB	LMRI	
	α_t	1	-	LMRI	
^{93m}Nb	$T_{1/2}$	0.85	-	PTB/NPL	
	P_x	3.2	-	CBNM	
^{94}Nb	$T_{1/2}$	12	-	PTB/NPL	
	P_γ	0.05	-	INEL	
	α_t	1	-	LMRI	

Table 4 (cont.)

Radio-nuclide	Data Type	Uncertainty Achieved(%)+	CRP activities Measurements	CRP activities Evaluations	Comments
^{95}Nb	$T_{1/2}$	0.02	-	PTB/NPL	
	P_γ	0.03	-	INEL	
	α_t	1-3	-	LMRI	
^{109}Cd	$T_{1/2}$	0.15	NIST	PTB/NPL	
	P_x	2.0	-	CBNM	
	P_γ #	0.6	PTB	LMRI	
	α_t	2	-	LMRI	
^{111}In	$T_{1/2}$	0.02	-	PTB/NPL	
	P_x	2.4	-	CBNM	
	P_γ #	0.1	-	Hiroshima Univ.	
	α_t	1.2	-	Hiroshima Univ.	
^{113}Sn	$T_{1/2}$	0.03	-	PTB/NPL	
	P_x	0.6	-	CBNM	
	P_γ #	0.2	-	INEL	
^{125}Sb	$T_{1/2}$	0.06	-	PTB/NPL	
	P_γ	1	INEL	LMRI	
^{125}I	$T_{1/2}$	0.02	NIST/NPL/PTB/CBNM	PTB/NPL	
	P_x	2.2	-	CBNM	
	P_γ #	1.2	PTB	LMRI	
	α_t	1.5	-	LMRI	
^{134}Cs	$T_{1/2}$	0.03	-	PTB/NPL	
	P_γ	0.06-1.3	-	Hiroshima Univ.	
^{137}Cs	$T_{1/2}$	0.4	NIST	PTB/NPL	
	P_x	2.9	-	CBNM	
	P_γ	0.24	-	LMRI	
	α_t	0.7	-	LMRI	
^{133}Ba	$T_{1/2}$	0.4	-	PTB/NPL	Resolution of 79 and 81 keV gamma transitions poses problems
	P_x	1.3	-	CBNM	
	P_γ *	0.3-0.8	OMH/PTB	OMH	
	α_t	5.5-7	-	LMRI	
^{139}Ce	$T_{1/2}$	0.02	-	PTB/NPL	
	P_x	2.8	-	CBNM	
	P_γ	0.08	-	LMRI	
	α_t	0.4	-	LMRI	

Table 4 (cont.)

Radio-nuclide	Data Type	Uncertainty Achieved(%)+	CRP activities: Measurements	CRP activities: Evaluations	Comments
^{152}Eu	$T_{1/2}$	0.2	NIST/NPL	PTB/NPL	
	P_X	1.6	-	CBNM	
	P_γ *	0.5	-	INEL	
^{154}Eu	$T_{1/2}$	0.09	-	PTB/NPL	
	P_X	2.3	-	CBNM	
	P_γ	1.1-1.7	INEL/NIST/NPL	Hiroshima Univ.	
^{155}Eu	$T_{1/2}$	2.8	PTB	PTB/NPL	
^{198}Au	$T_{1/2}$	0.03	-	PTB/NPL	
	P_X	7.1	-	CBNM	
	P_γ	0.5	-	AEA	
^{203}Hg	$T_{1/2}$	0.03	-	PTB/NPL	
	P_X	3.1	-	CBNM	
	P_γ	0.1	-	INEL	
^{207}Bi	$T_{1/2}$	6	-	PTB/NPL	Additional P_γ measurements are underway to resolve discrepant data
	P_X	5.2	-	CBNM	
	P_γ	0.03-0.6	INEL/NIST/PTB	Hiroshima Univ.	
	α_t	1.4	-	Hiroshima Univ.	
^{228}Th (and daughters)	$T_{1/2}$	0.9	-	NPL/PTB	
	P_γ	0.2-3.3	-	LMRI	
^{239}Np	$T_{1/2}$	0.17	-	PTB/NPL	
	P_γ	1.5	-	LMRI	
^{241}Am	$T_{1/2}$	0.15	-	PTB/NPL	
	P_X	2.0	-	CBNM	
	P_γ	1-4	PTB	CBNM	
^{243}Am	$T_{1/2}$	0.3	-	NPL/PTB	
	P_γ	1.5-1.9	-	AEA/LMRI	
	α_t	2	-	LMRI	

\+ Uncertainties for X-and γ-ray emission probabilities and internal conversion coefficients apply to the major transitions only, corresponding to 1σ confidence level.
* Measurement programme co-ordinated by ICRM.
\# Measurement programme co-ordinated as BIPM intercomparison.

It was not considered necessary to carry out evaluations of the X- and γ-ray energies, because the photon energies are only required to the nearest 1 or 0.1 keV. However, for completeness it was decided to include the best available energy values, many of which had been precisely measured and evaluated [28]. Most of the energy values were taken from Ref. [28]; original references were cited when such data were not available from this source. Internal conversion coefficients are often used in the evaluation of γ-ray emission probabilities, either directly in the determination of a particular emission probability or in testing the consistency of the decay scheme. Theoretical internal conversion coefficients were normally taken from Rösel et al. [29]; when necessary these data were obtained by interpolation using a computer program written at LMRI [30].

3.2 High-energy gamma rays

The radioactive sources discussed above permit the precise determination of the efficiency of a germanium detector up to about 2.7 MeV with either a ^{24}Na or ^{228}Th source, or to 3.6 MeV with a ^{56}Co source. Some sources of radiation can be used to extend the efficiency calibration to above 10 MeV, and were also considered. Except for one radioactive nuclide (^{66}Ga), these sources of radiation are based on nuclear reactions. While other reactions could be used, only thermal neutron capture and (p, γ) reactions were considered.

The high-energy γ-ray data were generally taken from a single reference, and were not subjected to the detailed evaluation of the other data. Furthermore, the data were of somewhat uneven quality. Some of the measurements had been undertaken with metrological goals in mind; other measurements were less well defined.

3.2.1 ^{66}Ga

^{66}Ga is the only radionuclide that has been used in the energy region above 3600 keV. This nuclide has a half-life of 9.5 hours, and can be produced by ^{63}Cu(α, n), ^{66}Zn(p, n) and ^{64}Zn(α, 2n) reactions. The γ rays with emission probabilities > 0.01 are listed in Table 5, including six lines from 3.2 to 4.8 MeV. However, two limitations are immediately apparent: half-life of 9.5 hours means that this radionuclide can only be used by spectroscopists with access to an appropriate production facility, and the uncertainties in the emission probabilities above 3 MeV range from 7% to 27% which does not result in a precise calibration.

Since a source of unknown activity would be used, the relative efficiencies would be measured and normalised to efficiencies determined previously at lower energies, for example at 1039 or 2752 keV. Despite a high decay energy of 5.2 MeV, the multiplicity of the γ-ray cascades is not high. Considering that the decay scheme consists only of the γ rays listed in Table 5, 6% of the decays produce three γ rays in cascade, 32% produce only two cascade γ rays, 10% produce only one γ ray, and 50% do not produce any γ rays at all. This means that any coincidence summing corrections will be similar to those of simple sources (e.g., ^{60}Co) with cascades of two γ rays (assuming X-rays from the electron-capture process do not reach the detector).

However, considerable improvements have been made with respect to ^{66}Ga γ-ray analysis since this CRP was completed (as noted in Section 4), and spectroscopists are urged to use the more recently recommended data on release.

Table 5. Gamma-ray Emission Probabilities from the Decay of ^{66}Ga (9.5 hours) for those Gamma Rays with Probabilities greater than 0.01 (Refs [31] and [32]).

E_γ (keV)	P_γ [a]
833.6	0.0603(12)
1039.4	0.379
1333.2	0.01232(25)
1918.8	0.0214(4)
2189.9	0.0571(11)
2422.9	0.0196(4)
2752.3	0.232(8)
3229.2	0.0148(11)
3381.4	0.0140(11)
3791.6	0.0102(11)
4086.5	0.0114(19)
4295.7	0.035(7)
4807.0	0.015(4)

a The uncertainties are those for the probabilities relative to that for the 1039-keV gamma-ray. A normalization uncertainty of 3.2% should be added (in quadrature) to obtain the overall uncertainty in the emission probabilities.

3.2.2 Thermal neutron capture reactions

Efficiency calibrations can be derived using γ rays from the thermal neutron capture reaction on selected target materials. Of the many thermal neutron capture reactions that could have been assessed, only a few were considered by the CRP.

^{14}N(n, γ)^{15}N reaction was judged to be of particular interest [33]: as shown in Table 6, there are twelve γ-ray emission probabilities (per neutron capture) ranging from 3 to 11 MeV that have uncertainties of ~ 1%. This accuracy was achieved in part because the level scheme is quite simple (for capture γ-ray decay), and the authors could use intensity balances at each level to constrain the deduced emission probabilities.

^{35}Cl(n, γ)^{36}Cl reaction was also assessed, with seventeen strong γ rays (> 0.020 photons per thermal neutron capture) ranging from 0.516 to 8.58 MeV of which eight are above 5 MeV [34]. The accuracy of the reported emission probabilities were not as good as the ^{14}N(n, γ)^{15}N data for several reasons, including a more complex scheme which precludes the confident use of intensity balances to constrain the values.

Some ratios of γ-ray emission probabilities are given in Table 7 (taken from Ref. [35]). The adoption of these reactions depends on the availability of a neutron source, and the usefulness of any particular reaction depends on the reaction cross section, a suitable sample, and the lack of any interference from background radiation (including the production of the same reaction outside the target).

Table 6. Gamma-ray Emission Probabilities per Neutron Capture (P_γ) for Prompt Gamma Rays from the $^{14}N(n, \gamma)^{15}N$ Reaction from Kennett et al. [33]).

E_γ(keV)	P_γ
1678.174(55)	0.0723(18)
1884.879(21)	0.1866(25)
2520.418(15)	0.0579(7)
3532.013(13)	0.0924(9)
3677.772(17)	0.1489(15)
4508.783(14)	0.1654(17)
5269.169(12)	0.3003(20)
5297.817(15)	0.2131(18)
5533.379(13)	0.1975(21)
5562.062(17)	0.1065(12)
6322.337(14)	0.1867(14)
7298.914(33)	0.0973(9)
8310.143(29)	0.0422(5)
9149.222(47)	0.0162(2)
10829.087(46)	0.1365(21)

Footnote: A.H. Wapstra [Nucl. Instrum. Meth. Phys. Res. A292, 671 (1990)] has given an alternate set of gamma-ray energies based on the average of three sets of measurements and a revised value of the neutron binding energy.

Table 7. Thermal Neutron Capture Reactions with Subsequent Emission of Gamma Rays in Cascade at Energies E_1 and E_2 and with Emission Probabilities P_1 and P_2.

Reaction	E_1	E_2	P_1/P_2
$^{35}Cl(n,\gamma)^{36}Cl$	5.716	2.864	0.86(7) [a]
	6.111	1.951	1.05(9) [a]
	6.111	0.517	0.87(7) [a]
	6.620	1.959	0.67(6) [a]
	6.978	1.601	0.65(6) [a]
	7.791	0.788	0.57(5) [a]
$^{48}Ti(n,\gamma)^{49}Ti$	4.882	1.499	0.92(3)
	6.419	0.342	1.23(2)
	6.761	1.382	0.54(2)
$^{52}Cr(n,\gamma)^{53}Cr$	5.618	2.231	1.00
$^{53}Cr(n,\gamma)^{54}Cr$	6.645	2.239	0.95
	7.100	1.785	1.07
	8.884	0.835	0.60

[a] Uncertainty includes statistical uncertainties, and 8% for the systematic uncertainty.

3.2.3 Proton capture reactions

Proton capture reactions can be used to provide γ rays to calibrate germanium detectors. Although there are some experimental difficulties, these reactions have the advantage that simple γ-ray spectra are often produced when the proton energy is chosen to coincide with a resonance. Some useful proton resonances and the related γ-ray emission probability ratios are listed in Table 8. Many other potentially useful resonances may also be identified from the review articles of Endt and van der Leun [36] and Ajzenberg-Selove [37].

Table 8. Proton Capture Reactions with Subsequent Emission of Gamma Rays in Cascade at Energies E_1 and E_2 and with Emission Probabilities P_1 and P_2; Proton Resonance Energy is E_p.

Reaction	E_p (MeV)	$E_{\gamma 1}$ (MeV)	$E_{\gamma 2}$ (MeV)	P_1/P_2
$^{11}B(p,\gamma)^{12}C$	0.675	12.14	4.44	1.000
	1.388	12.79	4.44	1.000
	2.626	13.92	4.44	1.000
$^{14}N(p,\gamma)^{15}O$	0.278	5.183	2.374	1.00
		6.176	1.381	1.00
		6.793	0.764	1.00
$^{23}Na(p,\gamma)^{24}Mg$	1.318	11.588	1.368	0.963(3)
	1.416	8.929	2.754	0.985(3)
$^{24}Al(p,\gamma)^{28}Si$	0.767	7.706	2.837	0.981(2)
	0.992	10.76	1.780	0.806(10)
	1.317	6.58	4.50	1.017(7)

3.3 Recommended X-ray and Gamma-ray Standards, 1990/91

A set of recommended half-life and emission probability data was prepared by participants of the IAEA Co-ordinated Research Project on X-ray and Gamma-ray Standards for Detector Calibration. The results from this work represented a significant improvement in the quality of specific decay parameters required for the efficiency calibration of X- and γ-ray detectors. Data inadequacies were highlighted, several of the identified inconsistencies remain unresolved, and further efforts are required to address these uncertainties. Accomplishments of this CRP included:

- assessment of the existing relevant data during 1986/87,
- co-ordination of measurements within the existing project and extensive cooperation among the participating research groups,
- performance of a large number of measurements stimulated by the CRP, and
- preparation of an IAEA-TECDOC report which consolidated most of the data needed for γ-ray detector efficiency calibration (IAEA-TECDOC-619, IAEA Vienna, Austria, 1991).

The resulting data were internationally accepted as a significant contribution to the improved quality of X- and γ-ray spectrometry. However, the recommended database that evolved from this CRP will soon be superseded by the results of a new CRP initiative that began in 1998 to update calibrant decay data (see Section 4).

4. Co-ordinated Research Project: Update of X-ray and Gamma-ray Decay Data Standards for Detector Calibration and Other Applications (both the technical document and database are still in preparation, 2005)

A strong recommendation was formulated at the 1997 biennial meeting of the International Nuclear Data Committee for the IAEA-NDS to re-visit and place further emphasis on the development of improved decay data for standards applications. This recommendation arose as a consequence of the publication of relevant measured data beyond 1990 that were not included in the original CRP (see Section 3, above). Many such studies had been catalysed by the demands of this earlier CRP, and new efforts were required to incorporate the new data and extend the existing database to encompass the related needs of a number of important applications such as environmental monitoring and nuclear medicine. High-quality decay data are essential in the efficiency calibration of X- and γ-ray detectors that are used to quantify radionuclidic content by determining the intensities of any resulting X- and γ rays. A Consultants' Meeting was held at IAEA Headquarters in 1997 to assess the current needs, and identify the most suitable radionuclides [38]. The expert participants at this meeting advised the establishment of a new Co-ordinated Research Project: Update of X-ray and Gamma-ray Decay Data Standards for Detector Calibration and Other Applications.

Members of the new CRP reviewed and modified the list of radionuclides most suited for detector calibration, and were able to include some of the specific needs of such nuclear applications as safeguards, material analysis, environmental monitoring, nuclear medicine, waste management, dosimetry and basic spectroscopy. CRP meetings were held at IAEA, Vienna (1998 [39]), PTB, Braunschweig (2000 [40]), and IAEA Vienna (2002 [41]) to monitor progress, promote measurements, formulate and implement the evaluation procedures, and agree upon the final recommended half-lives and X- and γ-ray emission probabilities. All evaluations were based on the available experimental data, supplemented with the judicious use of well-established theory. As with the previous CRP, three types of data (half-lives, energies, and emission probabilities) were compiled and evaluated. Consideration was also given to the use of the γ-γ coincidence technique for efficiency calibrations, as well as adopting a number of prompt high-energy γ rays from specific nuclear reactions. Well-defined evaluation procedures were applied to determine the recommended half-lives and emission probabilities for all prominent X- and γ rays emitted by each selected radionuclide.

4.1 Main issues

4.1.1 Update of 1991 IAEA database

IAEA-TECDOC-619 contains recommended decay data for 36 radionuclides, extending up to γ-ray energy of 3.6 MeV. These data were revisited and revised where appropriate, as a consequence of the availability of new experimental data measured and published after 1990. New measurements of half-lives have also been published for at least 29 of the original 36 radionuclides. Most of the γ-ray energies were taken from Ref. [42], while original references were cited when such data were not available from this source. Only average X-ray energies and their emission probabilities were given in IAEA-TECDOC-619 - the new work eliminates this shortcoming through a systematic analysis of the emissions of the individual $K_{\alpha1}$, $K_{\alpha2}$, $K_{\beta1}$ and $K_{\beta2}$ components. However, X-ray energies were not evaluated, but taken from Schönfeld and Rodloff [43] and Browne and Firestone [31].

4.1.2 Additional radionuclides

A comprehensive list of 68 radionuclides was originally prepared at the Consultants' Meeting, and adopted as a suitable starting point by the participants of the CRP. Decay data were compiled, evaluated and recommended for the half-lives, and X-ray and γ-ray emission probabilities. These radionuclides have been re-evaluated in an international exercise led by laboratories involved in the Decay Data Evaluation Project (DDEP) [44] and affiliated to the International Committee for Radionuclide Metrology (ICRM), with the IAEA-CRP providing additional impetus and the necessary co-ordination to achieve the desired objectives.

4.1.3 Extension of the energy range

New nuclear techniques (for example, radiotherapy) suffer from a lack of high-energy calibration standards. Hence, there is an urgent need to provide such data for the calibration of γ-ray detectors up to 25 MeV. Appropriate radionuclides and nuclear reactions have been identified, and γ-ray emission probabilities were compiled and evaluated. Various options were explored in order to provide energy and intensity calibration γ-lines above 10 MeV.

4.1.4 Other features

Angular correlation coefficients were evaluated for a few appropriate radionuclides of relevance to the γ-γ coincidence method of calibration. Attention was also focused on the analysis of uncertainties, including an investigation of the feasibility and usefulness of including error correlations in the evaluation procedures. A limited number of nuclides were evaluated in this manner. One conclusion arising from this exercise was the need to establish rules for the documentation of experiments that would enable the evaluators to estimate input covariances from the published decay data.

4.2 Specified radionuclides and nuclear reactions

A recommended list of 62 nuclides evolved from the meetings of the IAEA CRP (Table 9), including specific parent-daughter combinations and two heavy-element decay chains. A primary standard is a nuclide for which γ-ray emission probabilities are calculated from various data that do not include significant γ-ray measurements (emission probabilities are usually close to 1.0, expressed per decay); these data may include internal conversion coefficients and the intensities of weak beta branches. Secondary standards are nuclides for which the recommended γ-ray intensities depend on prior measurements of the γ-ray intensities. When relative intensities had been measured, these parameters were evaluated as well as the normalisation factor; this combination of data was then used to generate absolute emission probabilities. Thus, both relative intensities and absolute emission probabilities were included in the evaluation exercise, and both can be extracted from the database.

The following nuclear reactions were also adopted as γ-ray calibration standards:

$^{14}N(n, \gamma)^{15}N^*$
$^{35}Cl(n, \gamma)^{36}Cl^*$
$^{48}Ti(n, \gamma)^{49}Ti^*$
$^{50, 52, 53}Cr(n, \gamma)^{51, 53, 54}Cr^*$
$^{11}B(p, \gamma)^{12}C^*$
$^{23}Na(p, \gamma)^{24}Mg^*$
$^{27}Al(p, \gamma)^{28}Si^*$

Their cross sections, and the energies and transition probabilities of the most prominent high-energy γ rays have been evaluated.

Emphasis has been placed on the X- and γ rays most suited as detector efficiency calibrants, and only these emissions have been included in the final CRP dataset (i.e., only a limited number of strong lines are recommended). Detailed comments and complete decay-data listings will not necessarily be included in the final technical document; however, the user will be referred to relevant parallel publications by laboratories involved in the DDEP [45-47], and web pages located through: http://www.nucleide.org/DDEP_WG/DDEPdata.htm

4.3 Recommended X-ray and Gamma-ray Decay Data Standards: Revisited, 2004/05

A new set of recommended half-life and emission probability data has been prepared by participants in the IAEA-CRP to Update X- and Gamma-ray Decay Data Standards for Detector Calibration and Other Applications. The results from this work represent a further significant improvement in the quality of specific decay parameters required for the efficiency calibration of X- and γ-ray detectors. Examples of the data as presented to the reader of the technical report are given in Appendix B (these data are provisional, and subject to modification before release of the final database).

The accomplishments of the CRP include:

- re-evaluations of all existing relevant data from the 1986-90 programme;
- extension of the recommended database to satisfy the needs of a number of important applications;
- specific measurements were undertaken, particularly with respect to high-energy γ-ray emissions;
- preparation of an IAEA technical report which summarizes the recommended decay data for X- and γ-ray detector efficiency calibration and other applications.

As before, one important expectation is that the resulting set of data will be internationally accepted as a significant contribution to improving the quality of both X- and γ-ray spectrometry.

Table 9: Selected Radionuclides and Applications.

Nuclide	X/γ-Ray Standard	Dosimetry Standard	Medical Applications	Environmental Monitoring	Waste Management	Safeguards
^{22}Na	P	-	x	-	-	-
^{24}Na	P	-	-	-	-	-
^{40}K	S	-	-	x	-	-
^{46}Sc	P	-	-	-	-	-
^{51}Cr	S	-	x	-	-	-
^{54}Mn	P	-	-	x	x	-
^{56}Mn	P	-	x	-	-	-
^{55}Fe	S	-	x	-	x	-
^{59}Fe	S	-	x	-	-	-
^{56}Co	S	-	-	-	-	-
^{57}Co	P (122 keV)	-	x	-	-	x
^{58}Co	P	-	-	x	-	-
^{60}Co	P	-	x	x	x	x
^{64}Cu	-	-	x	-	-	-
^{65}Zn	S	-	-	x	x	-
^{66}Ga	S	-	x	-	-	-
^{67}Ga	S	-	x	-	-	-
^{68}Ga	-	-	x	-	-	-
^{75}Se	S	-	x	-	-	-
^{85}Kr	-	-	-	x	-	-
^{85}Sr	P	-	x	x	-	-
^{88}Y	P (1836 keV) S (898 keV)	-	-	-	-	-
^{93m}Nb	-	x	-	-	-	-
^{94}Nb	P	-	-	-	-	-
^{95}Nb	P	-	-	x	-	-
^{99}Mo	P (140.5 keV)	-	x	-	-	-
^{99m}Tc	P (140.5 keV)	-	x	-	-	-
^{103}Ru	-	-	x	x	-	-
^{106}Ru-^{106}Rh	S	-	x	x	-	-
^{110m}Ag	S	-	-	x	x	-
^{109}Cd	S	-	-	x	-	-
^{111}In	P	-	x	-	-	-
^{113}Sn	P	-	-	-	-	-
^{125}Sb	-	-	-	x	-	-
^{123m}Te	-	-	-	-	-	-
^{123}I	P	-	x	-	-	-
^{125}I	S	x	x	-	-	-
^{129}I	S	-	-	x	x	-
^{131}I	S	x	x	x	-	-
^{134}Cs	S	-	-	x	-	-

Table 9: Selected Radionuclides and Applications (cont.).

Nuclide	X/γ-Ray Standard	Dosimetry Standard	Medical Application	Environmental Monitoring	Waste Management	Safeguards
^{137}Cs	P	-	-	x	x	-
^{133}Ba	S	-	x	-	-	-
^{139}Ce	P	-	-	x	-	-
^{141}Ce	S	-	-	x	-	-
^{144}Ce	S	-	x	x	-	-
^{153}Sm	-	-	x	-	-	-
^{152}Eu	S	-	-	x	x	x
^{154}Eu	S	-	-	x	x	x
^{155}Eu	S	-	-	x	x	-
^{166m}Ho-^{166}Ho	S	-	x	-	-	x
^{170}Tm	S	-	-	-	-	-
^{169}Yb	S	-	x	-	-	-
^{192}Ir	S	x	x	-	-	-
^{198}Au	P	-	-	-	-	-
^{203}Hg	P	-	-	-	-	-
^{201}Tl	-	-	x	-	-	-
^{207}Bi	P (569.7 keV)	-	x	-	-	-
^{226}Ra decay chain	S	x	-	x	x	-
^{228}Th decay chain	P	-	-	x	-	-
^{234m}Pa	-	-	-	x	x	-
^{241}Am	P	-	-	x	x	x
^{243}Am	-	-	-	-	x	-

P primary efficiency calibration standard.
S secondary efficiency calibration standard.

5. Concluding Remarks

Decay-data studies undertaken under the auspices of the International Atomic Energy Agency are strongly linked to the needs of Member States, and are therefore applications oriented. Specific inadequacies in our knowledge of important decay-data parameters have been identified through IAEA-sponsored Advisory Group Meetings and Consultants' Meetings.

At various periods of time over the previous 30 years, staff in the IAEA Nuclear Data Section have been encouraged by Member States to organise four Co-ordinated Research Projects (CRPs) to resolve difficulties and uncertainties identified with:

- decay data of transactinium nuclides (two CRPs, 1977-85 and 2005-09 (in planning stage));
- X-ray and γ-ray decay data standards for detector calibration and other applications (two CRPs, 1986-1990 and 1998-2002).

New measurements have been performed and in-depth evaluations undertaken in order to formulate recommended decay data for the relevant radionuclides, as specified at the various Consultants' Meetings.

A comprehensive form of in-depth evaluation methodology has been developed in conjunction with the Decay Data Evaluation Programme (DDEP). The various agreed evaluation procedures have been applied to all relevant decay data for each individual radionuclide, representing a high degree of analysis. Such detail is extremely labour intensive, and the limited amount of expertise worldwide prevents general application to the full range of mass chain evaluations.

Much has been achieved to resolve a wide range of specific difficulties and discrepancies, and a number of extremely useful applications-based decay-data files have been assembled by the IAEA Nuclear Data Section to ensure that the most up-to-date values are adopted by users in Member States. Further work is merited, including the need to update the IAEA database of actinide decay data (indeed plans are being formulated to initiate such a CRP in 2005). One further intention will be to maintain strong technical links between the relatively modest number of experts to be found working within the DDEP and involved in IAEA-CRPs dedicated to the evaluation and recommendation of decay data.

Acknowledgements

Information was gratefully received from past and present colleagues of the IAEA Nuclear Data Section:

O. Schwerer (Introduction);
A. Lorenz (Decay Data for the Transactinium Nuclides);
A. Lorenz and H.D. Lemmel (X-ray and Gamma-ray Standards for Detector Calibration);
M. Herman (Update of X-ray and Gamma-ray Decay Data Standards for Detector Calibration and Other Applications).

References

[1] D.D. Sood, P. Obložinský, M. Herman and O. Schwerer, *Nuclear Data for Applications,*. Radioanal. Nucl. Chem., **243**, 227 (2000).

[2] See *http://www-amdis.iaea.org/*

[3] R.B. Firestone, V.S. Shirley, S.Y.F. Chu, C.M. Baglin and J. Zipkin, *Table of Isotopes,* 8th edition, John Wiley and Sons, New York, 1996.

[4] S.Y.F. Chu, H. Nordberg, R.B. Firestone and L.P. Ekström, *Isotope Explorer*; see *http://ie.lbl.gov/isoexpl/isoexpl.htm*

[5] G. Audi, O. Bersillon, J. Blachot and A.H. Wapstra, *The NUBASE Evaluation of Nuclear and Decay Properties,* Nucl. Phys., **A729**, 3-128 (2003); database available in electronic form, see *http://csnwww.in2p3.fr/amdc/web/nubase_en.html*

[6] V.G. Pronyaev, O. Schwerer, Nuclear Reaction Data Centres Network, IAEA report INDC(NDS)-401, Rev. 4, August 2003, IAEA Vienna, Austria.

[7] V.G. Pronyaev, A.L. Nichols, J. Tuli, *Nuclear Structure and Decay Data (NSDD) Evaluators' Network,* IAEA report INDC(NDS)-421, Rev. 1, March 2004, IAEA Vienna, Austria.

[8] O. Schwerer and H.D. Lemmel, *Index of Nuclear Data Libraries available from the IAEA Nuclear Data Section,* IAEA report IAEA-NDS-7, July 2002, IAEA Vienna, Austria; see also *http://www-nds.iaea.org/reports/nds-7.pdf*

[9] H.D. Lemmel and O. Schwerer, *Index to the IAEA-NDS Documentation Series,* IAEA report IAEA-NDS-0, July 2002, IAEA Vienna, Austria.
see also *http://www-nds.iaea.org/nds-0.html*

[10] *IAEA Nuclear Data Newsletter*, IAEA Vienna, Austria; issued twice per year, and also available through *http://www-nds.iaea.org/newslett.html*

[11] NDS services can be contacted through: *services@iaeand.iaea.org*

[12] International Atomic Energy Agency, *Transactinium Isotope Nuclear Data*, Proc. Advisory Group Meeting, Karlsruhe, 1975, IAEA-TECDOC-186, IAEA Vienna, Austria, 1976.

[13] A. Lorenz, *Measurement and Evaluation of Transactinium Isotope Nuclear Data*, Summary Report 1st IAEA Research Coordination Meeting, Vienna, 1978, IAEA report INDC(NDS)-96/N, IAEA Vienna, Austria.

[14] A. Lorenz, *Measurement and Evaluation of Transactinium Isotope Nuclear Data*, Summary Report 2nd IAEA Research Co-ordination Meeting, Aix-en-Provence, 1979, IAEA report INDC(NDS)-105/N, IAEA Vienna, Austria.

[15] A. Lorenz, *Measurement and Evaluation of Transactinium Isotope Nuclear Data*, Summary Report 3rd IAEA Research Co-ordination Meeting, Vienna, 1980, IAEA report INDC(NDS)-118/NE, IAEA Vienna, Austria.

[16] A. Lorenz, *Measurement and Evaluation of Transactinium Isotope Nuclear Data*, Summary Report 4th IAEA Research Co-ordination Meeting, Vienna, 1981, IAEA report INDC(NDS)126/NE, IAEA Vienna, Austria.

[17] A. Lorenz, *Measurement and Evaluation of Transactinium Isotope Nuclear Data*, Summary Report 5th IAEA Research Co-ordination Meeting, Geel, 1982, IAEA report INDC(NDS)-138/GE, IAEA Vienna, Austria.

[18] A. Lorenz, *Measurement and Evaluation of Transactinium Isotope Nuclear Data*, Summary Report 6th IAEA Research Co-ordination Meeting, Idaho Falls, 1983, IAEA report INDC(NDS)-147/GE, IAEA Vienna, Austria.

[19] A. Lorenz, *Measurement and Evaluation of Transactinium Isotope Nuclear Data*, Summary Report 7th IAEA Research Co-ordination Meeting, Vienna, 1984, IAEA report INDC(NDS)-164/GE, IAEA Vienna, Austria.

[20] International Atomic Energy Agency, *Transactinium Isotope Nuclear Data - 1979*, Proc. IAEA Advisory Group Meeting, Cadarache, 1979, IAEA-TECDOC-232, IAEA Vienna, Austria, 1980.

[21] International Atomic Energy Agency, *Transactinium Isotope Nuclear Data – 1984*, Proc. IAEA Advisory Group Meeting, Uppsala, 1984, IAEA-TECDOC-336, IAEA Vienna, Austria, 1985.

[22] A. Lorenz, *Decay Data for Radionuclides Used as Calibration Standards*, p. 89 in Nuclear Data Standards for Nuclear Measurements, IAEA Technical Reports Series No. 227, IAEA Vienna, 1985.

[23] A. Lorenz, *Gamma-ray Standards for Detector Calibration*, Summary Report of a Consultants' Meeting, Centre d'Etudes Nucleaires de Grenoble, France, May 1985, AEA report INDC(NDS)-171, IAEA Vienna, Austria.

[24] P. Christmas, A.L. Nichols and A. Lorenz, *Gamma-ray Standards for Detector Calibration*, Summary Report of Research Co-ordination Meeting, Rome, Italy, June 1987, IAEA report INDC(NDS)-196, IAEA Vienna, Austria.

[25] P. Christmas, A.L. Nichols and H.D. Lemmel, *Gamma-ray Standards for Detector Calibration*, Summary Report of Research Co-ordination Meeting, Braunschweig, Federal Republic of Germany, June 1989, IAEA report INDC(NDS)-221, IAEA Vienna, Austria.

[26] M.J. Woods and A.S. Munster, *Evaluation of Half-Life Data*, NPL report RS(EXT)95, 1988, National Physical Laboratory, Teddington, UK.

[27] W.L. Zijp, *On the Statistical Evaluation of Inconsistent Measurement Results Illustrated on the Example of the ^{90}Sr Half-Life*, ECN report ECN-179, 1985, Netherlands Energy Research Foundation, Petten, The Netherlands.

[28] R.G. Helmer, P.H.M. van Assche and C. van der Leun, *Recommended Standards for Gamma-ray Energy Calibrations (1979)*, At. Data Nucl. Data Tables, **24**, 39-48 (1979).

[29] F. Rösel, H.M. Fries, K. Alder and H.C. Pauli, *Internal Conversion Coefficients for all Atomic Shells*, At. Data Nucl. Data Tables, **21**, 91-514 (1978).

[30] N. Coursol, LMRI report RI-LPRI-102, November 1990, Departement des Applications et de la Metrologie des Rayonnements Ionisants, Gif-sur-Yvette, France.

[31] E. Browne and R.B. Firestone, *Table of Radioactive Isotopes*, John Wiley & Sons, New York, 1986.

[32] N.J. Ward and F. Kearns, *Nuclear Data Sheets for A*=66, Nucl. Data Sheets, **39**, 1-102 (1983).

[33] T.J. Kennett, W.V. Prestwich and J.S. Tsai, *The $^{14}N(n,\gamma)^{15}N$ Reaction as Both Intensity and Energy Standards*, Nucl. Instrum. Meth., **A249**, 366-378 (1986).

[34] A.M.J. Spits and J. Kopecky, *The Reaction $^{35}Cl(n,\gamma)^{36}Cl$ Studied with Non-polarised and Polarised Thermal Neutrons*, Nucl. Phys., **A264**, 63-92 (1976).

[35] K. Debertin and R.G. Helmer, *Gamma- and X-ray Spectrometry with Semiconductor Detectors*, North-Holland, Amsterdam, 1988.

[36] P.M. Endt and C. van der Leun, *Energy Levels of A=21-44 (VI)*, Nucl. Phys., **A310**, 1-752 1978).

[37] F. Ajzenberg-Selove, *Energy Levels of Light Nuclei A=11-12*, Nucl.Phys., **A433**, 1-158 (1985);
ibid, *Energy Levels of Light Nuclei A=13-15*, **A449**, 1-186 (1986);
ibid, *Energy Levels of Light Nuclei A=16-17*, **A460**, 1-148 (1986);
ibid, *Energy Levels of Light Nuclei A=18-20*, **A475**, 1 (1987);
ibid, *Energy Levels of Light Nuclei A=5-10*, **A490**, 1-225 (1988);
etc.

[38] A. Nichols and M. Herman, *Report on the Consultants' Meeting on Preparation of the Proposal for a Co-ordinated Research Project to Update X- and γ-ray Decay Data Standards for Detector Calibration*, IAEA Vienna, 24-25 November 1997, IAEA report INDC(NDS)-378, May 1998, IAEA Vienna, Austria.

[39] M. Herman and A. Nichols, *Summary Report of the First Research Co-ordination Meeting: Update of X- and γ-ray Decay Data Standards for Detector Calibration and Other Applications*, IAEA Vienna, 9-11 December 1998, IAEA report INDC(NDS)-403, July 1999, IAEA Vienna, Austria.

[40] M. Herman and A. Nichols, *Summary Report of the Second Research Co-ordination Meeting: Update of X- and γ-ray Decay Data Standards for Detector Calibration and Other Applications*, PTB Braunschweig, Germany, 10-12 May 2000, IAEA report INDC(NDS)-415, September 2000, IAEA Vienna, Austria.

[41] M. Herman and A.L. Nichols, *Summary Report of the Third Research Co-ordination Meeting: Update of X- and γ-ray Decay Data Standards for Detector Calibration and Other Applications*, 21-24 October 2002, IAEA report INDC(NDS)-437, December 2002, IAEA Vienna, Austria.

[42] R.G. Helmer and C. van der Leun, *Recommended Standards for γ-ray Energy Calibration (1999)*, Nucl. Instrum. Meth. Phys. Res., **A450**, 35-70 (2000).

[43] E. Schönfeld and G. Rodloff, *Energies and Relative Emission Probabilities of K X-rays for Elements with Atomic Numbers in the Range from Z=5 to Z=100*, PTB report PTB-6.11-1999-1, February 1999.

[44] E. Browne, M.-M. Bé, T.D. MacMahon and R.G. Helmer, *Report on Activities of the Decay Data Evaluation Project (DDEP)*, CEA report CEA-R-5990(E), October 2001.

[45] M.-M. Bé, N. Coursol, B. Duchemin, F. Lagoutine, J. Legrand, K. Debertin and E. Schönfeld, *Table de Radionucléides, Introduction*, CEA Saclay, ISBN 2-7272-0201-6, 1999.

[46] M.-M. Bé, V. Chisté, C. Dulieu, E. Browne, V. Chechev, N. Kuzmenko, R. Helmer, A. Nichols, E. Schönfeld and R. Dersch, *Table de Radionuclides (Vol. 1 – A = 1 to 150)*, Bureau International des Poids et Mesures, Monographie BIPM-5, ISBN 92-822-2206-3, 2004.

[47] M.-M. Bé, V. Chisté, C. Dulieu, E. Browne, V. Chechev, N. Kuzmenko, R. Helmer, A. Nichols, E. Schönfeld and R. Dersch, *Table de Radionuclides (Vol. 2 – A = 151 to 242)*, Bureau International des Poids et Mesures, Monographie BIPM-5, ISBN 92-822-2207-1, 2004.

APPENDIX A

TRANSACTINIUM DECAY DATA, 1985/86

EXAMPLE DATA AND RECOMMENDATIONS

I. HALF-LIFE

Recommended value: $(7.037 \pm 0.007) \times 10^8$ a

This value was adopted from the 1984 review by Holden [1].

The quoted uncertainty, corresponding to the 2σ level, has been reduced to 0.1%, being the minimum value adopted by the CRP participants for half-lives of long lived nuclides.

II. EMISSION PROBABILITIES OF SELECTED GAMMA RAYS

Evaluated by R. Vaninbroukx (CBNM, Geel, Belgium).

A. Recommended values

E_γ (keV)	P_γ
41.96	0.0006 ± 0.0001
74.8	0.0006 ± 0.0001
109.16	0.0154 ± 0.0005
140.76	0.0022 ± 0.0002
143.76	0.1096 ± 0.0008
150.93	0.0008 ± 0.0001
163.33	0.0508 ± 0.0004
182.61	0.0034 ± 0.0002
185.72	0.572 ± 0.002
194.94	0.0063 ± 0.0001
198.90	0.0042 ± 0.0006
202.11	0.0108 ± 0.0002
205.31	0.0501 ± 0.0005
221.38	0.0012 ± 0.0001
233.50	0.00029 ± 0.00005
240.85	0.00075 ± 0.00006
246.84	0.00053 ± 0.00003

E_γ (keV)	Vaninbroukx and Denecke (1982) [2]	Banham and Jones (1983) [3]	Helmer and Reich (1984) [4]
41.96		0.0006 *1*	
74.8		0.0051 *5*	
109.16		0.0153 *5*	
140.76		0.00214 *15*	
143.76	0.109 *2*	0.107 *2*	0.1101 *8*
150.93		0.00066 *10*	
163.33	0.050 *1*	0.0497 *10*	0.0512 *4*
182.61		0.00339 *17*	
185.72	0.575 *9*	0.573 *6*	0.572 *5*
194.94		0.00626 *13*	
198.90		0.00047 *6*	
202.11		0.0108 *2*	
205.31	0.050 *2*	0.0505 *5*	0.0496 *5*
221.38		0.00114 *6*	
233.50		0.00029 *5*	
240.85		0.00076 *6*	
246.84		0.00053 *3*	

C. Comparison with other measurements

E_γ (keV)	CRP measurements: Vaninbroukx and Denecke (1982) [2]	CRP measurements: Banham and Jones (1983) [3]	CRP measurements: Helmer and Reich (1984) [4]	Other measurements: Teoh et al. (1974) [5][a]	Other measurements: Vano et al. (1975) [6][a]	Other measurements: Olson (1983) [7]	Evaluated values[c]
41.96		0.0006 *1*		0.0007 *3*			0.0006 *1*
74.8		0.0051 *5*[b]		0.0005 *1*	0.0007 *1*		0.0006 *1*
109.16		0.0153 *5*		0.018 *2*	0.015 *2*		0.0154 *5*
140.76		0.00214 *15*		0.0026 *3*	0.0022 *3*		0.0022 *2*
143.76	0.109 *2*	0.107 *2*	0.1101 *8*	0.112 *11*	0.111 *11*	0.1093 *15*	0.1096 *8*
150.93		0.00066 *10*		0.0008 *1*	0.00081 *10*		0.0008 *1*
163.33	0.050 *1*	0.0497 *10*	0.0512 *4*	0.050 *5*	0.051 *5*	0.0507 *8*	0.0508 *4*
182.61		0.00339 *17*		0.0042 *14*	0.0044 *9*		0.0034 *2*
185.72	0.575 *9*	0.573 *6*	0.572 *5*			0.561 *8*	0.572 *5*
194.94		0.00626 *13*		0.0061 *9*	0.0062 *6*		0.0063 *1*
198.90		0.00047 *6*		0.00046 *6*	0.00033 *5*		0.0042 *6*
202.11		0.0108 *2*		0.0108 *11*	0.0107 *10*		0.0108 *2*
205.31	0.050 *2*	0.0505 *5*	0.0496 *5*	0.049 *4*	0.050 *5*	0.0503 *9*	0.0501 *5*
221.38		0.00114 *6*		0.0012 *3*	0.0012 *1*		0.0012 *1*
233.50		0.00029 *5*		0.0003 *1*	0.0003 *1*		0.00029 *5*
240.85		0.00076 *6*		0.0006 *2*	0.0008 *2*		0.00075 *6*
246.84		0.00053 *3*		0.0005 *2*	0.0008 *2*		0.00053 *3*

Notes to Table C

[a] The P_γ values have been calculated from the measured relative intensities using $P_\gamma = 0.572 \pm 0.005$ for the 185 keV reference line.

[b] The value, deviating by a factor of about 10 from the results of the other measurements, has not been considered in the calculation of the evaluated value.

[c] The evaluated values and uncertainties are based on weighted means calculated according to Topping [8].

REFERENCES

[1] HOLDEN, N.E., Total and Spontaneous Fission Half-lives of the Uranium and Plutonium Nuclides, Brookhaven Natl. Lab., Upton, NY, Rep. BNL-NCS-35514-R (1984).
[2] VANINBROUKX, R., DENECKE, B., Nucl. Instrum. Methods **193** (1982) 191.
[3] BANHAM, M.F., JONES, R., Int. J. Appl. Radiat. Isot. **34** (1983) 1225.
[4] HELMER, R.G., REICH, C.W., Int. J. Appl. Radiat. Isot. **35** (1984) 783.
[5] TEOH, W., CONNOR, R.D., BETTS, R.H., Nucl. Phys. **A228** (1974) 432.
[6] VANO, E., GAETA, R., GONZALEZ, L., LIANG, C.F., Nucl. Phys. **A251** (1975) 225.
[7] OLSON, D.G. Nucl. Instrum. Methods **206** (1983) 313.
[8] TOPPING, J., Errors of Observation and their Treatment, 3rd edn, Chapman and Hall, London (1963) 87 – 93.

I. HALF-LIFE

Evaluated by A.L. Nichols (UKAEA, AEE Winfrith).

I.1. Total half-life

Recommended value: 141 ± 2 a

Weighted mean with 1σ standard deviation.

Value (years)	Reference[e]
152 *7* [a,b]	Barnes et al. (1959) [1]
141.9 *17* [a,c]	Zelenkov et al. (1979) [2]
139.7 *18* [a,d]	Zelenkov et al. (1979) [2]

Notes to Table

[a] Quoted uncertainty estimated to be 1σ standard deviation.
[b] Derived from unpublished data and measured alpha half-life: recalculated, but includes erroneous identification of decay modes.
[c] In-growth of ^{242}Cm via ^{242}Am.
[d] Measurement of emission ratios of $^{242}Am^m$ and ^{242}Am.
[e] Exclusive consideration of 1979 measurements (see note b) results in a weighted mean half-life of 141 *1* years.

I.2. Alpha half-life

Recommended value: $(3.11 \pm 0.05) \times 10^4$ a

Weighted mean with 1σ standard deviation.

Value (years)	Reference
2.9 *2* $\times 10^4$ [a,b]	Barnes et al. (1959) [1]
3.12 *5* $\times 10^4$ [a]	Zelenkov et al. (1979) [2]

Notes to Table

[a] Quoted uncertainty estimated to be 1σ standard deviation.
[b] Recalculated from activity measurements using latest estimates of half-life data.

I.3. Spontaneous fission half-life

Recommended value: $(8.8 \pm 3.2) \times 10^{11}$ a

Value (years)	Reference
8.8 *32* $\times 10^{11}$ [a]	Caldwell et al. (1967) [3]

Note to Table

[a] Reported value of 9.5 *35* $\times 10^{11}$ years has been recalculated using latest values for the half-life of $^{242}Am^m$ and the branching fraction to ^{242}Cm.

I.4. Branching fractions

Alpha branching fraction: 0.0045 ± 0.0003.
Isomeric transition branching fraction: 0.9955 ± 0.0003.
Spontaneous fission branching fraction: $(1.6 \pm 0.6) \times 10^{-10}$.

REFERENCES

[1] BARNES, R.F., HENDERSON, D.J., HARKNESS, A.L., DIAMOND, H., J. Inorg. Nucl. Chem. 9 (1959) 105.

[2] ZELENKOV, A.G., PCHELIN, V.A., RODIONOV, Y.F., CHISTYAKOV, L.V., SHUBKO, V.M., At. Ehnerg. 47 (1979) 405; Sov. At. Energy (Engl. Transl.) 47 (1980) 1024.

[3] CALDWELL, J.T., FULTZ, S.C., BOWMAN, C.D., HOFF, R.W., Phys. Rev. 155 (1967) 1309.

APPENDIX B

X-RAY AND GAMMA-RAY DECAY DATA STANDARDS, 1998-2002

EXAMPLE DATA AND RECOMMENDATIONS

Health Warning: all recommended data are subject to change (see Section 4.3)

^{51}Cr

Half-life evaluated by M. J. Woods (NPL, UK), September 2003.
Decay scheme evaluated by E. Schönfeld (PTB, Germany) and R. G. Helmer (INEEL. USA), February 2000.

Recommended data:

Half-life

$T_{1/2}$ = 27.7009 (20) d

Selected gamma ray

E_γ (keV)	P_γ per decay
320.0835 (4) [a]	0.0987 (5) [b]

[a] from Ref. [1].
[b] from direct emission probability measurements.

Selected X-rays

Origin		E_X (keV)	P_X per decay
V	Kα	4.94 - 4.95	0.202 (3)
V	Kβ	5.43 - 5.46	0.0269 (7)

Input data:

Half-life

Half-life (d)	Reference
27.7010 (12) [a]	Unterweger *et al* [H1]
27.71 (3)	Walz *et al* [H2]
27.704 (3)	Rutledge *et al* [H3]
27.690 (5)	Houtermans *et al* [H4]
27.72 (3)	Lagoutine *et al* [H5]
27.703 (8)	Tse *et al* [H6]
27.75 (1) [b]	Visser *et al* [H7]
28.1 (17) [b]	Araminowicz and Dresler [H8]
27.76 (15) [b]	Emery *et al* [H9]
27.80 (51) [b]	Bormann *et al* [H10]
27.7009 (20)	

[a] uncertainty increased to (25) to ensure weighting factor not greater than 0.50.
[b] rejected as an outlier.

References - half-life

[H1] M. P. Unterweger, D. D. Hoppes, F. J. Schima, Nucl. Instrum. Meth. Phys. Res. **A312** (1992) 349
[H2] K. F. Walz, K. Debertin, H. Schrader, Int. J. Appl. Radiat. Isot. **34** (1983) 1191.
[H3] A. R. Rutledge, L. V. Smith, J. S. Merritt, AECL-6692 (1980).
[H4] H. Houtermans, O. Milosevic, F. Reichel, Int. J. Appl. Radiat. Isot. **31** (1980) 153.
[H5] F. Lagoutine, J. Legrand, C. Bac, Int. J. Appl. Radiat. Isot. **26** (1975) 131.
[H6] C. W. Tse, J. N. Mundy, W. D. McFall, Phys. Rev. **C10** (1974) 838.
[H7] C. J. Visser, J. H. M. Karsten, F. J. Haasbroek, P. G. Marais, Agrochemophysica **5** (1973) 15.
[H8] J. Araminowicz, J. Dresler, INR-1464 (1973) 14.

[H9] J. F. Emery, S. A. Reynolds, E. I. Wyatt, G. I. Gleason, Nucl. Sci. Eng. **48** (1972) 319.
[H10] M. Bormann, A. Behrend, I. Riehle, O. Vogel, Nucl. Phys. **A115** (1968) 309.

Gamma ray: measured and evaluated emission probability

Eγ (keV) [1]	[2]	[3]	[4]	[5]	[6]	[7]
320.0835	9.8 (6)	9 (1)	9.72 (15)	10.2 (6)	9.75 (20)	10.2 (10)

Eγ (keV) [1]	[8]	[9]	[10]	**Evaluated**
320.0835	9.85 (9)	10.30 (19)	9.86 (8)	9.87 (5)

Evaluated emission probabilities are the weighted averages calculated according to the Limitation of Relative Statistical Weights Method; no value has a relative weighting factor greater than 0.50.

References - radiations

[1] R. G. Helmer, C. van der Leun, Nucl. Instrum. Meth. Phys. Res. **A450** (2000) 35.
[2] M. E. Bunker, J. W. Starner, Phys. Rev. **97** (1955) 1272, and **99** (1955) 1906.
[3] S. G. Cohen, S. Ofer, Phys. Rev. **100** (1955) 856.
[4] J. S. Merritt, J. G. V. Taylor, AECL-1778 (1963) 31.
[5] K. C. Dhingra, U. C. Gupta, N. P. S. Sidhu, Current Sci., India **34** (1965) 504.
[6] J. Legrand, CEA-R-2813 (1965).
[7] C. Ribordy, O. Huber, Helv. Phys. Acta **43** (1970) 345.
[8] U. Schötzig, K. Debertin, K. F. Walz, Nucl. Instrum. Meth. **169** (1980) 43.
[9] S. A. Fisher, R. I. Hershberger, Nucl. Phys. **A423** (1984) 121.
[10] T. Barta, L. Szücs, A. Zsinka, Appl. Radiat. Isot. **42** (1991) 490.

Detailed tables and comments can be found on http://www.nucleide.org/DDEP_WG/DDEPdata.htm

^{203}Hg

Half-life evaluated by M. J. Woods (NPL, UK), September 2003.
Decay scheme evaluated by A. L. Nichols (IAEA and AEA Technology, UK), January 2002.

Recommended data:

Half-life

$T_{1/2}$ = 46.594 (12) d

Selected gamma rays

E_γ (keV)	P_γ per decay
279.1952 (10) [a]	0.8148 (8)

[a] from Ref. [1].

Selected X-rays

Origin		E_X (keV)	P_X per decay
Tl	L	8.953 - 14.738	0.0543 (9)
Tl	$K\alpha_2$	70.8325 (8)	0.0375 (4)
Tl	$K\alpha_1$	72.8725 (8)	0.0633 (6)
Tl	$K\beta_1'$	82.118 - 83.115	0.0215 (4)
Tl	$K\beta_2'$	84.838 - 85.530	0.0064 (2)

Input data:

Half-life

Half-life (d)	Reference
46.619 (27)	Unterweger *et al* [H1]
46.612 (19)	Walz *et al* [H2]
46.60 (1)	Rutledge *et al* [H3]
46.582 (2) [a]	Houtermans *et al* [H4]
46.76 (8) [b]	Emery *et al* [H5]
47.00 (3) [b]	Lagoutine *et al* [H6]
46.594 (12)	

[a] uncertainty increased to (9) to ensure weighting factor not greater than 0.50.
[b] rejected as an outlier.

References - half-life

[H1] M. P. Unterweger, D. D. Hoppes, F. J. Schima, Nucl. Instrum. Meth. Phys. Res. **A312** (1992) 349.
[H2] K. F. Walz, K. Debertin, H. Schrader, Int. J. Appl. Radiat. Isot. **34** (1983) 1191.
[H3] A. R. Rutledge, L. V. Smith, J. S. Merritt, AECL-6692 (1980).
[H4] H. Houtermans, O. Milosevic, F. Reichel, Int. J. Appl. Radiat. Isot. **31** (1980) 153.
[H5] J. F. Emery, S. A. Reynolds, E. I. Wyatt, G. I. Gleason, Nucl. Sci. Eng. **48** (1972) 319.
[H6] F. Lagoutine, Y. L. Gallic, J. Legrand, Int. J. Appl. Radiat. Isot. **19** (1968) 475.

Gamma ray: energy and emission probability

Comments:

γ-ray energy of 279.1952 keV have been adopted from Ref. [1].

279.1952-keV γ-ray is of mixed (25%M1 + 75%E2) multipolarity, and α_{tot} = 0.2271 (12) and α_K = 0.1640 (10) have been adopted from Ref. [2], in good agreement with specific measurements [3-6].

beta-particle emission probabilities were calculated from the limit of 0.0001 (1) set on the beta transition to the $½^+$ ground state of ^{203}Tl [7, 8], to give 0.9999 (1) for the transition to the first excited state of ^{203}Tl ($5/2^- \rightarrow 3/2^+$).

as defined above, transition probability of 0.9999 (1) for the 279.1952-keV γ ray was used in conjunction with α_{tot} to calculate an absolute emission probability of 0.8148 (8).

X-rays: energies and emissions

Calculated using the evaluated γ-ray data, and atomic data from Refs. [9-11].

References - radiations

[1] R. G. Helmer, C. van der Leun, Nucl. Instrum. Meth. Phys. Res. **A450** (2000) 35.

[2] H. H. Hansen, European Appl. Res. Rept., Nucl. Sci. Technol. **6**, No. 4 (1985) 777.

[3] J. G. V. Taylor, Can. J. Phys. **40** (1962) 383.

[4] C. J. Herrlander, R. L. Graham, Nucl. Phys. **58** (1964) 544.

[5] H. H. Hansen, D. Mouchel, Z. Phys. **267** (1974) 371.

[6] E. Schönfeld, H. Janβen, R. Klein, Appl. Radiat. Isot. **52** (2000) 955.

[7] N. Marty, C. R. Acad. Sci., Paris, Series B **240** (1955) 291.

[8] J. L. Wolfson, Can. J. Phys. **34** (1956) 256.

[9] E. Browne, R. B. Firestone, pp. C-19 – C-30, Table of Radioactive Isotopes, John Wiley & Sons, New York (1986).

[10] E. Schönfeld, H. Janβen, Nucl. Instrum. Meth. Phys. Res. **A369** (1996) 527.

[11] E. Schönfeld, G. Rodloff, PTB-6.11-1999-1, February 1999.

Detailed tables and comments can be found on:
http://www.nucleide.org/DDEP_WG/DDEPdata.htm

^{226}Ra with Daughters

Half-life evaluated by M. J. Woods (NPL, UK), September 2003.
Decay scheme evaluated by R. G. Helmer (INEEL, USA), August 2002.

Recommended data:

Half-life (^{226}Ra)
$T_{1/2} = 5.862\ (22) \times 10^5$ d

Selected gamma rays

Only γ rays with emission probabilities greater than 0.010 are included.

Parent	E_γ (keV)	P_γ per decay
^{214}Pb	53.2275 (21) [a]	0.01066 (14)
^{226}Ra	186.211 (13) [a]	0.03533 (28)
^{214}Pb	241.997 (3) [a]	0.0719 (6)
^{214}Pb	295.224 (2) [a]	0.1828 (14)
^{214}Pb	351.932 (2) [a]	0.3534 (27)
^{214}Bi	609.316 (3) [b]	0.4516 (33)
^{214}Bi	665.453 (22) [a]	0.01521 (11)
^{214}Bi	768.367 (11) [b]	0.04850 (38)
^{214}Bi	806.185 (11) [b]	0.01255 (11)
^{214}Bi	934.061 (12) [a]	0.03074 (25)
^{214}Bi	1120.287 (10) [a]	0.1478 (11)
^{214}Bi	1155.19 (2) [a]	0.01624 (14)
^{214}Bi	1238.110 (12) [a]	0.05785 (45)
^{214}Bi	1280.96 (2) [a]	0.01425 (12)
^{214}Bi	1377.669 (12) [a]	0.03954 (33)
^{214}Bi	1401.516 (14) [c]	0.01324 (11)
^{214}Bi	1407.993 (7) [b]	0.02369 (19)
^{214}Bi	1509.217 (8) [b]	0.02108 (21)
^{214}Bi	1661.316 (13) [b]	0.01037 (10)
^{214}Bi	1729.640 (12) [b]	0.02817 (23)
^{214}Bi	1764.539 (15) [b]	0.1517 (12)
^{214}Bi	1847.420 (25) [a]	0.02000 (18)
^{214}Bi	2118.536 (8) [b]	0.01148 (11)
^{214}Bi	2204.071 (21) [b]	0.0489 (10)
^{214}Bi	2447.673 (10) [b]	0.01536 (15)

[a] from Ref. [1].
[b] from Ref. [2].
[c] from Ref. [3].

Input data:

Half-life

Half-life (d)	Reference
584035 (853) [a]	Ramthun [H1]
585131 (3204)	Martin and Tuck [H2]
590609 (4135)	Sebaoun [H3]
592436 (4749)	Kohman *et al* [H4]
$5.862\ (22) \times 10^5$	

[a] uncertainty increased to (2250) to ensure weighting factor not greater than 0.50.

References - half-life

[H1] H. Ramthun, Nukleonik **8** (1966) 244.
[H2] G. R. Martin, D. G. Tuck, Int. J. Appl. Radiat. Isot. **5** (1959) 141.
[H3] W. Sebaoun, Ann. Phys., Paris **1** (1956) 680.
[H4] T. P. Kohman, D. P. Ames, J. Sedlet, Nat. Nucl. Energy Series **14** (1949) 1675.

Gamma rays: measured and evaluated relative emission probabilities

Eγ (keV)	[4]	[5]	[6] [a]	[7]	[8]	[3]	**Evaluated**
53.2	-	-	-	-	2.329 (23)	2.384 (20)	2.360 (27)
186.21	8.7 (11)	9.2 (10)	8.58 (5)	7.6 (8)	7.812 (31)	7.85 (5)	7.824 (26)
241.99	17.5 (17)	16.1 (24)	16.23 (10)	16.1 (10)	15.90 (5)	15.98 (6)	15.93 (4)
295.22	40 (4)	42 (5)	41.85 (26)	40.8 (12)	40.36 (12)	40.61 (13)	40.48 (9)
351.93	86 (9)	82 (11)	81.5 (5)	78.5 (24)	78.16 (23)	78.34 (23)	78.25 (16)
609.32	≡100	100	100	100	100	100	100
665.45	3.6 (4)	3.36 (37)	3.51 (20)	3.33 (10)	3.359 (17)	3.386 (21)	3.369 (13)
768.37	11.4 (12)	11.9 (17)	10.91 (8)	10.39 (31)	10.66 (5)	10.768 (29)	10.740 (29)
806.18	3.0 (4)	2.92 (43)	2.90 (22)	2.76 (11)	2.788 (22)	2.777 (14)	2.780 (12)
934.06	7.3 (7)	7.0 (9)	6.88 (5)	6.70 (20)	6.783 (34)	6.834 (36)	6.806 (25)
1120.29	34 (3)	-	33.13 (22)	32.3 (10)	32.71 (10)	32.77 (12)	32.73 (8)
1155.19	4.0 (5)	-	3.5 (4)	4.3 (7)	3.594 (36)	3.595 (17)	3.595 (15)
1238.11	14.9 (15)	-	12.87 (9)	12.7 (4)	12.83 (6)	12.80 (4)	12.810 (33)
1280.96	3.6 (5)	-	3.17 (17)	3.15 (11)	3.147 (28)	3.159 (16)	3.156 (14)
1377.67	9.9 (11)	-	8.82 (25)	8.52 (25)	8.69 (4)	8.794 (30)	8.755 (35)
1401.52	3.5 (4)	-	2.91 (16)	3.0 (4)	2.924 (20)	2.934 (13)	2.932 (11)
1407.99	6.2 (7)	-	5.37 (6)	5.5 (5)	5.233 (26)	5.250 (19)	5.245 (15)
1509.22	5.5 (5)	-	4.76 (5)	4.63 (15)	4.61 (6)	4.682 (31)	4.668 (31)
1661.32	2.72 (25)	-	2.33 (12)	2.37 (22)	2.271 (34)	2.299 (14)	2.296 (14)
1729.64	7.5 (7)	-	6.60 (4)	6.33 (15)	6.226 (31)	6.245 (32)	6.238 (25)
1764.54	40 (4)	-	34.48 (25)	33.3 (10)	33.54 (10)	33.63 (9)	33.59 (7)
1847.42	5.3 (5)	-	4.57 (6)	4.35 (13)	4.448 (36)	4.419 (28)	4.429 (25)
2118.54	3.03 (29)	-	2.56 (3)	2.65 (25)	2.536 (20)	2.548 (21)	2.543 (15)
2204.07	12.38 (27)	-	11.02 (9)	11.1 (3)	10.74 (5)	10.75 (9)	10.83 (20)
2447.67	4.0 (4)	-	3.42 (3)	3.30 (10)	3.402 (24)	3.409 (36)	3.402 (21)

[a] data rejected as outliers.

Evaluated emission probabilities are the weighted averages calculated according to the Limitation of Relative Statistical Weights Method, and using the data from Refs. [3-5, 7, 8]; no value has a relative weighting factor greater than 0.50.

Absolute emission probabilities for specific γ rays have been measured by several authors [9-13]. Generally, the uncertainties in the relative emission probabilities from these authors have larger uncertainties than those for the relative values in the above table. Therefore, the above relative emission probabilities have been normalized simply by use of P_γ(609 keV) = 0.4516 (33) from the average of the values from Refs. [9-13].

References - radiations

[1] Y. A. Akovali, Nucl. Data Sheets **75** (1995) 127; *ibid*, **77** (1996) 271.
[2] R. G. Helmer, R. J. Gehrke, R. C. Greenwood, Nucl. Instrum. Meth. **166** (1970) 547.
[3] G. L. Molnár, Institute of Isotope and Surface Chemistry, Chemical Research Centre, Budapest, Hungary, private communication; reported subsequently with minor rounding-up of uncertainties as G. L. Molnár, Zs. Révay, T. Belgya, “New intensities for high energy gamma-ray standards”, pp. 522-530 in Proc. 11th Int. Symp. on Capture Gamma-ray Spectroscopy and Related Topics, Pruhonice near Prague, Czech Republic, 2-6 September 2002, Editors: J. Kvasil, P. Cejnar, M. Krtička, World Scientific, Singapore (2003).
[4] A. Hachem, C. R. Acad. Sci., Paris, Series B **281** (1975) 45.

[5] H. Akcay, G. Mouze, D. Maillard, Ch. Ythier, Radiochem. Radioanal. Lett. **51** (1982) 1.
[6] G. Mouze, Ch. Ythier, J. F. Comanducci, Rev. Roum. Phys. **35** (1990) 337, as quoted in Ref. [7].
[7] D. Sardari, T. D. MacMahon, J. Radioanal. Nucl. Chem. **244** (2000) 463.
[8] J. U. Delgado, J. Morel, M. Etcheverry, Appl. Radiat. Isot. **56** (2002) 137.
[9] E. W. A. Lingeman, J. Konijn, P. Polak, A. H. Wapstra, Nucl. Phys. **A133** (1969) 630.
[10] D. G. Olson, Nucl. Instrum. Meth. Phys. Res. **206** (1983) 313.
[11] U. Schötzig, K. Debertin, Int. J. Appl. Radiat. Isot. **34** (1983) 533.
[12] W.-J. Lin, G. Harbottle, J. Radioanal. Nucl. Chem. **153** (1991) 137.
[13] J. Morel, M. Etcheverry, J. L. Picolo, Appl. Radiat. Isot. **49** (1998) 1387.

Detailed tables and comments can be found on http://www.nucleide.org/DDEP_WG/DDEPdata.htm

Nuclear Data Section
International Atomic Energy Agency
P.O. Box 100
A-1400 Vienna
Austria

e-mail: services@iaeand.iaea.org
fax: (43-1) 26007
cable: INATOM VIENNA
telex: 1-12645
telephone: (43-1) 2600-21710
Web: http://www-nds.iaea.org